UNIVERSIDAD AUTÓNOMA DE MADRID

Facultad de Ciencias

Departamento de Geología y Geoquímica

CLAY-BASED HYBRID NANOPLATFORMS: PREPARATION, CHARACTERIZATION AND EVALUATION OF PROPERTIES FOR CONTROLLED RELEASE OF BIOACTIVE SPECIES

Doctoral Thesis

Ediana Paula Rebitski

Supervisors:

Dr. Pilar Aranda
Dr. Margarita Darder

CSIC
CONSEJO SUPERIOR DE INVESTIGACIONES CIENTÍFICAS

Instituto de Ciencia de Materiales de Madrid (ICMM), CSIC.
Departamento de Nuevas Arquitecturas en Química de Materiales

February 2020

CONTENTS

ABSTRACT

This Doctoral Thesis is centered in the field of the nanostructured hybrid materials, and more specifically addresses the study of the so-called biohybrid materials resulting from the assembly of molecular and polymeric species of biological origin with inorganic substrates at the nanometer scale. The Thesis deals with the preparation and characterization of hybrid and biohybrid materials by intercalation of bioactive species in silicates of the type of clays and other related inorganic layered solids, and their integration into more complex systems such as bionanocomposites and nanoarchitectures, for application as controlled release systems of drugs and herbicides.

In this way, the first study focused on the development of controlled release systems of metformin (MF), the most commonly used oral drug for the treatment of type II diabetes and currently also explored in treatments of certain types of cancer. In a first stage, various hybrid materials were prepared by association of MF to clay minerals of the smectite group (montmorillonite and hectorite). Specifically, in this work a montmorillonite from Wyoming, marketed as Cloisite®Na (Mt), and a synthetic hectorite, commercialized under the tradename Laponite® XLG (Lap) were used. Laponite® XLG is usually used in cosmetics and pharmacy and was selected in view to have a well-regulated substrate for possible use in the production of pharmaceutical formulations. The combination of molecular modelling and experimental characterization techniques, such as FTIR, XRD, CHN chemical analysis and EDX, allowed to study the process of adsorption of the drug and the final molecular arrangement of MF species in the interlayered space of clays, confirming that the intercalated MF follows in both cases an ion-exchange mechanism. Furthermore, bionanocomposite systems in which the prepared intercalation compounds were incorporated into a

biopolymer matrix of pectin or chitosan were also explored, processing them in the form of microspheres (beads). These beads were then coated with one or two layers of those polymers in order to take advantage of the resistance properties of pectin to acidic pH environments, which may help to protect the hybrid at pH 1.2, and the mucoadhesive properties of chitosan, which can favor residence time and assimilation of the drug in the intestinal tract, thus overcoming problems linked to its rapid elimination as occurs in the most typical formulations used for MF administration. The produced beads were tested for water stability and *in vitro* release simulating the pH changes occurring throughout the gastrointestinal tract with the aim of establishing the performance of each system as a possible formulation for controlled release of metformin. The results obtained show that it is possible to establish a control on the release by varying the characteristics of the bionanocomposite system and the coatings of the microspheres, which may be useful in view of the application of this type of systems in pharmacology.

In a second study, the design of a controlled allantoin release system was addressed with the target of a possible topical application in skin disease treatments. Allantoin is a very particular molecule of great versatility for use in cosmetics and pharmacy, but it is very difficult to stabilize with other components for controlled release applications. In this sense, the preparation of hybrid materials by intercalation in layered metal hydroxides, typically layered double hydroxides (LDH), with different metals (MgAl or ZnAl) by different methods of synthesis (ion-exchange, reconstruction and co-precipitation) was explored. It was proven that hybrid materials based on LDH-MgAl incorporate up to a maximum of allantoin of approximately half of the LDH anionic exchange capacity, with the ion-exchange method being the least effective, and verifying that in all cases there is no intercalation of the associated allantoin. In the case of LDH-ZnAl, it is possible to incorporate a greater amount of allantoin, practically similar to the anion exchange capacity of the LDH, when the preparation of the hybrid is carried out by means of a co-precipitation process of the hydroxide in the presence of allantoin. The characterization of the resulting hybrid material indicates that actually the LDH was not formed because the Zn: Al ratio is much

smaller than the expected 2: 1, with practically no incorporation of Al in the structure of the precipitated solid. However, using only a Zn precursor, it was possible to successfully co-precipitate a compound in which allantoin is associated with a layered single hydroxide (LSH) of Zn. The obtained allantoin-Zn LSH hybrid was compared to the characteristics of a Zn-allantoin complex prepared according to a protocol previously reported in the literature, and for which the presence of Zn acts as an enhancer of the therapeutic effects of allantoin. A study of the release of allantoin from several of the prepared systems confirms that the allantoin-Zn LSH system is the most efficient, even better than the Zn-allantoin complex described in the literature. The incorporation of the systems developed in biopolymeric matrices such as agar, hydroxypropylmethylcellulose (HPMC) or nanocellulose, facilitates subsequent processing as stable films that can be used in applications, for example, as tissues for wound dressings, and in which the presence of Zn in the incorporated hybrid can play a bactericide action.

The third group of materials prepared in the Doctoral Thesis focused on the development of hybrid heterostructures of LDH-sepiolite for herbicide release system applications. Specifically, the synthesis of a LDH of Mg-Al in the presence of sepiolite fibrous clay and the herbicide known as MCPA (2-methyl-4-chlorophenoxyacetic acid) was addressed through co-precipitation in a single stage to prepare the hybrid nanoarchitecture. It has been proven that the co-precipitation of the LDH in the presence of the herbicide and sepiolite results in systems that incorporate a large amount of herbicide, much greater than the amount adsorbed when only the LDH is co-precipitated in the presence of MCPA or when the herbicide is intercalated in the LDH-sepiolite nanoarchitecture by ion-exchange. MCPA-LDH/sepiolite nanoarchitectures were characterized by various physicochemical techniques (XRD, FTIR and ^{29}Si NMR spectroscopy, CHN and FESEM analysis) revealing that LDH interacts and remains attached to the sepiolite fibers through silanol groups present on the external surface of the clay. It is also confirmed that MCPA is intercalated into the LDH as instead of an interlayer distance of 0.77 nm, characteristic of the LDH with chloride ions as

compensating interlayer anions, the actual interlayer distance in materials with MCPA is 2.32 nm. The herbicide release tests in water at pH 5.5, which simulates the characteristics of rainwater, show that the release from the sepiolite-LDH hybrid nanoarchitectures is much faster and more complete compared to the MCPA-LDH hybrid prepared by co-precipitation of the LDH in the presence of the herbicide, which confirms its suitability for agricultural applications. In order to have release systems for application in soils in which the hybrid nanoarchitecture may act as a reservoir for the herbicide and where a longer action can be established, a system of microspheres composed of the polysaccharide alginate and the hydrophobic zein protein was also developed. In *in vitro* tests and in columns prepared with soils, the release results were very satisfactory and allow to confirm a more controlled release process of the herbicide from the bionanocomposite systems at levels closer to the outermost surface of the soil, avoiding leaching processes of the herbicide at greater depths thereof. Other additional advantages of the developed systems refer to the use of encapsulation as a means to allow better management and transport of the herbicide and to the use of sepiolite present in the hybrid nanoarchitecture to incorporate other species of interest that could be released simultaneously to the environment.

RESUMEN

Esta Tesis Doctoral se encuadra en el campo de los materiales híbridos nanoestructurados, y más concretamente de los denominados materiales biohíbridos resultantes del ensamblaje de especies moleculares y poliméricas de origen biológico con sustratos inorgánicos a través de interacciones a escala nanométrica. La Tesis aborda la preparación y caracterización de materiales híbridos y biohíbridos basados en la intercalación de especies bioactivas en silicatos del tipo de las arcillas y otros sólidos inorgánicos relacionados laminares, y su integración en sistemas más complejos como bionanocomposites y nanoarquitecturas, para su aplicación como sistemas de liberación controlada de fármacos o herbicidas.

En concreto, se han desarrollado sistemas para actuación en la liberación controlada de metformina (MF), el fármaco oral más utilizado para el tratamiento de la diabetes tipo II y actualmente explorado en tratamientos de ciertos tipos de cáncer. En una primera etapa se han desarrollado materiales híbridos en los que la MF ha podido ser intercalada mediante procedimientos de cambio iónico en arcillas del grupo de las esmectitas (montmorillonita y hectorita). En concreto, en este trabajo se ha utilizado una montmorillonita de Wyoming, comercializada como Cloisite®Na (Mt), y una hectorita sintética, comercializada bajo el nombre de Laponite® XLG (Lap) y habitualmente empleada en cosmética y farmacia, seleccionada con vistas a tener un substrato bien regulado para su posible empleo en la producción de formulaciones farmacéuticas. La combinación de técnicas de modelado molecular y caracterización experimental, como FTIR, XRD, análisis químico CHN y EDX, ha permitido estudiar el proceso de adsorción del fármaco y la disposición molecular final de las especies de MF en el espacio interlaminar de las arcillas, confirmando que la intercalación de MF en ambos casos sigue un

mecanismo de intercambio iónico. Además, se ha explorado el desarrollo de sistemas bionanocomposites en los que los compuestos de intercalación desarrollados se han incorporado en una matriz biopolimérica de pectina o de quitosano, procesando el material bionanocomposite resultante en forma de microesferas. Estas fueron recubiertas posteriormente con una o dos capas de dichos polímeros para aprovechar las propiedades de resistencia a pHs ácidos de la pectina, que ayuda a proteger el híbrido a pH 1.2, y las propiedades de mucoadhesividad del quitosano, que pueden favorecer el tiempo de residencia y asimilación del fármaco en el tracto intestinal, venciendo así problemas ligados a su rápida eliminación como ocurre en las formulaciones más típicas del mismo. Las microesferas producidas se sometieron a pruebas de estabilidad al agua y de liberación *in vitro* simulando los cambios de pH a lo largo del tracto gastrointestinal con el objetivo de establecer el rendimiento de cada sistema como posible formulación para la liberación controlada de metformina. Los resultados obtenidos muestran que es posible establecer un control en la liberación variando las características del sistema bionanocomposite y de los recubrimientos de las microesferas, lo que puede ser de utilidad con vistas a la aplicación de este tipo de sistemas en farmacología.

Un segundo estudio realizado fue el diseño de un sistema de liberación controlada de alantoína para una posible aplicación tópica en tratamientos de enfermedades de la piel. La alantoína es una molécula muy particular de gran versatilidad para usos en cosmética y farmacia, pero que es muy difícil de estabilizar con otros componentes para aplicaciones en liberación controlada. En este sentido se ha explorado la preparación de materiales híbridos por intercalación en hidróxidos metálicos lamelares, típicamente hidróxidos dobles laminares (HDL), con distintos metales (MgAl or ZnAl) por diferentes métodos de síntesis (intercambio iónico, reconstrucción y co-precipitación). Se ha comprobado que los materiales híbridos basados en el HDL-MgAl incorporan hasta un máximo de alantoína de aproximadamente la mitad de la capacidad de cambio aniónico del HDL, siendo el método de cambio iónico el menos eficaz, y comprobándose que en todos los casos no se produce intercalación de la

alantoína asociada. En el caso del HDL-ZnAl se observa que es posible incorporar una mayor cantidad de alantoína, prácticamente similar a la capacidad de cambio del LDH, cuando se lleva a cabo la preparación del híbrido mediante un proceso de co-precipitación del HDL en presencia de alantoína. La caracterización del material híbrido formado indica que en realidad no se ha formado un HDL ya que la relación Zn:Al es mucho menor que la esperada de 2:1 no incorporándose prácticamente Al en la estructura del sólido precipitado. Sin embargo, utilizando sólo un precursor de Zn ha sido posible co-precipitar con éxito un compuesto en el que la alantoína se asocia a un hidróxido sencillo laminar (HSL) de Zn. El híbrido alantoína-Zn HSL obtenido ha sido comparado con un complejo de Zn-alantoína preparado de acuerdo con un protocolo previamente recogido en la literatura y para el que se había descrito un efecto de la presencia de Zn como potenciador de los efectos terapéuticos de la alantoína. Un estudio de la liberación de la alantoína a partir de varios de los sistemas preparados confirma que el sistema alantoína-Zn HSL es el más eficiente, incluso que el complejo Zn-alantoína descrito en la literatura. La incorporación de los sistemas desarrollados en matrices biopoliméricas como pueden ser el agar, la hidroxipropilmetilcelulosa (HPMC) o la nanocelulosa, facilita un posterior procesado como películas estables que puedan ser utilizadas en aplicaciones, por ejemplo, como tejidos para apósitos de heridas, y en las que la presencia de Zn en el híbrido incorporado puede ejercer un papel bactericida.

El tercer grupo de materiales preparados en la Tesis Doctoral se ha centrado en el desarrollo de heteroestructuras híbridas de hidróxidos dobles laminares-sepiolita como sistemas de liberación de herbicidas. En concreto, se ha abordado la síntesis de hidróxidos dobles laminares de Mg-Al en presencia de la arcilla fibrosa sepiolita y del herbicida conocido como MCPA (ácido 2-metil-4-clorofenoxiacético) para producir mediante co-precipitación en una sola etapa la nanoarquitectura híbrida. Se ha comprobado que el proceso de co-precipitación del HDL en presencia del herbicida y de sepiolita da lugar a sistemas que incorporan una gran cantidad de herbicida, mucho mayor que la cantidad adsorbida cuando se co-precipita sólo el HDL o cuando la nanoarquitectura

híbrida se prepara mediante un proceso de cambio iónico de los aniones Cl^- presentes en nanoarquitecturas de HDL-sepiolita previamente obtenidas en un proceso de co-precipitación similar pero en ausencia de herbicida en el medio. Las nanoarquitecturas MCPA-HDL/sepiolita se caracterizaron por diversas técnicas fisicoquímicas (XRD, espectroscopias FTIR y ^{29}Si NMR, análisis de CHN y FESEM) que revelaron interacciones del HDL con las fibras de sepiolita a través de los grupos silanol presentes en la superficie externa de las fibras de sepiolita, junto con la intercalación de MCPA en la LDH confirmada por el aumento del espaciado basal de 0,77 nm característico del HDL con aniones compensadores cloruro en la interlámina a espaciados de 2,32 nm en materiales con MCPA. Los ensayos de liberación del herbicida incorporado en las nanoarquitecturas híbridas en agua a pH 5,5, que simula las características de agua de lluvia, muestran que la liberación a partir de las nanoarquitecturas híbridas de sepiolita-HDL es mucho más rápida y completa en comparación a cuando el herbicida está incorporado en un LDH co-precipitado en presencia del herbicida, lo que confirma su idoneidad para aplicaciones agrícolas. Con el fin de contar con sistemas de liberación de aplicación en suelos donde la nanoarquitectura híbrida actúe como reservorio del herbicida y donde se pueda establecer una acción más prolongada, se desarrolló también sistema de microesferas compuestas del polisacárido alginato y de la proteína hidrofóbica zeína. En pruebas *in vitro* y en columnas preparadas con suelos los resultados de liberación son muy satisfactorios y permiten confirmar un proceso de liberación más controlado del herbicida a partir de los sistemas bionanocomposites en niveles más próximos a la superficie más exterior del suelo, evitando procesos de lixiviación del herbicida a mayores profundidades del mismo. Otras ventajas adicionales de los sistemas desarrollados se refieren al uso de la encapsulación como medio para permitir un mejor manejo y transporte del herbicida y a la utilización de la sepiolita presente en la nanoarquitectura híbrida para incorporar otras especies de interés que pudieran ser liberadas simultáneamente al medio.

CHAPTER 1

INTRODUCTION

This Thesis deals with the preparation, and characterization of hybrid and biohybrid materials based on the intercalation of bioactive species in layered inorganic solids, and their integration in more complex systems like bionanocomposites and nanoarchitectures. It deals also with the evaluation of the properties of the resulting materials for application as controlled release systems of drugs or herbicides. The developed materials are based on cationic clays of the smectite type, and anionic clays, such as layered double hydroxides or layered simple hydroxides, which are commonly used in the formation of hybrid, bionanocomposite and nanoarchitectured materials. This introductory chapter is intended to review some of the most important concepts that form the basis of the work reported in this Thesis. First, general concepts of controlled delivery will be described, both in pharmaceutical and agriculture areas, followed by a revision on the clays used for this purpose, with emphasis on the use of intercalation compounds and more complex systems (bionanocomposites and nanoarchitectures) as controlled release systems. Finally, the main objectives of this Thesis will be detailed.

1.1 CONTROLLED DELIVERY SYSTEMS

1.2 CLAY-BASED NANOCARRIERS IN DELIVERY SYSTEMS

1.3 OBJECTIVES OF THIS DISSERTATION

1.1 CONTROLLED DELIVERY SYSTEMS

There is currently an increasing progress in the development of controlled release systems in several sectors, both in the areas of food, cosmetics, and pharmaceutics (for oral, dermal, transdermal, intravenous, sublingual, or nasal administration, among others) as in the environmental field (for the controlled release of pesticides, fertilizers, etc.). In the health area, the controlled release can be defined as a technique or method in which the active chemical agent is delivered at specific rate over a period of time in order to achieve the intended therapeutic effect (Hoffman, 2008; Park, 2014; Yun et al., 2015), avoiding or minimizing side effects (Zhang and Cresswell, 2016; Robert et al., 2017; Mehtani et al., 2019). In the environmental sector, more specifically in the agrochemical sector, the development of these controlled release systems is being a potential solution to those problems related to the delivery efficiency and the environmental pollution derived from pesticides (Campos et al., 2014; Singh et al., 2020).

1.1.1 Controlled drug delivery systems

The search for new therapeutic materials capable of efficiently modifying the kinetics and release site of a drug, compared to a conventional release, has aroused great interest in the areas of biomedicine and tissue engineering. Figure 1.1 describes how a controlled release system works compared to conventional release formulations. As can be seen, the release rate of active ingredient from conventional formulations is generally very fast and complete after administration. This means that the concentration in the medium is initially very high, reaching toxic levels, and decreases rapidly to low and ineffective levels, which makes necessary the administration of multiple doses. In contrast, a controlled release system allows the gradual release of the active substance, maintaining its concentration within the therapeutic level with a single dose, and minimizing side effects (Park, 2014; Dalcanale et al., 2015).

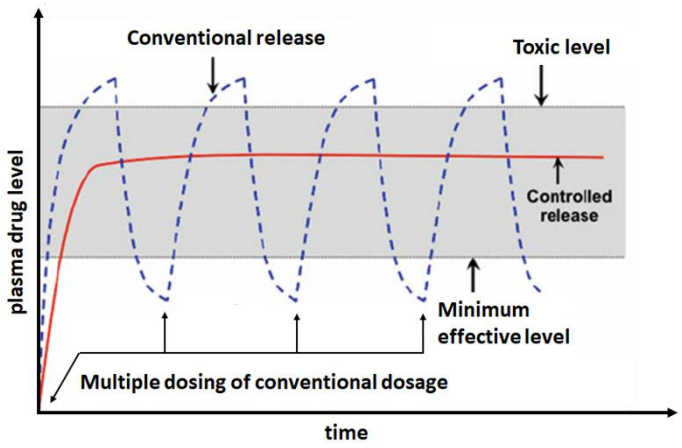

Figure 1.1. Drug levels in the plasma released from a traditional release system (blue dashed curve) that requires multiple doses, and a controlled release system (red continuous curve). (Adapted from Dalcanale et al. (2015)).

Often, in a controlled drug delivery system, the addition of excipients (pharmacologically inactive substances used as a vehicle for the active ingredient) is required (Park, 2014; Kaur et al., 2018). In addition, they can guarantee greater stability, improve the biopharmaceutical properties of the drugs and improve the organoleptic characteristics, thus contributing to a better acceptance of medication by patients. These excipients should have properties such as biocompatibility, biodegradability, and versatility, among others. Among the materials most commonly used as carriers or vehicles in release systems, we can find surfactants, lipids, polymers and inorganic materials (Yun et al., 2015; Mehtani et al., 2019). Among the last ones, clay minerals have shown great interest as controlled release systems of drugs, including natural silicates such as smectites, sepiolite or palygorskite, and also layered double hydroxides (LDH) (Gordijo et al., 2005; Aguzzi et al., 2007; Choy et al., 2007; Carretero and Pozo, 2009; Viseras et al., 2010; Oh et al., 2012; Siepmann et al., 2012; Kim et al., 2013; Hun Kim et al., 2016), as will be detailed in #section 1.2.1. The possibility of processing the formulations as powdered materials, films, foams or microbeads is of interest to select the more appropriate conformation depending on the type of administration in the body (oral, dermal, intravenous...) and the type of disease. For instance, administration can be carried out through the nasal

membranes (nasal route), the eye (ophthalmic route), the mucous membranes of the mouth (oral route), the skin (transdermal route), among others (Shingade, 2012; Tiwari et al., 2012; Park, 2014; Hun Kim et al., 2016; Ruiz-Hitzky et al., 2019; Viseras et al., 2019).

1.1.2 Controlled delivery of herbicides

Productivist agriculture has had an exponential increase in recent years, mainly due to the worldwide population increase, once plants are the main source of food in the world (Campos et al., 2014; Singh et al., 2020). This increase in world agricultural productivity has had a direct impact on the greater use of pesticides, together with new agricultural practices, providing the diffusion of new varieties of self-growing crops. In order to meet the current production needs of plants in general, the use of pesticides is essential since the plants are susceptible to approximately 100,000 diseases due to a wide variety of agents. The use of pesticide amounts in large excess tries to overcome its loss due to several factors, such as chemical/or biological degradation, photodecomposition and losses due to runoff and leaching along the soil profile (Chauhan et al., 2017; Singh et al., 2020) (Figure 1.2). Leaching of herbicides usually brings more serious consequences such as the increase in the residual activity of the herbicide since the microbial activity responsible for the degradation of most herbicides decreases with depth; reduction of the herbicide concentration in the upper part of the soil below the thresholds necessary for the control of weeds and excessive accumulation in the root zone of the crop to levels that jeopardize its safety; water can carry herbicides below the root, reaching and contaminating groundwater (Singh et al., 2020).

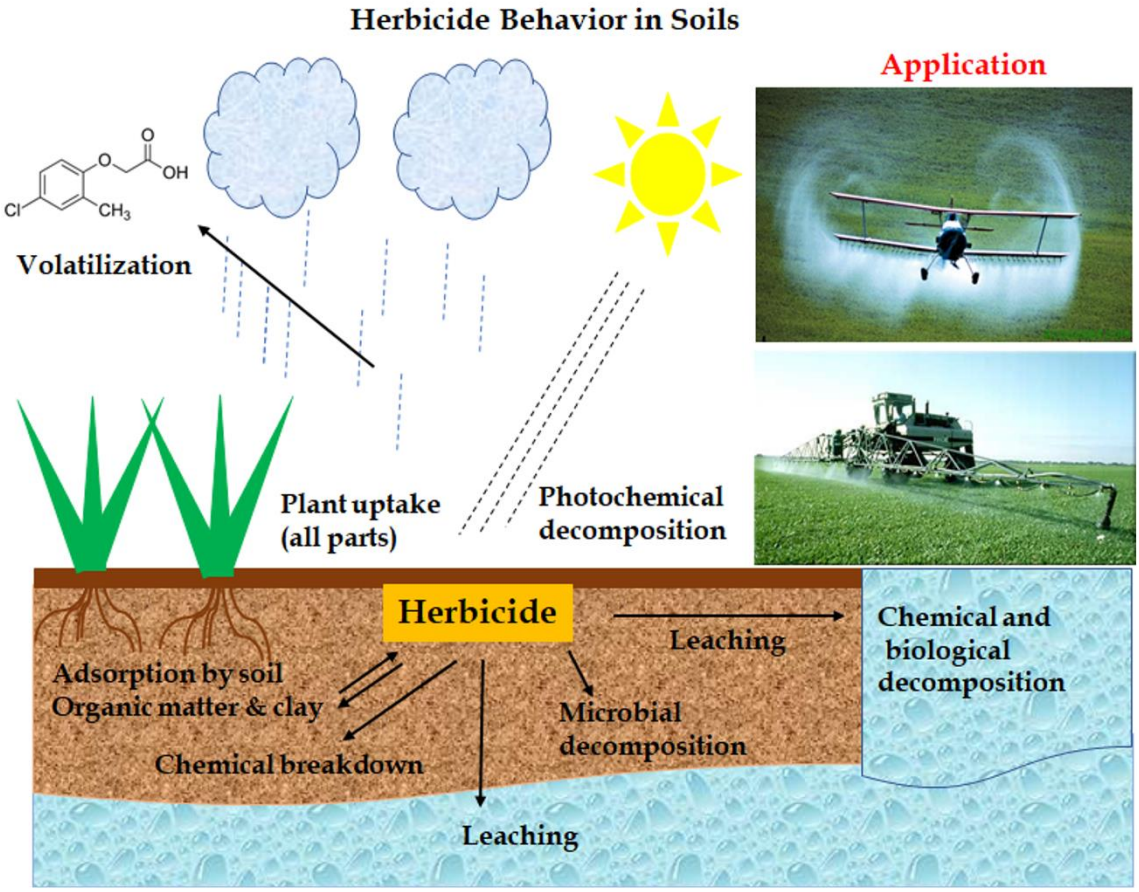

Figure 1.2. Behavior of herbicides in soils. (Adapted from Miller and Westra, (2004).

In the search for new alternatives to conventional systems that can reduce pesticide overdosing and environmental pollution, the formulations of controlled release of pesticides, similar to those of drugs, appear to reduce the risk in their use by increasing the safety of both the worker and the consumer, and being more efficient formulations where the loss of the active substance is minimized to the maximum (Nir et al., 2006; Singh et al., 2020). Similarly to controlled drug release systems, the design of controlled herbicide release formulations has the main purpose of maintaining for a longer time the concentration threshold of the active ingredient for the control of the pest in the soil or in the plant, through its release at adequate speed. The aim is to provide the amount required to achieve the proper biological effect, and thus reducing its level in the environment (Celis et al., 2002; Singh et al., 2020). Controlled release systems of herbicides are not intended to increase the persistence of herbicides

compared to conventional systems, but to control the release of the active ingredient to make it more available at the most appropriate time for crop protection. Numerous controlled delivery systems of herbicide have been developed by coating and microencapsulating pesticides using different techniques, such as atomization, encapsulation by nuclear reactors, complex co-acervation, organic co-acervation, interfacial polymerization, fluid bed coating, solvent evaporation, disk recovery swivels, encapsulation of the herbicide in biopolymers, clays or in bionanocomposite systems (Gerstl et al., 1998; Taki et al., 2001; Nir et al., 2006; Roy et al., 2014; Goyal, 2017; Prete et al., 2017; Singh et al., 2020).

1.2 CLAY-BASED NANOCARRIERS IN DELIVERY SYSTEMS

Clays minerals, known from the first days of humanity, are very abundant in nature and are used for multiple purposes, profiting from their low cost and the unique structural properties of these hydrated silicates containing alkali and alkaline earth metals (Bergaya and Lagaly, 2006; Brigatti et al., 2006). Among the layered clay minerals (phyllosilicates), only some of them, including kaolin, talc and smectites as well as fibrous clays (sepiolite and palygorskite), are commonly used as excipients in the formulation of different dosage forms, as solid, liquid or semi-solid (Carretero, 2002; Choy et al., 2007). The structure and general characteristics of the clay minerals used in this Thesis is here briefly described:

Montmorillonite: it is a dioctahedral clay mineral of general structural formula $(Na)_{0.33}(Al,Mg)_2(Si_4O_{10})(OH)_2 \cdot nH_2O$ belonging to the group of smectites. Its structure is 2:1 type, that is, with structural layers consisting of two sheets of tetrahedral silica and a central sheet of octahedral alumina, joined by oxygen atoms common to both sheets (Bergaya et al., 2013) (Figure 1.3). Among these sheets, isomorphic substitutions occur in octahedral sheet (typically Al by Mg) and frequently also in the tetrahedral one (Si by Al). These isomorphic

substitutions generate a positive charge deficiency, resulting in a negative global charge layer (Bergaya et al., 2013; Brigatti et al., 2013). The negative charge of the network is balanced by the presence of interlamellar cations, generally Na^+, Ca^{2+} or K^+ among others. The presence of these interlaminar cations gives montmorillonite interesting ion-exchange properties, as these cations can be exchanged by other cations of diverse origin by a topotactical chemical reaction, including organic species that lead to the formation of organic-inorganic hybrid materials (Ruiz-Hitzky et al., 2004).

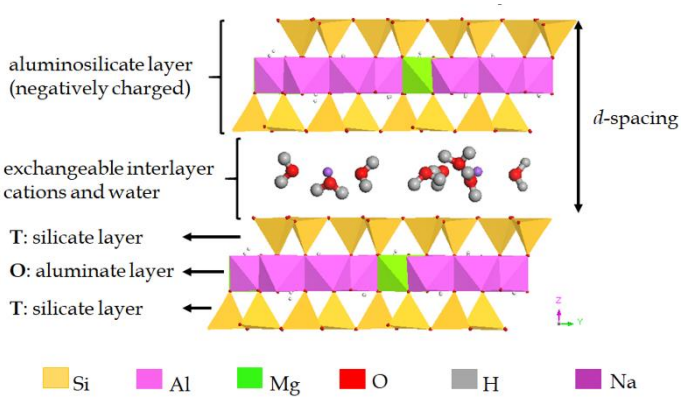

Figure 1.3. Schematic representation of the montmorillonite structure (T = tetrahedral sheet and O = octahedral sheet).

Laponite®: although less explored than montmorillonite, synthetic hectorites are also smectite clays of interest in diverse applications composition and purity can be controlled better than in natural clays (Christidis et al., 2018). This clay is a trioctahedral magnesium silicate, with the general formula $Na_{0.7}[(Si_8Mg_{5.5}Li_{0.3})O_{20}(OH)_4]$, being the most representatives those products commercialized under the trade-mark Laponite®, firstly by Laporte and currently by BYK Additives & Instruments. Normally, the negative charge is in this case compensated by Na^+ ions, which can be also exchanged for other cations through topochemical reactions. Figure 1.4 represents schematically the structure of Laponite®, where the negative charge in the clay layers is originated from the replacement of Mg^{2+} with Li^+ in the octahedral sheets of the crystal. The edges

have a positive charge (or less negative charge) depending on the protonation of the exposed hydroxyl groups (BYK Additives & Instruments, 2014).

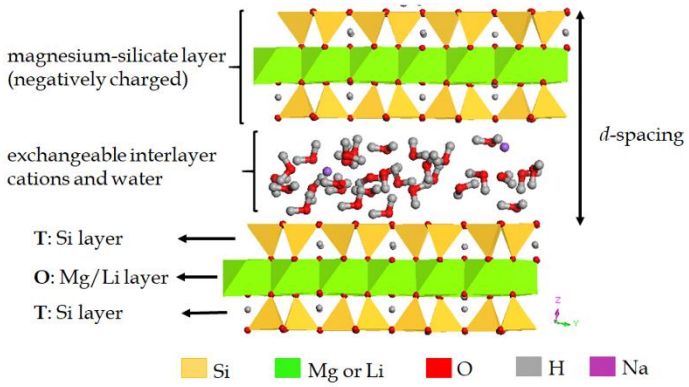

Figure 1.4. Schematic representation of the Laponite® structure. (T = tetrahedral sheet and O = octahedral sheet).

Sepiolite: is a natural magnesium silicate of microfibrous morphology of general formula $[Si_{12}O_{30}Mg_8(OH,F)_4](H_2O)_4\,8H_2O$ (Santaren et al., 1990; Ruiz-Hitzky, 2001). The crystalline structure of a fiber is the characteristic of 2:1 phyllosilicates, consisting of two tetrahedral silicon and oxygen sheets and a central octahedral sheet containing magnesium cations coordinated with oxygen, fluorine and hydroxyl (OH) groups, but defining blocks due to discontinuities in the octahedral sheet caused by a regular inversion produced every six units of the tetrahedron sheets (Brauner and Preisinger, 1956; Ruiz-Hitzky, 2001). Thus, the structural blocks of the sepiolite delimit tunnels of dimensions 1.08 x 0.4 nm, considering its cross section and channels on the outside of the fiber. In addition, due to the systematic discontinuities this silicate has a large number of silanol groups (≡Si-OH) regularly disposed on its outer surface (Figure 1.5).

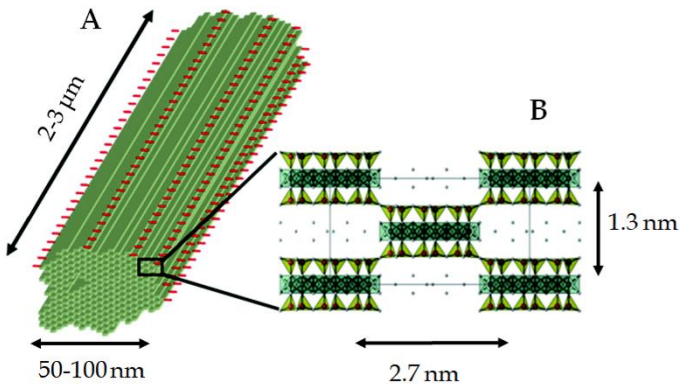

Figure 1.5. Schematic representation of a sepiolite nanofiber (A) and sepiolite crystalline structure (B). (Adapted from Fernandes et al. (2014))

Although it has no expansion properties, unlike smectite clay minerals, the special structure of tunnels and sepiolite channels gives rise to a specific high surface area of approximately 300 m^2/g, with almost half of this value attributed to the external surface. In addition, the presence of pores of different sizes, including the micropores defined by the structural tunnels, makes this mineral an excellent adsorbent material (Ruiz-Hitzky, 2001).

Layered double hydroxides (LDH): are considered "anionic clays" and are frequently also called "hydrotalcite-type" compounds. Hydrotalcites are natural magnesium-aluminum double hydroxides containing carbonate anions intercalated between their layers for compensating the deficit of charge in the inorganic solid (Cavani and Trifirb, 1991). The structure of layered double hydroxides is based on that of brucite ($Mg(OH)_2$), which is characterized by a laminar geometry of high symmetry where the Mg^{2+} cation is located in the center of an octahedron and coordinated to six OH groups (Constantino and Pinnavaia, 1995) (Figure 1.6). Although layered double hydroxides are not very abundant in nature, they can be easily synthesized in the laboratory (Bergaya and Lagaly, 2006; Forano et al., 2006). These compounds can be represented by the following general formula: $[M^{2+}{}_{1-x}\ M^{3+}\ x\ (OH)_2]^{x+}\ A^{m-}{}_{x/m}\ nH_2O]$, where M^{2+} represents a divalent metal cation (Mg^{2+}, Zn^{2+}, Fe^{2+}, Cu^{2+}...), M^{3+} a trivalent metal

cation (Al^{3+}, Cr^{3+}, Mn^{3+}, Fe^{3+}...) and A^{m-} corresponds to an anion with m- charge (Constantino and Pinnavaia, 1995; Costantino et al., 2008). The presence of divalent and trivalent cations results in sheets with positive charge, which are compensated by interlayer anions (typically CO_3^{2-}, NO^{3-}, Cl^-, or OH^-).

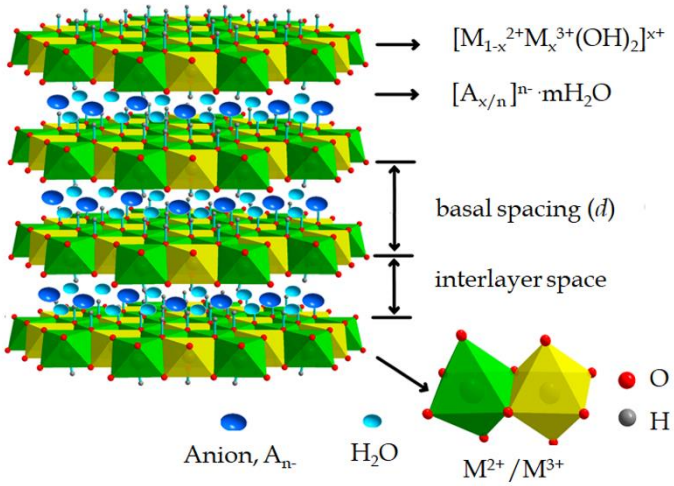

Figure 1.6. Schematic representation of the classical LDH structure. (Adapted from Li et al. (2017))

Layered Simple Hydroxides (LSH): have a related structure to that of LDH, but in LSH the inorganic layers are composed of a single type of metal cation, such as Mg^{2+}, Cu^{2+}, Zn^{2+} or Ni^{2+}, and can be represented by the general formula $[M^{II}_2(OH)_{4-x}(A^{m-})_x/m] \cdot nH_2O$ (Figure 1.7) (Hussein et al., 2012; Si et al., 2012; Abdul Latip et al., 2013). In this structure, the anions are coordinated with the metal ions in the plane and the inorganic layers are essentially neutral (Rogez et al., 2011). In more detail, quasi-planar array of edge-sharing octahedral, incomplete for LSH, where metal vacancies are charge balanced by two tetrahedral M(II) sites, one adjacently attached on each side of an octahedral void, and as much as one quarter of the octahedral sites of the metal hydroxide layers can be vacant at maximum (Stimpfling et al., 2016). The anions interleaved between the layers to compensate an excessive positive charge stemming from a divalent cation (Stimpfling et al., 2016; Langry et al., 2018) Thus, in the case of LSH, the metal-anion bond results in a strong interaction, and when ions derived from organic

molecules are intercalated between the inorganic metal network, they produce highly stable organic-inorganic hybrid compounds (Si et al., 2012).

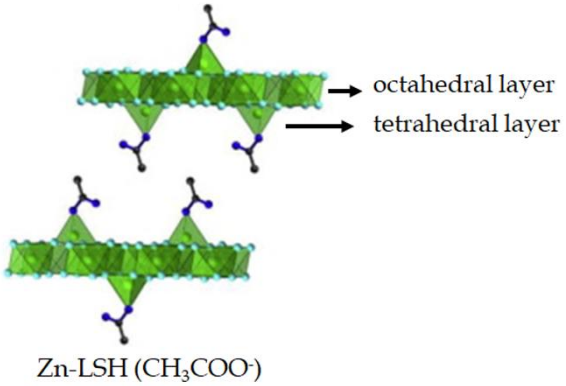

Figure 1.7. Schematic representation of the structure of layered simple hydroxides. (Adapted from Stimpfling et al., (2016))

1.2.1 Clay-based systems for application as controlled drug delivery systems

Clay minerals have been used in medicine for centuries to treat a wide variety of diseases, such as infections, or as antidotes against various toxins and poisons. Clays have also been used topically for dermatological treatments, such as malignant ulcers (Williams and Haydel, 2010; Williams, 2017) and also by geophagy (Allègre, 2002). This interest in the study of clays for health continues today, as revealed by the great number of publications related to this topic, which has continued to grow in the last years (Carretero, 2002; Choy et al., 2007; Carretero and Lagaly, 2007; Viseras et al., 2007; Carretero and Pozo, 2009, 2010; López-Galindo et al., 2011; Carretero et al., 2013; Sánchez-Espejo et al., 2014; Hun Kim et al., 2016; Ruiz-Hitzky et al., 2019).

One of the main properties of clays that makes them special and of great interest in many areas, including health, is due to their capacity for adsorption and ion-exchange properties, which make them capable, for example, of adsorbing and eliminating ammonia and other nitrogen compounds harmful to the human body, capture various types of toxins (such as cholera) and mycotoxins, as well

as toxic molecular compounds (alkaloids, stricalasin, etc.), including radionuclides, such as ^{137}Cs (Ruiz-Hitzky et al., 2019). These adsorption properties are also of great interest in the pharmaceutical field, as they can allow the development of drug release systems (DDS) or even controlled drug delivery systems (CDDS). For this purpose, typical hybrid drug carriers based on clays are produced through a process of intercalation/adsorption of the drug in the inorganic solid, forming drug-clay hybrids that allow the release of the drug in the gastrointestinal tract (oral drug administration) (Park et al., 2008; Oh et al., 2013; Cunha et al., 2017; Tian et al., 2018), through the skin for topic usages (e.g., treatment of burns, dermatological treatments, incorporation in wound dressing tissues, etc.) (Moraes et al., 2017; Caflisch et al., 2018; Rebitski et al., 2018; Viseras et al., 2019; Lisuzzo et al., 2020), or even in more sophisticated uses, such as vector in vaccines (Ruiz-Hitzky et al., 2009; Wicklein et al., 2012, 2016) or DNA transfection (Castro-Smirnov et al., 2016, 2017; Piétrement et al., 2018).

In addition to natural silicates, the anionic clays such as LDH and LSH are promising as nanocarriers in the pharmaceutical field due to their interesting properties mentioned above (Choy et al., 2007; Costantino et al., 2008; Bini and Monteforte, 2018; Mishra et al., 2018). In this way, numerous types of drugs such as DNA, anti-inflammatories (ibuprofen, diclofenac, etc.), steroids (L-tyrosine), anticancer (methotrexate) have been intercalated in these layered hydroxides for direct application as DDS (Choy et al., 2000; Gordijo et al., 2005; Oh et al., 2006; Del Hoyo, 2007; Zhang et al., 2014) or were further entrapped in polymers and biopolymers for developing CDDS (Alcântara et al., 2010; Ribeiro et al., 2014; Choi et al., 2018; Rebitski et al., 2019). These last drug-clay hybrid systems involving the use of polymers and biopolymers in the formulation can overcome some of the drawbacks of the just intercalated drug—LDH systems. For instance, the encapsulation increases the sensitivity to pH changes and improves thermal instability (Aguzzi et al., 2007; Matalanis et al., 2011; Modi et al., 2013). In this way, in general, the encapsulation of drug-clay hybrids, based on both LDH and clay minerals, in a protective polymer matrix is a methodology used more and more (Alcântara et al., 2010; Ribeiro et al., 2014; Rebitski et al., 2019). The resulting

composite systems show not only higher stability but, in many cases other interesting properties such as targeting for the searched application, better control of the release, greater protection of the drugs from pH changes (Ambrogi et al., 2008; Oh et al., 2012; Park et al., 2013). Besides, the use of biopolymers as encapsulating matrix may offer additional advantages such as biocompatibility, biodegradability and non-toxicity which can be of crucial relevance in this type of applications (Šimkovic, 2013; Alcântara and Darder, 2018; Ruiz-Hitzky et al., 2019). Some examples of biopolymers used in controlled delivery applications are zein, alginate, chitosan, pectin, carboxymethylcellulose, or xanthan gum, among others (Alcântara et al., 2010; Paliwal and Palakurthi, 2014; Ribeiro et al., 2014; Oliveira et al., 2017; Rebitski et al., 2018, 2019).

Alginate and pectin are hydrophilic polysaccharides very useful as encapsulating matrices due to their ability to form microspheres by crosslinking, typically with divalent cations such as Ca^{2+} and Zn^{2+} (Gombotz, 1998; Sande, 2005; Sriamornsak, 2011; Lee and Mooney, 2012) (Figure 1.8). The cross-linking effect is due to these divalent ions acting as bridges between the negatively charged groups of different units of guluronic acid, which favors the formation of a rigid gel with a characteristic structure called "egg-box" (Rees, 1981).

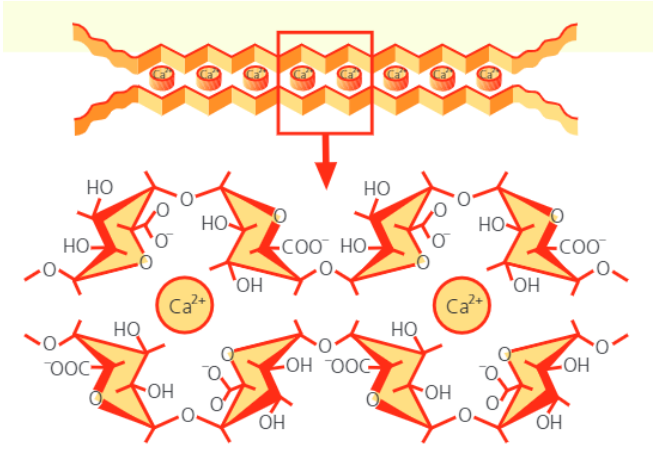

Figure 1.8. Egg crate model of calcium crosslinked pectin. (Adapted from Roy et al. (2014).

However, this type of polysaccharides typically presents a high-water absorption capacity, which may reduce the control in oral drug delivery applications. Thus, hydrophobic biopolymers such as zein can be used to modulate the hydrophilicity of various biopolymer matrices reducing its swelling capacity (Alcântara et al., 2010). Zein is a storage protein from corn composed mainly of non-polar amino acids, which are responsible for the hydrophobic properties (Shukla and Cheryan, 2001; Lawton, 2002). Other biopolymers such as chitosan have mucoadhesive properties that allow their interaction with negatively charged surfaces, such as that of mucous membranes (intestinal or nasal mucosa), increasing the residence time of the drug in the gastrointestinal tract (Shimoda et al., 2001; Donnelly et al., 2011; Cheung et al., 2015; M. Ways et al., 2018; Zhao et al., 2018). Chitosan is a hydrophilic polysaccharide, extracted from the exoskeleton of crustaceans and some insects, which is also widely used in biomedical applications due to its interesting properties (biocompatibility, antimicrobial activity, film forming ability, etc.) (Singh and Ray, 2000; Cheung et al., 2015).

A class of biopolymers that is gaining a growing interest mainly in applications of controlled topical release are those polysaccharides derived from cellulose, present mainly in plants as a structural component, such as hydroxypropylmethylcellulose (HPMC) or nanocellulose. HPMC shows good film forming ability, stability in the presence of heat, light, and moderate levels of moisture, and it is easy to incorporate additives or active species into the HPMC film (Siepmann and Peppas, 2001; Ghosal et al., 2011; Ford, 2014). In the recent years, the use of nanocellulose for biomedical applications is increasing due to its properties of non-cytotoxicity and immunogenicity, which make it promising for use as scaffolds for the engineering of blood vessels, neural tissue, bone, cartilage, liver, adipose tissue, to repair connective tissue and congenital heart defects, and to build lenses of contact and protective barriers (Klemm et al., 2006; Lin and Dufresne, 2014; Mohite and Patil, 2014; Jorfi and Foster, 2015a; Bacakova et al., 2019) Although bacterial cellulose would seem more appropriate for biomedical purposes, as it is obtained as a highly pure material (Mohite and

Patil, 2014; Fadel et al., 2017), cellulose nanomaterials derived from lignocellulosic biomass are becoming a common material for this type of applications (Xue et al., 2017). In this case, both cellulose nanofibers and nanocrystals are being used to develop suitable hydrogels as drug delivery systems and implants or scaffolds for tissue engineering, exploring also new processing methods like 3D printing (Wenyang et al., 2018; Du et al., 2019).

Figure 1.9 shows schematic representations of drug release systems based on clays, biopolymers, or clay-biopolymer composites. In drug-loaded clays (Figure 1.9a), the drug is contained in the channels or sheets of the inorganic solids, from which the drug is released by a diffusion process (Jafarbeglou et al., 2016; Sangeetha et al., 2019). In drug delivery systems using biodegradable biopolymers, the drug molecules initially dispersed in the polymer are released when the polymer begins to erode (with or without changes in chemical structure) or degrade (breakdown of the main chain links), as shown in Figure 1.9b, as a result of exposure to chemicals (water) or biological agents (enzymes) (Siepmann et al., 2012; Jafarbeglou et al., 2016). In the bionanocomposite systems, where the clay-drug hybrids are encapsulated in a biopolymer, a combination of the mechanisms mentioned above is expected (Figure 1.9c) (Jafarbeglou et al., 2016; Sangeetha et al., 2019). In this last case, the biopolymer matrix will act as an additional barrier to the diffusion of the drug molecules from the clay, improving the control in the release rate of the drug, and, in some cases, with the possibility of allowing a targeted release.

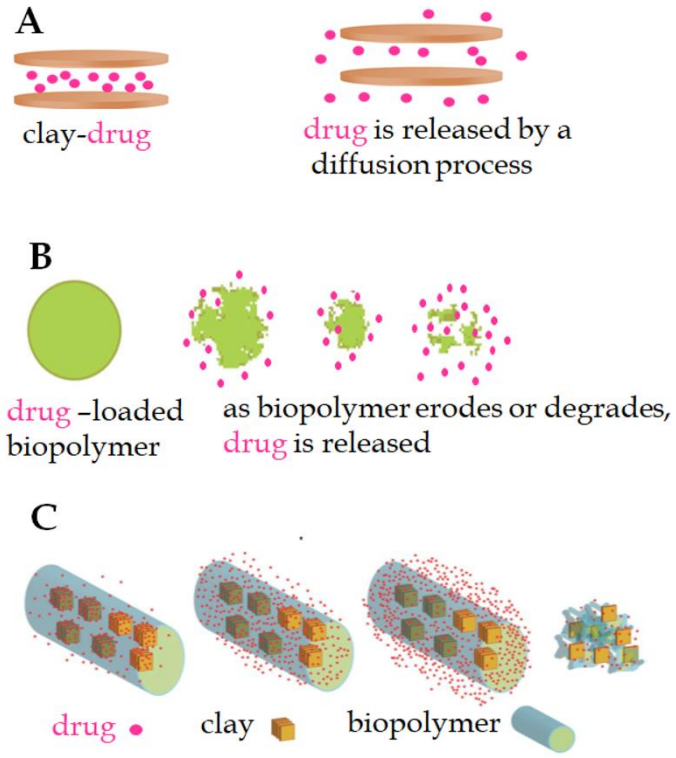

Figure 1.9. Different drug release systems based on: clays (A), biopolymers (B), and bionanocomposites (C). (Adapted from Sangeetha et al. (2019)).

1.2.2 Formulations for controlled delivery of herbicides based on clay minerals

Clay minerals are the components of the clay fraction of the soil (<2.0 μm) most important from the point of view of adsorption together with organic matter, not only because of their abundance in soils, but also due to their high specific surface area and ion-exchange capacity. Currently, pesticide formulations are attracting considerable interest as they may contribute to reduce the required dosage and the leaching, enhancing efficiency in their administration and so decreasing pollution of the environment (Nennemann et al., 2001; Undabeytia et al., 2003; Nir et al., 2006).In this context, to increase the efficiency of pesticides by reducing their leaching in air and water, it has been proposed the development of systems involving the reversible binding of the pesticide to clay minerals. Clays can protect the pesticide and increase its stability against volatilization and photodegradation, making overdosing unnecessary and, thus, reducing

environmental pollution (Margulies et al., 1985; El-Nahhal et al., 2001; Nir et al., 2006, 2013). Slow-release formulations designed to reduce leaching were prepared with organoclays, micelles, liposomes, clay minerals (montmorillonite, sepiolite, layered double hydroxides, etc), and polymers (Lakraimi et al., 2000; Undabeytia et al., 2000, 2003; Casal et al., 2001; El-Nahhal et al., 2001; Nennemann et al., 2001; Rytwo et al., 2002; Mishael et al., 2003; Bruna et al., 2009; Alromeed et al., 2015a). An example is the incorporation of the diuron herbicide in phosphatidylcholine (PC) vesicles absorbed in montmorillonite reported by Undabeytia et al., (2012). In that system, the clay was responsible for increasing the herbicide sorption capacity. In addition, in soil column experiments with sandy soil, herbicide formulations in PC-clay accumulated mainly in the upper part of the soil, and there was a reduction of one third in leaching compared to the commercial formulation. Other approaches that use clays and polymers have also been described. Similarly, to controlled drug release systems, these polymer-clay herbicide formulations are often prepared from biodegradable materials. These materials include synthetic polymers such as polyvinyl alcohol and polypeptides; biopolymers obtained from plants, animals and microorganisms, such as polysaccharides (for example, starch, cellulose, chitin, gums and pectin), proteins, polyesters, lignins, latex and resins; and modified biopolymers (Nir et al., 2006, 2013). In these controlled delivery systems, clays can be added to the matrix as modifiers to improve the slow release of the active ingredient. An illustrative example is the formulation of alginate-bentonite beads incorporating the insecticide imidacloprid that reduced its release rate and increased grain yield, thus producing a more efficient and economical formulation (Pepperman et al., 1991; González-Pradas et al., 1999). This same formulation was studied by Fernández-Pérez et al., (1999) and showed that alginate-bentonite formulations are efficient systems to reduce leaching of carbofuran in clay soils.

As reported, the use of clays for herbicide-controlled delivery systems allows different systems to be produced with combinations with various materials producing complex, bionanocomposite hybrid systems among others (Lakraimi

et al., 2000; Celis et al., 2012; Undabeytia et al., 2012), which are very efficient and an excellent alternative to avoid damage to the environment.

1.3 OBJECTIVES OF THIS DISSERTATION

This Thesis intends to contribute to the development of delivery systems that could be applied to solve specific problems of current treatments, as well as to address diverse specific delivery applications. For this purpose, inorganic solids were used, where the specific drug was incorporated to procure convenient reservoirs, and they were suitably combined with natural biopolymers to afford the adequate control and targeting, if possible, in the delivery. With this premise, the Thesis has focused on the development of controlled release systems based on the intercalation of bioactive compounds in layered clay minerals and layered hydroxides, using various synthesis strategies, followed by their encapsulation in protective biopolymer matrixes, typically abundant polysaccharides, to produce bionanocomposite systems that can be applied for the specific release of pharmaceuticals and pesticides for uses in biomedicine and agriculture.

The first target to be addressed involves the development of an effective system for the delivery of metformin, the most employed drug in the oral treatment of diabetes II, and recently also explored in the treatment of various types of cancer. In this way, in a first approach it will be explored the direct use of clay minerals as substrates where the drug could be intercalated and stabilized, profiting from the possibility to use it in its protonated form and, thus, exchange it with the interlayer cations of smectites. Natural clays of the smectite type, such as a montmorillonite, will be firstly explored, and in a second step synthetic clays, such as hectorites of the Laponite® type, will be used to exploit the advantages of such type of synthetic substrates in view to its real application in pharmacological production. Taking into account the different characteristics of those two lamellar silicates, their behavior as substrates for the adsorption of metformin will be also explored by applying computational modeling tools at the molecular level to better understand possible differences in the characteristics

and type of interactions between the drug and the clay host lattice. In a second step and with the aim of increasing biological half-life in the body, decreasing the daily dose and, presumably, avoiding other side effects described in the regular use of metformin, the produced clay-metformin hybrids will be associated with biopolymers to produce bionanocomposite materials that can procure a more controlled release, or even a possible targeting effect. In this way, core-shell bead systems will be designed using chitosan and pectin as components with the aim to profit from the stability that pectin could introduce in highly concentrated acids, such as the conditions found in the stomach, and chitosan mucoadhesive properties could contribute to improve adherence to the mucosa at the intestinal tract, favoring metformin absorption and increasing the effectiveness of the treatment. The presence of the drug intercalated in the layered silicate is expected to procure a convenient reservoir for a more controlled release, as well as other possible advantages related to the use of this type of clays that can also act as antidiarrheal agent, reducing other side effects due to accumulation of metformin in the intestinal tract. The release of the designed systems will be evaluated in *in vitro* tests that simulate the changes in the pH conditions along their passage through the gastrointestinal tract.

The second target to be addressed in this Thesis will be the design of a controlled release system of allantoin for potential topical application in skin diseases treatments. Allantoin is a very particular molecule of great versatility for uses in cosmetics and pharmaceutics, but which is very difficult to stabilize with other components for uses in controlled release. In this Thesis, the preparation of hybrid materials will be explored by intercalation of allantoin in layered metal hydroxides, typically layered double hydroxides, by different methods of synthesis (ion-exchange, reconstruction and co-precipitation). The developed systems will be used as components in the preparation of bionanocomposites using biopolymers, such as hydroxypropylmethylcellulose (HPMC), agar and nanocellulose as matrices, and processed as films in view to produce stable systems that could be applied as wound dressing tissues. Furthermore, metal hydroxide substrates containing elements such as Zn or Cu will be optimized in

view to incorporate antibacterial properties in the resulting hybrids and so in the produced bionanocomposite films.

Finally, the third targeted approach will explore the use of nanoarchitectured materials combining two types of inorganic host solids as substrate of the bioactive species, in view of possible combination of properties and/or use for a further incorporation of other functionalities. In this way, the use of nanoarchitectures where layered double hydroxides particles have been grown on the surface of sepiolite fibers will be explored. This nanoarchitecture will be used to incorporate 2-methyl-4-chlorophenoxyacetic acid (MCPA), a frequently employed herbicide in agriculture, using different approaches of synthesis: ion-exchange with interlayer cations of the LDH already assembled to sepiolite, and co-precipitation of the LDH in the presence of sepiolite and the herbicide to produce directly in one step the hybrid nanoarchitecture. The produced materials will be explored alone or encapsulated in a biopolymer matrix to evaluate their behavior for the controlled release of MCPA in view to their application in soils. The biopolymeric system to be used in this case will be based on a combination of alginate and zein biopolymers, as the presence of zein in the generated bionanocomposite beads will incorporate hydrophobicity to the system and, therefore, will procure controlled swelling properties in order to tune the release process.

CHAPTER 2

MATERIALS AND METHODS

2.1 STARTING MATERIALS

In this doctoral thesis, various bionanocomposite materials and nanoarchitectured hybrids based on clays of different nature (Na-montmorillonite, Laponite® XLG and sepiolite) and layered double hydroxides, were studied for application in the controlled delivery of different active molecules (drugs and herbicides).

2.1.1 Montmorillonite

Montmorillonite (Mt) from Wyoming (USA), marketed by Southern Clay Products corresponds to the commercial product known as Cloisite®Na whose structural general formula is $(Na)_{0.33}(AlMg)_2(Si_4O_{10})(OH)_2nH_2O$. The Mt used in this thesis has a cation exchange capacity (CEC) of approximately 93 mEq Na^+ per 100 g montmorillonite (Maes et al., 1979) and a particle size of 600 nm ± 92 nm (as measured in sonicated water dispersion with Zetasizer Nano ZS from Malvern).

2.1.2 Laponite® XLG

Laponite® XLG is a synthetic layered clay kindly provided by the company BYK Additives & Instruments with high purity, indicated especially for the control of rheology in personal care and cosmetic applications, where it is used to stabilize emulsions, lotions and creams. Laponite® XLG has $Na_{0.7}[(Si_8Mg_{5.5}Li_{0.3})O_{20}(OH)_4]$

general formula, CEC of 63 mEq per 100 g and disk-shaped crystals of approximately 25 nm in diameter and 0.92 nm in thickness (BYK Additives & Instruments, 2014; Tomás et al., 2018).

2.1.3 Sepiolite

The sepiolite (Sep) microfibrous clay used in this thesis is from Vallecas-Vicalvaro (Madrid-Spain), commercialized as Pangel® S9 by Tolsa S.A. This microfibrous clay has a total specific surface area determined from BET measurements of 320 m^2 per g, being its external surface 150 m^2 per g and its CEC approximately 15 mEq per 100 g (Brauner and Preisinger, 1956; Santaren et al., 1990). The chemical composition presented by this clay of purity <95% is shown in Table 2.1.

Table 2.1. Chemical composition of Pangel® S9 sepiolite (Santaren et al., 1990).

	SiO_2	**Al_2O_3**	**MgO**	**Na_2O**	**MnO_3**	**CaO**	**K_2O**	**F^-**
Sepiolite	62.5%	1.20%	25.2%	0.09%	0.5%	0.4%	0.3%	≈ 1%

2.1.4 Biopolymers

The biopolymers used for the preparation of the bionanocomposite materials of this thesis were: chitosan (CHT), pectin (PEC), alginate (ALG), zein (Z), hydroxypropylmethylcellulose (HPMC) and agar (A), all obtained from Sigma-Aldrich, and cellulose nanofibers (CNF) was kindly provided by "La Montañanesa" pulp mill (Torraspapel - Lecta Group, Spain).

Chitosan: it is a natural polycationic linear polysaccharide derived from the partial deacetylation of chitin (Galed et al., 2005; Cheung et al., 2015) (Figure 2.1). The chitosan used in this Thesis present deacetylation 75 - 85% medium molecular weight (190,000-310,000 Da).

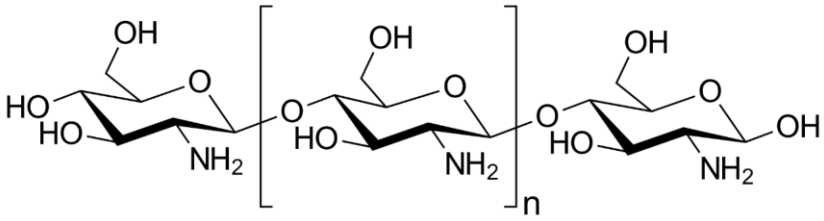

Figure 2.1. Molecular structure of chitosan.

Pectin: are typical polysaccharides found in vegetables that are commonly used in the food industry as gelling and stabilizing agents (Thakur et al., 1997; Munarin et al., 2012; Zhang et al., 2020). Basically, pectins are polymers of (1-4) α-D-galacturonic acid partially esterified with methyl (Thakur et al., 1997; Synytsya, 2003) (Figure 2.2). Pectins with more than 50% methyl-ester groups are classified as high methoxy (HM) and those with less than 50% methyl-ester groups as low methoxy (LM) (Synytsya, 2003). The pectin used in this Thesis is obtained from citrus peel and contains ≥ 74.0 % galacturonic acid groups.

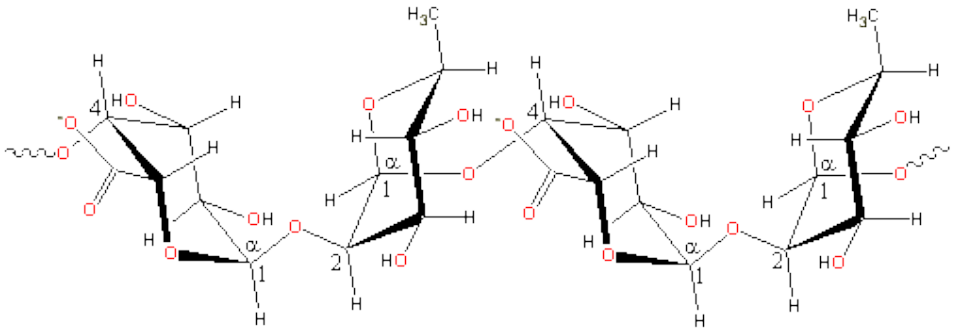

Figure 2.2. Molecular structure of pectin.

Alginate: is an anionic co-polymer consisting of β-D-manuronic acid (M) and α-L-guluronic acid (G) monomers that are organized in sequential blocks of only one of the monomers (-MMMGGG-) or in blocks in which the monomers alternate (-MGMGMG -) (Lee and Mooney, 2012), as shown in Figure 2.3. The alginate used in this Thesis is alginic acid sodium salt from brown algae medium viscosity.

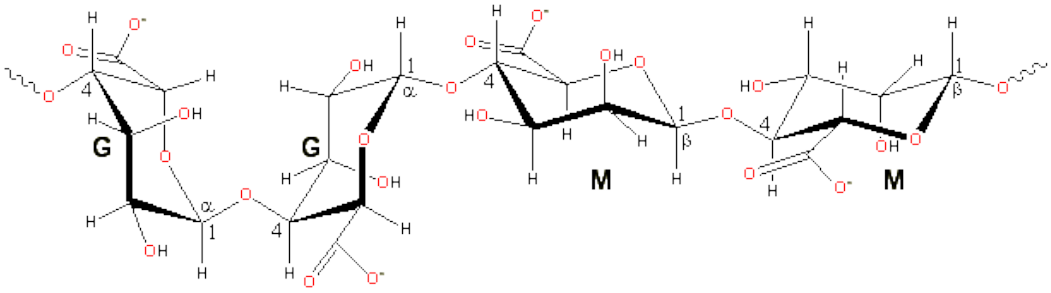

Figure 2.3. Molecular structure of alginate.

Zein: is a protein of prolamin class found in corn with a molecular weight of approximately 40 kDa (Figure 2.4). The zein used in this Thesis is a class of prolamine protein found in maize (corn).

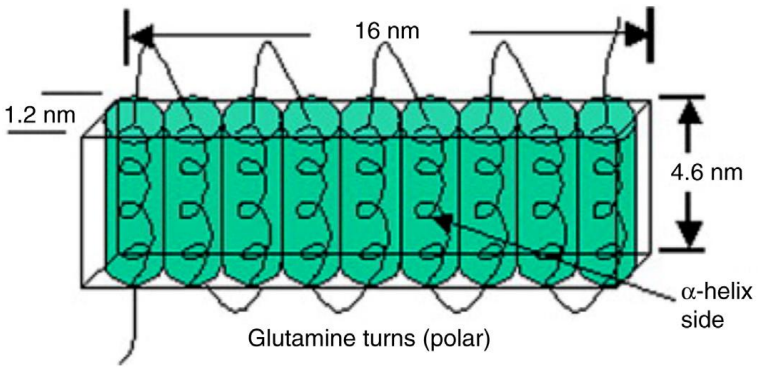

Figure 2.4. Molecular structure of zein.

Hydroxypropylmethylcellulose (HPMC): is a cellulose backbone with ether-linked methoxy and hydroxypropyl side group substituents linked via ether bonds to the cellulosic chain hydroxyl groups (Figure 2.5). The properties of the polymer are strongly influenced by the methoxyl and hydroxypropyl substitution ratio.

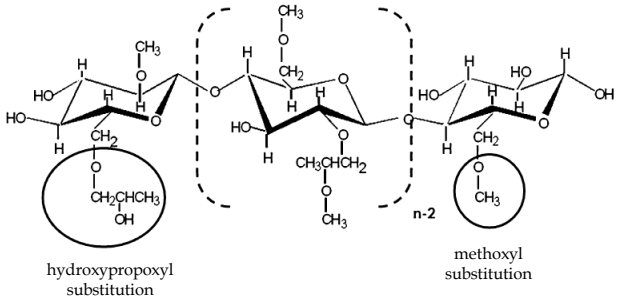

Figure 2.5. Molecular structure of hydroxypropylmethylcellulose (HPMC). (Adapted from Ford, (2014).

Cellulose nanofibers: is a linear polymer of glucose prepared from cellulose the most abundant biopolymer in nature. Cellulose is a homopolysaccharide composed of β-1,4-D-glucopyranose units (Figure 2.7). Vegetable nanocellulose can be obtained from abundant sources derived from trees, shrubs, various herbs, flowers, tubers, succulents, etc (Jorfi and Foster, 2015b; Bacakova et al., 2019). The cellulose nanofibers used in this Thesis was prepared from fully bleached eucalyptus pulp. This never-dried pulp was first exchanged to their sodium form and then refined in a PFI mill (until Schopper-Riegler degree above 90^{o}) to enhance fiber accessibility and fibrillation efficiency. The refined fibers were processed in a high-pressure microfluidizer (Microfluidizer M-110P, Microfluidics Corp.) The fibers were passed thirteen times though an intensifier pump that increased the pressure, followed by an interaction chamber, which defibrillated the fibers by shear forces and impacts against the channel walls and colliding streams. The first six steps were carried out using only one chamber of 200 μm, while the rest of the steps were performed adding a second chamber of 100 μm. The obtained slurry of nanofibrillated cellulose was stored at 4^{o}C until use.

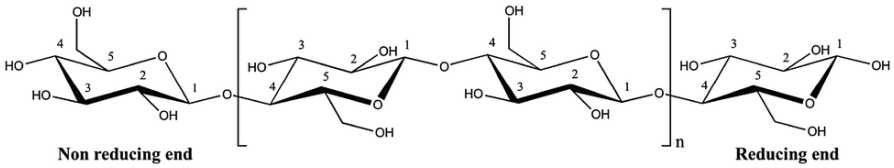

Figure 2.6. Molecular structure of cellulose nanofibers.

Agar: is a polysaccharide extracted from the Gelidiaceae and Gracilariaaceae seaweed families and it is composed mainly of repeating units of d-galactose and 3,6-anhydro-l-galactopyranose that alternate along the polymer (Armisén, 1991; Lai and Lii, 1997; Labropoulos et al., 2002) (Figure 2.7). The agar is insoluble in cold water, but melts on heating and cooling, and this cycle can be repeated for an indefinite number of times without compromising the mechanical properties of the gel (Wang and Rhim, 2015). One of the most significant uses of agar is in the preparation of microbiological media, stable and firm gels that can be used as support for the cultures, therefore it is commonly employed in the food, biomedical and other areas which that purpose (Settanni and Corsetti, 2008; Shukla et al., 2012; Fekete et al., 2019). The agar used in this Thesis is or agar-agar is a jelly-like substance, obtained from red algae.

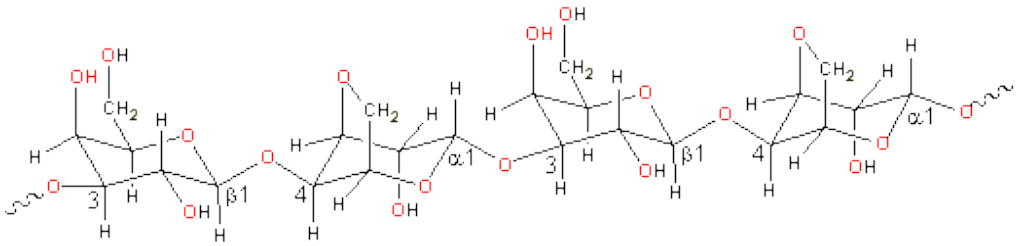

Figure 2.7. Molecular structure of agar.

2.1.5 Organic compounds

The organic compounds used in this Thesis as active species in the release study were:

Metformin: is the drug most frequently used for the treatment of type II diabetes and was purchased from Sigma Aldrich as 1,1-dimethylbiguanide chloride ($C_4H_{12}ClN_5$) (Figure 2.8), with a molecular weight of 165.62 g mol^{-1} and a 97% purity.

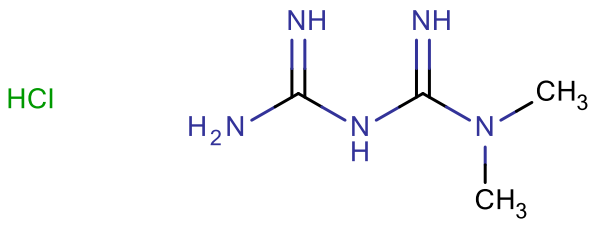

Figure 2.8. Molecular structure of metformin hydrochloride.

Allantoin: is a compound widely used in cosmetics and pharmacy as a complement in various treatments for skin diseases. Allantoin is also known as 5-ureidohydantoin or glyoxylic (acid) diureide, with chemical formula $C_4H_6N_4O_3$ (Figure 2.9), and molecular weight 158.12 g mol^{-1}. It was acquired from Sigma Aldrich with 98%purity.

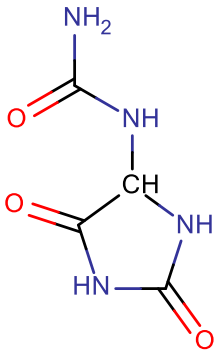

Figure 2.9. Molecular structure of allantoin.

4-Chloro-2-methylphenoxyacetic acid: is an herbicide used to combat weeds, and commonly referred as MCPA. Its chemical formula is $C_9H_9ClO_3$ (Figure 2.10), and

its molecular weight 200.62 g mol^{-1}. It was purchased from Sigma Aldrich with 95% purity.

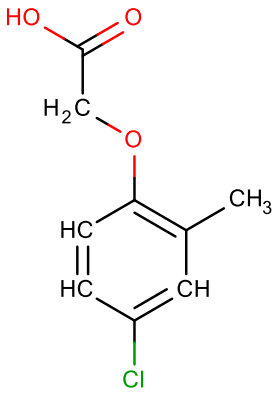

Figure 2.10. Molecular structure of 4-chloro-2-methylphenoxyacetic acid.

2.1.6 Other reagents and solvents

Other reagents used in this work, including its formula, provenance and purity are listed in Table 2.3. The deionized water (resistivity of 18.2 MΩ cm) was obtained with a Maxima Ultrapure Water system from Elga.

Table 2.3. Reagents used in this work with its corresponding formula, supplier and purity.

Reagent	Formula	Supplier	Purity (%)
Aluminum chloride hexahydrate	$AlCl_3 \cdot 6H_2O$	Sigma Aldrich	≥99%
Magnesium chloride hexahydrate	$MgCl_2 \cdot 6H_2O$	Sigma Aldrich	≥99%
Aluminum nitrate nonahydrate	$Al(NO_3)_3 \cdot 9H_2O$	Sigma Aldrich	≥99%
Zinc chloride hexahydrate	$ZnCl_2 \cdot 6H_2O$	Sigma Aldrich	≥99%
Zinc nitrate hexahydrate	$Zn(NO_3)_2 \cdot 6H_2O$	Sigma Aldrich	≥99%
Sodium carbonate anhydrous	Na_2CO_3	Sigma Aldrich	≥99%
Sodium hydroxide anhydrous	NaOH	Sigma Aldrich	≥97%
Calcium chloride	$CaCl_2$	Sigma Aldrich	≥93%
Sodium phosphate monobasic monohydrate	$NaH_2PO_4 \cdot H_2O$	Sigma Aldrich	≥98%
Sodium chloride	NaCl	Sigma Aldrich	≥99.5%
Hydrochloric acid 37%	HCl	Sigma Aldrich	A.C.S.
Ethanol	C_2H_5OH	Panreac	A.C.S.
Glacial acetic acid	CH_3CO_2H	Sigma Aldrich	A.C.S.

2.2 SYNTHESIS AND PREPARATION METHODS

2.2.1 Preparation of bionanocomposite systems containing clay-metformin hybrids and biopolymers

For the preparation of the oral systems for the release of the drug metformin, two hybrid systems were prepared using as host matrices two layered clays with different characteristics and properties: Na-montmorillonite and Na-Laponite® XLG.

a) Montmorillonite-metformin and laponite-metformin hybrids

➢ *Preparation of montmorillonite-metformin hybrids:* the adsorption of metformin into the Na-montmorillonite (Mt) clay mineral was carried out by first dispersing a certain amount (150 mg) of the starting Mt in water to facilitate the intercalation of the drug by swelling the clay in water. Subsequently, variable amounts of metformin (MF) (5, 10, 25, 30, 50, 100, 200, 300 and 500 mg) were slowly added to the dispersion under continuous magnetic stirring that was maintained at 23 ºC for 24 h. The Mt–MF hybrid compounds were recovered in two ways: (1) one part was centrifuged, washed with water and dried overnight at 60 °C and (2) another part was only centrifuged to separate the solid from the supernatant, without further washing, and then dried overnight at 60 °C. The resulting hybrid materials were denoted as "Mt-MF/X" for the centrifuged samples without washing and "Mt-MF/Xw" for the washed samples, where X indicates the initial amount of MF (mg) added per 150 mg of Mt. The Mt-MF/X series was used to establish the corresponding MF adsorption isotherm. Afterwards, the hybrid materials were characterized by various physicochemical techniques.

➢ *Preparation of Laponite® XLG-metformin hybrids:* the intercalation of MF in Laponite® XLG (Lap) was performed by adding one, two and three times the CEC of the clay (63 mEq per 100 g), that is, 20.86, 41.73 and 62.58 mg of metformin, respectively, to a dispersion of 0.2 g of the clay in 20 ml of water. The system was maintained under slow magnetic stirring for 48 h at room temperature. A part of the solid was recovered by centrifugation (Lap-MF/X) and dried in an oven at 60 °C, and the other one was centrifuged and the recovered solid was washed 3 times to remove any excess of MF weakly adsorbed on the clay surface (Lap-MF/Xw), where X indicates the relative CEC proportion of MF used (i.e., 1, 2 or 3).

b) Bionanocomposite beads based on Mt-MF and Lap-MF hybrids incorporated in chitosan and pectin

➢ *Preparation of bionanocomposite beads based on chitosan-pectin/Mt-MF:* the bionanocomposites based on the washed and unwashed Mt-MF hybrid were prepared in the form of spheres, *beads*, using the biopolymers chitosan and pectin. The experimental procedure proposed by Ribeiro et al., (2014) and schematized in Figure 2.12 was used as reference for the preparation of these systems, with the exception of some adaptations according to the need of the experiment as described:

Step 1: In this step, spheres of chitosan have been prepared incorporating the pure MF drug or the Mt-MF hybrids as follows: i) a chitosan gel was prepared from 1 g of chitosan in 100 ml of 1% acetic acid solution. This gel was maintained under magnetic stirring at room temperature for approximately 4 h until a homogeneous gel was obtained. Adding dropwise 1 M NaOH solution, the pH of the gel was increased to approximately 5, to avoid possible alterations in the clay at acid pH, since the minerals are usually sensitive to very acid pH. In this case the pH of the gel should not exceed a maximum of ≈ 5 to prevent the chitosan gel from precipitating; ii) 0.1 g of pure drug (in the form of MF·HCl) or the amount of Mt-MF hybrid containing exactly the same amount of metformin is added to the chitosan gel prepared in the previous step. This system is maintained in magnetic stirring until a homogeneous system is obtained. The resulting gel is introduced into a burette and small drops were poured slowly into a 2 M NaOH solution. The drops are formed into rigid gel spheres due to the insolubility of chitosan at alkaline pH values, which are collected after approximately 20 min and washed with water in abundance to remove the residual Na^+ ions and reach a neutral pH. The materials were labelled as CHT/MF, CHT/Mt-MFw or CHT/Mt-MF.

Step 2: The spheres prepared as explained in step 1, were coated by pectin using a dispersion of the biopolymers at concentrations of 0.5, 1 or 1.5% (v/w). The chitosan spheres remained approximately 10 min in contact with the pectin gel.

Then, they were collected using a funnel Büchner and immersed in a 10% solution of $CaCl_2$ for approximately 15 min. The spheres were collected, rinsed thorough by with water, and labelled as: PEC0.5%@CHT/Mt-MFXw, PEC0.5%@CHT/Mt-MF, PEC1%@CHT/Mt-MFXw, and PEC1.5%@CHT/Mt-MFXw. The prepared microspheres of the bionanocomposites were frozen at -20 °C with liquid nitrogen and lyophilized (Cryodos -80, Telstar) to produce the final beads tested in the controlled release application.

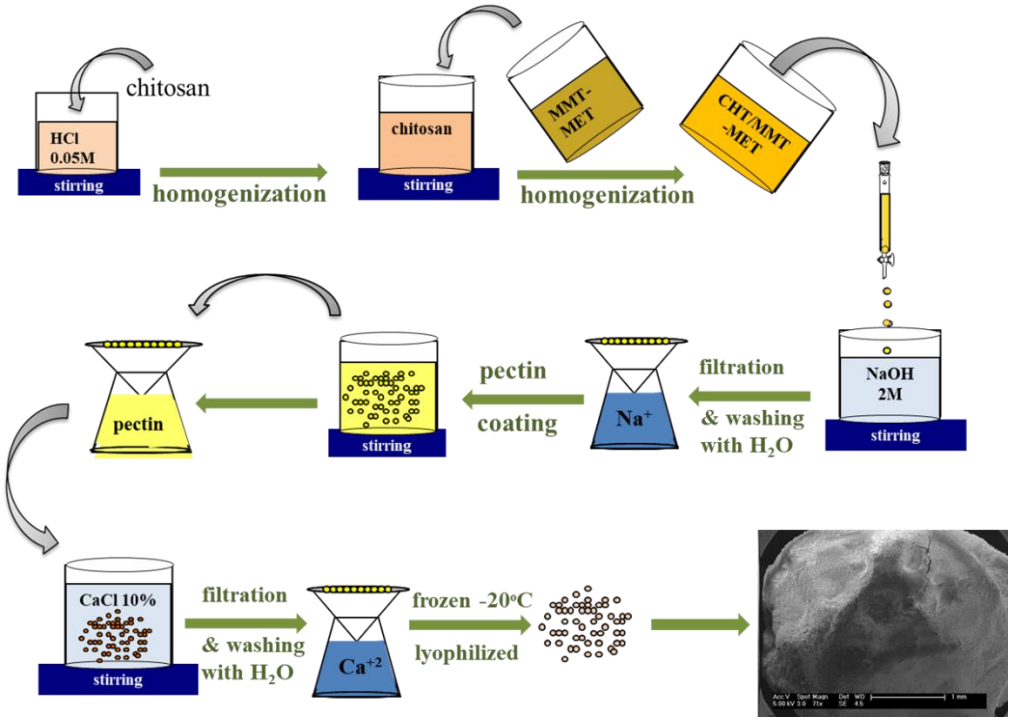

Figure 2.12. Scheme of the general procedure used for the preparation of the chitosan-pectin beads entrapping the drug metformin, directly or incorporated in the hybrids prepared from montmorillonite.

➢ *Preparation of bionanocomposite beads based on PEC-CHT-PEC / Mt-MF and Lap-MF:* pectin spheres, incorporating MF drug or the Mt-MF and Lap-MF hybrid materials, and then coated with a layer of chitosan and another layer of pectin was carried out as followed:

Step 1: the pectin gel was prepared by dispersion of pectin in 100 ml of bidistilled water at 5% (v/w). Subsequently, 0.1 g of the drug, or the suitable amount of Mt-

MFw, Mt-MF or Lap-MF hybrid containing the same amount of MF i.e. 0.1 g, was added, maintaining the system under stirring until its complete homogenization. The resulting gel was then introduced into a burette and slowly dripped into a 10% (v/w) $CaCl_2$ solution for about 20 min. The formed spheres were collected and washed with water in abundance to remove residual Ca^{+2} ions, being the products denominated as PEC/MF, PEC/Mt-MFw, PEC/Mt-MF and PEC/Lap-MF.

Step 2: The previously prepared pectin spheres were coated with a layer of chitosan by immersing them in a 0.5% aqueous dispersion of chitosan (pH ≈ 3) for 10 min, removed by filtration and incorporated then into a 2 M NaOH solution for approximately 10 min. After that there were collected by filtration and washed with abundant water. Subsequently these spheres went through an additional coating by immersing them in a 0.5% (v/w) pectin solution. After 10 min, they were transferred to a 10% $CaCl_2$ solution to consolidate the coating, followed by washing with abundant water. The bionanocomposite beads were denominated as PEC@CHT@PEC/MF, PEC@CHT@PEC/Mt-MFw, PEC@CHT@PEC/Mt-MF and PEC@CHT@PEC/Lap-MF. All the prepared materials were frozen at -20 °C with liquid nitrogen and lyophilized in a Cryodos -80, Telstar equipment, to produce the consolidated beads for later application as drug delivery systems.

2.2.2 Preparation of hybrid systems based on allantoin and layered double hydroxides

Various routes of synthesis were explored to obtain hybrid layered double hydroxide materials incorporating allantoin. These procedures involved the use of diverse layered double hydroxides (LDH) containing different inorganic anions in the interlayer region and with different salts.

a) Allantoin- layered double hydroxide hybrids

- *Synthesis of layered double hydroxides:* Mg/Al and Zn/Al LDH with a 2:1 M^{II}/M^{III} ratio and containing different anions in the interlayer (Cl^- and CO_3^{-2}) were prepared by co-precipitation following the procedure described by Constantino and Pinnavaia (1995).

For the preparation of the MgAl-LDH, a mixture of $MgCl_2 \cdot 6H_2O$ (9.34 mmol) and $AlCl_3 \cdot 6H_2O$ (4.68 mmol) was dissolved in 250 ml of double distilled water. This aqueous solution was added dropwise at a rate of 2 ml $\cdot min^{-1}$, with the help of a 800 Dosino equipment from Metrohm, to 200 ml of bidistilled water maintained under nitrogen flow to remove CO_2. Simultaneously, a solution of 1 M NaOH was added dropwise to the aqueous system to maintain a constant pH of ≈ 8 during the synthesis, all automatically controlled by the Dosino unit. The resulting suspension was vigorously magnetic stirred under nitrogen flow for 24 h for aging the formed LDH. The solid product was isolated by centrifugation, washed three times with bidistilled and degassed water and dried at 60 °C overnight. The material is denoted as MgAl-LDH.

For the synthesis of ZnAl-LDH, also with 2:1 (M^{II}/M^{III}) ratio and, containing Cl^- or CO_3^{2-} ions, the co-precipitation reaction was carried out at a constant pH of 9.0 according to the procedure described above. In this case, a mixture of $ZnCl_2 \cdot 2H_2O$ (15.58 mmol) and $AlCl_3 \cdot 6H_2O$ (7.79 mmol) was dissolved in 250 ml of decarbonates double-distilled water. This aqueous solution was added dropwise at a rate of 2 ml $\cdot min^{-1}$ to 200 ml of deionized water maintained under nitrogen flow to remove the CO_2. Simultaneously, a solution of 1 M NaOH was added dropwise to the aqueous system to maintain a constant pH of ≈ 8 during the synthesis. The resulting suspension was vigorously magnetic stirred under nitrogen flow for 24 h. The solid product was isolated by centrifugation, washed three times with bidistilled and degassed water and dried at 60 °C overnight. The material was denoted as ZnAl-LDH.

The ZnAl-LDH/CO_3^- was obtained analogously to the ZnAl-LDH described above, including the same salts and their respective concentrations, except that

the nitrogen flow was not used in the different stages of the synthesis, and the pH of precipitation (≈ 8) was adjusted with a 0.2 M $Na_2CO_3^-$ aqueous solution instead of NaOH. Once formed, the ZnAl-LDH/CO_3^- was recovered, washed and dried in an oven at 60 °C overnight. The material was denoted as ZnAl-LDH/CO_3^-.

- *Allantoin-LDH hybrids preparation*

Ion-exchange method: for the preparation of all the hybrids by ion-exchange method, 0.5 g of allantoin was dissolved in 250 ml of bidistilled water. The pH of the solution was adjusted to approx. 9 with 1 M NaOH. This solution was slowly added to a suspension containing 1 g of the selected LDH (MgAl-LDH and ZnAl-LDH) described above, and then kept at room temperature under magnetic stirring and nitrogen flux for 72 h. Subsequently, the solid product was isolated by centrifugation, washed with distilled water and dried at 60 °C overnight. The resulting materials were labelled as: allant$_{ie}$:MgAl-LDH and allant$_{ie}$:ZnAl-LDH.

Co-precipitation method: the allantoin hybrids based on MgAl and ZnAl LDH were prepared by the co-precipitation method as described in the previous section, but in this case the salts were dropped into 200 ml of 1% (w/v) allantoin solution. The resulting suspensions were stirred at room temperature under nitrogen flow for 24 h. The solid fraction was separated by centrifugation, washed with bidistilled water and dried at 60 °C overnight. The hybrid materials synthesized by the co-precipitation method were labelled as allant$_{cop}$:MgAl-LDH and allant$_{cop}$:ZnAl-LDH.

Reconstruction method: the synthesis of allantoin-LDH hybrid materials by the reconstruction method was performed by a calcination-rehydration reaction of the corresponding LDH-carbonate solids. Thus, 0.5 g of ZnAl-LDH containing carbonate ions in the interlaminar space (ZnAl-LDH/CO_3^-) was calcined in a muffle furnace at 350 ^oC heating the sample from room temperature at 10 ^oC min^{-1} and then maintained at that temperature for 5 h to assure the formation of the corresponding dehydrated layered double oxide (ZnAl:LDO). On the other hand,

allantoin (1.56 g) was dissolved in 250 ml of bidistilled water and the pH was adjusted to 9 with 1 M NaOH, similarly to that described for the ion-exchange reaction. Then, 0.5 g of ZnAl-LDO was added to the allantoin solution, while the system was maintained under magnetic stirring and nitrogen atmosphere to prevent the formation of LDH-carbonate. The solid product was separated by centrifugation, washed and dried at 60 °C overnight. The resulting hybrid material was labelled as allant$_{rec}$:ZnAl-LDH.

b) Allantoin-zinc systems

➢ *The allantoin-Zn layered single hydroxide:* the LSH hydrid was prepared according to the same procedure followed in the preparation of allant$_{cop}$:ZnAl-LDH, but in this case, no aluminum was added to the salts solution. Thus, a solution of $ZnCl_2 \cdot 2H_2O$ (15.58 mmol) in 250 ml was dropped at a rate of 2 ml min^{-1} into an allantoin solution (2 g in 200 ml of bidistilled water) using the 800 Dosino from Metrohm. The material was kept under stirring under nitrogen atmosphere for 24 h. The solid product was separated by centrifugation, washed with bidistilled water and dried at 60 °C overnight. The resulting hybrid material was labelled as allant:Zn-LSH. A Zn-LSH (in this case an LSH is not formed, it is only used as a nomenclature) has also been prepared under the same conditions without the presence of allantoin.

➢ *Allantoin-Zinc complexes:* the allantoin-zinc complex was prepared based on the patent by Margraf (1974), using in this case 2 g of allantoin and 3.51 g of $ZnCl_2$, which were added to 62 ml of warm double-distilled water (60 °C). The pH was neutralized to approximately 7-8 by adding 1 M NaOH. Upon addition of NaOH, a white precipitate started to form. It was recovered by centrifugation, washed several times with bidistilled water, and dried at room temperature in a desiccator for 48 h. The resulting product was labelled as allant:Zn-complex. Under the same conditions a reference sample (blank) was prepared without the presence of allantoin, labelled as Zn-NaOH.

c) Preparation of bionanocomposite films by incorporating the allantoin hybrids in biopolymers

For the studies of antibacterial activity, the materials based on ZnAl-LDH (without allantoin), allant:ZnAl-LDH, allant:Zn-LSH and the allant-Zn complexes were incorporated in the agar (A), hydroxypropylmethylcellulose (HPMC) and cellulose nanofibers (CNF) biopolymers.

Agar: for this purpose, a 1.5% w/v agar solution was prepared in hot water until the gel was completely homogeneous. Before the agar solution reached room temperature, a certain amount of hybrid material containing 8.5 mg of zinc was added. After total homogenization, the resulting dispersions were placed in Petri dishes and dried in an oven at 40 °C for approx. 48 h. The resulting materials were labelled as: A/allant, A/Zn, A/LDH, A/allant:LDH, A/LSH, A/allant:complex, A/Zn-complex and A/allant:LSH.

Hydroxymethylcellulose: the same materials cited for the agar biopolymer were incorporated into the HPMC films and the same drying conditions were used. Except in this case, a 2% w/v HPMC solution was prepared at room temperature.

Nanocellulose fibers: In this case, nanocellulose fiber films incorporating pure allantoin and allant:Zn-LSH hybrid were prepared, using the same conditions as in the previous preparations. Except in this case, a 0.6% w/v nanocellulose fiber solution was prepared at room temperature.

2.2.3 MCPA-LDH /sepiolite hybrid nanoarchitectures

The preparation of MgAl-LDH/Sep nanoarchitectures involves the formation of a MgAl-LDH in the presence of a suspension of sepiolite (Gómez-Avilés et al., 2016). In this work, this procedure was followed to produce organic-inorganic hybrid nanoarchitectures associating organic molecules to the MgAl-LDH/Sep nanoarchitectures by ion-exchange reaction, or in one step process by co-

precipitation of the LDH in presence of sepiolite and the organic specie, in this study the herbicide MCPA. For comparative purposes, hybrids resulting from MCPA intercalation on the neat MgAl-LDH were also prepared.

a) *Layered double hydroxide materials*

MgAl-LDH was prepared by co-precipitation reaction following the method described in #Section 2.2.2. The resulting solid was labelled as MgAl-LDH.

b) *MCPA-LDH hybrids*

Ion-exchange method: 1.5 g of MCPA was dissolved in 125 ml of bidistilled water and, then, the pH slowly adjusted to 7 by adding 1 M NaOH to assure the presence of the herbicide in its anionic form (Figure 2.13). The resulting herbicide solution was slowly added to a suspension of 0.5 g of MgAl-LDH (prepared as described above) in 125 ml of bidistilled water. This system was kept at room temperature under stirring and nitrogen flow for 72 h. Subsequently, the solid was recovered by centrifugation, washed 3 times with water and dried at 60 °C overnight. The resulting solid was labelled as $MCPA_{ie}$:MgAl-LDH.

Co-precipitation method: here again the LDH is prepared following the method described by Constantino and Pinnavaia (1995), but in this case the aqueous metal salts solution was here added slowly to 350 ml of a MCPA (2.5 g) water solution. Once the addition is completed, the system is kept at room temperature under stirring and N_2 flow for 24 h, in order to complete the reaction. Then, the solid was recovered by centrifugation, washed three times with bidistilled water and oven dried at 60 ^{o}C overnight. The resulting solid is labelled as MCPA:MgAl-LDH.

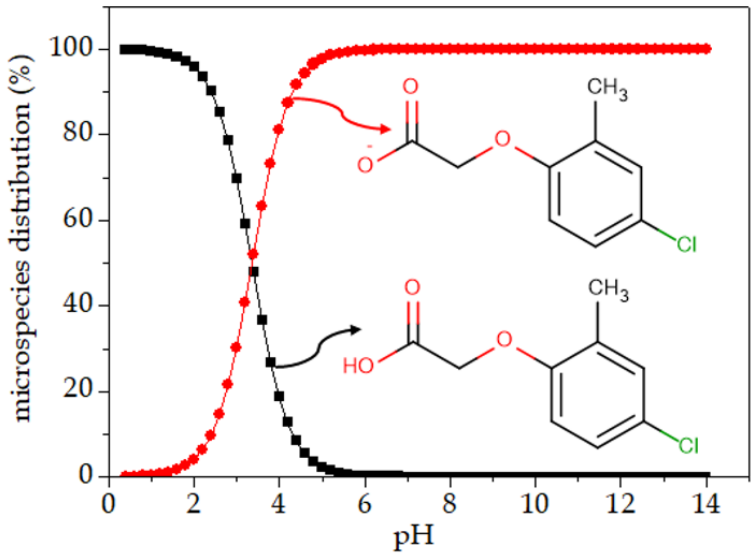

Figure 2.13. Diagram showing the distribution (percentage) of the protonated and anionic species of the MCPA molecule at different pH (obtained with the MarvinSketch program 6.1.5 software).

c) *Preparation of LDH /sepiolite nanoarchitectures*

The LDH/Sep nanoarchitectures were prepared according to a previously reported procedure (Gómez-Avilés et al., 2016), by forming the MgAl-LDH from a solution of $MgCl_2 \cdot 6H_2O$ (9.34 mmol) and $AlCl_3 \cdot 6H_2O$ (4.68 mmol) in 500 ml of bidistilled water that was dripped with the 800 Dosino equipment from Metrohm to a dispersion of 4 g of sepiolite in 350 ml of bidistilled water. At the same time, the system was maintained at pH ≈ 9 by controlled addition of 1 M NaOH solution. After the complete addition of the salts, the system was kept under magnetic stirring and nitrogen flow for 24 h to complete the formation of the LDH crystals. In this study, LDH:sepiolite materials with 2:1, 1:1, 0.5:1 and 0.3:1 theoretical ratio were prepared. The product was then centrifuged, washed 3 times with water and dried in the oven at 60 °C or, alternatively heated at 26 °C/h until reaching 150 °C, and then kept it at this temperature for 3 h (nitrogen flow of 100L $\cdot min^{-1}$) to achieve its drying and the consolidation of the formed nanoarchitecture (Gómez-Avilés et al., 2016).

d) *Preparation of MCPA-LDH /sepiolite hybrid nanoarchitectures*

To obtain the hybrid nanoarchitectures, two methods were studied: ion-exchange method and co-precipitation.

Ion-exchange method: the previously prepared LDH/Sep nanoarchitectures were used to incorporate MCPA by an ion-exchange process. For this purpose, 1.5 g of MCPA was solubilized in 125 ml of bidistilled water and the pH was adjusted to 7 to have the herbicide in its anionic form. On the other hand, 0.5 g of a given nanoarchitecture was dispersed in an equal volume of water. The herbicide solution was slowly added to the nanoarchitecture dispersion and the system was kept under stirring for 72 h. Then, it was centrifuged, washed 3 times with water, and dried at 60 °C overnight. The hybrid nanoarchitectures were prepared from LDH/Sep nanoarchitectures of 2:1 and 0.5:1 LDH:sepiolite theoretical ratio consolidated at 60 and 150 °C. The resulting hybrid nanoarchitectures were labelled as: $MCPA_{ie}$-LDH/Sep2:1_60C, $MCPA_{ie}$-LDH/Sep2:1_150C, $MCPA_{ie}$-LDH/Sep 0.5:1_60C, $MCPA_{ie}$-LDH/Sep 0.5:1_150C.

Co-precipitation method: MCPA-LDH/sepiolite hybrid nanoarchitectures were also obtained in a single step by co-precipitation of the LDH in the presence of sepiolite and MCPA. In this case, the amount of Mg^{+2} and Al^{+3} chlorides required to obtain LDH:sepiolite of 2:1, 0.5:1 and 0.3:1 theoretical ratios was dripped into a dispersion containing 4 g of sepiolite and 2.5 g of MCPA in 500 ml of water. The solid recovered by centrifugation was then heated at 60 °C or 150 °C for 3 h under nitrogen flow (100 $ml \cdot min^{-}$) to consolidate the resulting hybrid nanoarchitectures. They were labelled as: MCPA-LDH/Sep2:1_60C, MCPA-LDH/Sep2:1_150C, MCPA-LDH/Sep0.5:1_60C, MCPA-LDH/Sep0.5:1_150C, MCPA-LDH/Sep0.3:1_150C and MCPA-LDH/Sep0.5:1_60C.

e) *Bionanocomposite beads based on the incorporation of MCPA hybrid systems in alginate-zein matrices*

The biopolymers alginate and zein were selected for the encapsulation of the MCPA hybrid systems, following the protocol described by Alcântara et al. (2010). Thus, i) 1.66 g of alginate in the solution was dissolved in 80 ml of water previously heated to 60 °C; ii) 0.34 g zein (corresponding to 17% of the total amount of biopolymers), to obtain a 2% concentration of biopolymers (considering the total amount of zein and alginate), together with 34 mg of MCPA, or the required amount of MCPA-LDH hybrid or MCPA-LDH/Sep nanoarchitecture that contains 34 mg of MCPA, were incorporated in 20 ml of ethanol-water (80%, v/v); iii) then, this mixture was homogenized and slowly added to the alginate solution, and kept under stirring for about 30 min; iv) the formed gel was poured drop by drop with a burette in a 5% $CaCl_2$ solution to form spheres that were kept under constant stirring for 15 min; at the end of the process, the beads were washed with double distilled water to remove residual Ca^{+2} ions; and, finally, v), the recovered bionanocomposite beads were dried at 40 °C overnight. The resulting materials were labelled as: ALG-Z@MCPA-LDH (incorporating the MCPA-LDH hybrid material) and ALG-Z@MCPA-LDH/Sep (incorporating the MCPA-LDH/Sep hybrid nanoarchitecture).

2.3 CHARACTERIZATION METHODS

The characterization of the prepared materials and the study of their controlled release properties were carried out by means of various physicochemical characterization techniques.

2.3.1 Powder X-ray diffraction (XRD)

The structural information of crystalline materials was obtained using powder X-ray diffractometry (XRD). In this study, this technique was essential to characterize materials derived from montmorillonite and Laponite® clays, and from layered double hydroxides, where changes in the basal spacing deduced from the position of reflections provide useful information on the intercalation of molecules in the interlaminar space. The diffractograms of the samples were obtained in a D8-ADVANCE unit from Bruker, equipped with a "Lynxeye" detector using the characteristic radiation for the copper Kα line (λ_1 = 0.154060 nm and λ_2 = 0.154439 nm). The voltage and current of the source used were 40 kV and 30 mA, respectively. The diffractograms were obtained with a goniometer speed of 0.3 s/step between 3 and 70 degrees of 2θ angle values.

2.3.2 Elemental chemical analysis (CHN)

Elemental chemical analysis was used to determine the amount of organic component present in the prepared hybrid materials. The samples were analyzed in duplicate either in a LECO CHNS-932 or in a PERKIN ELMER 2400 analyzer.

2.3.3 Infrared spectroscopy (FTIR)

Fourier transform infrared spectroscopy (FTIR) is a widely used technique for the identification of functional groups especially in organic compounds, as well as in organo-inorganic hybrid materials, which can also provide information on interaction mechanisms. FTIR was applied to characterize diverse samples prepared in this work using a BRUKER IFS 66v/S spectrophotometer. In general, the samples were diluted in KBr (~ 2%) and pellets were formed under a pressure of 10 tons prior to obtain the corresponding spectrum from 4000 to 400 cm^{-1} with a resolution of 2 cm^{-1}. The samples based on sepiolite were prepared as a free-standing film (from a 2% w/v suspension) that was directly placed in the sample

holder. This configuration was required in order to detect changes in the characteristics O-H stretching vibrations of Si-OH of this silicate appearing around 3720 cm^{-1}.

2.3.4 Thermal analysis (TG/DTA)

Thermal analysis is an analytical technique that allows the study of both mass and thermal variations provoked when a sample is heated in a controlled atmosphere. The thermal behavior of the different prepared materials was analyzed from the simultaneously recorded thermogravimetric (TG) and differential thermal analysis (DTA) curves in a SDT Q600-TA equipment, in experiments carried out under air atmosphere (flux of 100 ml/min) from room temperature to 1000 ^{o}C at 10 ^{o}C/min heating rate.

2.3.5 UV-visible spectroscopy (UV-Vis)

Ultraviolet-visible spectroscopy is an instrumental technique that provides qualitative and quantitative information based on the process of absorption of ultraviolet-visible radiation (with wavelength between 160 and 780 nm) by a molecule or solid. In this Thesis, this technique was used in the quantitative evaluation of the content in solutions containing the drug or herbicide released from the hybrid and bionanocomposite materials in *in vitro* release assays. The measurements were carried out in a UV-1201 spectrophotometer from Shimadzu, using quartz cuvettes with 1 cm path length. The determination of concentration of the specie of interest was obtained by applying the *Lambert-Beer* law.

2.3.6 Electron microscopy

a) Field Emission Scanning Electron Microscopy (FESEM)

Scanning electron microscopy is an important technique used in the characterization of materials as it allows to investigate their morphology and texture as well as other relevant aspects such as homogeneity and composition. In this work, the morphology of the prepared materials was studied with a field emission scanning electron microscope FEI NOVA NANO 230 high resolution scanning electron microscope with an EDAX-Ametek detector, which allowed to quantify semiquantitatively the elements (e.g., sodium, chloride, aluminum, magnesium and zinc) present in the studied samples. The sample preparation was carried out by adhering the sample particles on a carbon adhesive tape and they were visualized directly without the need of any conductive coating. In some studies, the EDX analysis was carried out in a Hitachi S-3000N scanning electron microscope.

b) Transmission electron microscopy

Transmission Electron Microscopy (TEM) allows the study of the structure and morphology of particulate materials, in a very small scale with nanometric resolution. For the observation of some of the hybrids, the samples as powders were dispersed in bidistilled water and submitted to ultrasonic stirring for 15 min. A drop of the resulting dispersion was deposited on a copper grid covered with a carbon conductive coating and allowed to dry at room temperature. The images of the corresponding samples were obtained with a JEOL JEM1010 (100 kV) or JEOL 2100F STEM 200 kV microscope.

2.3.7 High resolution solid state nuclear magnetic resonance spectroscopy (NMR)

Through Nuclear Magnetic Resonance (NMR) spectroscopy that uses electromagnetic radiation in atomic nucleus, physical or chemical properties of

atoms or molecules in which they are contained can be determined. From the spectra of the ^{3}C and ^{29}Si nucleus, information about the structure of the metformin molecule or its organization in the inorganic solid can be obtained, or disturbances in the structure of a solid, a silicate, for example, as is the case with sepiolite.

^{13}C solid state NMR spectra were recorded at room temperature with a Bruker AV-400-WB spectrometer on a 2.5 mm twin channel probe using ZrO_2 rotors with Kel-F plug. The pulse sequence used in the ^{13}C spectra was cross polarized (CP-MAS) ^{1}H-^{13}C. The working frequencies were 400.13 MHz for ^{1}H and 100.32 MHz for ^{13}C. The rotational speed was set to 10 kHz. The spectra were recorded using a spectral width of 35 kHz, an excitation pulse π/2 ^{1}H of 1.8 µs, a contact time of 3 ms and a relaxation time of 4 s, with a decoupling of ^{1}H type tppm 15 at 80 kHz. The number of scans was 1024 for MF. The spectra of the Mt-MF300 and Mt-MF300w samples were accumulated throughout the night. The ^{13}C chemical shift was referred to the tetramethylsilane (TMS) signal as the main reference and to the CH_2 signal of adamantane (29.5 ppm) as a secondary reference. The ^{29}Si NMR spectra were obtained using the same equipment and speed of rotation of the sample (10 KHz) but applying 79.49 MHz as the resonance frequency for ^{29}Si, a pulse of π/2 for 5 µs and collecting between 1200 and 2000 accumulations with a waiting time of 5 s between successive accumulations. TMS was used as the standard reference signals for the ^{29}Si nucleus, respectively.

2.3.8 Total reflection X-Ray Fluorescence (TXRF)

Total reflection X-Ray Fluorescence (TXRF) is a technique used in atomic chemical analysis, being based on the classical X-ray fluorescence spectroscopy (XRF). This technique allows to qualitative and quantitative evaluate the elements of the periodic table preferentially from Z=13 to Z=92, with a dynamic range of 5 orders of magnitude and a sensitivity of ppb (ng/ml) in liquids, and the percentage of weight (% wt) in solids. In this work, the technique was used

to determine the content of Zn in the materials based in allantoin in the release assays. The TXRF S2 PicoFox Bruker spectrometer of fixed geometry was used.

2.3.9 Total Organic Carbon (TOC)

The analysis of total organic carbon was used to determine the concentration of allantoin released from the samples prepared in this work. The samples were analyzed with an Analytik Jena multi N/C 2100 equipment.

2.3.6 Zeta potential

Zeta Potencial is a measure of the stability of a particle and indicates the potential that is required to penetrate the surrounding ion layer in the particle to destabilize it. Therefore, the zeta potential is the electrostatic power that exists between the separation of the layers surrounding the particle. In this Thesis to determine the zeta potential of allantoin and the various hybrid systems prepared from allantoin was used an equipment NanoBrook 90Plus PALS from Brookhaven Instruments, using the BI-ZEL electrode, in the diluted aqueous dispersion of the samples.

2.4 COMPUTATIONAL MODELING

To complement the studies of the hybrids based on the intercalation of MF in Mt and Lap, theoretical studies of computational models were necessary. For this purpose, a theoretical materials package from Materials Studio was used. This software presents a simple graphical interface to prepare the models and systems to study. In addition, it presents a variety of available methods and various types of calculations in combined theoretical-experimental studies in which it allows the use of theoretical-chemistry at an interpretive level of the atomistic point of experimental results. Among the variety of modules with specific functions for

different studies and theoretical problems integrating the Materials Studio Software, FORCITE (FF) and CASTEP was used in this Thesis.

a) Computational methodology

A Force field (FF) based on empirical interatomic potentials previously refined by Heinz et al., (2005) for organics and clays was used in the optimization of the atomic structures, applying the Forcite code and periodical boundary conditions within the Materials Studio package (Biovia, 2018). This method yielded satisfactory results in similar systems previously studied (Borrego-Sánchez et al., 2016, 2018). The Ewald method was used for the Coulomb and Van der Waals interactions with a cut-off at 15 Å. The SPC water model (Rick et al., 1995) was used with atomic charge values of 0.41 and -0.82 for the H and O atoms, respectively. To set up the FF to the MF molecule, DFT calculations were applied for the optimization of this molecule using the Dmol3 code, calculating the atomic charges adjusted to the electrostatic potential (ESP charges) (Cox and Williams, 1981). These charges were compared with those calculated by the same FF and by the QEq method (Rappe and Goddard, 1991).

In addition, quantum mechanical calculations have been performed using the Castep code (Clark et al., 2005) based on a plane wave DFT (Density Functional Theory) with periodical boundary conditions for comparison with previously applied FF. The generalized gradient approximation (GGA) and Perdew–Burke–Ernzerhof (PBE) correlation exchange functional were used (Perdew et al., 1997) with an energy cutoff of 630 eV. On-the-fly generated (OTFG) ultra-soft pseudopotentials were used with Koelling-Harmon relativistic treatment (Vanderbilt, 1990). The effect of the dispersion corrections of Tkatchenko were included (Tkatchenko and Scheffler, 2009).

b) Mineral and molecular models

Models of Mt and Lap with a composition similar to the experimental one were used as a starting point, applying periodic boundary conditions to reproduce the crystallinity of this material. A periodic crystalline structure of the dioctahedral smectite, montmorillonite, with the unit-cell formula $Na_{0.6}(Al_{3.4}Mg_{0.6})Si_8O_{20}(OH)_4$ was created and a 2x2x1 supercell model was generated with a formula $Na_2(Al_{14}Mg_2)Si_{32}O_{80}(OH)_{16}$. The Mg atoms were placed in the octahedral sheet taking into account their dispersion tendency observed in previous work (Ortega-Castro et al., 2010). For the structure of the trioctahedral smectite, Laponite®, we created a model close to the experimental composition the Laponite® XLG used $Na_{0.7}(Mg_{5.5}Li_{0.3}\square_{0.2})Si_8O_{20}(OH)_4$, with no tetrahedral substitution and Li substitutions and vacant sites in the octahedral sheet. A 2x2x1 supercell was generated with formula $Na_3(Mg_{22}Li_1\square_1)Si_{32}O_{80}(OH)_{16}$. The Li substitution and the octahedral vacancy were placed in a maximal dispersion way in order to avoid charge concentration generated by these alterations of the Mg octahedral sheet. Then, both mineral solid models were studied for the MF adsorption in the interlayer space of the clays. In the experimental conditions MF is protonated being a monocation extracted from experimental crystal structure (Childs et al., 2004). Then, in the cation exchange we replaced in the intermediate layer a Na^+ cation by a MF cation that would be intercalated, keeping the entire system electrically neutral. The quantity of water present in the pure clays and in the MF intercalated clays used in the calculations were the experimental values obtained from TG/DTA measurements.

2.5 Evaluation of the properties of the hybrid and bionanocomposite materials

2.5.1 Metformin-based materials

a) *Water absorption properties of MF-loaded bionanocomposite beads*

Water absorption properties of pectin-chitosan bionanocomposite beads were evaluated at room temperature by immersing the beads (≈ 10 mg) in 25 ml of

water or a solution simulating the pH of the first intestinal zone (around 6.8) using a phosphate buffer solution. At predetermined times, the beads were removed from the liquid and the excess of water whipped with absorbent paper, and then weighed on an analytical balance. The percentage of adsorbed water was determined by equation (1).

$$water\ absorption\ g/g = \frac{\mathrm{Wt} - \mathrm{W0}}{\mathrm{W0}} \quad (1)$$

where W_t and W_0 are the wet and initial mass of beads, respectively.

b) *Determination of the efficiency of encapsulation of metformin in pectin-chitosan bionanocomposite beads*

After incorporation of the drug MF in montmorillonite and Laponite® and in the chitosan/pectin bionanocomposite beads, the amount of drug incorporated, and the encapsulation efficiency were determined. For this purpose, 0.2 g of spheres were immersed in a buffer solution of pH 6.8 prepared with 0.030 g of NaOH, 0.40 g of $NaH_2PO_4{\cdot}H_2O$ and 0.62 g of NaCl to completely extract the drugs from the beads. The system was maintained under magnetic stirring at 37 °C for 24 h. The supernatant was recovered by centrifugation at 9000 rpm for 10 min, and then, the MF content was determined using UV-spectroscopy. Thus, the absorbance of the solution at 233 nm was determined and the concentration calculated by applying the *Lambert-Beer* law.

The percentage of incorporated metformin and encapsulation efficiency were calculated using equations (2) and (3) (Babu et al., 2006), respectively.

$$\%\ drug\ loading = \frac{\text{amount of drug in beads}}{\text{amount of beads}}\ \ x100 \quad (2)$$

$$\%\ encapsulation\ efficiency\ = \frac{amount\ of\ drug\ loading}{\text{theoretical loading}}\ x100 \qquad (3)$$

c) *In vitro evaluation of metformin release*

A preliminary assay of MF release from the Mt-MF or Lap-MF hybrids was performed in bidistilled water for 5 h. Then, the *in vitro* release study that simulates the gastrointestinal tract was performed for 8 h. This study aims to simulate the sequential pH changes and time of residence that occur during the passage of the formulation through the gastrointestinal tract in the *in vivo* process. The materials selected for this study were first maintained for 2 h in a 0.006M HCl solution (pH 1.2) containing 0.1% by weight NaCl to simulate the fluid in the gastric tract. The *in vitro* release studies of the different prepared materials were carried out by putting approximately 5 mg of the Mt-MF or Lap-MF hybrids, or around 50 mg of bionanocomposite beads, into 100 ml of the selected delivery medium, which was kept in a thermostatic bath at 37 °C for the selected time. Then, it was kept at pH 6.8 for other 2 h, by adding a buffer prepared by the addition of 0.03 g of NaOH, 0.40 g of $NaH_2PO_4 \cdot H_2O$ and 0.62 g of NaCl to the solution of pH 1.2, in order to simulate the pH of the first zone of the intestinal fluid (small intestine). Finally, the system was kept for 4 h at pH 7.4 by adding 1 M NaOH to the solution of pH 6.8, in order to simulate the pH of the intestinal colon area. At appropriate time intervals, an aliquot of 3 mL was withdrawn, and the amount of MF released from the drug-loaded beads was determined by UV spectrophotometry (λ = 233 nm) by applying the *Lambert-Beer* law. After the measurement, the aliquot was added back to the solution, in order to maintain the volume constant. All the experiments were carried out in triplicate. For the measurement of the MF released at pH 1.2, the pH has to be raised to 7 by adding a buffer solution, so that the MF band at λ= 233 nm can be observed. In this case, the collected aliquot (1 ml) is not returned to the main solution, and 1 mL of fresh pH 1.2 solution is replenished to keep the volume constant.

2.5.2 Allantoin-based materials

a) Release of allantoin in phosphate buffered saline

The release of allantoin from the prepared hybrid systems was investigated by immersing a quantity of the selected compound containing 55 mg of allantoin in 100 ml of phosphate buffer solution (PBS) (pH ≈ 5.5) that simulates the pH of the human skin. The systems were kept at 36 °C under slow stirring in a thermostatic bath (50 rpm) for 24 h. In order to determine the concentration of the drug in the liquid, 5 ml of the solution was taken at certain time intervals and 5 ml of the phosphate buffer were added in order to keep a constant volume. The content of allantoin in the aliquot was determined by analyzing the total organic carbon in the solution and, then, the released allantoin was calculated considering the gravimetric factor.

b) Study of the antibacterial properties of allantoin containing materials

The antibacterial activity of the different samples obtained from allantoin-Zn systems was evaluated *in vitro* by the disc diffusion method (Hudzicki, 2012) using Mueller-Hinton agar (MHA) (Sigma-Aldrich) with inhibition zones determined in millimeters (mm). Gram-positive bacteria (*Staphylococcus aureus* CECT 239) and Gram-negative bacteria (*Escherichia coli* K 12 CECT 433) were used for this study previously grown in LB broth (10 g L^{-1} tryptone, 5 g L^{-1} yeast extract, and 5 g L^{-1} NaCl) at 36 ± 1 °C for 24 h. Each bacterial suspension (100 µL, 108 CFU ml^{-1}) was inoculated on MHA and spread with a sterile Drigalski handle. The 5-6 mm cm disks of agar agar (A) or Whatman filters (W) containing each one of the tested materials (A/allant, A/Zn, A/LDH, A/allant:LDH, A/LSH, A/allant:complex, A/Zn-complex and A/allant:LSH; W/allant, W/Zn, W/LDH, W/allant:LDH, W/LSH, W/allant:complex, W/Zn-complex and W/allant:LSH) were placed in the previously inoculated agar plates and

incubated at 36 ± 1 °C for 24 h. After incubation, the diameter of the inhibition zone was measured.

2.5.3 MCPA-based materials

a) Release of MCPA in water

The release of MCPA herbicide from the MCPA-LDH hybrid, MCPA-LDH/Sep nanoarchitectures and the alginate/zein (ALG-Z) bionanocomposite materials was performed in 100 ml of bidistilled water at pH 5.5, with the addition of the required quantity of material to provide 20 mg of MCPA. The experiment was maintained at room temperature under slow magnetic stirring for 48 h or 8 days. At predetermined times, aliquots of 3 ml were removed from the system and then the MCPA concentration was evaluated by measuring the absorbance at 279 nm in a UV-Vis spectrophotometer and applying the *Lambert-Beer* law. After the analysis, the collected solution was returned to the initial solution to keep the volume constant. All the experiments were performed in triplicate.

b) Experiments MCPA release in the soil column

The soil used in this experiment was collected from an area of Madrid (Spain) located at the campus of the Autonomous University of Madrid. The soil has a sandy appearance on the surface (Figure 2.14A) and was removed from about 10 cm under the surface and its color suggests the presence of some organic matter content. Before its incorporation in a column, it was sieved at 2 mm and allowed to dry at room temperature.

The soil release studies were based on those described by Alromeed et al., (2015) where a methacrylate tube was used to build a 20 cm column. The column was covered at the opposite end of the 8 cm unit using a 1 mm nylon mesh padded with a thin layer of glass wool (0.5 g) to keep the soil in the column. The sand soil

(0.164 kg) was placed from the top of the column creating a 16 cm column Figure 2.14B. Approximately 3 ml of a suspension of the prepared formulations (pure MCPA, MCPA-LDH hybrid, MCPA-LDH/Sep nanoarchitectures, and ALG/Z@MCPA-LDH/Sep beads) were sprayed on the soil surface. Distilled water simulating the equivalent to 70 mm of rain (50 ml) was added to the top of the column throughout 24 h. The leachate was collected and analyzed by HPLC to determine the level of herbicide.

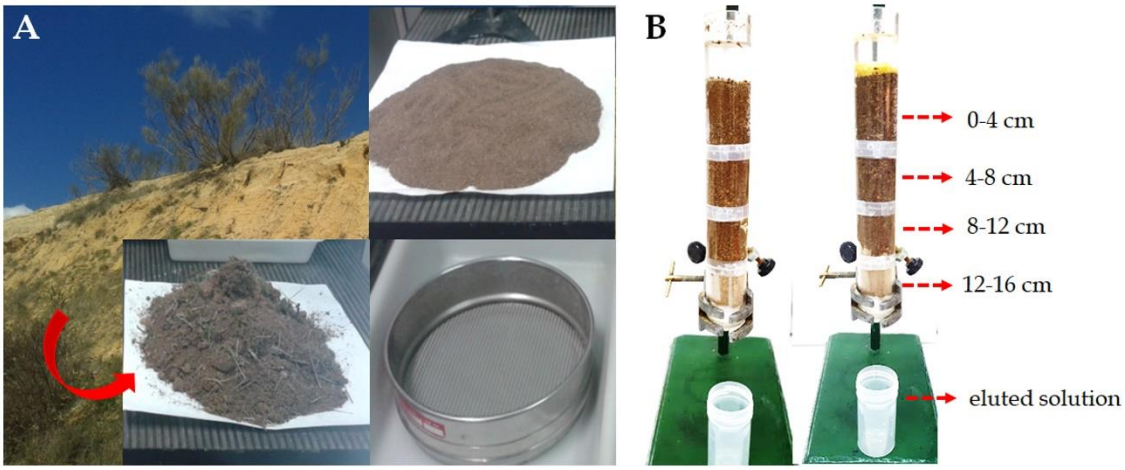

Figure 2.14 Soil used in the experiments of this work (A) and columns used for the release of MCPA from the formulations (B).

CHAPTER 3

CLAY- BASED BIONANOCOMPOSITES AS CONTROLLED DRUG DELIVERY SISTEMS FOR RELEASE OF METFORMIN

This chapter presents a comparative study on the use of two layered clays, a natural montmorillonite from Wyoming (Mt) and a synthetic hectorite known as Laponite® XLG (Lap), to encapsulate metformin (MF), which is the oral drug most used to treat type II diabetes. The objective was to evaluate the suitability of Mt and Lap as substrates for controlled release of MF in order to have a convenient and well-regulated clay-based component to produce pharmaceutical formulations. The combination of molecular modeling and experimental characterization techniques allowed to study the adsorption process and the final molecular arrangement of MF in the interlayer region of each of the silicates. As observed in "in vitro" release tests, the large release of MF in acidic media from both systems makes additional encapsulation in a protective polymer matrix necessary to increase the drug delivery in the small intestine. Promising results were obtained using chitosan and pectin as encapsulating matrix in a core shell configuration, leading to a gradual release of MF in the simulated gastrointestinal tract.

3.1 INITIAL CONSIDERATIONS

Metformin (MF) is a biguanide type medication widely prescribed for more than 60 years for the treatment of type II diabetes (Sirtori, 1994; Turner, 1998). This is a chronic metabolic disease whose main feature is to raise blood glucose levels (hyperglycemia), which may be associated with a body's resistance to insulin causing long-term serious problems in blood vessels, eyes, heart, kidneys and nerves (King et al., 2001; Lenhard and Gottschalk, 2002; Krentz and Bailey, 2005; Levetan, 2007; Chatterjee et al., 2017). Type 2 diabetes mellitus is a progressive and complex disorder that is difficult to treat effectively in the long term. Most patients are overweight or obese at diagnosis and will be unable to reach or sustain near normoglycemia without oral antidiabetic agents. A considerable proportion of patients will eventually require insulin therapy to maintain long-term glycemic control, either as monotherapy or in conjunction with oral antidiabetic therapy (Turner, 1998; Krentz and Bailey, 2005; Levetan, 2007).

According to the World Health Organization (WHO) the number of deaths from diabetes reached 1.6 million in 2016, which made this disease the seventh cause of death in the world (WHO, 2019). Currently, metformin hydrochloride is the reference drug used for the treatment of type 2 diabetes, being able to decrease blood glucose concentration by mechanisms other than insulin or sulphonylurea (Sirtori, 1994; Rojas and Gomes, 2013; Pala and Rotella, 2014; Sterrett et al., 2016; Chatterjee et al., 2017). This drug also decreases plasma insulin concentrations, contributing to increase peripheral glucose uptake and decreasing hepatic glucose production (Laliberte and Neumiller, 2010; Sterrett et al., 2016). Metformin does not promote weight gain and has beneficial effects on various cardiovascular risk factors (Turner, 1998; UK Prospective Diabetes Study Group, 1998; Krentz and Bailey, 2005). For these reasons, the World Health Organization, has listed metformin as an essential medicine (WHO, 2019), being the most used oral medication for diabetes. Moreover, this drug is gaining great prominence in recent years, showing high efficacy as antitumor agent mainly in the treatment of prostate, colon, polycystic ovary syndrome and breast cancers (Lord, 2003; Gupta et al., 2013, 2018; Aldea et al., 2014). However, this drug has several

disadvantages caused by the low absolute bioavailability of 50-60% and the plasma half-life is 1.5–4 h, which implies the administration of high doses for an optimal therapeutic effect that can produce serious gastrointestinal problems (Pala and Rotella, 2014; Markowicz-Piasecka et al., 2017). Besides approximately 30–50% of an oral dose is excreted in the urine as unchanged drug within 24 h, and 30% of the dose is eliminated unchanged with the feces (Graham et al., 2011; Emami Riedmaier et al., 2013; Markowicz-Piasecka et al., 2017). In this context, the design of controlled drug delivery systems (CDDS) is required to offer a controlled release and, consequently, to diminish these side effects. Currently, there is a commercial extended-release formulation of metformin, GLUCOPHAGE® XR, which contain the inactive ingredients sodium carboxymethyl cellulose, hydroxypropyl methylcellulose, microcrystalline cellulose, and magnesium stearate (Bristol-Myers Squibb. U.S. FDA., 2009). However, with a view to having even more efficient results, MF support materials based mainly on biopolymers are still being investigated (Ghazaie et al., 2017; Martínez-Gómez et al., 2017; Verma and Ahuja, 2017), considering that they are biocompatible, biodegradable and also some biopolymers can offer mucoadhesive properties increasing the effectiveness of a CDDS system. Other materials studied are inorganic mesoporous solids (X. Li et al., 2017; Shariatinia and Zahraee, 2017), porous silicon (García-Briones et al., 2019). In particular, clay minerals that to date have not been studied as CDDS for MF, are frequently used as carriers of a wide variety of medications in CDDS or DDS (Carretero, 2002; Aguzzi et al., 2007; Viseras et al., 2010; Hun Kim et al., 2016; Yang et al., 2016; Alcântara and Darder, 2018; Massaro et al., 2018; Ruiz-Hitzky et al., 2019), and so they could also serve as substrates for MF. Based on these premises, the possibility of using smectites, such as montmorillonite and hectorite, to stabilize metformin is evaluated here, which will allow its subsequent incorporation into a formulation that can increase its biological half-life, decrease the daily dose and, presumably, other side effects associated with the regular use of metformin (Figure 3.1A). The selected clays in this study have been a natural montmorillonite from Wyoming commercialized as Cloisite® (Mt) and a

synthetic hectorite commercialized as Laponite® XLG (Lap) which is commonly used in cosmetic and pharmacology. Taking into account the different characteristics of these two layered silicates, this study was set with the aim of exploring and analyzing in a comparative way their behavior as substrates for adsorption and release of metformin.

Computational modeling tools at the molecular level are here applied for a better understanding of the interactions between the drug and clays. Computational modeling allows to determine the geometrical structure of metformin, the structural dimensions of the unit cell, the distribution of the drug along the interlayer space, the interpretation of the clays interlayer spacing shift, atomic organization etc., including the interaction energy associated with the adsorption process. Several works based on computational modeling have achieved results of great relevance in the understanding of the interactions between diverse molecules (drugs, herbicides, surfactants, etc.) and clay minerals (sepiolite, palygorskite, halloysite, montmorillonite, Laponite®, etc.) as for example the adsorption of sulfonamides on phyllosilicate (Francisco-Márquez et al., 2017), pilocarpine on Laponite® (Cunha et al., 2017), surfactants on montmorillonite (Borrego-Sánchez et al., 2018), neomycin on montmorillonite and sepiolite (Rebitski et al., 2018), or to study the interaction of ethambutol with palygorskite (Meirelles et al., 2019). The final objective of the present study is also to evaluate and compare the release of MF intercalated in the Lap and Mt substrates incorporated in a biopolymers matrix of chitosan and pectin, forming bionanocomposite materials (Figure 3.1B). Bionanocomposites are known as good carriers of different types of drugs (Darder et al., 2007) like ibuprofen (Alcântara et al., 2010b; Ribeiro et al., 2014c), diclofenac (Lisuzzo et al., 2019), or amoxicillin (Rebitski et al., 2019) among others. The selected biopolymers has been chitosan and pectin that present properties of biocompatibility, biodegradability, and have very interesting mucoadhesive properties, especially in the case of chitosan, for biomedical applications, while pectin may improve the stability of the developed systems at the pH of the stomach (Shimoda et al.,

2001; Chourasia and Jain, 2003; Thirawong et al., 2007; Rajpurohit et al., 2010; Liu et al., 2012; Yadu et al., 2017; Zhao et al., 2018; George et al., 2019).

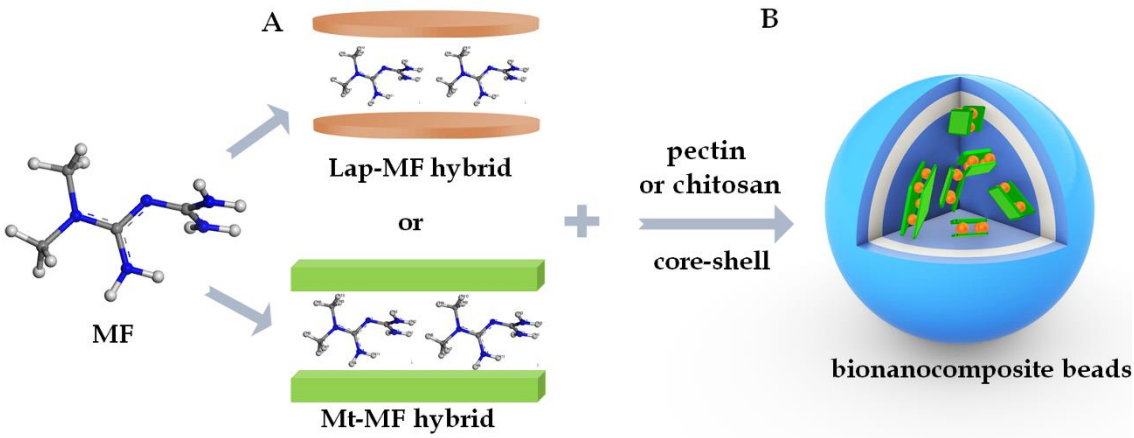

Figure 3.1. Schematic representations of the formation of the Lap-MF and Mt-MF hybrids (A) and the bionanocomposite systems based on chitosan and pectin core-shell (B).

3.2 METFORMIN-MONTMORILLONITE HYBRIDS

3.2.1 Intercalation of metformin in montmorillonite

Metformin is a biguanide, a hydrophilic organic molecule that is a strong base with a pKa of 12.4. Therefore, it exists mainly in protonated form with positive charge under physiological conditions. MF contains 5 nitrogen atoms with different tendencies towards protonation. Within a large pH range (between ca. 1.5 and 10.5), the main species correspond to mono-protonated molecules Figure 3.2 (Foretz et al., 2014; Kinaan et al., 2015).

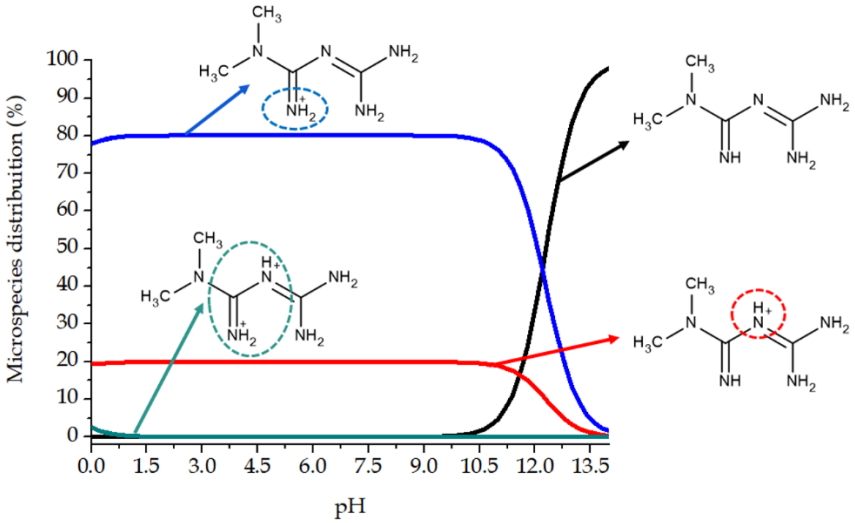

Figure 3.2. Graphic showing the percentage of the various protonated species of the metformin molecule stable at different pH values (obtained by simulated calculations with the MarvinSketch program 6.1.5 software).

The positive charge in MF contributes to its spontaneous adsorption in Mt from aqueous solutions of MF hydrochloride. As described in the Chapter 2 #section 2.2.1, the adsorption isotherm at 298 K (Figure 3.3A) was constructed from the data of adsorbed amounts of MF that were determined from CHN elemental analysis. These results can be fitted to a L-type (Langmuir) adsorption isotherm (equation 1) according to the Giles classification (Giles et al., 1960). The fitting to the Langmuir isotherm data (R = 0.986) is indicative of the high affinity (b = 7.163 $mmol^{-1} \cdot L$) between the adsorbate (MF) and the adsorbent (clay).

$$r = \frac{bx_m C_s}{1+bC_s} \qquad (1)$$

where r represents in the present case the adsorbed amount of MF in a specific point of the isotherm, Cs is the equilibrium concentration, x_m is the maximum amount of adsorbed MF and b is the constant affinity between the MF organic adsorbate and the montmorillonite clay adsorbent.

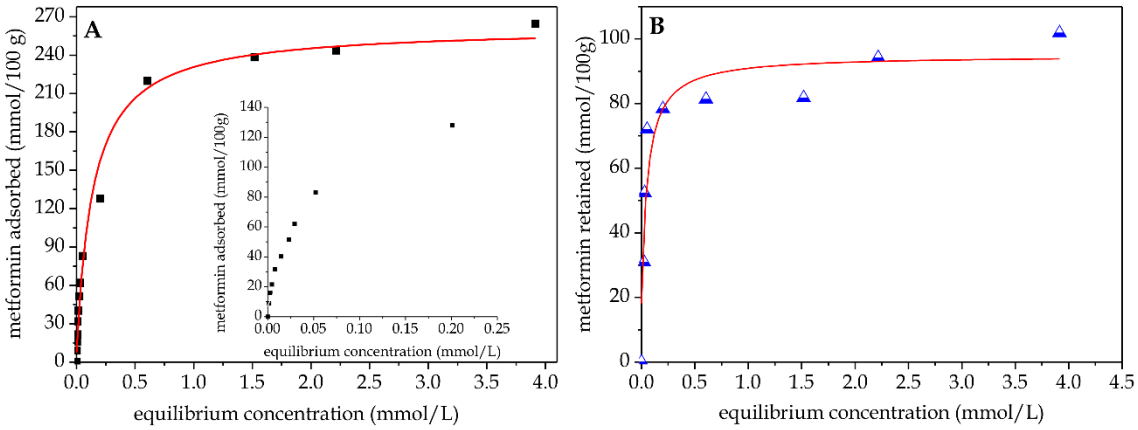

Figure 3.3. Adsorption isotherm at 298 K of MF (water solutions) in Na-montmorillonite (A), retained amounts of MF in Na-montmorillonite after washing the samples (B).

The constant b can be related to the Gibbs energy of the adsorption process, calculated by the equation 2:

$$\Delta G_{ads} = -RT\ ln\ K \qquad (2)$$

where R is the gas constant, T the adsorption temperature, and K corresponds to $(b\rho/4)^2$ for ionic species (Miller et al., 2002), where ρ is the ratio of the solvent (water) density to its molecular weight ($\rho \approx 1000/18$). Thus, the calculated Gibbs energy is ΔG = -76.5 kJ mol^{-1}, indicating an elevated tendency to the adsorption of the MF species on the montmorillonite clay surface. This value is comparable to the Gibbs energy obtained from adsorption of other type of cationic organic in Na-montmorillonite also involving intercalation processes (Colilla et al., 2005; Wicklein et al., 2010).

It is known that the CEC of the commercial montmorillonite Cloisite®Na is 93 mEq per 100 g, but the values of the adsorption isotherm plateau correspond to a drug content of about 260 mEq per 100 g, around thrice the CEC of the employed montmorillonite clay mineral (Figure 3.3A). The inset of Figure 3.3A shows the detailed evolution of the isotherm for the lowest values of the equilibrium concentration, which can be attributed mainly to intercalation

through an ion-exchange mechanism. Higher equilibrium concentration values lead to the adsorption of MF on the outer surface of the clay particles, which are easily removed by washing the samples. The "pseudoisotherm" representing the retained amount of MF after washing (Figure 3.3B) shows a plateau corresponding to 94 meq per 100 g, that is, almost coincident with the CEC value of this montmorillonite. Semi-quantitative EDX analyses of the hybrids produced at each point of the isotherm indicate a progressive decrease in the content of Na^+ in the clay with the concomitant increase in adsorbed MF-H^+ species (Figure 3.4A). Unwashed samples corresponding to equilibrium concentration values greater than *ca.* 100 mEq per 100 g contain also chloride species (Figure 3.4B) that must be related to the presence of adsorbed MF·HCl species, which most probably remain assembled on the outer surface of the clay, in some cases forming even crystallites as deduced from the corresponding XRD patterns (Figure 3.5A).

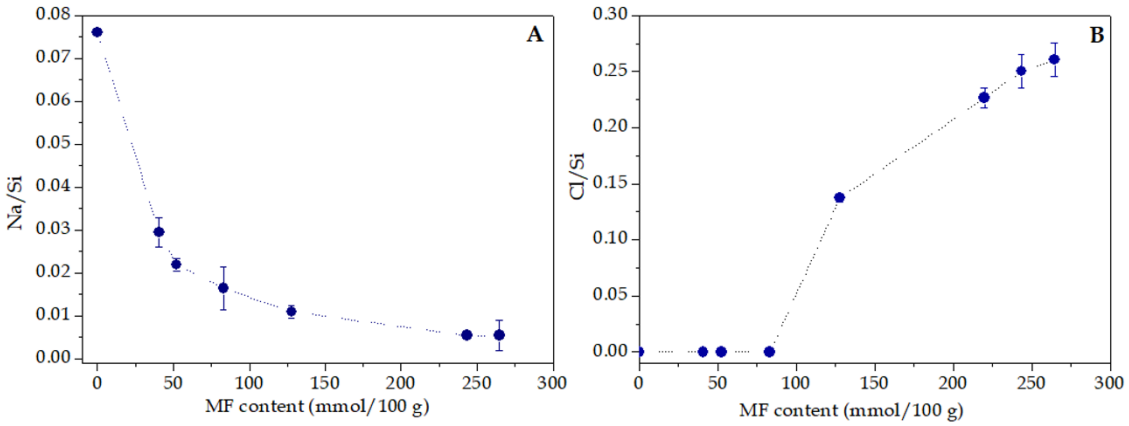

Figure 3.4. Evolution of the Na/Si ratio in samples with different amount of adsorbed MF on Na-montmorillonite (A), and content in chloride species in samples with different amount of adsorbed MF on Na-montmorillonite (samples from the adsorption isotherm study, i.e., without washing) (B). Note: sodium to silicon and chloride to silicon ratios in atomic % are deduced from EDX measurements and represented as a function of MF content in mmol per 100 g of the composite.

Taking into account that the total accessible surface area of montmorillonite is 750 $m^2\ g^{-1}$ (Olphen, 1977), and that the clay used in this study has a CEC of 93 meq per 100 g, it can be calculated a value of 0.66 nm^2 available per monovalent

cation, taking into account also such ion is sandwiched between two silicate sheets. The packaging of MF, deduced from the molecular models, is estimated to be around 0.4 nm^2, which is below the area available per cation. Therefore, protonated MF species are compatible with the available area of this clay and, therefore, could easily exchange interlayer Na^+ ions, and be freely accommodated in the interlayer space as a monolayer, leading to the formation of montmorillonite-MF intercalation compounds.

The intercalation of MF in the interlamellar space of MT is deduced from the XRD patterns of the prepared hybrids containing different amounts of adsorbed drug (Table 3.1), before and after washing (Figure 3.5A & B). The intercalation is clearly deduced by the change in the position of the most intense peak, attributed to the (001) reflection plane, towards lower angles in 2θ. Given that the thickness of a single layer of montmorillonite is approximately 0.96 nm (Bergaya et al., 2013), it is possible to deduce a basal spacing increase of around 0.4 nm in the prepared Mt-MF hybrids due to the intercalation of MF. In addition, other (*00l*) reflections peaks, e.g. the d_{002} reflection peak at around 13.5° in 2θ, start to be also detected, confirming that at least a part of metformin is easily adsorbed in the interlamellar space of the clay mineral. The basal spacing of 1.20 nm in the initial Mt increases to values of around 1.35 nm in the Mt-MF hybrids, independently of the concentration of the drug used in the preparation or the washing processes. In samples prepared with high MF contents and without further washing, additional peaks related to the presence of crystalline MF·HCl adsorbed at the external surface of the clay may be also observed (Figure 3.5A).

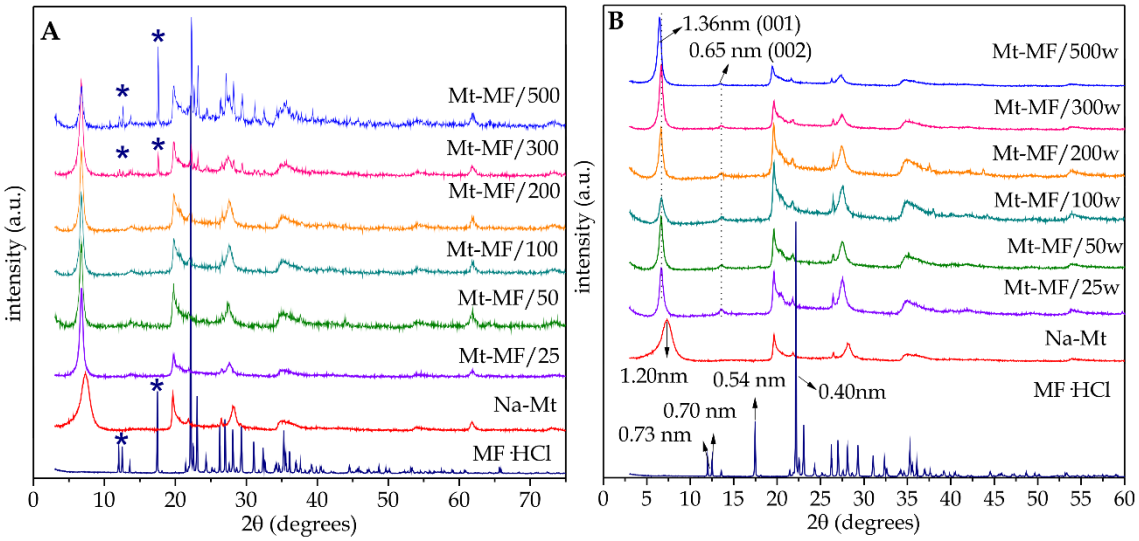

Figure 3.5. X-ray diffraction patterns of metformin (MF), Na-montmorillonite (Mt) and various Mt-MF hybrids obtained after adsorption of MF at different equilibrium concentrations without further washing (A) and X-ray diffraction patterns of metformin (MF), Na-montmorillonite (Mt) and washed Mt-MF hybrids with different content in metformin (B).

Table 3.1 Amount of MF adsorbed on Na-montmorillonite before and after washing in samples preapred at 298 K in different equilibrium conditions.

Sample	**Unwashed** **mEq MF per 100 g Mt**	**Washed** **mEq MF per 100 g Mt**	**Sample**
Mt-MF5	40.02	30.9	Mt-MF5w
Mt-MF10	52.2	51.6	Mt-MF10w
Mt-MF25	83.0	72.0	Mt-MF25w
Mt-MF50	127.8	78.3	Mt-MF50w
Mt-MF100	219.9	81.3	Mt-MF100w
Mt-MF200	238.6	81.8	Mt-MF200w
Mt-MF300	243.6	94.2	Mt-MF300w
Mt-MF500	264.7	101.8	Mt-MF500w

The proposed ion-exchange mechanism supports the high observed tendency of MF to intercalate Na-montmorillonite according to the Gibbs energy value calculated above. In fact, only by mixing both components in a mortar, the

ambient humidity is sufficient to spontaneously promote rapidly a partial intercalation according to XRD patterns (Figure 3.6).

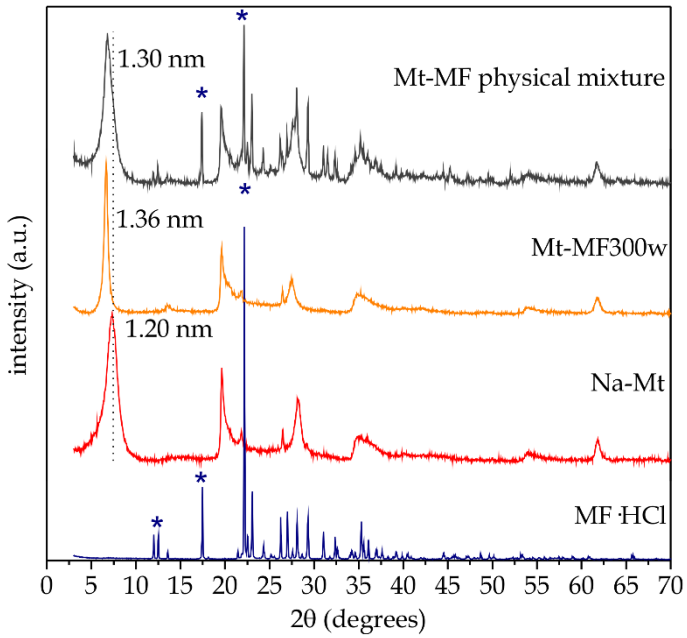

Figure 3.6. X-ray diffraction patterns of MF·HCl, Na-Mt, Mt-MF300w hybrid and the physical mixture Mt-MF with a content in MF similar to Mt-MF300w sample.

FTIR spectroscopy corroborates the formation of Mt-MF hybrids. The spectrum of the used montmorillonite (Figure 3.7a) shows the typical vibration bands of this type of phyllosilicate, which also shows vibration bands at approximately 1635 cm^{-1} ascribed to water directly coordinated with the exchangeable cations of the clay (Porubcan et al., 1978; Madejová et al., 1999). The spectrum of metformin hydrochloride (Figure 3.7b) shows a series of ν_{N-H} vibrations bands centered at around 3370, 3300 and 3170 cm^{-1} that can be assigned to the primary and secondary amine groups, respectively. The band attributed to the bending vibration mode of the primary amine appears as a double band at 1635 and 1625 cm^{-1}, while the NH flexion of the imine group with the contribution of the secondary NH flexion amine is also shown as a double band at 1580 and 1565 cm^{-1}. The bands between 1475 and 1415 cm^{-1} can be assigned to the bending vibration modes involving CH_3 groups, and those that are around 1060, 940 and

740 cm^{-1} to the stretching ν_{C-N} and bending and wagging vibration modes involving NH groups, respectively (Gunasekaran et al., 2006). The spectra of the washed and unwashed Mt-MF hybrids (Figure 3.7c, d and f) show bands within the typical regions where Mt and MF bands were observed but with some differences, especially with respect to those assignable to the organic molecule. These differences reveal the existence of interactions between MF and the montmorillonite substrate. Firstly, a new band is observed at around 3470 cm^{-1}, while the band at 3370 cm^{-1} relatedto the ν_{N-H} of the primary amine groups is still visible. Actually, the vibration band attributed to the ν_{N-H} of the secondary amine is disturbed and changes to higher wave numbers, now appearing at around 3200 cm^{-1}. More significant are the changes in the band observed at around 3300 cm^{-1} related to the stretching mode of the imine group, which is less visible within the broad background and only clearly defined in the spectrum of the Mt-MF300 hybrid, probably due to to the presence of MF located on the external surface of the clay, involved here in low interaction with the silicate substrate. Other changes affect the bands in the region of 1400-1600 cm^{-1}, involving both an enlargement of the bands and, in some cases, also slight changes in the frequency. IR bands of MF that appear in the 1000-1100 cm^{-1} region are not detected due to the highly intense ν_{Si-O} silicate vibration bands. The same applies to bands in the region of 700-950 cm^{-1}, although the band of MF that appears at around 940 cm^{-1} is still detectable in the spectrum of Mt-MF300 near that of the silicate at approximately 935 cm^{-1}, pointing again to the presence of a greater amount of MF in this hybrid sample with a part of it scarcely perturbed.

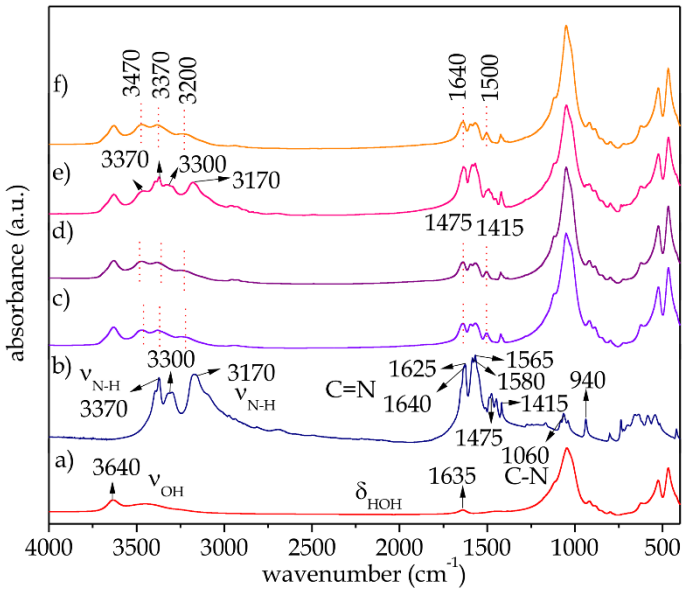

Figure 3.7. FTIR spectra of the Na-montmorillonite (a), metformin hydrochloride (b), and the Mt-MF25 (c) Mt-MF25w (d), Mt-MF300 (e) and Mt-MF300w (f) hybrids.

Figure 3.8 shows the TG/DTA curves obtained in the air atmosphere for Na-montmorillonite, MF, and the four selected Mt-MF hybrids. The curves corresponding to the initial Mt (Figure 3.8a) show the typical pattern of this type of silicate with a loss of mass at moderate temperatures that is accompanied by an endothermic peak at around 80 °C, which corresponds to the removal of water physically adsorbed water, approximately 7%. At higher temperatures, there is a progressive and small mass loss, probably associated with the elimination of water molecules attached to the cations between layers and the characteristic dehydroxylation of clay at temperatures between 600 and 700 °C, also associated with an endothermic process (Heller-Kallai, 2013). In the case of pristine MF (Figure 3.8b), the first significant event is the melting process observed at 235 °C. Above this temperature, the compound begins to degrade, losing about 80% of the mass between 300 and 400 °C in an endothermic process with a maximum at about 330 °C, although there is still another mass loss between 550-600 °C to complete the degradation of the molecule (Santos et al., 2008; Ghazaie et al., 2017). In the case of the Mt-MF hybrid materials, the TG and DTA curves (Figure 3.8c, d, e, and f) are very complex, even assuming the superposition of the effects observed in the two components separately, which indicates the existence of

interactions between the two counterparts, MF and clay ore. In all cases, a small mass loss is observed at temperatures below 100 ºC also associated with an endothermic peak, which is related to the elimination of physisorbed water as in pure silicate. In intercalation compounds, water removal occurs in a similar temperature range, with mass losses of around 3-4%. Metformin removal begins at temperatures of around 200 ºC and can also last up to temperatures of 650-700 ºC, being more complex and continuous than in pure MF and accompanied by several endothermic effects. The endothermic peak attributed to the fusion of MF is not clearly defined as in pure MF, but it could be the maximum observed at around 220 ºC on the Mt-MF300 DTA curve (Figure 3.8e), indicating a different aggregation state of the MF molecules. In this case, the sample contains an excess of crystalline MF·HCl on the outer surface of the clay as determined from the corresponding XRD pattern. Although it is not evident, the presence of MF on the outer surface of Mt-MF25 (Figure 3.8c) can not be discarded since certainly the thermal decomposition of MF in this hybrid is complex and slightly different from that of the sample after washing (Figure 3.8d). An endothermic peak near 245 ºC can be distinguished, which is the temperature where MF fusion occurs. Finally, it is also remarkable that the TG and DTA curves of all washed hybrid materials are quite similar regardless of the initial MF content in the sample, indicating that once the samples are washed, the remaining MF should be located in the interlayer region of the clay.

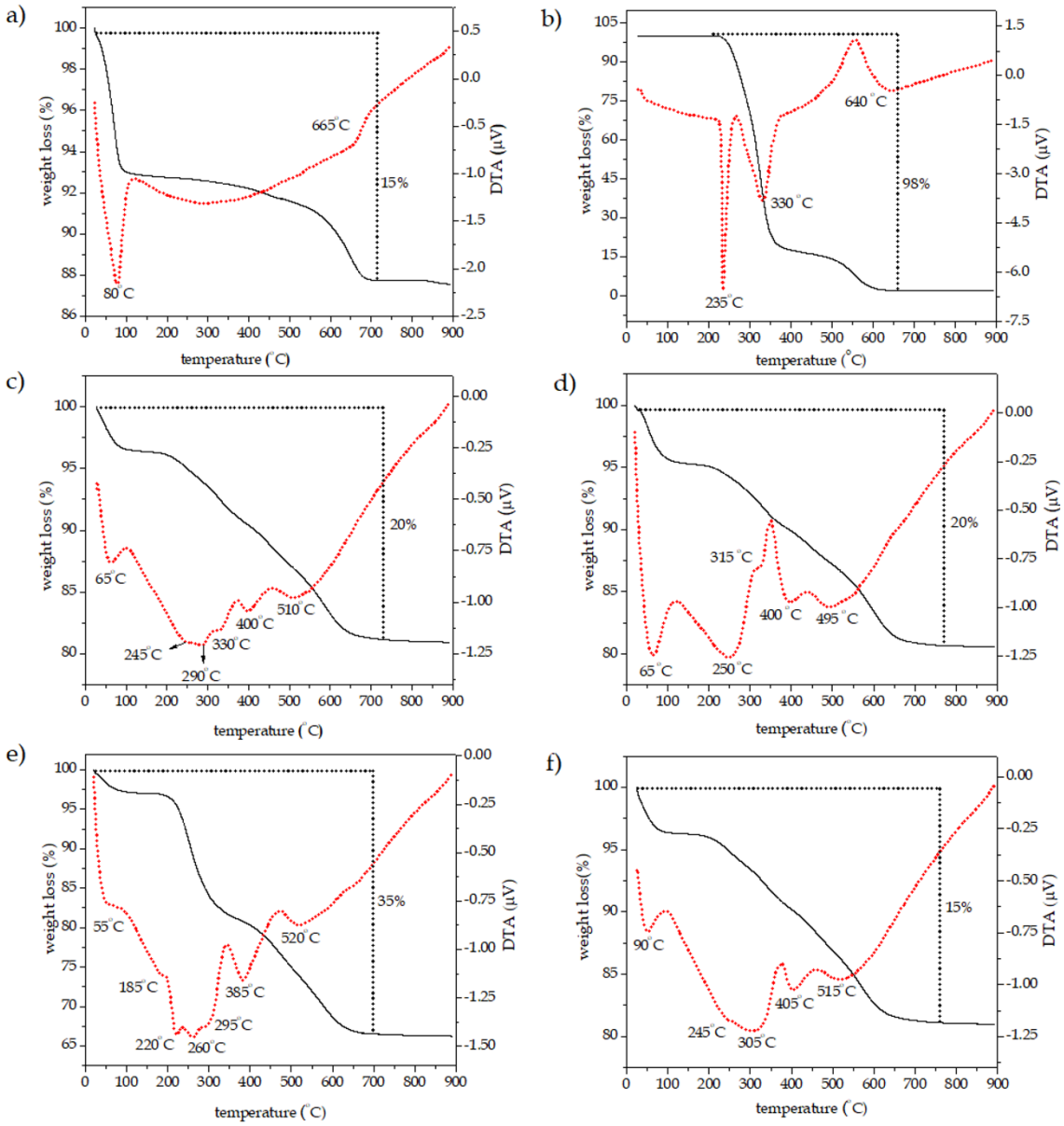

Figure 3.8. TG (black, solid line) and DTA (red, dashed line) curves of Na-montmorillonite (a), metformin hydrochloride (b) and the Mt-MF25 (c) Mt-MF25w (d), Mt-MF300 (e), and Mt-MF300w (f) hybrids. Experiments carried out in air atmosphere.

The ^{13}C NMR spectrum of starting metformin hydrochloride (Figure 3.9) shows resonance signals at 38, 40, 157 and 160 ppm described in greater detail in Table 3.2. The two signals C*1* and C*2* at higher field are assigned to the carbon nuclei of the two methyl groups in the molecule. The two other signals, (C*3* and C*4*) appearing at 157 and 160 ppm are attributed to the carbons involved in the bonds with the imine group of the molecule, respectively (Gadape and Parikh, 2011).

The spectra of the Mt-MF300 hybrid before and after washing show signals at close chemical shifts but with a very large background, especially in the 140-70 ppm region, that is more evident in the sample without washing, confirming the presence of MF in excess in the outer surface of the clay in this last case. Beyond the possible changes due to the presence of MF intercalated within the clay, which may produce enlargement of the signals making difficult to distinguish them as two separated peaks as in pure MF, the notorious background indicates the existence of MF intermolecular interactions that can strongly affect the conformation of MF. In the samples where MF is only located at the interlayer region of the clay, this effect is much lower because the MF molecules remain isolated only in interaction with the clay surface.

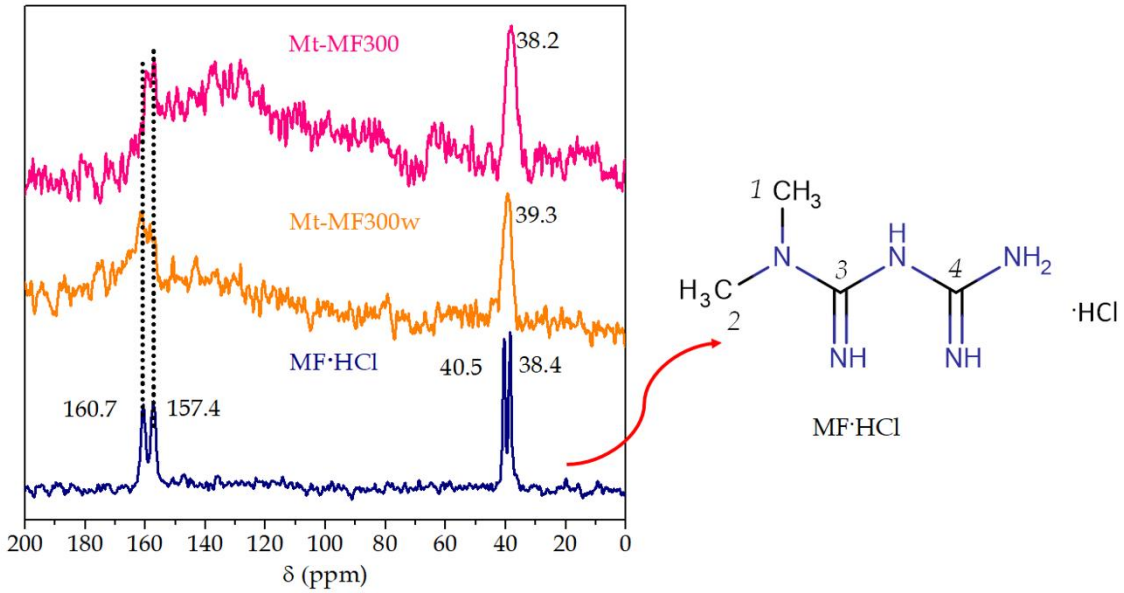

Figure 3.9. ^{13}C NMR spectra of metformin hydrochloride (MF·HCl), and the Mt-MF300w and Mt-MF300 hybrids.

Table 3.2 Assignments of ^{13}C NMR signal in the spectrum of MF·HCl

Type of Carbons	**Assignation**	**^{13}C ppm (δ)**
2-CH_3 (aliphatic)	1, 2	38.4, 40.5
1-C (1-imine)	3	157.4
1-C (1-imine)	4	160.7

3.2.2 Molecular modeling of the intercalation of MF in Mt

Computational modeling studies are used in this Thesis to understand at a molecular level the interactions between MF and clay (detailed in Chapter 2 #section 2.4). Computational modeling has revealed the geometric structure of intercalated metformin, the structural dimensions of the unit cell, the distribution of the drug along the interlayer space, the interpretation of the increase in the interlayer distance of clays, the atomic organization, etc., including the interaction energy associated with the adsorption process and all this information was compared to the results obtained experimentally.

For the simulation, several tautomers of MF mono-protonated salt have been considered and we selected that considered as the most stable in previous studies (Wei et al., 2014). For the application of the Forcite (FF) to this protonated MF molecule, several atomic charges were explored finding that those calculated by Density Functional Theory **(**DFT) and associated with the electrostatic potential yielded the best results. Hence, these charges were used for the rest of calculations with FF. Nevertheless, the conformational structures were similar in all cases (Figure 3.10). This preoptimized protonated MF molecule was placed in a periodical box of 2x2x2 nm and was re-optimized. The re-optimized MF molecule has slightly changed its conformation from the original. The two terminal NH_2 groups (N3 - N2) acquire a more planar conformation, forming a C2–N1–C1–N2 torsion angle of 72.09º. The terminal CH_3 groups form an C4–N5–C2–N4 angle of 11.74º and the central N form a torsion C4–N5–C2–N4 angle of -178.88º (Table 3.3).

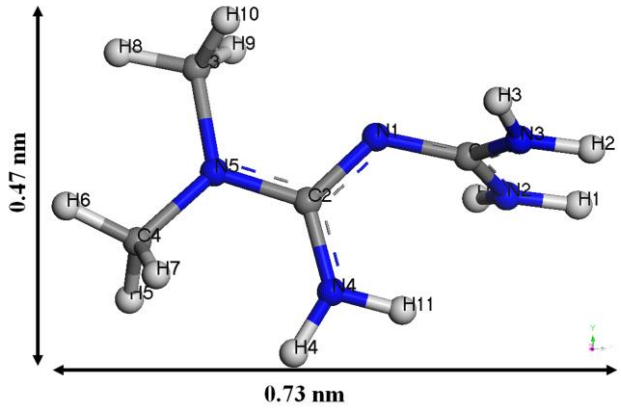

Figure 3.10. Molecular structure of metformin obtained by Castep program. Atoms in white-gray, gray and blue colors are H, C, N atoms, respectively. This color assignment is extended to the rest of figures of this Chapter.

An initial model of montmorillonite was prepared and optimized taking into account the chemical composition and the water content (7%) found in in TG-DTA (see figure 3.8a). Then, the 2x2x1 supercell of montmorillonite with 12 water molecules per supercell was fully optimized relaxing the atomic positions and lattice cell parameters, yielding a basal spacing of d_{001}=1.198 nm, matching the experimental value of 1.2 nm. This result validates the FF and methodology used in this work (Figure 3.11A).

The water content decreases during the intercalation of MF to 3.5 - 4.5% (Figure 3.8f). This means that there will be 8 water molecules per supercell during the adsorption of MF. Hence, two Na^+ cations were substituted by two protonated MF cations per supercell and the intercalation complex was optimized with two MF protonated cations (Mt-MF) (Figure 3.11B). The (001) interlayer spacing of the optimized structure is d_{001}=1.363 nm, matching the experimental value of 1.365 nm (see figure 3.5). The intercalated MF remains in the center of the interlayer space with H atoms of the protonated N atoms oriented towards the tetrahedral O atoms of the mineral surface forming a monolayer of MF. The MF molecules H forms bridges with the O of the clay surface and also with the water O atoms through the H atom of the terminal CH_3 and central and terminal NH_2 groups with a distances range of 1.95 nm - 2.50 nm (Figure 3.11B). In addition, the MF changes its conformation after intercalation, with the terminal CH_3 groups in a

more coplanar way compared to the starting MF, acquired new torsion angles (Table 3.2), and new dimensions of 0.34 x 6.72 nm, a value that approximates that obtained experimentally 0.39 nm for intercalated MF.

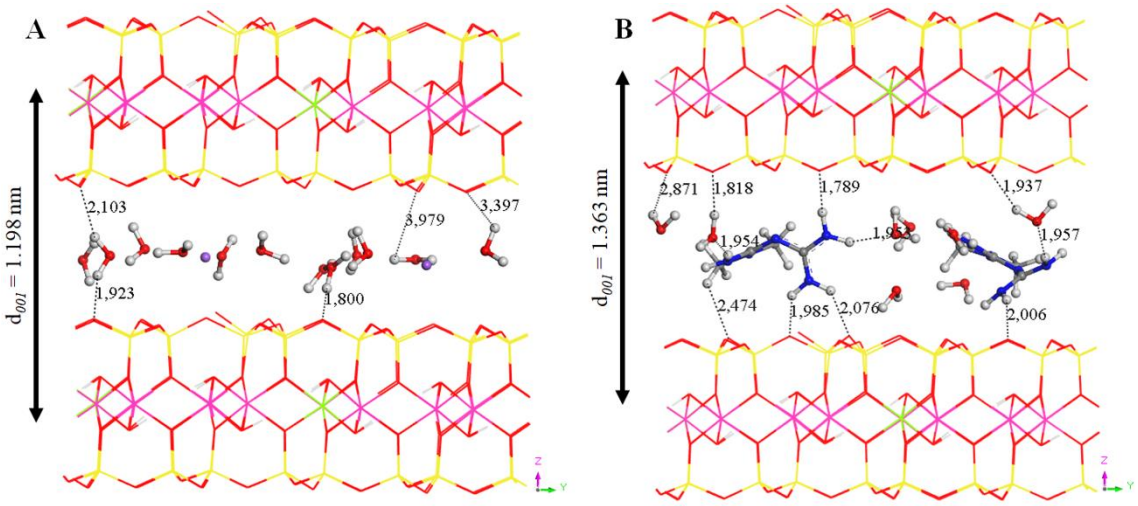

Figure 3.11. Supercell 2×2×1 of montmorillonite intercalated with Na^+ cations with 12 molecules of water (A), and metformin cations with 8 water molecules (B) per supercell. Atoms in white-gray, red, gray, blue, yellow, pink and green colors are H, O, C, N, Si, Al, and Mg atoms. This is extended to the rest of figures of this chapter.

Table 3.3 Torsion angles comparison of FF and CASTEP methods results for protonated MF and intercalated in Mt and Lap.

Torsion angle	**MF^+**	**Mt-MF (FF method)**	**Mt-MF (CASTEP method)**	**Lap-MF (CASTEP method)**
C2–N1–C1–N2	72.04°	11.40°	17.36°	20.84°
N5–C2–N1–C1	-178.88°	70.02°	-159.37°	-144.14°
C4–N5–C2–N4	11.74°	5.30°	7.98°	6.71°

To calculate the adsorption energy, we have to consider all the species involved in the interaction process by cation exchange mechanism. Then, we prepared a Mt supercell with 2 Na^+ cations with 8 water molecules (Mt-Na) and optimized in the same conditions, obtaining a (001) spacing basal of d_{001}=1.197 nm close to

the experimental value. Besides, one box of MF hydrochloride with 4 water molecules (MFCl4w), and another one with Na chloride with 4 water molecules (NaCl4w) were optimized in the same conditions at constant volume. Hence the adsorption energy was calculated using equation (3):

$$E_{ads} = E_{Mt\text{-}MF} + E_{NaCl4w} - (E_{Mt\text{-}Na} + E_{MFCl4w}) \quad (3)$$

yielding an energy of -42.73 kcal·mol^{-1}. This means that the intercalation of MF in Mt is energetically favorable.

This intercalation process was studied also at quantum mechanical level. These species involved in the intercalation process were optimized with CASTEP. The adsorption energy was -47.28 kcal·mol^{-1} similar to that obtained above with FF (Figure 3.12A and B). However, the (001) interlayer space of the calculated structures is shorter than experimental value, d_{001} = 1.192 nm for the Mt and d_{001} = 1.275 nm for the Mt-MF, due to that the CASTEP method overestimates the interactions between the tetrahedral sheets in the interlayer space.

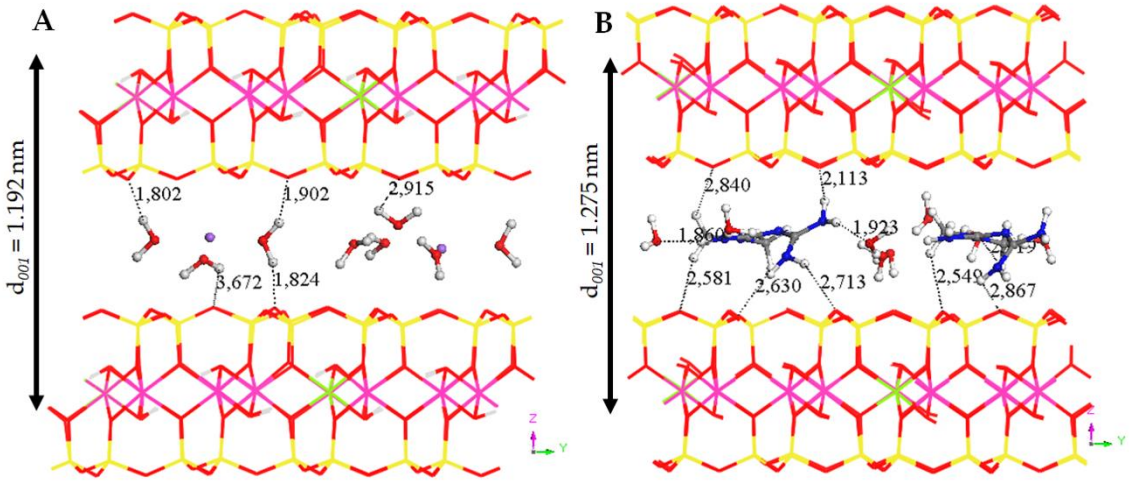

Figure 3.12. Structure of montmorillonite with Na^+ (A) and two molecules of MF (B) in the 2×2×1 supercell in presence of 8 molecules of water.

3.3 METFORMIN-LAPONITE® HYBRIDS

3.3.1 Intercalation of the metformin in Laponite®

To prepare the MF-Lap hybrids the results of the previous study on the intercalation of MF in the clay mineral Mt was used and so, in that case, a given amount of Mt was mixed with a set of MF solutions with a concentration that varies from 1 to 30 times the CEC of the clay but for the intercalation of MF in Lap the process was carried out using amounts of MF 1, 2 and 3 times the CEC of the clay following the same experimental conditions of the previous isotherm study. The Table 3.4 shows the content of MF in the prepared samples both before and after washing of the formed hybrids. In contrast to the Mt system, Lap-MF samples do not show large excesses of absorbed MF with respect to the CEC of the clay, regardless of the amount of drug present in the reaction medium, observing only a small excess in unwashed samples compared to the final washed products.

Table 3.4 Amount of MF adsorbed on Laponite® XLG (Lap) and Cloisite®Na (Mt).

Sample	**Unwashed meq MF per 100 g Lap**	**Washed meq MF per 100 g Lap**	**Sample**
Lap-MF1	53.6	52.6	Lap-MF1w
Lap-MF2	69.0	62.5	Lap-MF2w
Lap-MF3	76.0	68.3	Lap-MF3w

Similarly to the Mt-MF hybrid systems, the fact that MF intercalation occurs through a cation-exchange process is supported by the EDX analysis, which shows the decrease in sodium content after MF adsorption, since the initial Na/Si ratio is reduced from 0.069 in pristine Lap to 0.020, 0.012 and 0.018 in the Lap-MF1w, Lap-MF2w and Lap-MF3w hybrids, respectively.

The XRD patterns of the Lap-MF2w and Lap-MF3 hybrid compounds show a shift of the (001) reflection peak towards angles greater than 2θ, giving basal spaces that vary from 1.44 nm for the pristine Lap to 1.317 and 1.321 nm for the intercalation compounds, regardless of the concentration of MF used, which leads to a interlayer distance increase of 0.35-0.36 nm in the hybrids (Figure 3.13). The fact the interlayer distance in the hybrids is lower than in the pristine silicate can be associated with a large amount of water present in Lap, which shows a basal space increase of 0.44 nm, *i.e.*, twice that observed in the used Mt. The reflection d_{002} can be observed in the XRD patterns of the hybrids, which shows that there is an alteration in the stacking of the clay layers due to the presence of intercalated organic species. In contrast to the XRD pattern of the unwashed Mt-MF hybrid that shows reflections related to the presence of crystalline MF·HCl on the surface of Mt (Figure 3.5), the Lap-MF3 diffractogram (Figure 3.13), which contains a small amount of excess MF, does not show any characteristic peak attributed to crystalline MF·HCl.

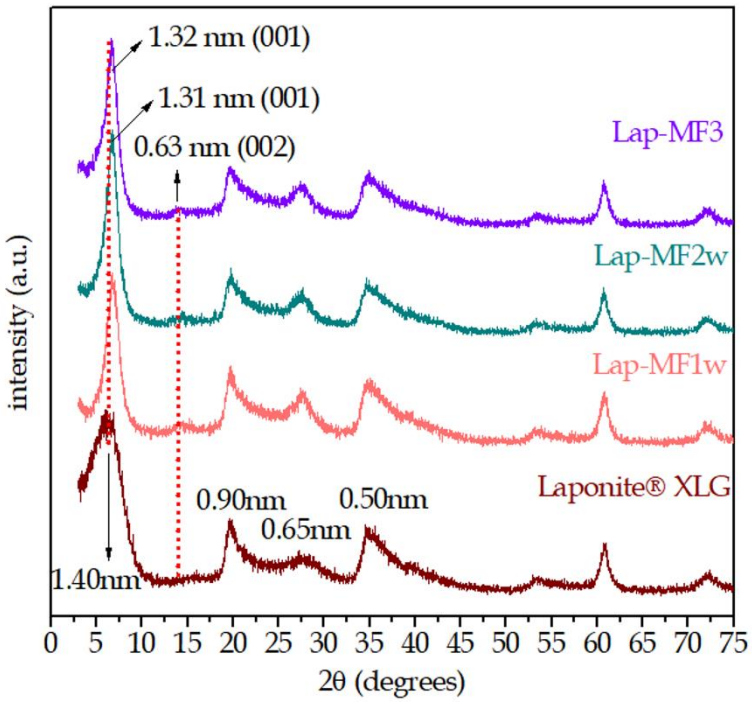

Figure 3.13. XRD patterns of pristine Laponite® XLG (Lap), Lap-MF1w, Lap-MF2w and Lap-MF3 hybrids.

Figure 3.14 shows the TG curves of pristine Lap and Lap-MF2w intercalation compounds. The neat clay mineral shows a main mass loss of 15% below 100 °C, which corresponds to the removal of water. Dehydroxylation processes occur above 600 °C in clay, taking place at lower temperature in Lap than Mt as typically occurs in hectorites (Bergaya and Lagaly, 2013). In the intercalation compounds, removal of water occurs in a similar interval of temperatures but revealing much lower content (7 % for the Lap-MF2w sample). The mass loss ascribed to the combustion of MF occurs in a very large interval of temperatures (200-650 °C) in what seems two steps, as observed in MF·HCl (see inset Figure 3.14). The amount of MF in the Lap-MF2w hybrid that can be deduced from the TG curve is approximately 11 %, which is in good accordance with the MF content deduced from the elemental chemical analysis.

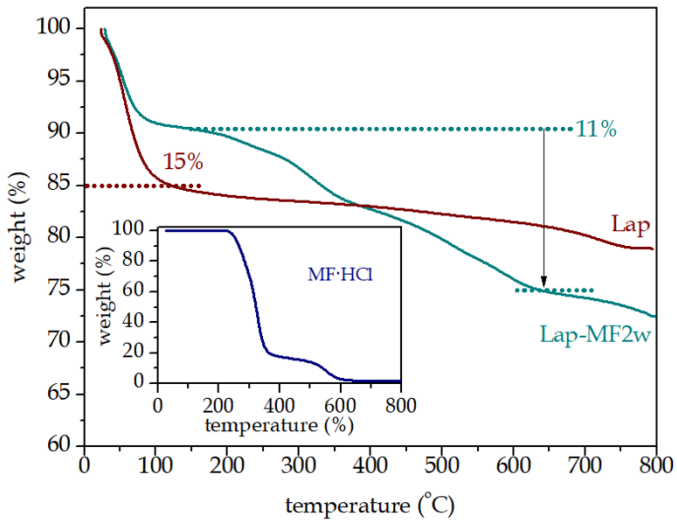

Figure 3.14. TG curves of Lap and the Lap-MF2w intercalation compound. The inset includes the TG curve of MF·HCl. Experiments carried out in air atmosphere.

The interactions between MF species and the clay substrate were studied by FTIR, as shown in Figure 3.15. The spectra of the hybrid materials show the characteristic bands of the clay and those of MF species, being observed changes in some of the bands assignable to the organic molecule The spectrum of pristine Lap shows the characteristic bands assigned to Si-O stretch vibration modes with

a maximum centered at around 1005 cm^{-1} (Ding et al., 2016). The bands in the 3700-3300 cm^{-1} region and the one at around 1643 cm^{-1} ascribed to ν_{OH} and δ_{OH} vibration modes of water molecules reveal the presence of physisorbed water in Lap (Herrera et al., 2005; Pálková et al., 2010). In the case of the hybrids, it is important to highlight the presence of bands in the region of 3370-3170 cm^{-1} corresponding to the asymmetric and symmetric stretching vibrations of N-H and the bands at 1630-1520 cm^{-1} attributed to C=N stretching and N-H deformation vibrations. Analyzing these areas in more detail, changes and displacements of all bands with respect to the ones in the spectrum of the MF·HCl are observed, confirming the interaction of the MF intercalated with the clay substrate. Since bands of MF·HCl do not appear in the spectrum of Lap-MF3 as observed in some of the Mt-MF hybrid with excess of MF it is clear evidence that in the Laponite® system the adsorption of MF on the surface external of the clay is not significant.

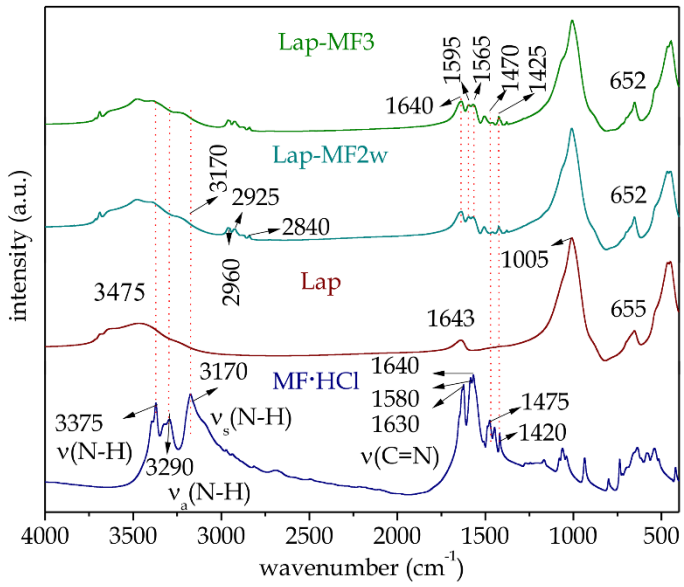

Figure 3.15. FTIR spectra of pure MF·HCl, pristine Lap, Lap-MF2w and Lap-MF3 hybrids.

3.3.2 Molecular modeling of the intercalation of MF in Lap

Laponite®-based hybrids were also simulated using the previously described molecular modeling (Chapter 2 #section 2.4), also applied to study the Mt-MF hybrids, and the model contrasted with experimental results in order to understand, at a molecular level, the interactions between MF and this new clay. In the present case the study was carried out using only DFT calculations. The replacement of Li in the octahedral sheet and the existence of a vacancy in this octahedral sheet generates a structure impedes the use of the Forcite model. Therefore, Lap-Mf hybrids were simulated using only the CASTEP model based on DFT calculations. Thus, similarly than for the DFT calculations used in Mt-MF, all species involved in the interaction process have been considered to evolve through a cation exchange mechanism. In this way, an initial Lap model was prepared taking into account its chemical composition and water content (15%) determined from the TGA experimental results, (Figure 3.14). Based on these data, a Lap 2x2x1 supercell with 30 water molecules per supercell was created and completely optimized by relaxing the atomic positions and lattice parameters, producing a (001) interlayer spacing equal to d_{001}=1.439 nm, which is close to the experimental value of d_{001}=1.44 nm (Figure 3.16A).

In the intercalation process of MF in Lap, the water content decreases to 7% in our experiments (see figure 3.14). This amount of water corresponds to 9 water molecules per the 2x2x1 supercell of our Lap model. Therefore, initially two Na^+ cations were replaced by two protonated MF cations per supercell as a cation exchange process and the intercalation complex was optimized (Figure 3.16B). The (001) basal spacing of the optimized structure is d_{001}=1.318 nm, which is coincident with the experimental value (see figure 3.13). The intercalated MF molecule remains at the center of the intercalated space with H atoms of the protonated N atoms oriented towards the tetrahedral O atoms of the mineral surface forming a monolayer of MF. The MF intercalated in Lap presents new torsion angles Table 3.3, compared to the starting MF and also with respect to MF intercalated in Mt. In addition, the bond sizes, in the case of the MF intercalated

in the Lap are greater than in the Mt-MF hybrid, it should be noted that this result may justify the different behavior of MF in the release test (see later).

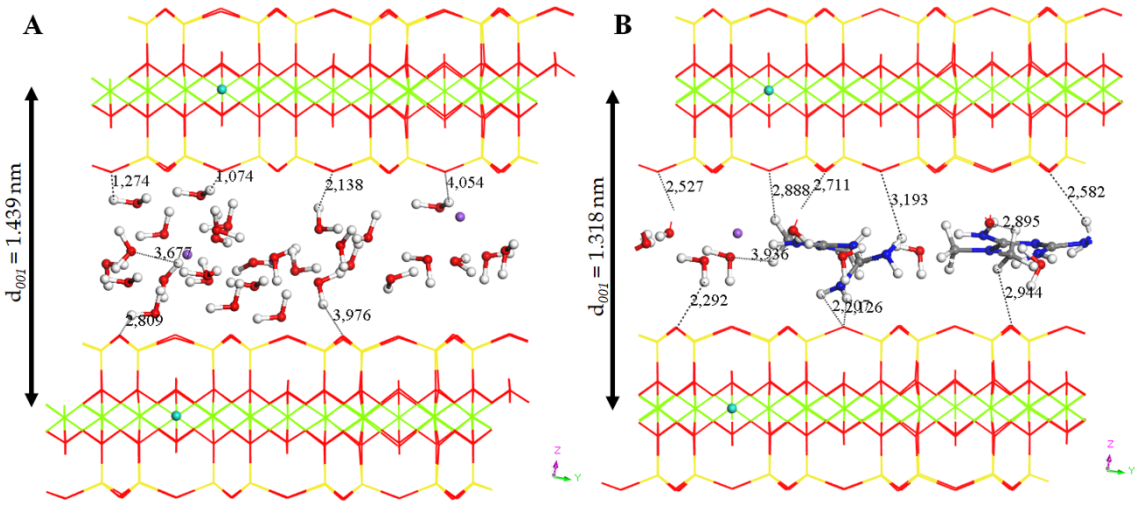

Figure 3.16. Supercell 2×2×1 of Lap intercalated with Na^+ cations with 30 molecules of water (A), and metformin cations with 9 water molecules (B) per supercell. Atoms in green are Li, highlighted in the form of a ball.

In a second stage, several amounts of MF cations were intercalated in the Lap interlayer with one and three cations per supercell. The optimization of the hybrid complex with the cation exchange of one MF cation per Na^+ yielded a basal spacing of 1.249 nm slightly shorter than the above calculated with two MF cations per supercell and close to the experimental one (Figure 3.17A). The optimization of the complex where the three Na^+ cations were exchanged with 3 MF cations per supercell showed an (001) interlayer spacing of d_{001}=1.361 nm been higher than the one found in the experimental that was d_{001}=1.31 nm (Figure 3.17B). This result indicates that the exchange of 3 Na^+ cations by MF per supercell is not likely to be produced.

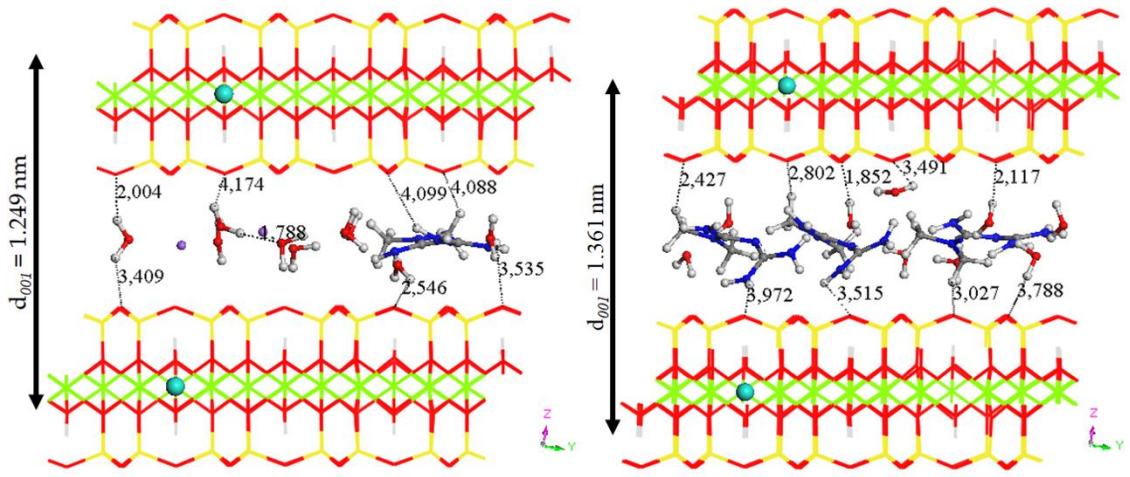

Figure 3.17. Lap structure with 2 cations of Na^+ and one MF (A) and 3 molecules of MF (B) in the 2×2×1 supercell in presence of 9 molecules of water. Atoms in green is Li, highlighted in the form of a ball.

For the adsorption energy calculations, we prepared a Lap supercell with 3 Na^+ cations with 9 water molecules (Lap-Na) optimized in the same conditions obtaining a (001) basal spacing of d_{001}=1.257 nm, shorter than the experimental value in the pristine Lap because the amount of water is lower in the calculated model. In addition, one periodical box with two MF hydrochloride ion pairs with 8 water molecules (MF_2Cl_2w8), and another one with two pairs of Na-Cl species with 8 water molecules (Na_2Cl_2w8) were optimized in the same conditions at constant volume. Hence the adsorption energy was calculated using equation (4):

$$E_{ads} = E_{Lap\text{-}MF} + E_{Na2Cl2w8} - (E_{Lap\text{-}Na} + E_{MF2Cl2w8}) \quad (4)$$

producing an energy of -60.69 kcal·mol^{-1} for the cation exchange of two MF cations per supercell. This energy is more negative than in the montmorillonite case, indicating that the adsorption can be easier in Laponite® than in montmorillonite. Similar procedure was performed for the adsorption models with the exchange of one MF cation yielding -32.1 kcal·mol^{-1}. This means that the intercalation of MF in Lap is energetically favorable.

3.4 *IN VITRO* TESTS OF METFORMIN RELEASE FROM THE METFORMIN-CLAY HYBRIDS

3.4.1 *In vitro* release of MF from MF-clay hybrids in water

For the release studies of metformin from the various hybrids prepared using Mt and Lap clays, a first study was performed putting the systems in bidistilled water at pH ≈ 5.5 for 5 h (Figure 3.18). The Mt-MF25w, Mt-MF300w, Mt-MF300, and Lap-MF2w formulations were selected for this study. The unwashed Mt-MF25 was not evaluated since its MF content is close to that of the washed sample and slightly lower than the clay CEC in both Mt-MF hybrid materials. For the Mt-MF25w hybrid, the release of the drug after 5 h is approximately 15% and then it remains constant over time. In the case of the compound Mt-MF300w the release of drug reaches a constant value of around 25% after 3 h. In both cases, the use of the washed formulations show a slower initial release than that observed for the unwashed Mt-MF300 hybrid, which releases 50% of the drug in a few minutes and then remains almost constant until the end of the experiment. This rapid release is probably due to the fact that the excess of MF associated with the external surface of the clay is easily removed in contact with water, while the release of intercalated MF, which is more strongly assembled to the support, occurs much more slowly. In the case of the Lap-MF2w hybrid, the release of MF reaches a vaule of about 25% after 3 h, similar to that found for the Mt-MF300w hybrid (Figure 3.18).

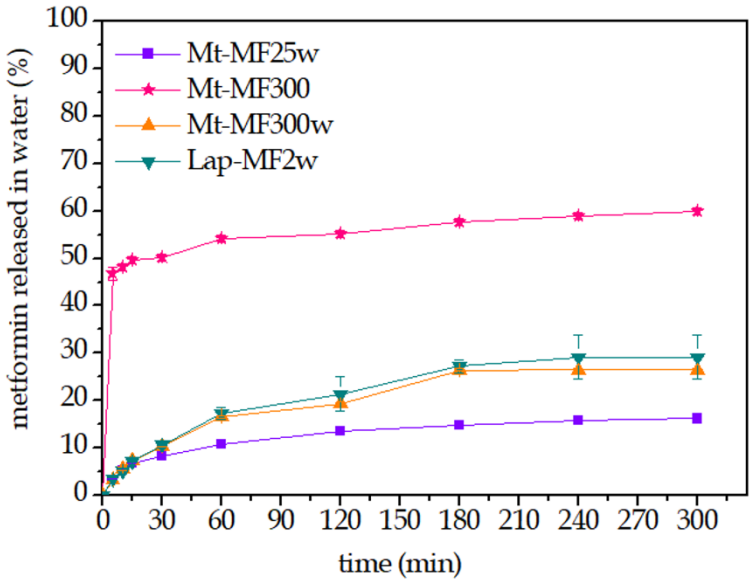

Figure 3.18. Percentage of MF released from montmorillonite and Laponite® formulations in contact with bidistilled water (pH ≈ 5.5). Error bars are not visible in this graphic due to their small value.

3.4.2 In vitro release of MF from MF-clay hybrids in simulated media of the gastrointestinal tract

The *in vitro* release of metformin from the hybrid materials based on Mt and Lap was evaluated in a simplistic manner under release conditions that simulate the sequence of pH changes when in the human body. Considering the residence time and the different pH values in each section of the gastrointestinal tract, the samples are initially maintained a pH of 1.2 for 2 h (mimicking stomach fluid), moving to pH 6.8 for 2 h (mimicking fluid from the small intestine) and changing to pH 7.4 in the last 4 h (mimicking fluids in the colon section of the intestine) (Figure 3.19). For these MF release tests, the same formulations previously evaluated in the release study carried out in water were also selected. As shown in Figure 3.19, all Mt-based formulations show a rapid initial release of MF at pH 1.2, loosing approximately 60% of the adsorbed MF in the first 2 h and reaching 80% total release at the end of the 8 h experiment. Meanwhile, the Lap-MF2w hybrid already releases the 100% of the intercalated drug in the first 2 h. This dissimilar behavior of release of metformin from the two clays may be ascribed

to some of the different characteristics of the two involved smectites such as particle size, which is lower in Lap than in Mt and may favor the more rapid kinetic release of intercalated MF, as well as a possible magnesium release in the case of Laponite® due to the low pH conditions that may alter the silicate structure, making even faster the release process. As a whole, the process of release occurring at the pH of the stomach can be explained considering the presence of H^+ ions that replace intercalated MF^+ cations following ion-exchange reactions. Despite this hostile environment, in the case of the montmorillonite systems the silicate structure seems to remain unchanged as determined by the XRD patterns recorded after the acid-media release experiment (Figure 3.20). In the case of the Laponite® systems, the characterization by XRD was not performed because practically all the drug is released in the first two hours.

The release in neutral media can also take place by ion-exchange of the remained intercalated MF with sodium ions present in the simulated intestinal fluid, being observed the release of greater amounts of MF than those determined in the above mentioned tests performed in bidistilled water (Figure 3.18). For better visualization, the amount of MF released per mg of hybrids is depicted in Figure 3.19B. These results show that the release of MF from clay minerals was not as successful as expected since in both clay-based systems the majority release of MF occurs in acidic medium, which corresponds to the conditions the formulation will find at the beginning of its travel though the digestive tract. Therefore, an additional optimization of the formulation is required and so its encapsulation in a convenient shell that may procure s adequate protection during its passage through the stomach was proposed with the aim to use the hybrid as a metformin reservoir able to afford a greater release of MF in the intestine.

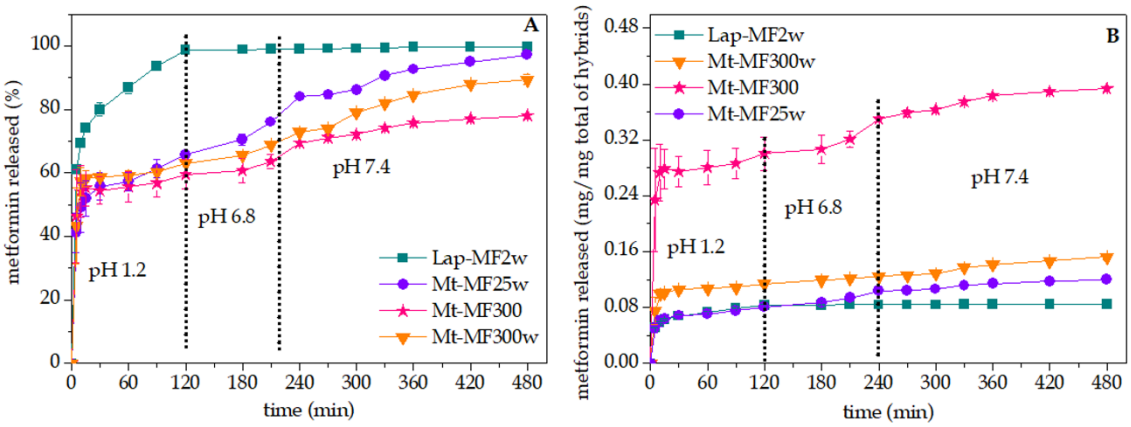

Figure 3.19. Percentage of MF released from Lap-MF2w and Mt-MFw in the simulated gastrointestinal tract pH conditions (A), and amount of MF released referred to the mass of in hybrids (B).

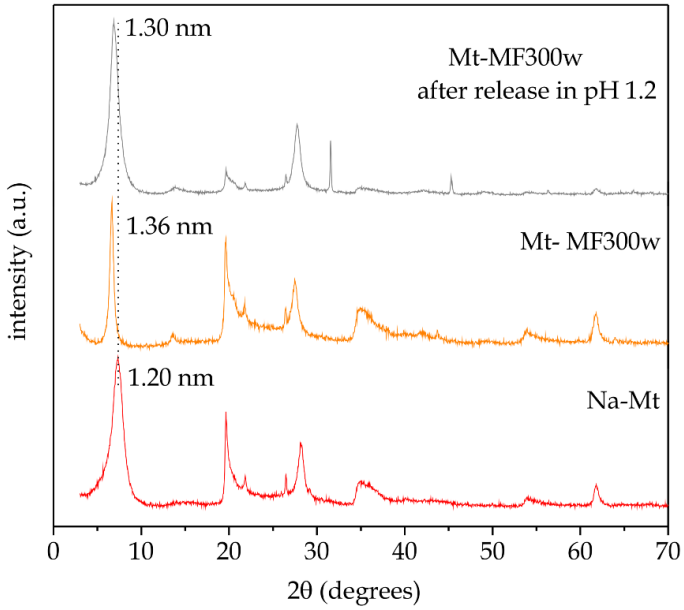

Figure 3.20. X-ray diffraction patterns of Na-Mt, Mt-MF300w and Mt-MF300w after release in pH 1.2.

3.5 BIONANOCOMPOSITE SYSTEMS BASED ON CLAY-METFORMIN HYBRIDS

As the clay-MF hybrid systems were not satisfactory formulations for application as controlled release system for oral administration of metformin they were combined with biopolymers to improve their delivery properties. Thus, new

delivery systems were designed by combining the clay-metformin hybrids with pectin and chitosan biopolymers. The approach consists on the incorporation of a montmorillonite-metformin hybrid (Mt-MF) in chitosan, forming beads that were later coated with a pectin layer in a core-shell configuration. In a second stage clay-metformin hybrids (Mt-MF300w and Lap-MF2w) were incorporated in pectin beads that were later coated with a first layer of chitosan and a second layer of pectin. As pectin is very resistant to acidic pH, the external coating will protect the drug to be release in the stomach, assuring its presence of the delivery system in the intestinal tract where metformin is absorbed. The presence of the chitosan shell can be used to increase its permanence in the gastrointestinal tract due to its mucoadhesive properties and then, the drug can be slowly released from the clay-pectin bionanocomposite.

3.5.1 Pectin@chitosan/Mt-MF bionanocomposite systems

Bionanocomposite were first prepared by dispersing the Mt-MF300w intercalation compounds in a chitosan matrix. These bionanocomposite systems were processed into beads, as explained in Chapter 2 #section 2.2 by dripping the chitosan solution in a 2M NaOH solution. Subsequently, the beads were coated with pectin to procure resistance to acid pH to the produced beads. Pectine was adsorbed onto the bionanocomposite beads from solutions of the biopolymer dispersed at 0.5, 1 and 1.5% w/w in water. For comparison, analogous core-shell beads were prepared but incorporating pure MF·HCl in chitosan instead of the clay-MF hybrid. Additionally, core-shell beads incorporating the Mt-MF300 hybrid in chitosan were coated with the 0.5% pectin dispersion. Table 3.5 shows the amount of MF loaded in the beads as well as the efficiency of the encapsulation in each system. The systems incorporating the pure drug (CHT/MF) have a lower loading and efficiency of encapsulation compared to the materials loaded with the Mt-MF hybrids , showing only encapsulation efficiency values of 25.0, 29.5 and 31.8%, for the system prepared for incorporating 0.1, 0.3 and 0.5 g of metformin, respectively. This result may be

related to the fact that though MF·HCl is a neutral specie if they are dissociated the protonated MF species may suffer scarce affinity and even electrostatic with the biopolymer, making difficult to increase the loading of drug into the chitosan matrix. In fact, the increase of the starting amount of MF added to chitosan does not result in an increase of the drug loading. Therefore, 0.1 g of MF was used as reference to prepare the other bionanocomposite systems. In the case of incorporate the MF stabilized in the hybrid Mt-MF300w it is possible to load a large amount of drug with encapsulation efficiencies close to 60% independently if the bead contains just chitosan or if it was later on coated with different amounts of pectin, indicating the good stability of the chitosan-hybrid bionanocomposite system. The system prepared using the non-washed hybrid (Mt-MF), with MF content about three times higher than that of the Mt-MFw hybrid, showed a very close encapsulation efficiency (60.9%), which suggests that the use of clay-based hybrids with large excess of drug adsorbed on the external surface of the clay is not necessary.

Table 3.5 Encapsulation efficiency and relative content of MF loaded in the beads of MF, either as pure drug or as Mt-MF, in different polymer systems.

Formulation	**MF loaded (%)**	**Encapsulation efficiency (%)**
CHT/MF0.1	2.5 ± 0.2	25.0 ± 0.8
CHT/MF0.3	1.9 ± 0.4	29.5 ± 1.0
CHT/MF0.5	1.2 ± 0.5	31.7 ± 0.6
CHT/Mt-MF300w	5.8 ± 0.2	58.2 ± 0.8
PEC0.5%@CHT/Mt-MF300w	5.7 ± 0.1	56.8 ± 1.0
PEC0.5%@CHT/Mt-MF300	6.1 ± 0.3	60.9 ± 1.0
PEC1%@CHT/Mt-MF300w	5.7 ± 0.2	57.3 ± 0.9
PEC1.5%@CHT/Mt-MF300w	5.7 ± 0.2	57.5 ± 1.2

Figure 3.21 shows SEM images of the surface and interior of a PCT@CHT/Mt-MF bionanocomposite bead. In the cross-section image it is possible to distinguish the pectin coating covering CHT/Mt-MF bionanocomposite core. The externa surface of the bead is fairly homogeneous and smooth while the interior presents a quite homogeneous and porous pectin layer over a more compact and bulky material in the bionanocomposite core. The CHT/Mt-MF bionanocomposite is very homogeneous without segregation of phases where the Mt-MF300w hybrid could be agglomerated, confirming the good dispersion of the hybrid in the polymer matrix. The two biopolymers phases seems to be in good interaction confirming the adherence between these two biopolymers already reported in other works (Ribeiro et al., 2014a; Chinnaiyan et al., 2019).

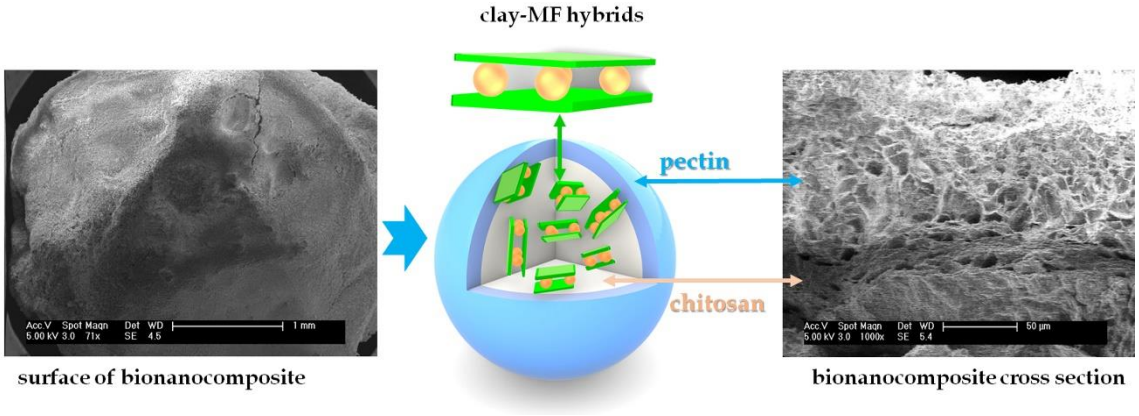

Figure 3.21. SEM images of the external surface and cross-section of PEC@CHT/Mt-MF300w bionanocomposite beads, together with and schematic illustration of the core-shell configuration.

Figure 3.22 shows the FTIR spectra of the pure biopolymers as well as of beads with and without the pectin coating. In the spectrum of chitosan (Figure 3.22b) are clearly defined the characteristic bands of amide II and amine at 1650 and 1585 cm^{-1}, respectively. The bands appearing at 2925 and 2875 cm^{-1} can be assigned to ν_{C-H} vibration modes and those between 3400 and 3300 cm^{-1} to ν_{N-H} and ν_{O-H} vibration modes of functional groups in the biopolymer (Domszy and Roberts, 1985; Negrea et al., 2015). In the spectrum of the CHT/Mt-MF beads, the bands ascribed to amide II and amine groups, which appear in pure chitosan at

1660 and 1580 cm^{-1}, respectively, are no longer appreciated in the CHT/Mt-MF beads, which is related to the δ_{NH2} inversion modes due to an almost complete deprotonation of the chitosan amine groups during the beads formation process (Ribeiro et al., 2014b). Moreover, in the CHT/Mt-MF bionanocomposite spectrum (Figure 3.22d) are observed bands at 1075 and 950 cm^{-1} bands attributed to characteristic vibration modes of the montmorillonite structure, confirming the presence of the clay mineral (ν_{Si-O} and δ_{OH}) (Madejová and Komadel, 2001). The spectra of the CHT/Mt-MF bionanocomposite beads coated with pectin (figure 3.22c, d and e) present similar profiles to that of the neat beads except for some additional bands that could be ascribed to the presence of pectin. In the spectrum of pectin (Figure 3.22a) are clearly defined bands at 1750 and 1620 cm^{-1}, attributed to the $\nu_{C=O}$ vibration mode of carbonyl ester groups and to the symmetric and antisymmetric stretching vibration of carboxilic groups, respectively (Gnanasambandam, 2000; Synytsya, 2003). However, in the spectra of the beads covered with the pectin coating (Figure 3.22c, d and e) it is appreciated a unique band at 1640 cm^{-1} probably due to the blocking of the carboxylic groups once crosslinked by Ca^{+2} during the process of formation of the bead.

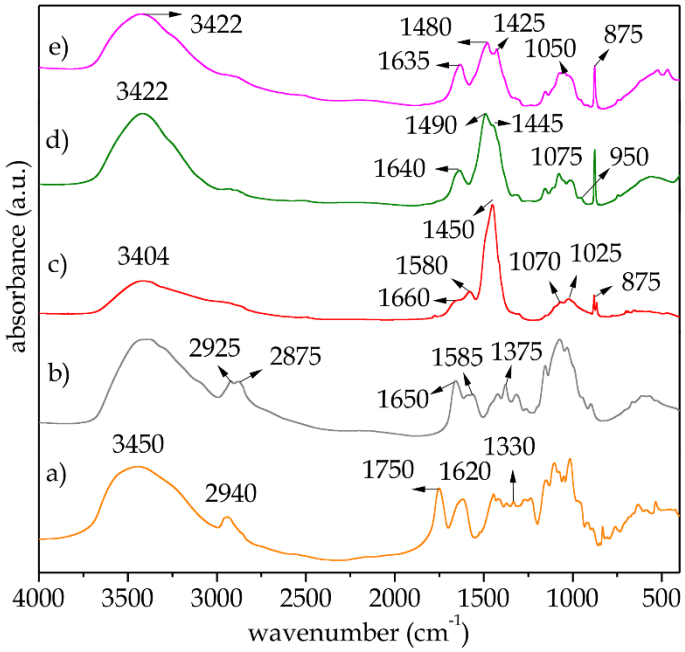

Figure 3.22. FTIR spectra of PEC (a), CHT (b), CHT/Mt-MF (c), PEC@CHT/MF (d) and PEC@CHT/Mt-MF (e).

3.5.1.1 Water absorption properties of the beads

For controlled drug release applications, it is important to study the water uptake capacity and swelling properties of the beads. Thus, these parameters were evaluated in the different prepared systems using aqueous media at pH 1.2 and 6.8 corresponding to a HCl solution and phosphate buffer, respectively. Figure 3.23 shows the evolution in the content of water absorbed by the beads as a function of their time in contact with the aqueous media. It is observed that water uptake of the different beads strongly depends on the pH of the medium. At pH 1.2 (Figure 3.23 graphic on the left), chitosan beads directly incorporating MF·HCl shows a fast water uptake, and in just 10 minutes of contact the absorbed water is enough to produce the disintegration of the beads making impossible to continue the measurements. In previous studies, this behavior was explained considering the ability of the amino groups in chitosan t to become easily protonated, provoking the gradual dissolution of the biopolymer till the complete disintegration of the beads (Ribeiro et al., 2014). However, when the chitosan beads is covered with a pectin coating, the stability in the presence of

that large amount of H^+ increases and all the beads show lower absorption of water without their complete disintegration within the time set for the experiment. The uptake of water is reduced in core-shell beads incorporating the bionanocomposite in the core, probably due to a physical crosslinking effect within the hybrid component and the chitosan matrix as there are not relevant differences between beads with different pectin coatings.

Figure 3.23 (graphic on the right) shows the evolution of water uptake in various types of beads immersed in the phosphate buffer at pH 6.8. In this case, beads CHT/MF and CHT/Mt-MF prepared just with chitosan exhibit the greatest stability with very similar swelling profiles. However, the pectin-coated systems shows larger uptake of water probably affected by the presence of phosphate ions in the medium that can favor the release of Ca^{+2} ions acting as crosslink points of pectin chains in the bead (Remunan-López and Bodmeier, 1997). From the results of these water uptake experiments it is confirmed that the pectin coating in the beads is crucial to protect the chitosan core from became fast disintegrated in low pH conditions as that of the stomach, allowing the beads to reach the gastrointestinal tract where the drug can be release upon a fast and progressive uptake of water by the bead favored by the presence of the pectin coating.

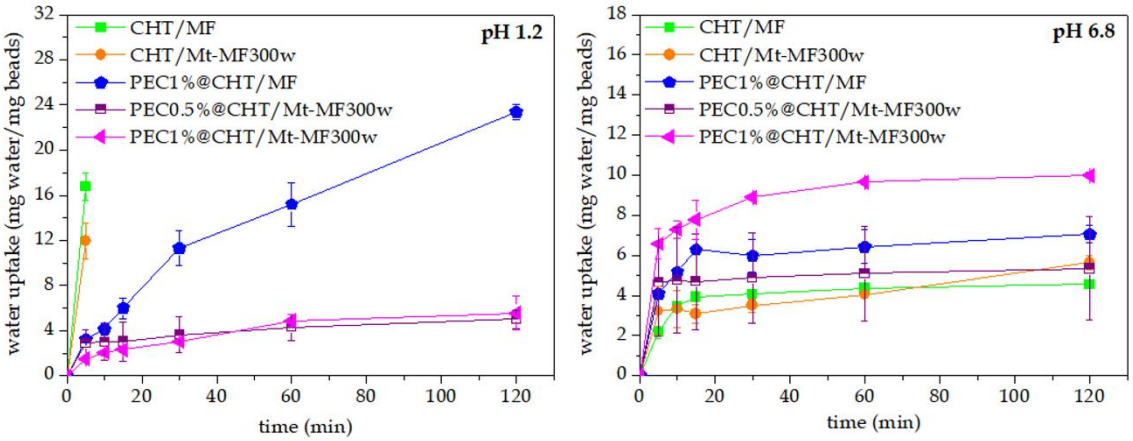

Figure 3.23. Water uptake of various types of beads immersed in water at pH 1.2 (HCl 0.1 M) and pH 6.8(phosphate buffer). Each value is the mean ± S.D. n = 3.

3.5.1.2 In vitro tests of the release of metformin from the beads

The *in vitro* release tests of the various prepared beads were carried out simulating the the sequence of pH conditions that the formulation would follow along its passage through the gastrointestinal tract (Figure 3.24).

Firstly it was analyzed the system based on the direct incorporation of MF·HCl in the beads showing that in the case of the CHT/MF beads the drug was completely released in the first two hours (Figure 3.24). This result was already expected because chitosan is not resistant to acid pH as shown in the previous water uptake study. The core-shell beads in which the chitosan bead was further coated with pectin show a higher resistance at low pH, obtaining a more controlled release over the 8 hours of the experiment (Figure 3.24).

When comparing core-shell incorporating a clay-MF hybrid in the chitosan core the release of metformin depends on the characteristics of the bionanocomposite that forms the core and also the thicknes of the pectin coating. Thus, the bead incorporating in the core the bionanocomposite prepared from the unwashed hybrid (PEC0.5@CHT/Mt-MF300), presents a fast initial release at pH 1.2 with about 40% of the metformin liberated in those conditions, reaching after the 8 h a total release of 80%. The large amount of MF released at the stomach pH may be associated with the presence of drug within the biopolymer matrix coming from MF released from that adsorbed at the external surface of the clay in the Mt/MF300 hybrid during the bead preparation. Although the PEC0.5%@CHT/Mt-MF300 beads exhibit an initial release greater than the washed hybrid, the release is gradual in comparison with the Mt-MF300 hybrid alone (Figure 3.19). In contrast, the PEC0.5@CHT/Mt-MF300w bead shows a more controlled release with a about the 20% liberated at the stomach conditions but a really progressive and continuous release following the squence of pH conditions in the intestinal tract till a practically complete MF release upon the 8 h of the experiment. When the beads present a thicker coating of pectin, i.e., those prepared using pectin solutions of concentration 1 and 1.5% (PEC1%@CHT/Mt-MF300w and PEC1.5%@CHT/Mt-MF300w beads, respectively) it is possible to reduce further the release of metformin at the pH conditions of the stomach.

However, the release in the conditions of the intestine is also slowered, reaching in both cases upto a 60% of liberated MF at the end of 8 hours experiment.

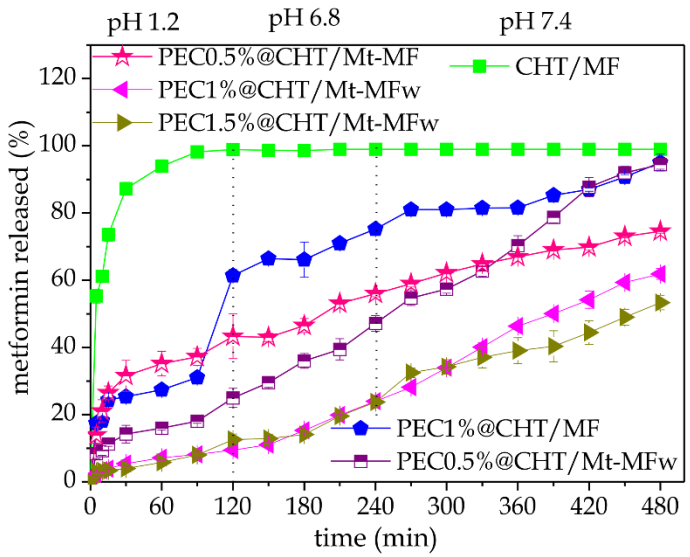

Figure 3.24. Profiles of the *in vitro* release of metformin (MF) from various types of beads incorporating MF·HCl or Mt-MF hybrids into chitosan with and without a pectin coating. The experiment simulates the pH conditions that occur in the passage through the gastrointestinal tract (pH and residence time) and was carried out at 37 °C. Each value is the mean ± S.D. n = 3.

3.5.2 Pectin-chitosan@pectin/clay-MF bionanocomposite systems

Given that all the prepared beads of the pectin@chitosan/clay-MF system showed an encapsulation efficiency below 60%, it was further explored other alternative biopolymer-based systems in order to increase the amount of entrapped drug. To improve the approach, it was considered that the possible reason of the low encapsulation efficiency values found in the pectin@chitosan systems could be due to a partial replacement of the intercalated MF by the protonated chitosan chains during the preparation of the bionanocomposite. In order to overcome this problem, it was explored the preparation of the bead core from bionanocomposites of the clay-MF hybrids in a pectin matrix, then produce a double coating of the bead, first with chitosan and at the exterior with pectin. As pectin is an anionic polymer it is expected that during the preparation of the

bionanocomposite it will not compete with the intercalated MF molecules producing a partial release from the hybrid.

In the present study it was developed beads based on the hybrid Mt-MF300w previously investigated in the pectin@chitosan beads and also one of the hybrids based on the incorporation of MF in Laponite® clay (Lap-MF2w). Both intercalation materials were so dispersed in a pectin gel and processed as beads as detailed in Chapter 2 #section 2.2.1, then the beads were first coated with chitosan coating, and finally with an external coating of pectin, using in both cases biopolymers solution at a concentration of 0.5% w/w. The idea is that the double coating will give the systems greater stability at the acidic pH (first zone of the gastrointestinal tract) due to the pectin that will be progressively dissolved in the conditions of the intestinal tract and then the chitosan coating will provide mucoadhesive properties while the bead is desintegrated and metformin is liberated from the pectin core.

Table 3.5 shows the loading drug and the encapsulation efficiency values for all the prepared pectin-core based beads. All these materials show higher encapsulation efficiency than the systems prepared with chitosan. For instance, the encapsulation of the pure drug in chitosan (CHT/MF) gave rise to values of 25% for, while almost a 70% of encapsulation efficiency was reached in pectin (PEC/MF). The PEC/Mt-MF300w and PEC/Lap-MF2w beads exhibit very good encapsulation efficiency reaching values of 87 and 91%, respectively, clearly also higher than when using encapsulated the MF·HCl. As in the chitosan system, this result may be associated with the protective effect exerted by the clay minerals, where the drug is protected within the sheets of the mineral. Here again, the encapsulation efficiency of pectin beads and the core-shell system is practically the same, confirming there is not loss of drug during the coating of the beads to produce the shell.

Table 3.5 Encapsulation efficiency and amount of MF loaded, either as pure drug or as clay-based hybrids, in different polymer systems.

Formulation	MF loaded (%)	Encapsulation efficiency (%)
PEC/MF	6.9 ± 0.4	69.3 ± 1.1
PEC/Mt-MF300w	8.7 ± 0.3	87.3 ± 0.9
PEC@CHT@PEC/Mt-MF300w	8.6 ± 0.2	86.2 ±0.8
PEC/Lap-MF2w	9.1 ± 0.9	91.1 ± 1.1
PEC@CHT@PEC/Lap-MF2w	9.0 ± 1.2	90.0 ± 1.2

Figure 3.25 shows images of the morphology of various beads encapsulating MF·HCl and the Mt-MF300w hybrid in just pectin and also this las one but after the double coating with chitosan and then with pectin. It is clear that the freeze-drying process produce certain deformation of the spheres but all of them show a very homogeneous aspect. When observed the surface of the beads by FESEM it is confirmed that they are quite smooth and do not present polymer agglomerates. Specially, in the case of the PEC/Mt-MF300w beads it FESEM images (Figure 3.25b) shows the Mt-MF300w hybrid is homogeneously dispersed in the pectin matrix and the external surface of the bead does not show practically any roughness or cracking confirming an excellent integration of the hybrid between the biopolymer matrix. In Figure 3.25c it is shown a cross-section of a PEC@CHT@PEC/Mt-MF300w bead, being possible to distinguish in more detail the two layers of the coating (chitosan sandwiched between the external pectin coating and the internal pectin bionanocomposite core). The three phases are very homogenous though show different type of roughness probably ascribed to the presence of porosity created during the lyophilization process used to produce the final bead.

.

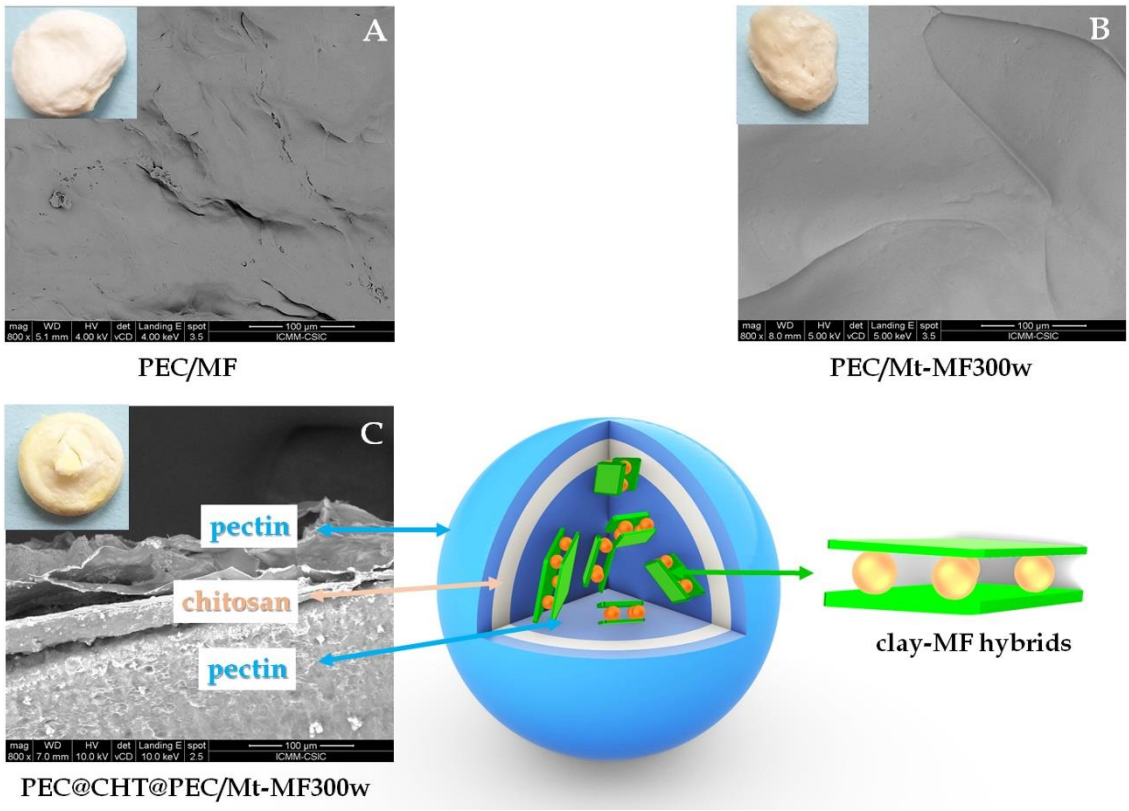

Figure 3.25. FESEM images of the external surface of PEC/MF (A), PEC/Mt-MF300w (B) and a cross-section of the PEC@CHT@PEC/Mt-MF300w (C) bionanocomposite beads.

3.5.2.1 Water adsorption properties of the beads

Swelling and water absorption properties of the prepared beads was evaluated I aqueous media at pH 1.2 and at pH 6.8, corresponding to a HCl solution and phosphate buffer, respectively. Figure 3.26 shows the evolution in the content of water absorbed by the beads as a function of their time in contact with the aqueous media, revealinga different behavior chitosan-based beads (Figure 3.23). In the present case it is clearly observed that at pH 1.2 all the beads present a rapid uptake of water that after 5 minutes remain constant, reaching water uptakes values upto 10%. This result was expected because pectin spheres had greater stability in the presence of acidic pH, as discussed in the previous study. Here again, the maximum uptake corresponds to the beads prepared with MF·HCl though in the present case the beads do not completely desintegrate. The lower uptake of water corresponds to the beads based on pectin and the hybrids,

being larger in the bionanocomposite based on the Laponite® clay. This effect may be associated with the good synergy between biopolymer/clay improving its properties, offering greater resistance to swelling of the bead. Besides, this is supported by the SEM images (Figure 3.24b), where it is observed that the bead of PEC/Mt-MF300w is quite compact, with practically no porosity and cracking. The beads containing the double coating show higher water uptake though in this case the water directly intereact with pectin insteead of the bionanocomposite, which confirms the existence of intereactions between pectin and the hybrid in the prepared bionanocomposites.

An interesting result is observed in the study of water absorption test carried out at pH 6.8. At previously indicated (#section 3.5.1.1), in this medium pectin begins to disintegrate due to the presence of phosphate ions in the solution, which capture the calcium ions acting as bridges between the polymer chains and facilitates the increase of water uptake. Here again the highest water uptake corresponds to the beads incorporating the MF·HCl in pectin. However when compared the beads prepared just with pectin and the two hybrids the one involving the motmorillonite intercalation compound is again the most stable but the one based on Laponite® shows water uptakes higher than the double-coated beads. This result confirms clearly that though the presence of clay hybrid may reduce the water intake in the bionanocomposite systems the nature of the hybrid determine different swelling properties, probably related to the degree of physical crosslinking effect of the dispersed phase in the biopolymer matrix. Based on these results of the low swelling of the systems at both 1.2 and 6.8pHs, the thernary core-shell beads can be proposed as promising system for the release of metformin, and as the chitosan coating may be preserved until it reaches the gastrointestinal tract it will be possible to useits mucoadhesive properties to favour a better adsorption of metformin.

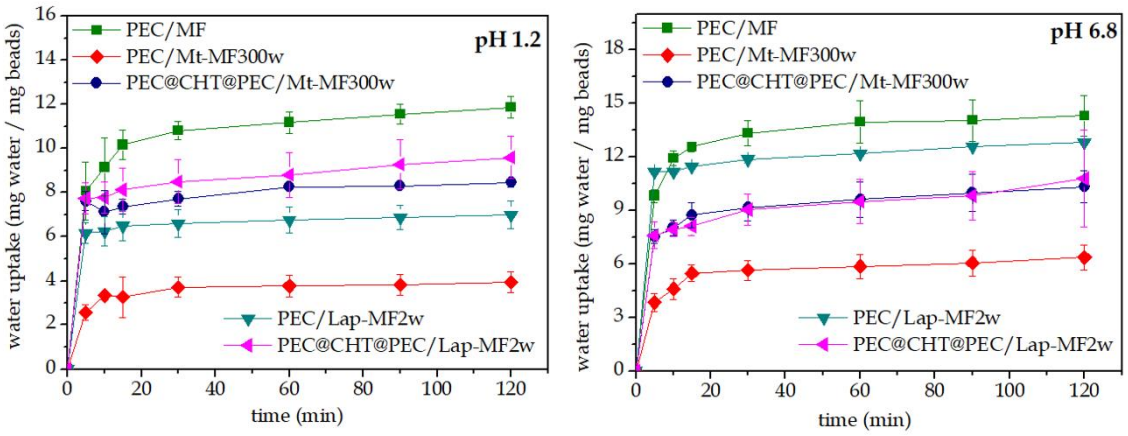

Figure 3.26. Water uptake of various types of beads beads immersed in water media at pH 1.2 (HCl 0.1 M) and pH 6.8 (phosphate buffer). Each value is the mean ± S.D. n = 3.

3.5.2.2 In vitro tests of the release of metformin from the beads

Firstly it was analyzed the system based on the direct incorporation of MF·HCl. The *in vitro* release tests of the various prepared beads were carried out similating the sequence of pH conditions that the formulation would follow along its passage through the gastrointestingal tract (Figure 3.27). The beads prepared from pectin incorporating MF·HCl exhibit an initial release of about 40% at pH 1.2, releasing 100% MF at pH 6.8 in the conditions that simulat the first zone of the gastrointestinal tract. Thus the PEC/MF system is much more satisfactory than the one encapsulating the MF in CHT (CHT/MF) which releases all the drug in approximately 60 min in the pH 1.2 medium. For the systems incorporating the clay-MF hybrids, i.e., PEC/Mt-MF300w and Lap-MF2w, the release at pH 1.2 is considerably reduced (Figure 3.27), specially for the system based on the montmorillonite hybrid. This behaviour can be related to the presence of the clay that reduces the swelling capacity, as observed in the water uptake study (#section 3.5.2.1), the different protection afforded by the host inorganic solid in the intercalation compounds explaining the differences in the release reached in this medium. Once in the medium at pH 6.8 the presence of phosphate anions capture the calcium ions serving as bridges to crosslink the biopolymer and the drug is libered at a quite constant rate, reaching 100% of MF released in approximately 6 hours. I the case of the double-coateed core-shell

beads, PEC@CHT@PEC/Mt-MF300 and PEC@CHT@PEC/Lap-MF2w, both systems shows a quite similar behaviour with a initial slow kinetic in the release in the acidic medium, which corroborates the protective effect exerted by the external pectin coating. In these systems, a significant slow release rate is kept at the high pH values, 6.8 and 7.4, providing a controlled release of MF alone the whole gastrointestinal tract.

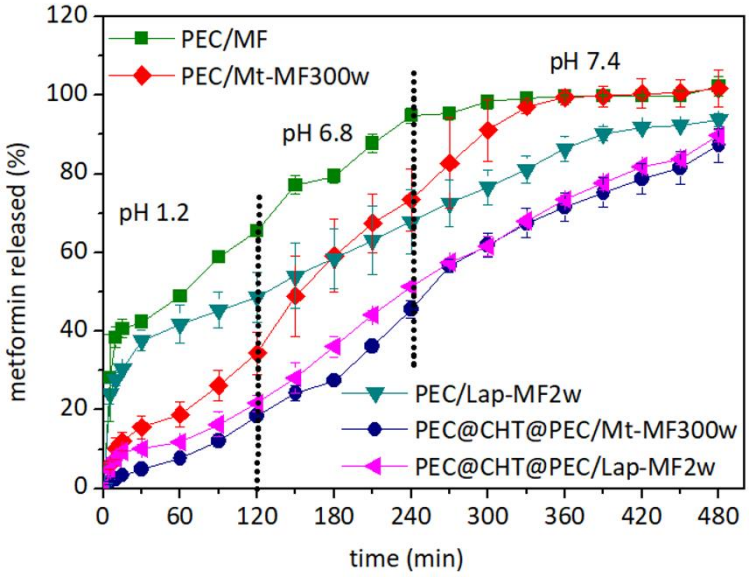

Figure 3.27. Profiles of the *in vitro* release of metformin from various types of beads based on a pectin core and protected or not with a double coating of chitosan and pectin. The experiment simulates the pH conditions that occurs in the passage through the gastrointestinal tract (pH and residence time) and was carried out at 37°C. Each value is the mean ± S.D. n = 3.

3.6 CONCLUDING REMARKS

This chapter reports a comparative study on the suitability of two lamellar clays, a synthetic hectorite and natural montmorillonite, as supports for the controlled release of metformin, the most used drug for the treatment of type II diabetes. Metformin was intercalated in both clays following an ion exchange mechanism and may led to hybrid materials with intercalated quantities that coincide with the CEC of each clay. The computational methods confirmed the experimental results, giving rise to basal spacing (001) similar to the experimental ones, 1.36

nm for the Mt-MF300w hybrid and 1.31 nm for the Lap-MF2w hybrid. The calculations indicate an energetically favorable cation exchange reaction with MF forming a monolayer in the space between layers of both clays. According to the calculations result more favorable adsorption energy values for Lap than Mt, that is, the intercalation process is more favorable for producing the Lap-MF hybrid. The resulting hybrid materials were studied as new release systems for controlled oral administration of MF. The tests carried out in simulated gastrointestinal media indicate the controlled release of MF was not as successful as expected due to a high amount of drug liberated at pH 1.2, conditions of the first zone of the gastrointestinal tract. To improve the control in the MF release, the intercalation compounds were encapsulated in two core-shell systems based on chitosan and pectin, designed to combine the advantages of the three components, pectin, chitosan, and clays:

(i) the outer pectin coating will protect the DDS in acidic media, in the first zone of the gastrointestinal tract (stomach);
(ii) the chitosan matrix, used as encapsulating matrix or as protective coating on pectin beads, will provide the DDS with mucoadhesive properties of interest for specific adsorption in the intestinal tract; and
(iii) the incorporation of the drug intercalated into the layered clay will offer the possibility of controlling the kinetics of drug release when the biopolymeric matrix was degrading.

The first core-shell system studied consists in the incorporation of a Mt-MF intercalation in a chitosan matrix prepared as a bead that was further coated with a pectin layer, e.g., PCT@CHT/Mt-MF300. *In vitro* test of MF release in fluids simulating the changes in pH and residence time that occur during the *in vivo* passage of the drug through the gastrointestinal tract demonstrated higher efficacy of those core-shell bionanocomposite systems than those based solely on chitosan or on the direct incorporation of the drug without the Mt host. Another important factor is that the release kinetics can be controlled by adjusting the thickness of the pectin coating. However, the encapsulation efficiency of these all

system with chitosan core is relatively low, which may be due to a partial replacement of the intercalated drug by the positively charged chitosan chairs.

This drawback in the use of chitosan for preparing the bionanocomposite core of the beads led to design a more complex core-shell system based on the use of pectin as biopolymeric matrix of the core in the beads. Thus, the new systems consist in the preparation of beads of pectin incorporating MF·HCl or a MF-clay hybrid (Mt-MF300w or Lap-MF2w), which were coated first with a chitosan layer and then with an external pectin coating. This second configuration has proven to be more efficient as controlled drug delivery because it is able to encapsulate around 90 % of metformin in contrast to the upto 60 % reached in the first system preparations. In addition, the second configuration provides a very slow release at low pH, allowing to deliver most part of metformin in the intestinal tract, as it is desired for this drug.

These results may be of special relevance to prepare appropriate formulations for the controlled oral administration of this medicament, this will allow the ingestion of lower amounts than those usually indicated to obtain an optimal therapeutic effect. With the proposed bionanocomposite controlled drug delivery system (CDDS), the residence time of MF in the intestinal region could be increased and, consequently, its efficiency may be higher, avoiding also many of the common side effects. In addition, the possibility of including more specific functionalities in the chitosan and/or pectin could be exploited to make the release location even more specific depending on the disease to be treated with metformin, for instance, in those cases where it is used as a targeted delivery will be preferred. The advantages of these bionanocomposites for application as CDDS are their availability, biocompatibility, biodegradability and low cost, which make them a very promising approach for the treatment of different diseases.

CHAPTER 4

ANIONIC CLAYS AS NANOPLATAFORM FOR CONTROLLED DELIVERY OF ALLANTOIN

This chapter presents a study based on the use of layered double hydroxides and layered single hydroxides involving different metals (Mg, Zn or Cu) as substrates for stabilizing allantoin. Allantoin is a compound of natural origin that can be synthetically produced, being widely used as a component of numerous cosmetic and pharmaceutical compounds due to its properties to promote healing and regenerate the skin. In this Chapter it has been explored the association of this molecule with hydroxide layered solids, mainly in the presence of Zn, seeking to increase its stability and control its action in various applications for improving its effectiveness compared to the formulations existing in the market today. In this sense, the release properties of these materials were evaluated in a phosphate saline solution, simulating the skin pH (≈ 5.5), conditions in which the hydroxide may slowly dissolve. Likewise, these hybrid allantoin systems were also incorporated in a polymer matrix (hydroxyproplymethylcellulose (HPMC), agar and nanocellulose), evaluating their activity against bacteria cultures on agar plates in view to their possible application as wound dressings.

4.1 INITIAL CONSIDERATIONS

Allantoin, also known as (2,5-dioxo-4-imidazolidinyl) urea o 5-ureidohydantoin, is produced by many animals and plants, being for instance extracted from aloe vera or from snail's slime (Fu et al., 2006; Akena Fine Chemicals S.r.l., 2012; Xu et al., 2015) (Figure 4.1), and it can be also synthetically produced in large amounts from the chemical reaction between urea and glyoxylic acid (Becker et al., 2010). Allantoin is used by its medical properties for more than 70 years, especially in dermatology to treat skin problems such as irritations, burns, ulcerations, etc(Loren, 1995; Fu et al., 2006; Araújo et al., 2010). Allantoin is used in a wide variety of cosmetic products, such as creams and foams of shaving and post-shave products, shampoos, lipsticks, toothpaste, moisturizing lotions (body or facial), bar soaps, after sun creams, post depilatory cosmetics (Becker et al., 2010). Also, in dermatology for the treatment of burns, resistant ulcers, seborrhea, ichthyosis, psoriasis, and other dermatological conditions, as it is a very versatile and highly effective product. One of the most important properties of allantoin is its keratoitic action, stimulating the desquamation of the skin, that is, it has a great capacity to cause a cutaneous renewal and, in this way, to refine the most superficial layer of human skin acting like a mild exfoliation. And at the same time, this epidermal regeneration collaborates in the formation of collagen, the dermal fiber responsible for giving support to the skin (Fu et al., 2006). Another important characteristic of allantoin is its high power to act as a restructuring agent in the cornea layer due to its soothing and anti-irritant properties, promoting healing and acting as a very mild natural anesthetic (Fu et al., 2006). Allantoin can also promote the healing of internal tissues by inducing cell proliferation, for instance promoting tissue repair in the whole gastrointestinal tract (Fu et al., 2006; Xu et al., 2011).

Recent studies have shown that the properties of allantoin could be enhanced through the formation of complexes with different metals such as zinc, copper or silver among others (Margraf, 1974; Loren, 1995; Xu et al., 2015). There are also some studies where allantoin was incorporated into porous

silice/polycaprolactone nanofiber materials to obtain controlled release systems of allantoin (Ke et al., 2016). As described, the association of this molecule with an inorganic solid or in polymers, or even the formation of complexes allows to increase its stability, improving its properties and controlling its action in various applications. Thus, in this Thesis, the intercalation of allantoin in layered hydroxides systems from different salts and precursor metals has been proposed with the aim of forming hybrid materials that could show greater efficiency compared to the formulations existing today in the market. Likewise, the incorporation of these allantoin hybrid systems in a polymer matrix (agar, HPMC or nanocellulose) was discussed, evaluating their activity against bacteria cultures on agar plates, in view to their possible application as wound dressings, facial masks, etc.

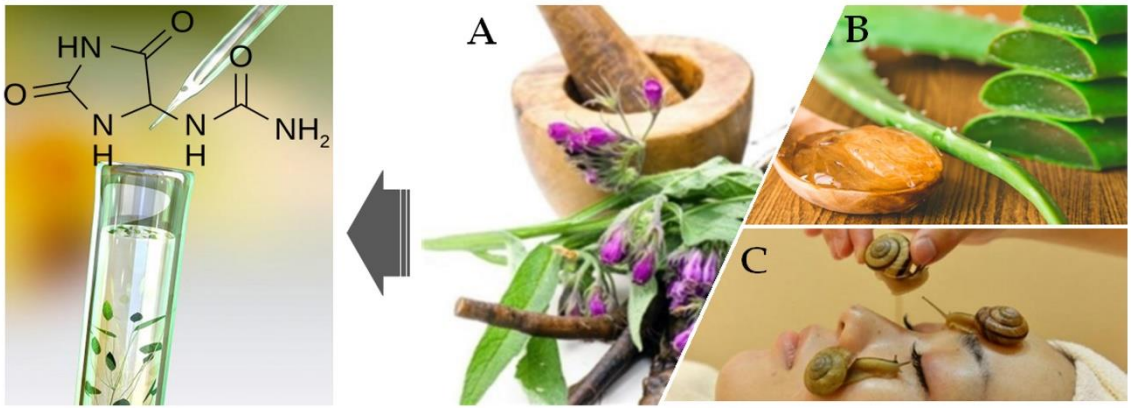

Figure 4.1. Main natural sources of allantoin: comfrey (Symphytum officinale) (A), aloe vera (B) and snail slime (C).

4.2 ALLANTOIN:MgAl-LDH

Allantoin is a nitrogenous amphoteric molecule derived from hydantoin, with a zeta potential of -20.23 ± 1.21 mV, determined in this work with a NanoBrook 90Plus PALS from Brookhaven Instruments, using the BI-ZEL electrode, in water. Hydantoins are considered weak acids and for the maximum relocation of the conjugate anion charge to occur, being the first deprotonation at the nitrogen N2 (pKa ≈ 8.5) (Oliveira et al., 2008), as shown in Figure 4.2. But allantoin may exist

in solution as a tautomeric mixture of ketonic and enolic forms in equilibrium, as shown in Figure 4.2B (Becker et al., 2010). Figure 4.2 also shows that allantoin is neutral at acid pH and presents several deprotonated species at pH higher than ≈ 9, as observed in the simulation obtained with the MarvinSketch software 6.1.5. Therefore, this anionic species may intercalate inorganic solids such as layered double hydroxides (LDH), also known as anionic clays, showing anion exchange properties.

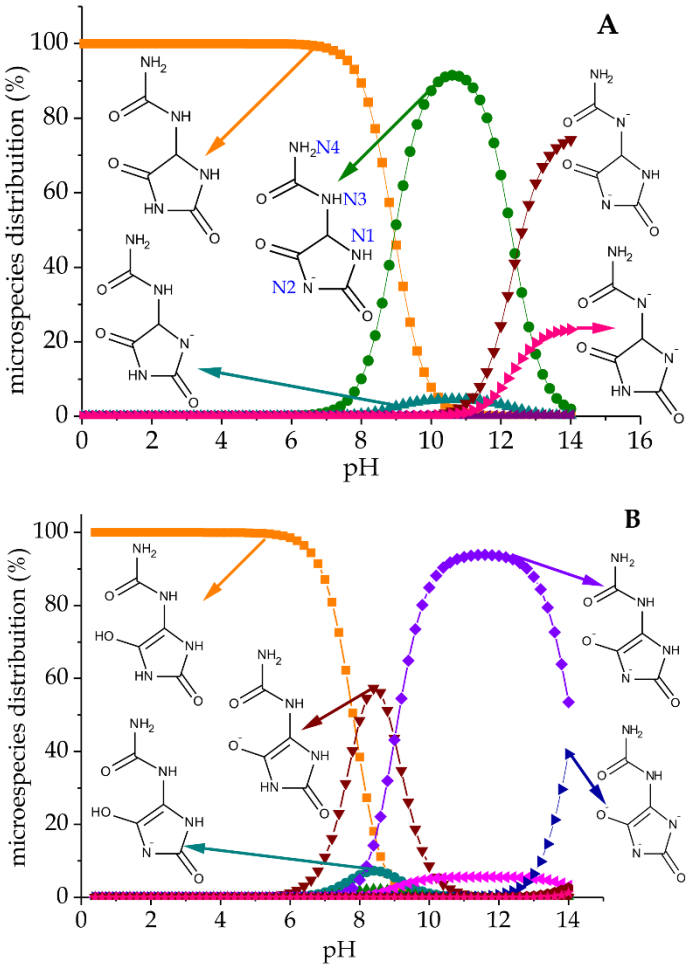

Figure 4.2. Distribution diagram of allantoin species at different pH values (A) and allantoin as a tautomeric mixture of ketonic and enolic forms (B) (obtained with the MarvinSketch software 6.1.5).

The first approach to intercalate allantoin here explored was in a 2:1 magnesium-aluminum LDH (MgAl-LDH), the most typical of the LDH solids. Thus,

intercalation was intended by ion-exchange reaction and by co-precipitation of the LDH in presence of allantoin, as described in Chapter 2 #section 2.5.2. The XRD pattern (Figure 4.3) of the starting LDH shows the characteristic peaks of the inorganic solid structure with the most intense diffraction reflection at 11.35° 2theta angle, which corresponds to the (003) reflection. The additional diffraction peaks were assigned to (006), (012), (015), (018), (110) and (113) (double) to the characteristics LDH structure reflections corresponding to 0.37, 0.25, 0.23, 0.19, 0.151 and 0.149 nm, allowing to confirm the structure of the hydroxide and a interlayer distance of 0.76 nm (Miyata, 1977; Bish, 1980; Meyn et al., 1990; Rives, 2001). Taking into account the thickness of the LDH brucite sheet is about 0.48 nm, a basal spacing increase of 0.28 nm is determined, confirming the presence of Cl^- ions in the interlayer region (Cavani et al., 1991). The intercalation of allantoin in the MgAl LDH prepared by the ion-exchange or the co-precipitation methods is not evident because there is no shift of the (00l) reflections towards a lower 2theta angle. However, the elemental chemical analysis shows a significant amount of allantoin in the hybrid compounds with a content of 142 and 50 mEq per 100 g for allant$_{cop}$:MgAl-LDH and allant$_{ie}$:MgAl-LDH, respectively, clearly below the AEC of LDH which is of approximately 330 mEq per 100g (Inacio et al., 2001; Forano et al., 2013). In the diffractogram of the allant$_{ie}$:MgAl-LDH hybrid (Figure 4.3), various additional peaks probably ascribed to allantoin are observed, though two of the most intense ones cannot be observed which may suggest a preferred orientation of allantoin crystals precipitated on the surface of the LDH. In fact, from EDX (Table 4.1) it is confirmed that the allant$_{ie}$:MgAl-LDH hybrid contains practically the same amount of Cl^- ions than the starting MgAl-LDH, which confirms that there is not intercalation of allantoin by an ion-exchange process. In the case of the allant$_{cop}$:MgAl-LDH hybrid from the EDX study (Table 4.1) it is observed a decrease in the amount of Cl^- ions compared to the expected one for the formation of a pure MgAl-LDH, going from a total of approx. 15.4 in the MgAl-LDH to 9.7% in the allant$_{cop}$:MgAl-LDH. This result in combination with the data obtained by CHN suggest that a part of the allantoin may be intercalated between the LDH sheets during the synthesis process

although neither changes in position of the (00l) reflection peaks of the LDH beyond broadening nor presence of reflections from the organic compound are detected in the XRD diffractogram (Figure 4.3). Thus, this observation may be related to the presence of some allantoin species associated with the precipitated solid by electrostatic interactions, perhaps neutralizing part of the charge of a low crystalline LDH formed in these particular experimental conditions.

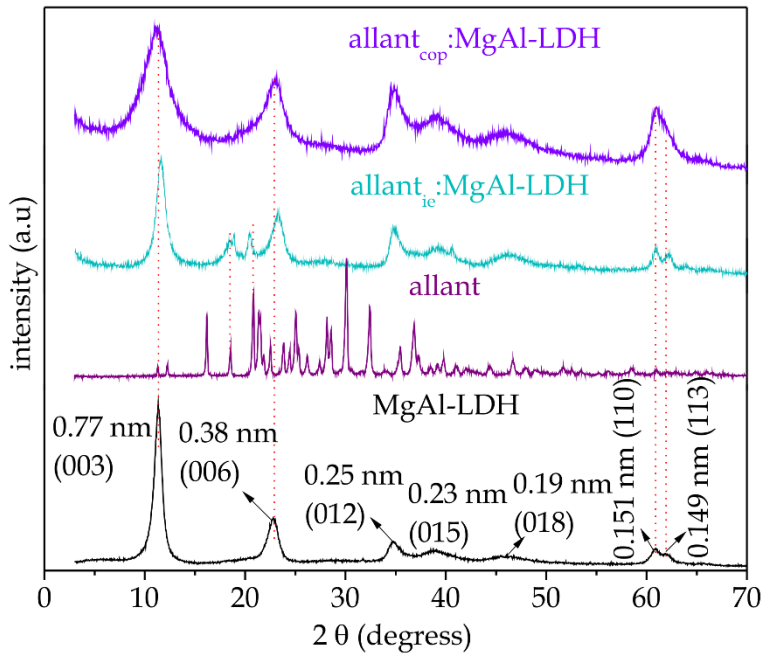

Figure 4.3. X-ray diffraction patterns of allantoin, the MgAl-LDH and the hybrids prepared from allantoin by ion-exchange (ie) and coprecipitation (cop) methods.

Table 4.1 Relative content of various elements in LDH-based systems deduced by EDX.

Element	**MgAl-LDH** **(At %)**	**allant$_{cop}$:MgAl-LDH** **(At %)**	**allant$_{ie}$:MgAl-LDH** **(At %)**
Al	36.3 ± 1.9	30.3 ± 3.4	36.3 ± 2.1
Mg	46.9 ± 1.0	45.5 ± 2.9	40.7 ± 0.5
Cl	15.4 ± 1.9	9.7 ± 0.3	13.5 ± 1.1
Na	1.4 ± 0.2	0.4 ± 0.1	0.5 ± 0.1
N	--	14.0 ± 2.8	5.2 ± 1.1

The interactions between the inorganic solid and the allantoin molecules in the hybrid material prepared by the co-precipitation method were corroborated by infrared spectroscopy Figure 4.4. The intense bands at 3460 cm^{-1} and 1630 cm^{-1} that appear in the spectra of the neat LDH and the hybrids, correspond to the stretching vibrations of hydroxyl groups and the bending vibration of water $\delta(H_2O)$, respectively (Badreddine et al., 1998; Lakraimi et al., 2000). The bands at around 785, 660 and 435 cm^{-1}observed in the spectrum of the LDH correspond to the reticular vibration modes Mg-O, Al-O and O-M-O, respectively (Miyata, 1977; Cavani et al., 1991; Badreddine et al., 1998; Houri et al., 1999; Lakraimi et al., 2000; Pavlovic et al., 2005), appearing at the same frequencies in the hybrid compound. It should be noted the presence of the band at 1360 cm^{-1}, characteristic of vibration modes of CO_3^{2-} species, indicates that despite the precautions taken during the synthesis of the materials a small contamination by carbonate is present in the produced LDH solids.

Table 4.2 summarizes the vibration bands observed in the FTIR spectrum of allantoin (Kuş et al., 2009; Alam and Ahmad, 2015). Figure 4.4 shows the spectrum of allantoin and next to the graph it is represented the species of deprotonated allantoin originated at pH 8-9, pH where the hybrid materials were prepared. Allantoin (1) shows the deprotonation of the N2 and allantoin (2) shows the possible existence of the tautomeric species with the deprotonated O2. In the spectrum of allantoin the bands in the 3440 - 3345 cm^{-1} region with medium to strong intensity are assigned to antisymmetric and symmetric vibrations of NH_2, respectively. These bands do not appear in the $allant_{cop}$:MgAl-LDH hybrid, as they may be overlapped by a wide band due to the ν_{O-H} vibrations of the LDH sustrate. The NH_2 scissoring vibration ($\beta_{ciss}NH_2$) band is observed at 1603 cm^{-1} in allantoin and in the hybrid appears at 1611 cm^{-1}. The bands that appear at 1431 cm^{-1} referring to the plane bending of $\beta_{[(N1-C4)+(C2-N6)]}$ of the molecule ring (Kuş et al., 2009; Alam and Ahmad, 2015). The band at 1284 cm^{-1} is ascribed to the contributions of the plane bending and asymmetric stretch vibrations of the allantoin ureidyl group and it is not observed in the spectrum of the hybrid. The band at 1326 cm^{-1} referring to the stretching vibrations of the N2-C1 does not

appear in the hybrid. According to the studies carried out using the MarvinSketch software 6.1.5, the N-H group involving the N2 is deprotonated at the studied pH (approx. 8-9), as shown in Figure 4.2 B. Then, the disappearance of this band and the alterations of the ring bands points out to the existence of interactions of a deprotonated N^- (N2) with the LDH sheets. In addition, the bands at 1782 and 1716 cm^{-1} ascribed to the symmetric stretching vibration modes of the C4=O1 and C1=O2 groups do not appear in the hybrid material. This result may be associated with the existence of allantoin also in its tautomeric form of keto-enol with a deprotonated oxygen (O2 of C1), which may also be interacting with the LDH sheets.

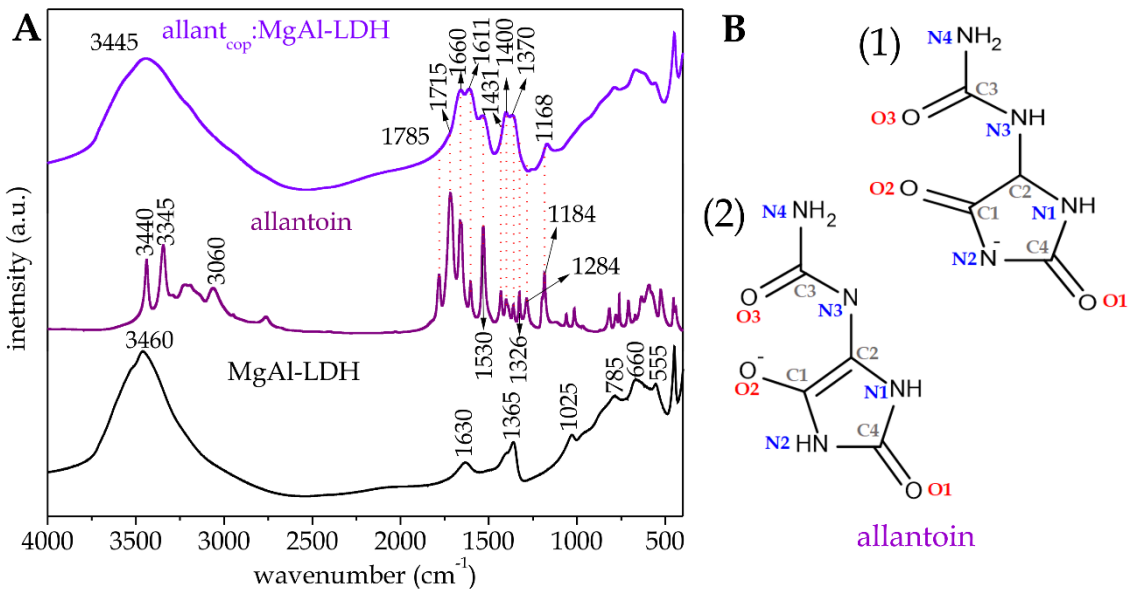

Figure 4.4. FTIR spectra of the MgAl-LDH, allantoin and allant$_{cop}$:MgAl-LDH hybrid(A). At the right side the Allantoin (1) shows the deprotonation of the N2 and allantoin (2) shows the possible existence of the tautomeric species with the deprotonated O2 (B) obtained with the MarvinSketch software 6.1.5.

Table 4.2 Assignation (Kuş et al., 2009; Alam and Ahmad, 2015) of infrared bands of allantoin observed in it the spectrum obtained in a KBr diluted sample.

wavenumber	**assignment**	**wavenumber**	**assignment**
3343	$\nu_s NH_2$	1194	$_{\nu}$ring
3190	νNH (imide)	1184	$_{\nu}$[N3-C2]+βC2– C1
3061	νC2-H	1115	νN-H
2948	νC-H	1060	$_{\nu}$N1-C2+rNH2
1780	ν_sC4=O1+ C1=O2 (ring)	1015	$_{\nu}$ring
1716	$_{\nu as}$C4=O1+ C1=O2 (ring)	967	$_{\delta}$RU
1660	ν_sC3=O3 (amide)	867	$_{\nu}$C-N
1603	$\beta_{ciss}NH_2$	816	$_{\nu}$ring
1530	β[N3-C+βC2–N3]+[N3-C+N1-C2]	778	$_{\delta}$C=O (amide)
1431	β[N1-C4+βC2– N3]	761	$_{\delta}$C=O (ring)
1402	$_{\nu}$ring	707	$_{\delta}$ring
1385	$_{\delta}$CH	670	$_{\delta}$C=O (ring)
1359	$_{\delta}$NH (ring)	632	$_{\delta}$ring
1326	β[N2-C1+C1-C2]	593	$_{\gamma}$NH (ring)
1285	$_{w}$RU	524	$_{\gamma}$NH (ring)

$_{\nu}$, stretching; δ, bending; $_{w}$, wagging; γ, rocking; as., anti-symmetric; s., symmetric; RU means movements of the ring (R) in relation to the ureidyl moiety (U).

Figure 4.5 shows TG-DTA curves corresponding to the MgAl-LDH, pure allantoin and the allant$_{cop}$:MgAl-LDH hybrid. In the curve of the MgAl-LDH is observed the loss (approx. 20%) of physically adsorbed and interlayer water molecules in a continuous process between 95-165 °C. Events related to the dehydroxylation of the brucite sheets are evidenced between 165 and 395 °C, with a total mass loss of approximately 43% (Constantino and Pinnavaia, 1995). On the other hand, allantoin is thermally stable up to approx. 200 °C, being observed its melting point at 237 °C as described in the literature (Kuş et al., 2009), point from which starts its decomposition with a first mass loss of 30 %, and then

several more up to slightly above 600 °C, representing a total mass loss of 96% (Kuş et al., 2009). These degradation processes were accompanied by other representative endothermic peaks at 255, 323 and 427 °C. In this case of the allant$_{cop}$:MgAl-LDH hybrid it is clearly observed differences in the decomposition profile expected for the incorporated allantoin while maintains the two endothermic peaks attributed to desorption of physically adsorbed water and interlayer water in the LDH now at 57 and 200 °C. Above this last temperature it is observed an endothermic event at 292 °C that is assigned to a partial decomposition of allantoin with a total mass loss of 5%, followed by other endothermic process at 395 °C assigned to the dehydroxylation of the MgAl-LDH layers. These last events are associated with a total mass loss of 31% that lasts till 500 ^{o}C and includes also the final steps of decomposition of allantoin. It should be noted that in the hybrid it is not observed the melting point of allantoin and a different pathway in the decomposition process, confirming the interaction of the organic molecule with the LDH, possibly as discrete species intercalated in a non-well stacked layered solid particles.

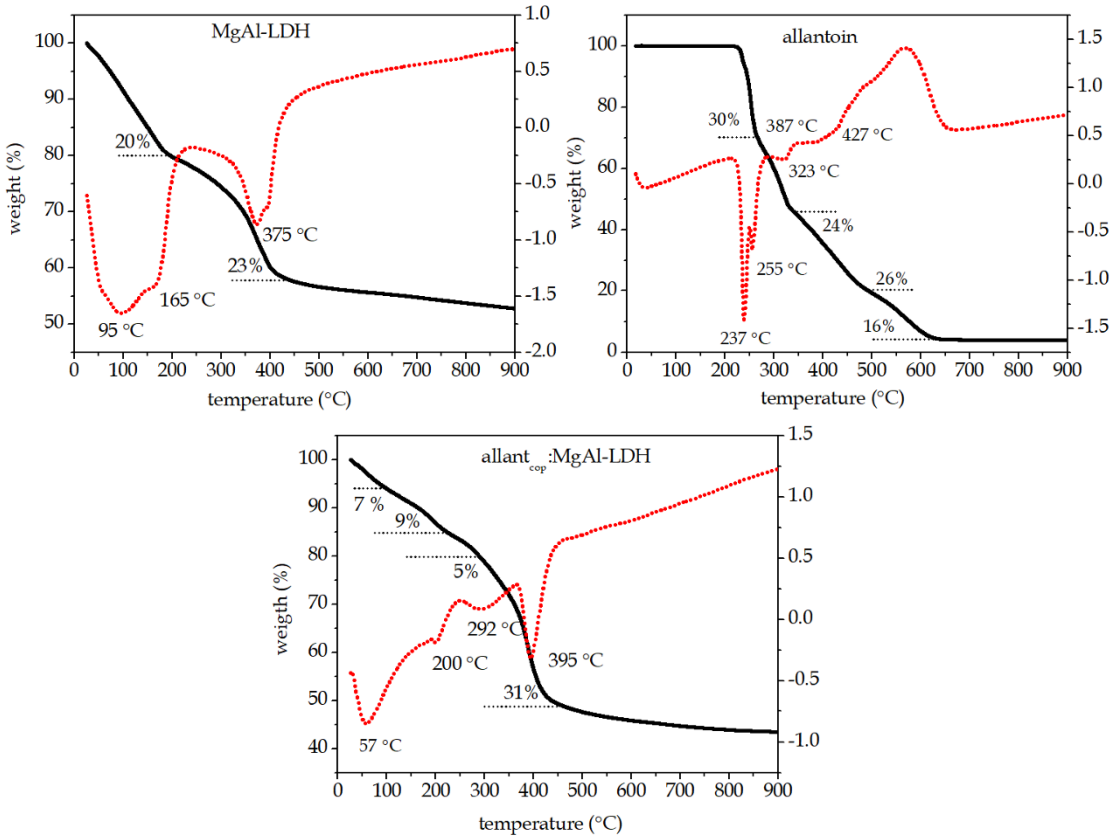

Figure 4.5. TG (black, solid line) and DTA (red, dashed line) curves of MgAl-LDH, allantoin and allant$_{cop}$:MgAl-LDH hybrid.

Figure 4.6 shows FESEM images of MgAl-LDH where it is possible to observed the characteristic morphology of this solid with laminar particles that form a compact *sandrose* structure (Costantino et al., 1998; Leroux et al., 2004). The aspect of the allant$_{cop}$:MgAl-LDH hybrid, in which the LDH is formed in presence of allantoin, shows a morphology less compacted where the lamellar particles appear to be aggregated in planes (Figure 4.6B).

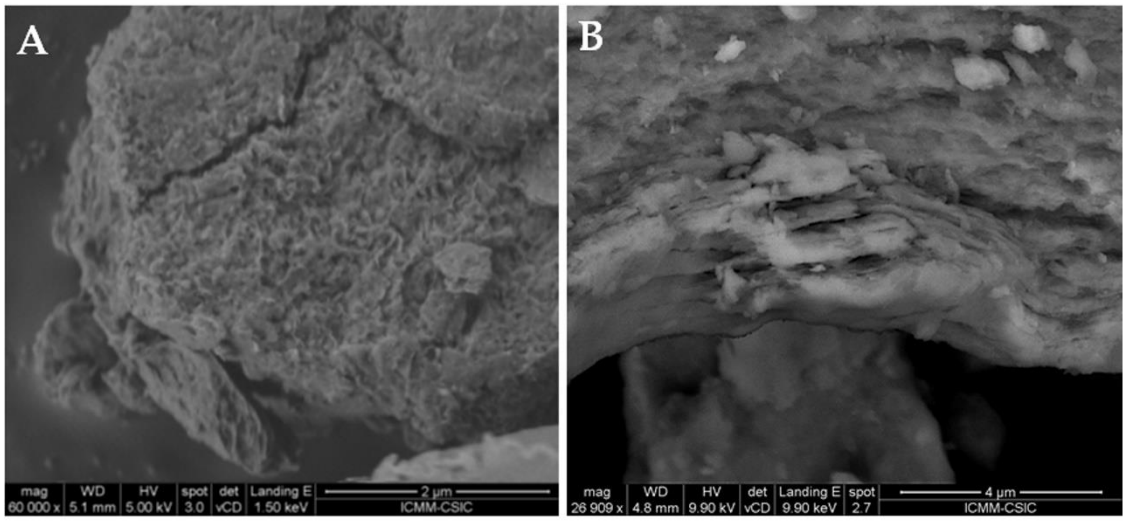

Figure 4.6. FESEM images of the MgAl-LDH (A) and the allant$_{cop}$:MgAl-LDH hybrid (B).

4.3 ALLANTOIN:ZnAl-LDH

4.3.1 Synthetic approaches to allantoin:ZnAl-LDH hybrids

Considering that the amount of allantoin incorporated in the MgAl-LDH system, by co-precipitation method, is relevant for applications in systems of topical uses of allantoin, it was then proposed to prepare a hybrid incorporating the allantoin into a ZnAl-LDH. Considering that zinc has antibacterial properties, it was assumed that the presence of this specie in the solid will add more value to the resulting hybrid system. In fact, it has been reported allantoin complexes with various metals (Zn, Ag, Cu, etc.) where the presence of the metal in the final material introduces antibacterial properties that improves also the generation of skin cells, which is advantageous for treatments of various skin diseases, burns, hair usages, among others, etc, (Margraf, 1974; Klippel et al., 1977; Loren, 1995).

Taking into account these premises, the preparation of hybrids based on a ZnAl-LDH was explored using the methods of co-precipitation, ion-exchange and reconstruction (Figure 4.7), as described in Chapter 2 #2.2.2.

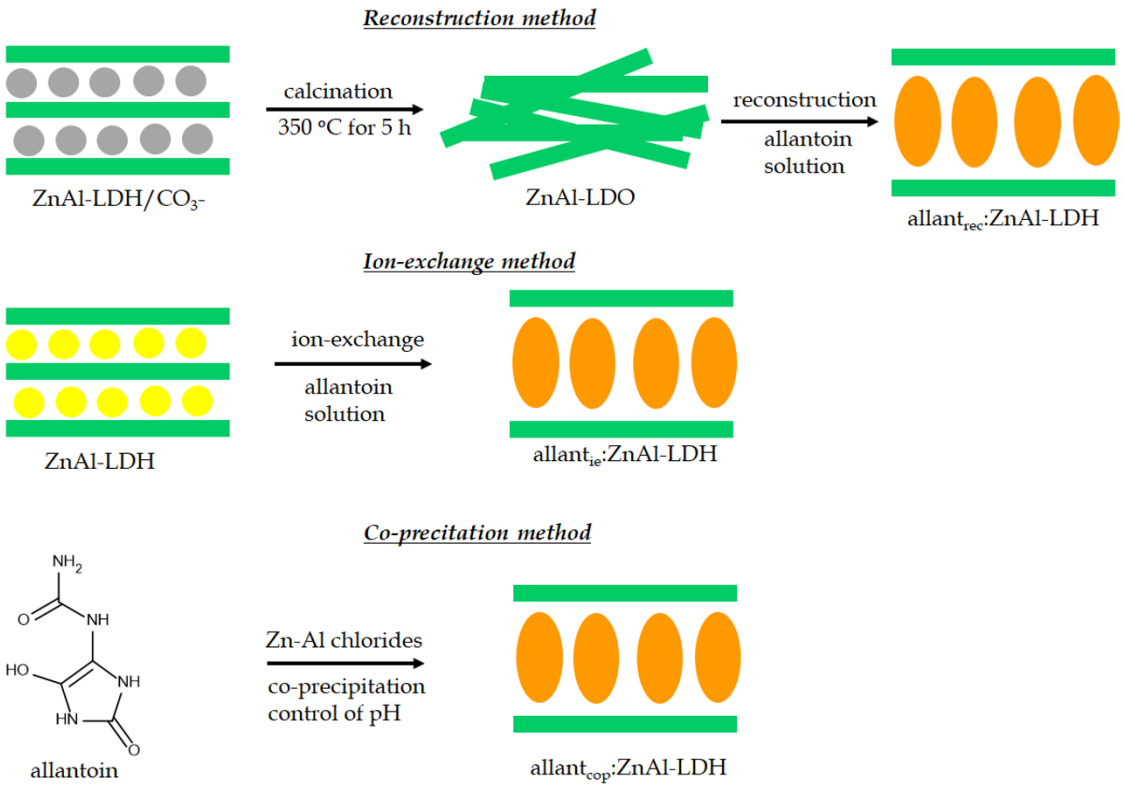

Figure 4.7. Synthesis strategies for allant:ZnAl-LDH hybrids.

Figure 4.8 shows the zeta potential of allantoin, the ZnAl-LDH and the allantoin:ZnAl-based hybrids resulting from each of the three explored synthetic methods. It is observed a correlation between the zeta potential and the content in allantoin in the hybrid. Thus, the pristine ZnAl-LDH shows a positive value of +52.3 mV, which was modified towards more negative values as increases the content in allantoin in the hybrid, showing values of +45.0 mV for the allant$_{ie}$:ZnAl-LDH with 46 mEq per 100g, +25.9 mV for the allant$_{rec}$:ZnAl-LDH with 135 mEq per 100 g and +11.2 mV for the allant$_{cop}$:ZnAl-LDH hybrid that contains 348 mEq per 100g. It should be noted that this last hybrid shows a zeta potential slightly positive, indicating that possibly the incorporated amount of allantoin is able to neutralize most of the charge of the LDH.

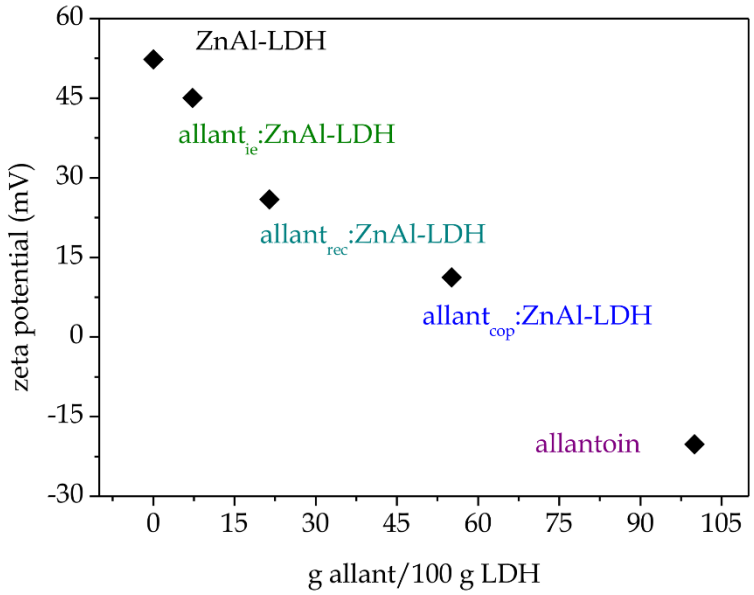

Figure 4.8. Zeta potential of allantoin, ZnAl-LDH, and allant$_{rec}$:ZnAl-LDH, allant$_{ie}$:ZnAl-LDH and allant$_{cop}$:ZnAl-LDH hybrids in relation to the relative content of allantoin in the solid.

Figure 4.9 shows the diffractogram of the hybrid prepared by reconstruction method of a ZnAl-LDH previously heated to 350 ºC for 5 h to produce a phase that in presence of allantoin may lead to the formation of the intercalation compound, following a methodology that has proved efficient in the preparation of other LDH hybrid materials such as the assembly of organic polymers, anionic surfactants, dichlophenac and porphyrins (Bonnet et al., 1996; Leroux and Besse, 2001; Leroux et al., 2001; Dupin et al., 2004; Starukh et al., 2016; Duan et al., 2017). Figure 4.9 shows the diffractograms of the LDH when the reconstruction method is applied to produce the hybrid. Thus, the diffractogram of the starting ZnAl-LDH prepared incorporating carbonate ions in this case, shows the characteristic pattern of the LDH but it is calculated a basal spacing of 0.75 nm slightly lower than in the LDH incorporating Cl^- ions. Upon calcination in air at 350 ºC for 5 h a mixture of zinc and aluminum oxides is obtained, the LDH is transformed into the so-called double laminar oxide phase (ZnAl-LDO) that shows the reflections in the XRD pattern of ZnAl calcined LDH in which are visible some characteristics peaks of ZnO wurtzite phase (Starukh et al., 2016). It is known that, at a certain temperature, the original hydrotalcite becomes a mixture of

oxides that have "memory" of the original structure (Kooli et al., 1997). In fact, in the presence of aqueous solutions, these oxides regenerate the double hydroxides in the form of brucite type sheets and the positive charges are balanced with anions presented in solutions. When the ZnAl-LDO is reconstructed in water in order to verify it is possible to reconstruct the solid, the corresponding XRD pattern shows again the characteristic peaks of the LDH (Figure 4.9), confirming in the present case the reversibility of the thermal transformation carried out at 350 ºC. Thus, the ZnAl-LDO was then treated with an allantoin solution at pH ≈ 8-9 (addition of NaOH) to achieve the formation of the allant$_{rec}$:ZnAl-LDH hybrid. As shown in Figure 4.9, the pattern of the resulting hybrid shows a characteristic pattern of the LDH but it does not show any displacement of the *d*(00l) reflections towards lower 2 theta angles though the hybrid contains 135 mEq of allantoin per 100 g of ZnAl-LDH. Therefore, it is clear that the formed hybrid material does not correspond to an intercalation compound.

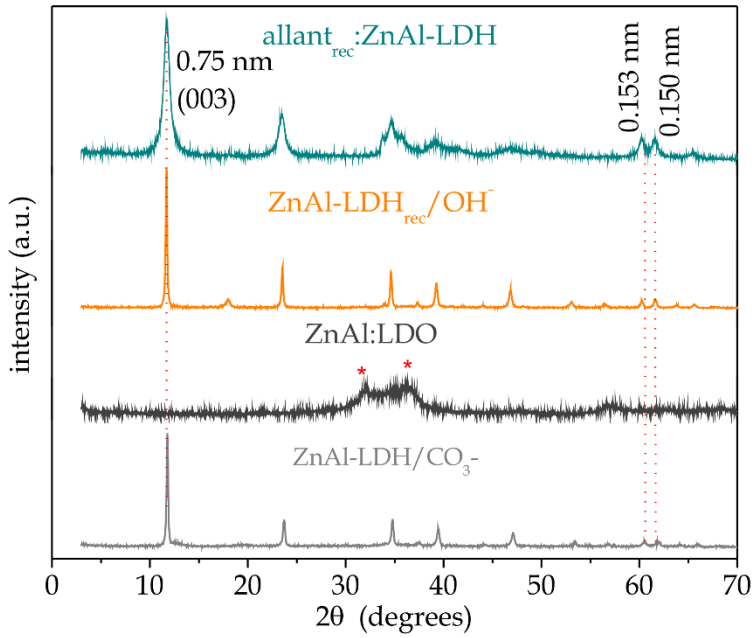

Figure 4.8. X-ray diffraction patterns of ZnAl-LDH/CO_3^-, the ZnAl-LDO produced by calcination of the former at 350 ºC (* peaks of the ZnO wurtzite phase), ZnAl-LDH$_{rec}$/OH^- obtained after reconstruction of the LDO in water at pH ≈ 8-9 and, allant$_{rec}$: ZnAl-LDH obtained by reconstruction of the LDO in presence of an allantoin solution at pH ≈ 8-9.

The XRD pattern of the hybrid prepared by ion-exchange method (allnt$_{ie}$:ZnAl-LDH) (Figure 4.10), is very similar to the one of the hybrid prepared from MgAl-LDH, except no peaks ascribed to crystalline allantoin are detectable (Table 4.3). The allant$_{ie}$:ZnAl-LDH hybrid incorporates 46 mEq of allantoin per 100 g of ZnAl-LDH, value also pretty close to the one of the allant$_{ie}$:MgAl-LDH hybrid. Thus, here again, the hybrid formed by ion-exchange reaction of allantoin with the ZnAl-LDH containing Cl^- ions and interlayer anions, does not correspond to an intercalation compound.

Interestingly, in the XRD diffractogram of the allant$_{cop}$:ZnAl-LDH hybrid prepared by the co-precipitation method (Figure 4.10), it can be observed the (003) and (006) reflection peaks shifted towards lower 2θ angles together with other characteristic (hkl) peaks of the LDH structure (Table 4.3). From those 00l peaks it can be estimated a basal spacing of 1.68 nm which leads to a basal spacing increase of 1.20 nm considering a thickness of 0.48 nm for the brucite-like layer (Cavani et al., 1991), which confirms in this case the intercalation of allantoin. From the CHN analysis of the allant$_{cop}$:ZnAl-LDH hybrid it is calculated a content of 348 mEq of allantoin per 100 g of ZnAl-LDH, which coincides practically with the AEC of LDH (≈ 330 mEq per 100g). This finding points out to the presence of allantoin anionic species as the counter-ion of the formed LDH solid. Based on these data and considering the dimensions of allantoin as 0.40 x 0.61 nm (Figure 4.11A), it can be proposed two possible intercalation models to explain the arrangement of allantoin in the interlayer region of the inorganic solid, with intercalated anionic species organizing in a bilayer or in a three-layer between the ZnAl-LDH sheets (Figure 4.11B & C). At this point, it is quite complex to ascertain the actual organization though the bilayer model seems to be more favorable for an easier compensation of charge and interaction with the hydroxide layers. Anyway, theoretical calculations would be necessary to confirm the real organization of allantoin in the hybrid.

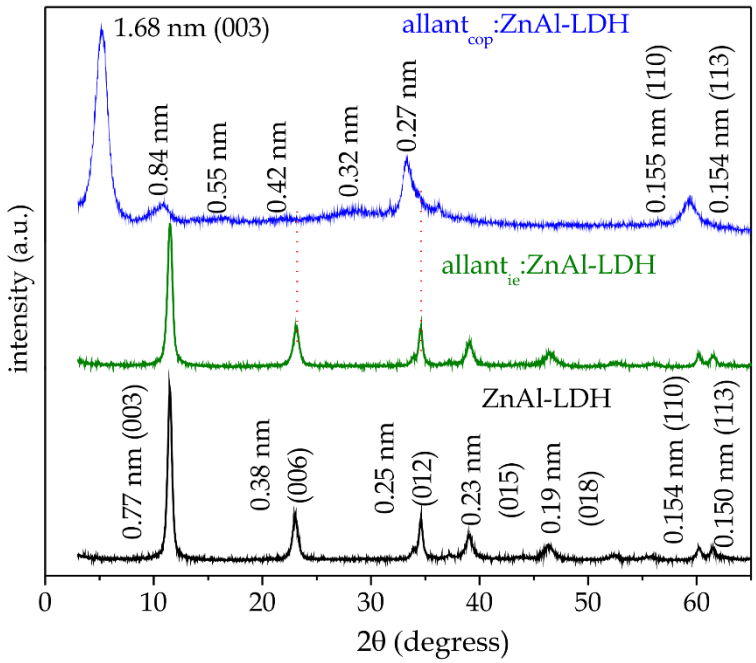

Figure 4.9. X-ray diffraction patterns of allantoin, ZnAl-LDH and of the allant$_{ie}$:ZnAl-LDH and allant$_{cop}$:ZnAl-LDH hybrids prepared by ion-exchange and co-precipitation, respectively.

Table 4.3. Interplanar distances (d_{hkl}) and 2θ (λ = 1.54 Å) obtained from XRD data of ZnAl-LDH, allant$_{ie}$:ZnAl-LDH and allant$_{cop}$:ZnAl-LDH hybrids.

ZnAl-LDH/Cl		**allant$_{ie}$:ZnAl-LDH**			**allant$_{cop}$:ZnAl-LDH**		
2θ (degrees)	*d* (nm)	2θ (degrees)	*d* (nm)	*hkl*	2θ (degrees)	*d* (nm)	*hkl*
11.49	0.77	11.49	0.77	003	5.23	1.68	003
23.04	0.38	23.04	0.38	006	10.45	0.84	006
34.58	0.26	34.58	0.26	012	15.94	0.55	009
39.05	0.23	39.11	0.23	015	21.27	0.42	0012
46.44	0.19	46.41	0.19	018	28.56	0.31	0015
60.26	0.152	60.20	0.152	110	59.40	0.155	110
61.57	0.150	61.57	0.150	113	59.83	0.154	113

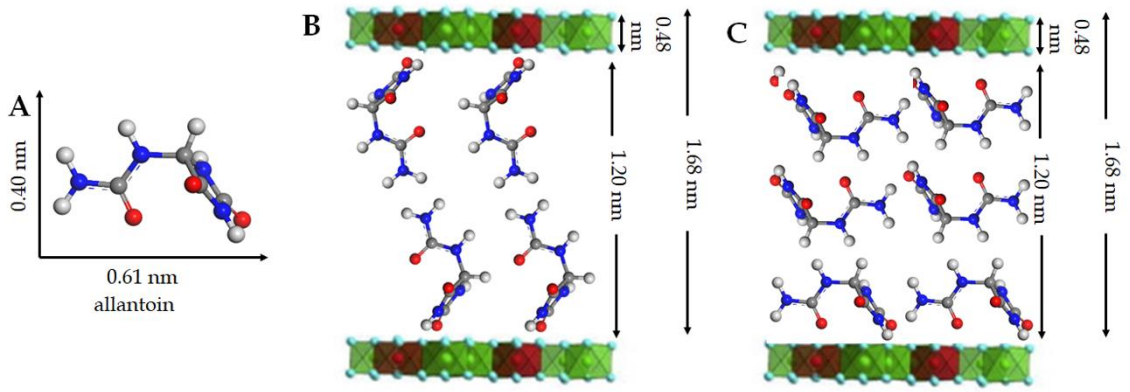

Figure 4.10. Schematic dimensions of allantoin molecule (A), schematic arrangement of allantoin in bilayer (B) or three-layer (C) in the ZnAl-LDH interlayer. (Adapted from Stimpfling et al. (2016a).

As the allant$_{cop}$:ZnAl-LDH hybrid seems to be the one with the most appropriated stoichiometry and it is confirmed the presence of allantoin in the interlayer region, this compound was futher analyzed in depth to obtain a more complete characterization of the hybrid. From the EDX analysis (Table 4.4) it was determined a acontent in Zn much larger than that expected for the formation of a LDH with a Zn:Al 2:1 ratio. In fact, the hybrid shows a very low content in Al that suggests the precipitated solid could most possibly be a layared single hydroxide (LSH) instead of the intended 2:1 ZnAl-LDH. This conclusion is quite plausibe considering possible strong interactions between Zn and allantoin, which has been already addressed in the literature in relation to the formation of allantoin-zinc-based complexes (Margraf, 1974). Based on these data, the model previously defined for the intercalation of allantoin in a co-precipitated ZnAl-LDH would not be valid and additional characterization should be done to understand the nature of the allant$_{cop}$:ZnAl-LDH hybrid.

Table 4.4. Relative content of element in ZnAl-LDH and allant$_{cop}$:ZnAl-LDH hybrid determined from EDX analysis.

Element	**ZnAl-LDH (At%)**	**allant$_{cop}$:ZnAl-LDH (At%)**
Al	30.8 ± 0.5	8.5 ± 4.5
Zn	51.5 ± 1.6	40.1 ± 2.0
Cl	17.6 ± 2.1	0.7 ± 0.1
N	--	50.6 ± 2.7
Na	--	--

Firstly, it should be noted that the FTIR spectra of the hybrids based on ZnAl hybrids (Figure 4.12) show differences in the intensity of the bands ascribed to allantoin that varies with the content of organic compound in the hybrid. The bands at 1780 and 1600 cm^{-1} referring to $\nu_{C=O}$ vibrtion mode of the carbons C3 and C4in the ring and the δ_{NH2} of the amide, respectively, disappear in all the hybrids. The band at 1660 cm^{-1} is related to the $\nu_{C=O}$ of the carbonyl of the amide (C3) and it is displaced to lower wave numbers in the allant$_{ie}$:ZnAl-LDH and allant$_{rec}$:ZnAl-LDH hybrids, appearing at 1645 cm^{-1}. The spectra of hybrids prepared by ion-exchange and reconstruction methods are quite similar however, in the allan$_{cop}$:ZnAl-LDH hybrid this last band is shifted to 1640 cm^{-1}, confirming a more intesnse interaction between allantoin and the inorganic substrate, some how different than in the solids prepared by the other methods. A careful analysis of the bands appearing in the low frequency region of the spectra of LDH-based materials show differences amongst the samples in the bands at 830 and 615 cm^{-1}, assignated to M-O vibration modes (M = Zn and Al), and the one at 430 cm^{-1}, assigned to O-M-O (Zn,-Al) vibration modes, of the inorganic solid. These bands are clearly observed in spectra of the ZnAl-LDH/Cl, and the allant$_{rec}$:ZnAl-LDH and allan$_{ie}$:ZnAl-LDH hybrids at the same frequencies. However, in the spectrum of allant$_{cop}$:ZnAl-LDH, the band at 615 cm^{-1} appears with a low intensity, and the O-M-O band is shifted to higher wave numbers appearing at 460 cm^{-1}. Additionally, the spectrum of the allant$_{cop}$:ZnAl-

LDH hybrid shows a band at 785 cm^{-1}, which could be assigned to a Zn-O stretching vibration mode according to the literature, which could be associated with the existence of allantoin-Zn interactions as those observed in complexes of allantoin with Zn (Xu et al., 2015). This important observation suggests that in the synthesis carried out by the co-precipitation method carbonyl groups in the allantoin molecule may react with Zn^{2+} ions to produce a complex (Xu et al., 2015) that seems to be further involving in the precipitation of the hydroxide solid. This result would explain the facility for incorporating allantoin in the samples and the lower amount of Al with respect to the Zn in the formed $allant_{cop}$:ZnAl-LDH hybrid (Table 4.4).

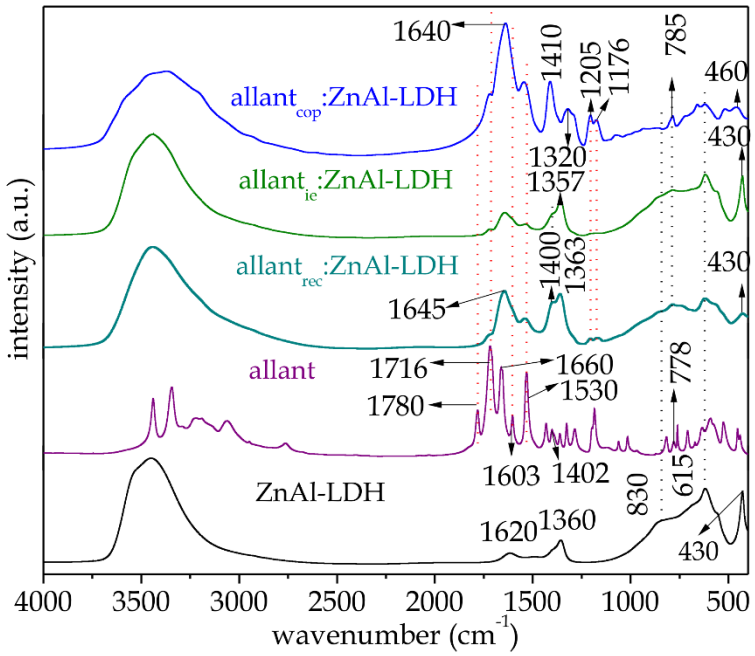

Figure 4.12. FTIR spectra of the ZnAl-LDH, allantoin, $allant_{rec}$:ZnAl-LDH, $allant_{ie}$:ZnAl-LDH and $allant_{cop}$:ZnAl-LDH hybrids.

The TG/DTA results also show differences in the thermal behavior between the hybrid prepared by co-precipitation and the ones formed by the other methods (Figure 4.13). In the TG curve of the neat ZnAl-LDH it is clearly observed four main mass losses. The first one associated with an endothermic event at 42 °C is attributed to the elimination of weakly adsorbed water (11 %). The second mass loss (7 %), also associated with an endothermic process at 138 °C, is ascribed to

the removal of water from the interlayer of the ZnAl-LDH. Between 173 and 261 ^{o}C the percentage of mass loss (7 %) is ascribed to the progressive dihydroxylation of the LDH and stabilization of oxide phases (Perioli et al., 2008). The observed mass losses steps in the allant$_{ie}$:ZnAl-LDH hybrid are very similar to that of the ZnAl-LDH except for the absence of the endothermic event at 173^{o}C and a total mass loss of 14 % instead of 7%. This difference in the mass loss could be ascribed to the presence of allantoin (45 mEq per 100 g) that is removed in the interval of temperatures in which the dihydroxylation of the LDH also takes place. However, the TG/DTA curves of the hybrids prepared by the reconstruction and co-precipitation methods show very different profiles, especially in the process taking place above 200 ^{o}C. In the case of the allant$_{rec}$:ZnAl-LDH hybrid it is observed a three mass losses (12%, 11% and 5%) between 150 to 650 ^{o}C that account of dihydroxylation of the inorganic solid and the decomposition of allantoin, being accompanied by three endothermic events at 210, 450 and 580 °C. In the case of the allant$_{cop}$:ZnAl-LDH hybrid the TG curve is quite different and it is observed a progressive and continuous mass loss from practically 200 ^{o}C up to 650 ^{o}C, being detectable various endothermic events at 35, 85, 294 and 566 °C, attributed to losses of masses of 4, 7, 21 and 16%, respectively. Besides, three exothermic processes are observed at 207, 480 and 650 °C, the most notable being the exothermic process at 650 °C, which may be related to the complete removal of allantoin strongly bonded to Zn that leads to the formation of zinc oxide with a wurtzite-type structure (De Roy et al., 2006).

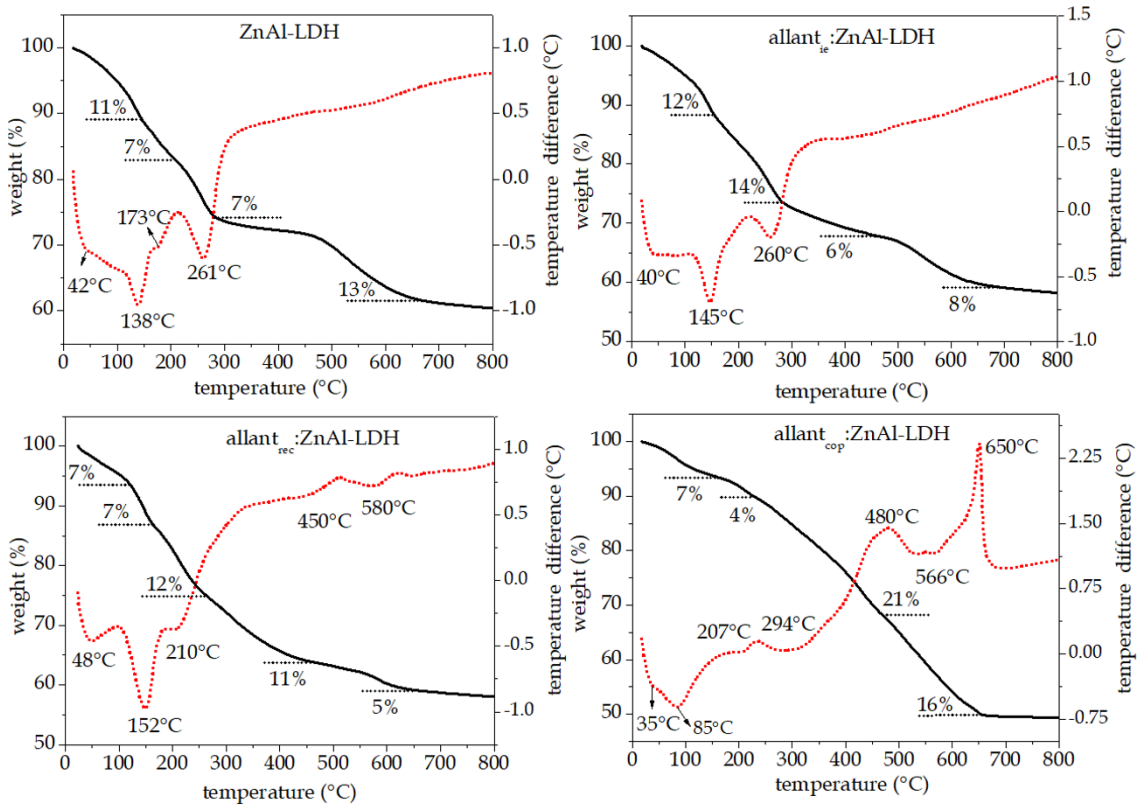

Figure 4.13. TG (black, solid line) and DTA (red, dashed line) curves of ZnAl-LDH, allant$_{ie}$:ZnAl-LDH, allant$_{rec}$:ZnAl-LDH and allant$_{cop}$:ZnAl-LDH hybrids.

Figure 4.14 shows FESEM and TEM images the ZnAl-LDH and the allant$_{cop}$:ZnAl-LDH hybrid. The first shows the characteristic aspect of LDH materials with aggregation of particles in typical *sandrose* structures. In contrast, the hybrid seems to be formed by platelets particles that form aggregate in more compact porous blocks. TEM images show that in fact the allant$_{cop}$:ZnAl-LDH hybrid (Figure 4.14D) is formed by aggregation of hexagonal platelet nanoparticles of typical 20 nm diameter size, much smaller than the ones of the ZnAl-LDH (Figure 4.14B).

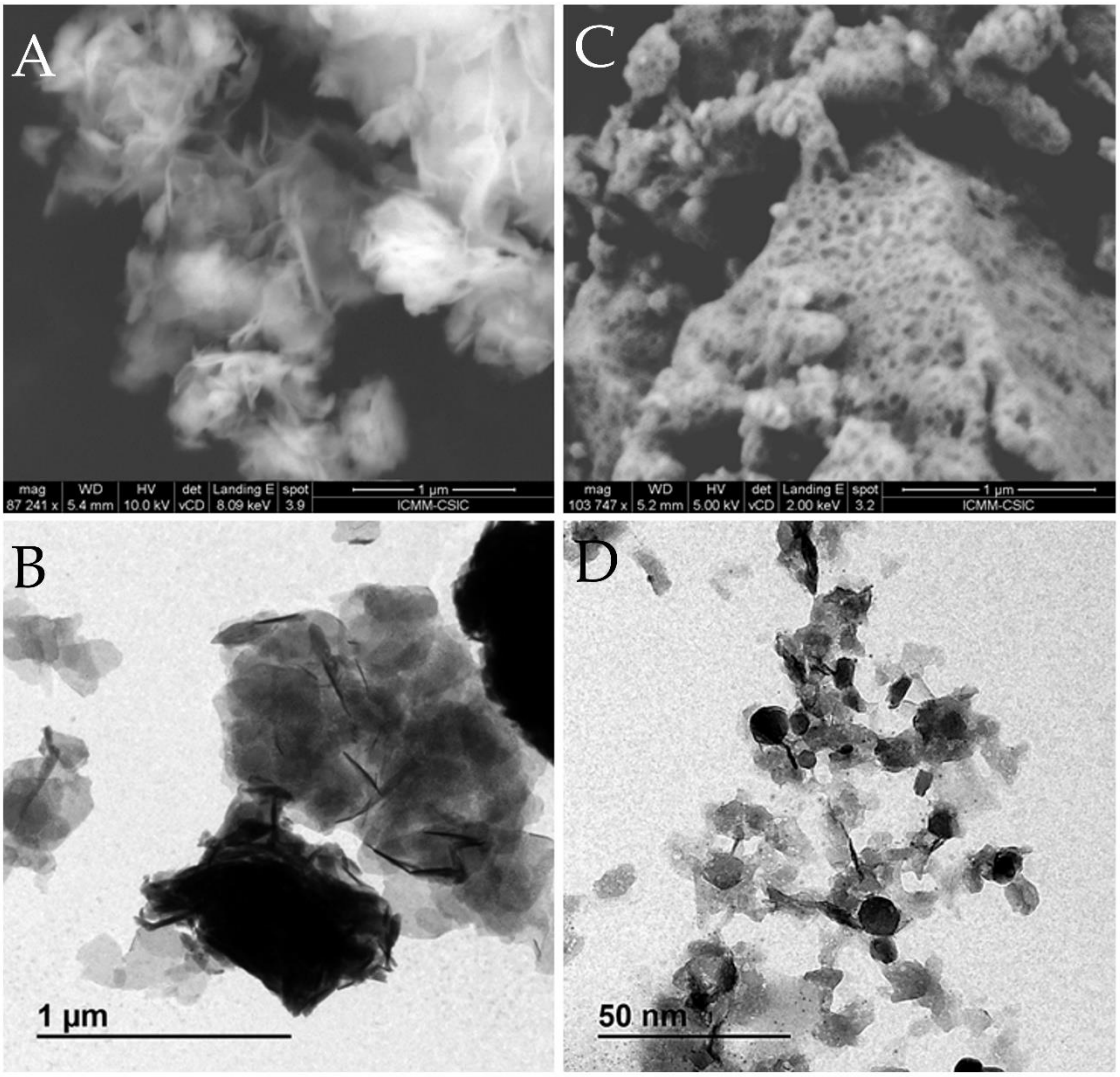

Figure 4.14. FESEM and TEM images of ZnAl-LDH (A-B) and allant$_{cop}$:ZnAl-LDH hybrid (C-D).

4.4 ALLANTOIN-ZINC SYSTEMS

According to the literature, allantoin easily forms complexes with different metals (Margraf, 1974). Based on these data and taking into account that in the process of ZnAl-LDH formation, the preference of allantoin for Zn was observed the preparation of the allant:Zn-complex following the protocol described in the patent by Margraf, (1974) was explored. The idea is to understand what it is the process of interaction of Zn^{2+} ions and allantoin that leads to the formation of

phases reach in Zn when intended the co-precipitation of the ZnAl-LDH in presence of allantoin, as it has been observed in the formation of the allant$_{cop}$:ZnAl-LDH hybrid (#section 4.3). Additionally, it was intended the precipitation of a Zn layered singly hydroxide in presence of allantoin (allant:Zn-LSH) to compare its similitudes with the LDH hybrid. The allant:Zn-complex prepared according to the protocol described in the patent by Margraf, (1974) contains 259 mEq of allantoin per 100 g of Zn-complex and there is no data in the literature on its characterization that could be used for comparison in this study. The XRD pattern of the allant:Zn-complex (Figure 4.15A) shows a very intense reflection peak at 2.56 nm with other broad reflections of much lower intensity, suggesting the formation of low crystalline phases that may resemble to LDH and LSH hybrids here developed (Figures 4.10 & 4.15A), though it is difficult to index the pattern due to low definition of peaks. On the other hand, the allant:Zn-LSH hybrid was successfully prepared according to the XRD diffractogram shown in Figure 4.15A, which can be indexed as indicated in Table 4.5. The presence of zinc hydroxides is overruled as none of the peaks of the Zn-NaOH solid are observed in the pattern of the allant:Zn-LSH hybrid. From the observed (00l) rational reflections values in Table 4.5 it is possible to establish a basal spacing increase of 1.28 nm for the allant:Zn-LSH hybrid. Taking into account 0.40 x 0.61 nm as dimensions of allantoin molecule (Figure 4.10A) it can be proposed a model in which allantoin species would be intercalated forming a bilayer between the Zn-LSH sheets, which would produce precisely a spacing increase of 1.28 nm (Figure 4.15B).

Curiously, the allant:Zn-LSH hybrid shows a quite similar diffractogram pattern than the allant$_{cop}$:ZnAl-LDH hybrid with just small displacements in the position of some of the peaks (Figure 4.15A). This observation suggests that, in the case of the allant$_{cop}$:ZnAl-LDH hybrid, it was in fact formed a Zn-LSH structure with the presence of small amounts of Al ions which would account of the small differences between XRD patterns. In that case, the allant$_{cop}$:ZnAl-LDH hybrid should be contemplate as a LSH structure instead of a LDH structure. In fact, the

allant:Zn-LSH hybrid incorporates 364 mEq of allantoin per 100 g of Zn-LSH, which is also similar to that incorporated in allant$_{cop}$:ZnAl-LDH hybrid.

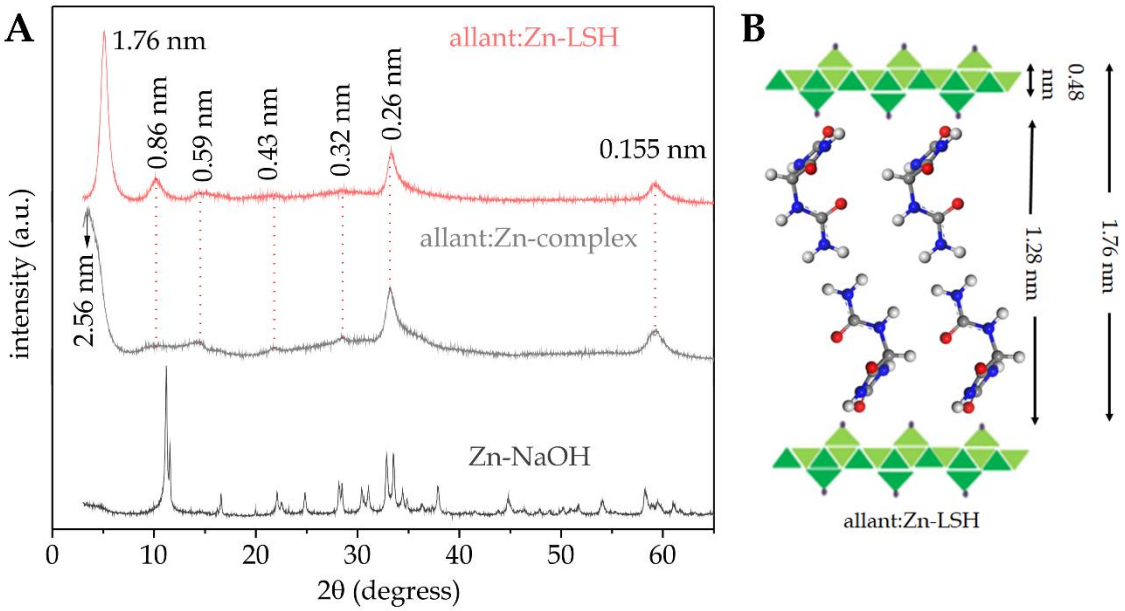

Figure 4.15. X-ray diffraction patterns of Zn-NaOH, allant:Zn-complex and allant:Zn-LSH hybrid (A) and schematic arrangement of allantoin in the Zn-LSH interlayer (B), adapted from Latip et al. (2013).

Table 4.5. Assignation of diffraction peaks observed in the diffractogram of the allant:Zn-LSH hybrid

allant:Zn-LSH		
hkl	2θ (degrees)	*d* (nm)
001	5.00	1.76
002	10.23	0.86
003	14.80	0.59
004	20.69	0.43
005	28.00	0.32
100	33.30	0.26
110	59.20	0.155

The FTIR spectra of the allant:Zn-complex and the allant:Zn-LSH hybrid (Figure 4.16) are quite similar to the one of the allant$_{cop}$:ZnAl-LDH (Figure 4.12) previously discussed (#section 4.3). Here again, the interactions of Zn and allantoin can be clearly discerned from the analysis of band in the region at lower wavenumbers. The band at 761 cm^{-1} referring to vibrations of the carbon (C=O) of the ring in pure allantoin, appears displaced at greater wavenumbers, to 785 cm^{-1}, in the spectra of the allant:Zn-complex and the allant:Zn-LSH hybrid. The band at 1780 cm^{-1} associated with ν_{as}C=O disappears in the allant:Zn-complex and allant:Zn-LSH hybrid and the band of allantoin at 816 cm^{-1} ascribed to the ring vibration (ɣ ring) that appears in the allant-Zn/complex at 830 cm^{-1} is not observed in the allan:Zn-LSH hybrid. In addition, similar to what occurs in the allant$_{rec}$:ZnAl-LDH and allant$_{cop}$:ZnAl-LDH hybrids the intense band at 1184 cm^{-1} ascribed to the ring stretching vibrations ν[(R + N3 + C2) +(β C2 + C1]) of allantoin molecule (see Table 4.2) does not appear in the spectra of the allant:Zn-complex and allant:Zn-LSH hybrid. In its place two other bands at 1205 and 1176 cm^{-1} appear in those spectra, which may be related to changes in the movement of the ring in relation to the rest of the molecule, due to the disturbance generated by interactions with Zn species as those occurring in the Zn complex. Thus, these changes in allantoin bands observed in the FTIR spectra of the allant:Zn-LSH and allant$_{cop}$:ZnAl-LDH hybrids and their similarity with that observed in the allant:Zn-complex spectrum, will clearly demonstrate the existence interaction of Zn in the precipitated hydroxides with the deprotonated carbonyl group of allantoin, in this case related to passing from C=O to C-O^{-} through the keto-enol tautomery.

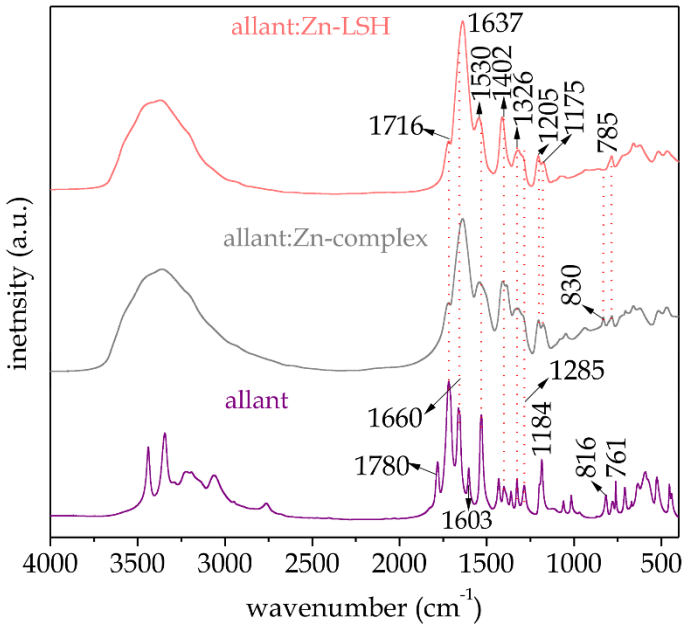

Figure 4.16. FTIR spectra of allantoin (allant), allant:Zn-complex and allant:Zn-LSH.

Figure 4.17 shows de TG/DTA curves of the allant:Zn-complex and the allant:Zn-LSH hybrid. The thermal decomposition of the allant:Zn-complex shows various consecutive thermal processes of decomposition and mass losses less differenced than in the profile of the allant:Zn-LSH hybrid. The first event occurs at 70 °C involving the loss of weakly adsorbed water. Then, the TG-DTA curves show several endothermic processes between 180 and 550 °C related to the decomposition of allantoin, followed by an exothermic peak at 665 °C in the allant:Zn-complex, similar to what happens in the allant:Zn-LSH hybrid but in that last case at 615 °C instead. These differences in the thermal processes may be related to the morphology of the material, which is different for both materials, being more aggregated in the case of allant:Zn-complex, as seen the FESEM and TEM images in Figure 4.18.

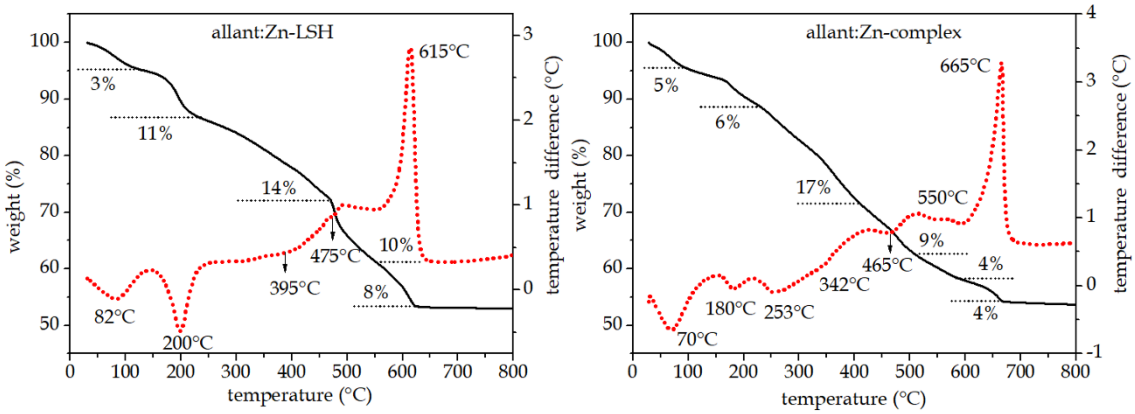

Figure 4.17. TG (solid line) and DTA (dashed line) curves of allant:Zn-complex and allant:Zn-LSH hybrid.

Images A and B in Figure 4.18 show the aspect of the allant:Zn-complex where it can be appreciated the solid is formed by aggregated particles of probably lamellar morphology. The aspect of the allant:Zn-LSH hybrid (Figure 4.18C & D) is more homogeneous and from the TEM images it is clearly distinguished the presence of platelet nanoparticles of hexagonal morphology and around 20-30 nm diameter, typical of Zn-based layered hydroxide materials (Altuntasoglu et al., 2010). The different aspect of the allant:Zn-LSH hybrid particles compare to the allant:Zn-complex ones indicate that both type of materials are different and so their properties regarding possible applications may be also different.

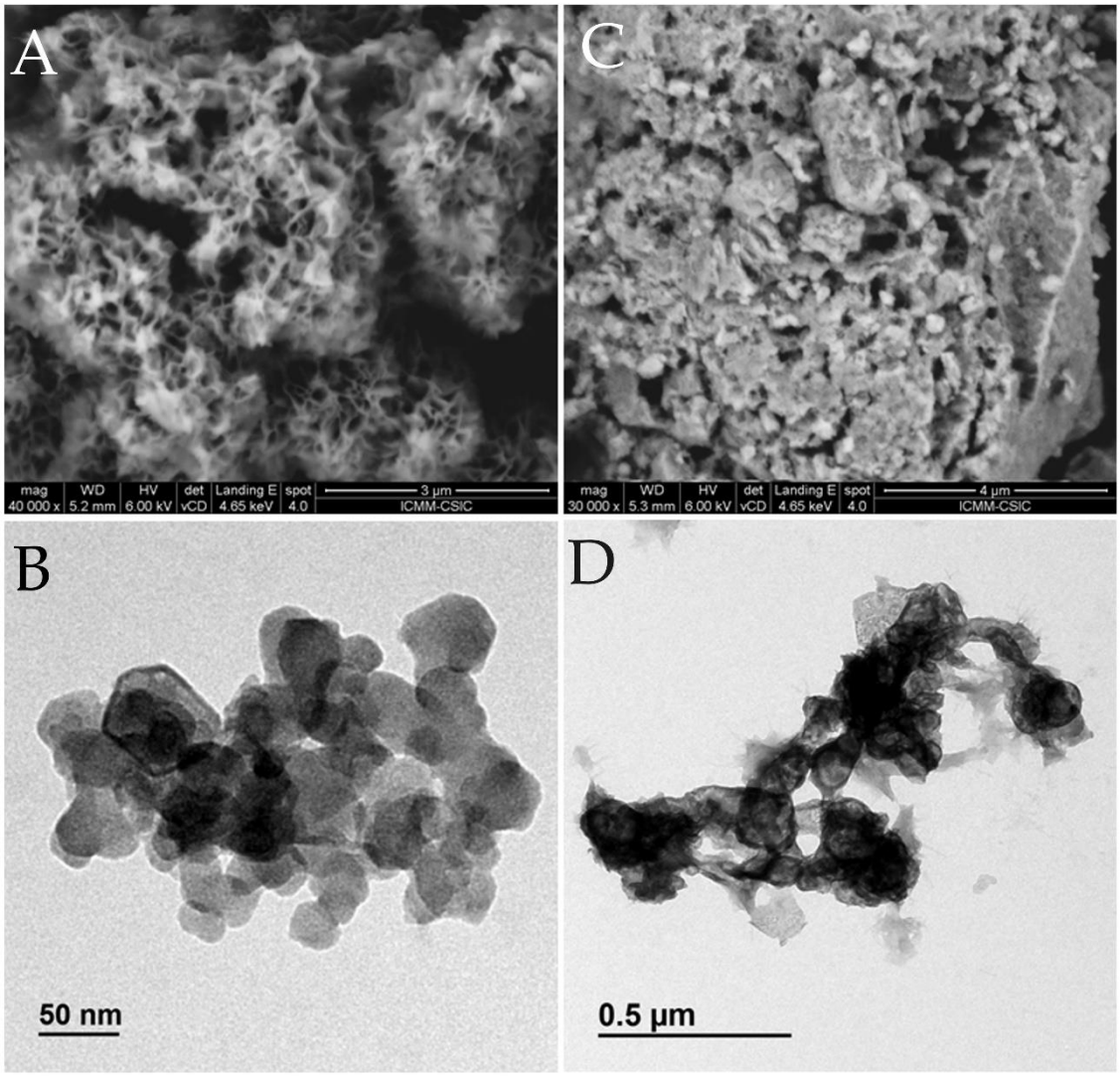

Figure 4.18. FESEM and TEM images of of allant:Zn-LSH hybrid (A-B) and allant:Zn-complex (C-D).

4.5 EVALUATION OF PROPERTIES OF ALLANTOIN-BASED HYBRIDS

4.5.1 *In vitro* release of allantoin from allantoin-based hybrids in aqueous buffer solution

As above indicated, one of the potential applications of the developed materials is related to the action of allantoin as active component in wound dressings, facial masks, etc., therefore a first study of properties of the allantoin-based hybrids is the direct release of allantoin from them. Thus, the allant$_{cop}$:ZnAl-LDH and allant:Zn-LSH hybrids together with the allant:Zn-complex were selected for

experiments of controlled release in conditions simulating the pH of the skin (pH ≈ 5.5) using a phosphate-buffer solution, following the protocols described in Chapter 2 #section 2.5.2. Figure 4.19 shows the profiles in the release of allantoin from the selected materials, which are quite similar for the three systems. In all the formulations it is observed a rapid initial release rate, achieving around a 60% of release in the first two hours. The small differences between the three systems point out to a slightly faster release in case of the allant:Zn-LSH hybrid. After the first 2 h of release, a slower kinetics is observed with allantoin release values of approximately 77, 85 and 82 % for the allant$_{cop}$:ZnAl-LDH, allant:Zn-LSH and allant:Zn-complex systems, respectively. In a study published by Ke et al. (2016) in which allantoin was loaded in composites prepared from porous silica nanoparticles and polycaprolactone nanofibers, it was observed an initial release of just 5% in the first hours, with approx. 40 % in 100 h. In contrast, in the present study it is observed a release of approx. 80 % in the first 8 hours. Taking into account that, in these *in vitro* test experiments the allantoin systems is directly in contact with a solution, and that in a real application, involving a dressing tissue or a cream in contact with the skin, the moisture will be lower it is expected that allantoin will show a much slower release rate and so it could exert at an adequate path its healing role *sur place*. Moreover, in view to applications dealing with wound dressing tissues the control in the release could be further improved as the allantoin-based systems must be associated with a substrate. In this way, the developed systems were also incorporated in various polymeric matrix, as described in the next section, in view to confirm their appropriateness for this application.

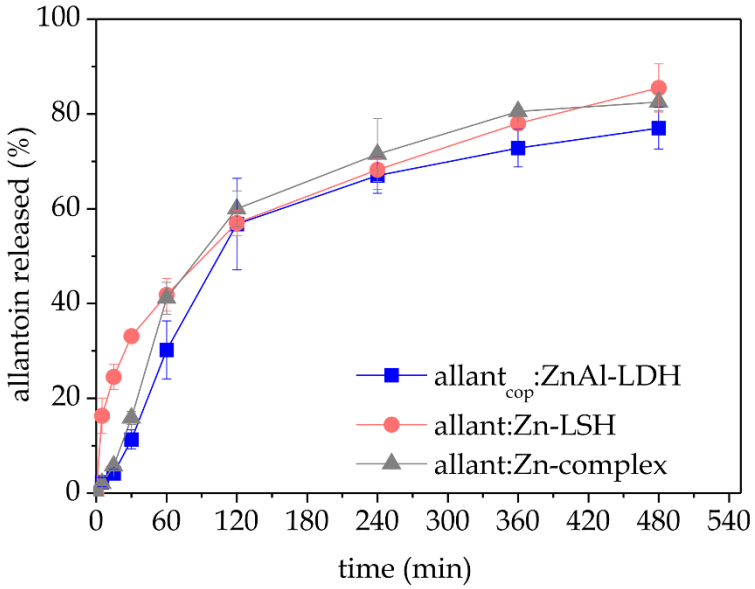

Figure 4.19. Studies of allantoin release in the different preparations in a buffer solution at pH 5.5.

4.5.2 Incorporation of the allantoin-based systems in polymer matrices and evaluation of their antimicrobial activity

For an initial study of antimicrobial activity and to evaluate possible topical applications various allantoin-Zn based systems, the allant:Zn-complex and the allant:Zn-LSH and allant$_{cop}$:ZnAl-LDH hybrids, were incorporated in polymer matrix of hydroxypropylmethylcellulose (HPMC). Thus, films were prepared by the casting method from dispersion of the allantoin-based system in an aqueous solution of the biopolymer and slow evaporation of the solvent (see Chapter 2 #section 2.2.2). To evaluate the antimicrobial activity properties of prepared materials, antibacterial tests were performed against bacterial cultures on agar plates. For this evaluation we selected two microorganisms: a Gram-positive bacterium (*Staphylococcus aureus*) and a Gram-negative bacterium (*Escherichia coli*). *Staphylococcus aureus* is considered an opportunistic human pathogen, a spherical bacterium, frequently found in the skin and also in the nostrils in healthy people. At the same time, they can cause certain diseases such as acnes, cellulitis or even more serious diseases such as pneumonia, endocarditis, etc (Harris et al., 2002). On the other hand, *Escherichia coli* is a seemingly harmless

bacillary bacterium normally found in lower gastrointestinal tract. But it can also cause serious food poisoning in humans through contaminated food. Together with *Staphylococcus aureus* it is one of the most common and ancient bacteria of humanity. For these reasons, both bacteria were selected for the tests with the materials prepared in this Thesis.

Figure 4.20 shows the aspects of films prepared using the HPMC. The film prepared with just HPMC shows a perfectly homogenous aspect and has a totally transparent appearance. The incorporation of allantoin to the HPMC produced films with an inhomogeneous aspects where allantoin is seggregated probably due to the low allantoin solubility. If the pH of the allantoin water solution that is around 3, was raised till ≈ 7 before incorpoating the HPMC and then prepared the allant$_{pH7}$/HPMC film it is produced a most homogeneous material (Figure 4.20), though it is still possible to distingue the presence small crystals within the polymer matrix. When the film is prepared from dispersions of allant: Zn-LSH in HPMC the resulting allant: Zn-LSH/HPMC material is again highly homogenous, though the film is quite stiff and little plastic. When the films were tested for antimicrobial activity, it was not possible to measure the inhibition halo since the films dissolved in the agar plates, probably due to the high hydrophilicity of the HPMC. This result indicated that the preparation of bionanacomposite systems for this application require to choose a polymeric matrix with a higher stability in aqueous environments.

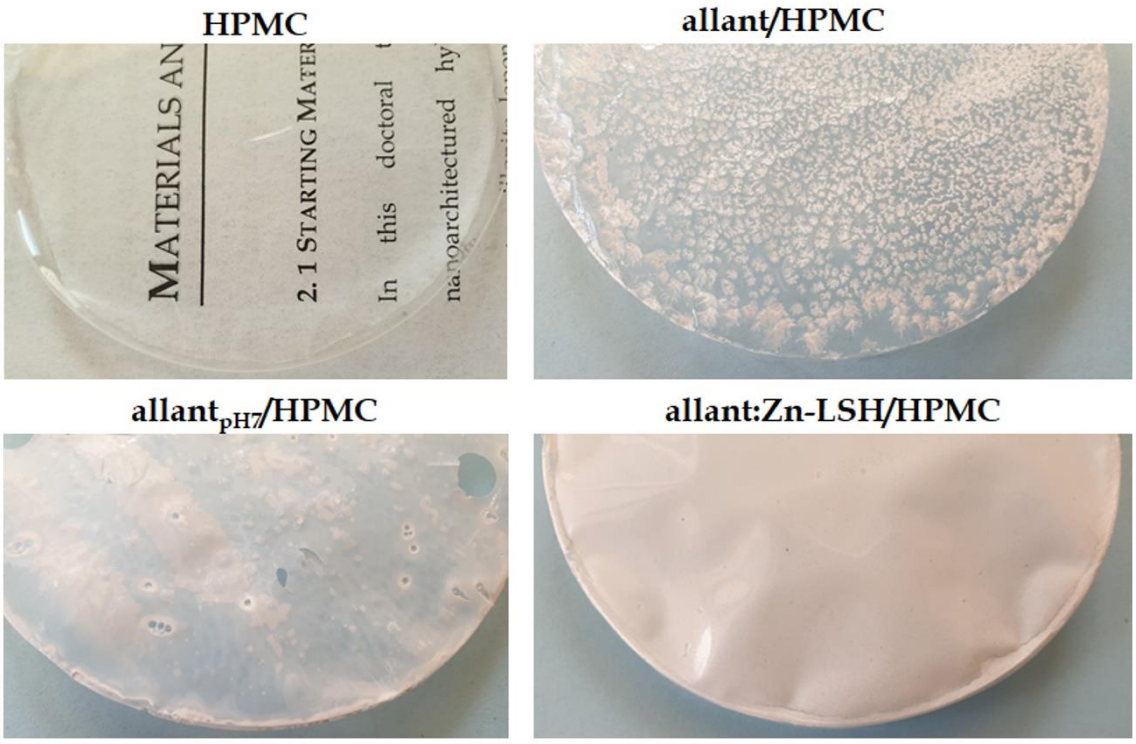

Figure 4.20. Images of HPMC films with allantoin and the allant:Zn-LSH hybrid.

Then, to overcome the problem of high hydrophilicity of the HPMC and to make possible the evaluation of the inhibition halo, it was explored agar as biopolymeric matrix of the bionanocomposite films. The agar-based bionanocomposite films were prepared also by the casting method from dispersions of the allantoin-based systems in an aqueous solution of the biopolymer and slow evaporation of the solvent (see Chapter 2 #section 2.2.2). In addition, for comparative purposes the allantoin-based systems were directly deposited in Whatman filters to determine their bactericide activity when they are not incorporated in the biopolymeric matrix, i.e., they can release species freely from the allantoin-based system.

Figure 4.21 shows images of the antimicrobial study performed, in duplicate, using materials prepared from the allantoin-based materials directly incorporated in Whatman filters (noted with W), referring to samples labelled from 1 to 8, and in the develoed agar bionanocomposite films (noted with A) referring to samples labelled from 9 to 16. In Table 4.6 is colleted the characteristics, names and abbreviations of the tested materials for easier

identification. It should be noted that $ZnCl_2$ was used as a Zn blank, Zn-LSH as a allant:Zn-LSH blank, Zn-NaOH as a allant:Zn-complex blank and also allantoin alone was checked, to discard/confirm any activity of this molecule.

Table 4.6. Identification labells of the various samples evaluated in the antimicrobial study showed in Figure 4.21.

Number	**Sample**	**Number**	**Sample**
1	allant@W	9	allant@A
2	Zn@W	10	Zn@A
3	ZnAl-LDH@W	11	ZnAl-LDH@A
4	$allant_{cop}$:ZnAl-LDH-@W	12	$allant_{cop}$:ZnAl-LDH@A
5	Zn-LSH@W	13	Zn-LSH@A
6	allant:Zn-complex@W	14	allant:Zn-complex@A
7	Zn-NaOH@W	15	Zn-NaOH@A
8	allant:Zn-LSH/W	16	allant:Zn-LSH@A

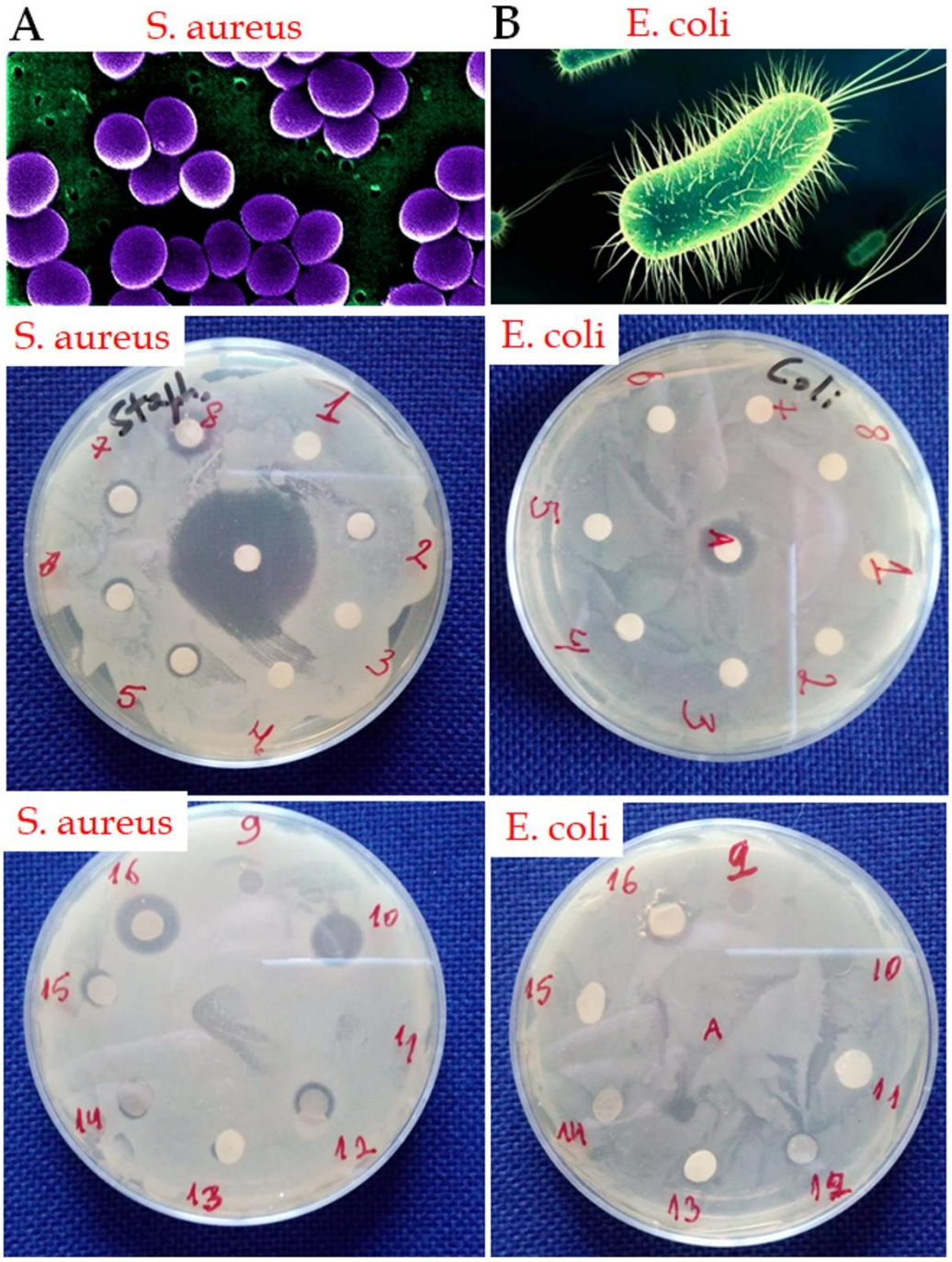

Figure 4.21. Images showing the evolution in the growth of the microbial population after 24 hours of *Staphylococcus aureus* (A) and *Escherichia coli* (B) colonies. The materials corresponding to each nunber are detailed in Table 4.6. The central sample carrying the antibiotic azithromycin is used as a positive control.

As detailed in the Chapter 2 #section 2.5.2, the bacteria growth on agar plates were observed after 24 h of incubation at 37 °C. The materials tested in the agar plates containing the *E. Coli* bacteria showed no inhibition halo. This result was observed for both type of samples, the systems directly embebed into the Whatman filter (1-8) and on the allantoin-Zn systems incorporated in the agar films (9-16). In contrast, in tests with the *S.aureus* bacteria, inhibition halos are observed in various of the samples, being oberved certain differences that depends if the active phase was directly deposited in the support (W samples) or if it was integrated within the polymeric matrix of the support (A samples), the lastest showing all inibition halos. However in the W series, samples 1, 3, 4, 5 and 6 do not exhibit inhibition halos, while samples 2, 5, 7 and 8, the ones containing $ZnCl_2$ (Zn), Zn-LSH , Zn-NaOH and allant:Zn-LSH hybrid, respectively, show inhibition halos though smaller tha the ones of the equivalent system incorporated in the agar film.

Anayzing the results in Figure 4.21 with more detail it should be noted that for both tested bacteria, the pure allantoin (samples 1 and 9) does not show any inhibition halo, which is an expected result considering that allantoin does not have bactericidal properties. The antibacterial effect of Zn^{2+} is proven by the halo displayed by samples containing $ZnCl_2$ (2 and 10) as the ions can be released directly to the medium, the observed differences of efficiency being related to the different release from each support. The ZnAl-LDH system (samples 3 and 11) do not show inhibition halo, which may be related to the fact the Zn ions are well stabilized in the LDH structure and so they cannot diffuse easily to the culture medium. In the case of the $allant_{cop}$:ZnAl-LDH hybrid it is again observed activity in the case of the material incorporating the hybrid in the biopolymer matrix (sample 12), indicating that in this case the Zn present in the hydroxide is more available than in the neat LDH. The results with the allant:Zn-LSH hybrid are more satisfying as it is possible to observe the formation of halos when directly supporte in the Whatman substrate (sample 8) as well as incorporated in the agar matrix (sample 16), being again more efective the biopolymer film substrate. Moreover, the inhibition halos are greater than the ones observed in

the equivalent samples involving the use of the allant:Zn-complex and Zn-NaOH (samples 6, 7, 14 and 15), proving so the allant:Zn-LSH hybrids could be of interest for applications involving the use of the complex patented by Margraf, (1974).

To better study the amount of Zn^{2+} released in the systems prepared in this work, various suspensions in water of the allantoin-Zn systems (allant:Zn-complex, Zn-complex, $allant_{cop}$:ZnAl-LDH, allant:Zn-LSH) and a Zn-LSH (used as blank) were prepared incorporating in all the cases the necessary amount of solid for containing 8.5 mg of Zn^{2+}. These suspensions were kept at 37 ºC for 48 hours in closed recipient so that the suspension did not evaporate. Then the supernatant was analyzed by XTRF. The results shown in the Table 4.7 clearly indicate that the allant:Zn-LSH hybrid and the allant:Zn-complex are the two materials that release the largest amount of Zn^{2+} ions in water. Though this experiment show very similar release of Zn^{2+} ions from both systems, the antibacterial tests show a higher efficiency of the allant:Zn-LSH system, which is relevant for further applications of the developed materials.

Table 4.7 Amount in mg of Zn^{+2} released in water.

Samples	**Zn^{+2} released (mg)**
allant:Zn-complex	0.66
Zn-complex	0.78
$allant_{cop}$:ZnAl-LDH	0.10
allant:Zn-LSH	0.80
Zn-LSH	0.27

Due to the good antibamicrobial results obtained mainly with the allant:Zn-LSH hybrid it will be intersting to study other supports most commonly used in the preparation of films for topical application. Recently, our group has reported the

preparation of bionanocomposite systems based on the combination of cellulose nanofibers (CNF), sepiolite and halloysite clays were used to produce stable films for release of silicic acid and ibuprofen of potential interest in wound dressing tissue applications (Lisuzzo et al., 2019). Nanocellulose is of great interest in the development of biomedical materials, mainly when using CNF obtained from bacteria, due to its low cost, biodegradability, biocompatibility, good mechanical properties, availability, sustainability and low cytotoxicity (Jorfi and Foster, 2015b; Bacakova et al., 2019). Nanocellulose, in general, has proven over the years as a good candidate for applications in wound healing, and skin tissue engineering (Bacakova et al., 2019). In addition, there are studies that showed a remarkable conformability to several body measurers, maintaining an adequate water balance and significantly reducing the pain in the wounds (Petersen and Gatenholm, 2011; Fu et al., 2013; Jorfi and Foster, 2015b). For instance, histological studies will exhibit significant tissue regeneration, hair formation and cell proliferation superior to conventional materials such as Vaseline gauze and Algisite M (Petersen and Gatenholm, 2011; Fu et al., 2013; Jorfi and Foster, 2015b). In this way, it has been here explored the preparation of nanocellulose films containing allantoin and the allant:Zn-LSH hybrid. Figure 4.22 shows the aspect of various films formed from cellulose nanofibers. The pure nanocellulose film is transparent and homogeneous. However, when allantoin is added to the CNF matrix, the result is very similar to that found in films based on HPMC, with the formation of small crystals of allantoin (Figure 4.22). Here again, the allant:Zn-LSH hybrid can be more easily dispersed in a hydrogel of CNF allowing the preparation of homogeneous films, apparently with a good distribution of the hybrid within the nanocellulose matrix (Figure 4.22). In this case, the produced allant:Zn-LSH/CNF bionanocomposite film is more flexible and has some adhesiveness when it comes in contact with skin humidity compared to the agar-based films, which make very promising the system for the intended application as wound-healing tissues. Further work regarding a systematic characterization, from mechanical properties to evaluation of antimicrobial activity, as well as

optimization of the content in the active component is still required to complete the study.

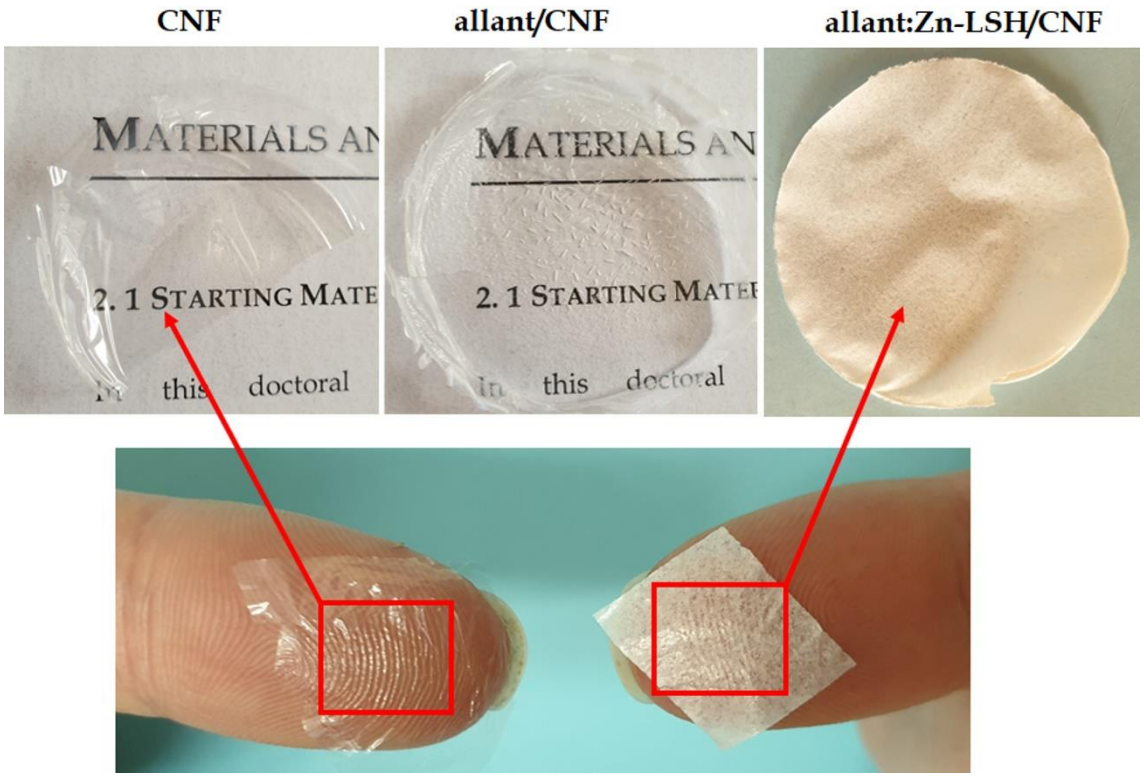

Figure 4.22. Images of CNF-based films prepared with the biopolymer alone and with allantoin and the allant:Zn-LSH hybrid.

4.7 CONCLUDING REMARKS

This chapter reports a study related to the association of allantoin with inorganic solids, including layered double hydroxides of brucite-type structure (LDH) or layered single hydroxides (LSH), starting from different salts and metals. Allantoin is a compound of natural and also synthetic origin widely used as a component of numerous cosmetic and pharmaceutical formulations due to its healing, soothing and keratolytic properties. The incorporation of allantoin in the Mg-Al LDH prepared by the co-precipitation and by ion-exchange method is not evident through XRD analysis. However, an amount of allantoin approximately equivalent to half of the ACE of LDH (330 mEq/100 g) for the co-precipitation (142 mEq/100 g) and lower for the ion-exchange (50 mEq/100 g) produced

materials, is deduced from the characterization results performed by CHN elemental analysis. The co-precipitation protocol has been effective in the preparation of the Zn-Al LDH in the presence of allantoin, proving that the solid formed contains an amount of allantoin similar to the LDH anionic exchange capacity. Elementary chemical analysis CHN allows to calculate a content of 348 mEq of allantoin /100 g of ZnAl-HDL. However, by EDX analysis it is confirmed that this material contains mainly Zn and very little amount of Al, so that the expected LDH structure with a Zn:Al 2: 1 ratio is not formed, but the resulting material seems to be closer to a layered single hydroxide (LSH) stoichiometry instead. Based on this result it has prepared a new material using the same LDH preparation conditions but without Al, obtaining in this case a layered material with a large amount of associated allantoin that remains in the interlayer region of the precipitated Zn-LSH structure. The release properties of these materials in a phosphate saline solution were also studied simulating the pH of the skin (≈ 5.5). All the materials have proven efficient in the release of allantoin; however, the LSH-based material exhibits a slightly faster initial release and almost releases 100% allantoin after 8 hours. Likewise, the incorporation of these hybrid allantoin systems in a agar polymer matrix or directly embedded in Whatman filters was carried out in order to evaluate their activity against cultures of two bacteria, a Gram-positive bacterium (*Staphylococcus aureus*) and a Gram-negative bacterium (*Escherichia coli*) on agar plates. In these studies, no halo of inhibition was seen for any material tested on agar plates containing *Escherichia coli*. On the other hand, various of the materials tested with the *Staphylococcus aureus* bacteria, have proven to be effective against this microorganism, being the best results obtained for those containing the allant:Zn-LSH hybrid, which presented a greater halo of inhibition compared to any of the other active systems, even better than those based on the patented Zn-allantoin complex. In this study, it has been seen that the incorporation of allantoin in a Zn-based LSH will improve the properties of the final material, by benefiting from the use of Zn as an antibacterial agent. In view to its possible application as wound dressings, allantoin and the LSH system were also incorporated into two cellulose-based

polymeric matrices, HPMC and CNF. In this study, the cellulose nanofibers matrix has proven to be more effective, since it produces more flexible bionanocomposite films, unlike the HPMC films that are more brittle. As CNF has a good capacity to absorb water and it has adhesive properties when it comes in contact with the skin, this type of bionanocomposite systems could be of interest in view to further development of effective wound dressing tissues. Another important point is that the incorporation of allantoin in an inorganic solid improves its stability and allows to form homogeneous films, avoiding the crystallization and segregation that take place when the drug is directly incorporated in the various tested polymers. The allantoin:Zn-LSH hybrid presents advantages both in the release of allantoin in *in vitro* test, and in antibacterial activity carried out on agar plates, compared to materials based on Zn-allantoin found in the literature, with suggest a high potential for their possible application as wound dressings, in cosmetic uses or in dermatological treatments.

CHAPTER 5

BIONANOCOMPOSITES BASED ON LAYERED DOUBLE HYDROXIDE-SEPIOLITE HYBRID NANOARCHITECTURES FOR CONTROLLED RELEASE SYSTEMS OF HERBICIDES

This chapter focuses on the exploration and development of hybrid nanoarchitectures based on a magnesium-aluminium layered double hydroxide (LDH) supported on sepiolite, taking advantage of the properties that both materials possess as nanoarchitectures to incorporate an anionic herbicide, 2-methyl-4-chlorophenoxylacetic acid (MCPA) and to apply them as controlled release systems. For this purpose, the incorporation of MCPA was first studied in LDH/sepiolite nanoarchitectures by ion-exchange and then explored the preparation of the hybrid nanoarchitectures by direct co-precipitation of the LDH in a medium containing sepiolite and the herbicide. Besides, MCPA-LDH hybrid materials and the hybrid nanoarchitectures were incorporated into an alginate-zein matrix to produce bionanocomposite materials conformed as beads for evaluation in controlled delivery of MCPA. The main objective is to compare the characteristics of various type materials and propose a system that allows a more sustainable management of the herbicide. The results of the in vitro release proved to be efficient and applicable to a controlled release from the bionanocomposite system based on the nanoarchitecture hybrid of MCPA.

5.1 INITIAL CONSIDERATIONS

In recent years there has been a great growth in the development of inorganic-inorganic heterostructured materials also now called nanoarchitectonic materials or just nanoarchitectures, that allow, to take advantage of the properties of both assembled components. The building up of certain nanoarchitectonics contemplates the assembly of components in interaction at their interface which can modify their properties, adding more potential for the development of new functional materials (Aono et al., 2012; Khan et al., 2017; Komiyama et al., 2017; Ariga et al., 2019). Based on this context, various nanoarchitectures were developed based on layered clays over the years, from classical pillared clays (Brindley and Sempels, 1977; Gil et al., 2008; Gil et al., 2010) and porous clay heterostructures (PCH) (Galarneau et al., 1995, 1997) to more innovative materials that include the assembly of diverse types of nanoparticles and other species to clays of different origin and morphology (Ruiz-Hitzky et al., 2012; Ruiz-Hitzky and Aranda, 2014; Aranda et al., 2015; Aranda and Ruiz-Hitzky, 2018) as explained in more detail in Chapter 2 #section 2.2.3.

Based on these premises, on this Thesis new hybrid nanoarchitectures were prepared taking advantage of the anion exchange properties of MgAl-LDH/sepiolite nanoarchitectures and also it was developed a new methodology that allows they formation in one-step processes by co-precipitation of the MgAl-LDH in a dispersion of sepiolite in water in which it was also present the organic specie to incorporate. The current aim is to ascertain if it is possible to develop organic-inorganic hybrid materials using LDH-sepiolite nanoarchitectured materials, as the presence of an organic counterpart could be of interest for introducing additional functionalities. In this way, we have explored in this study the incorporation of anionic species, the 2-methyl-4-chlorophenoxyacetic acid (MCPA) herbicide in its ionic form (Figure 1C), as it is expected its easy association with the LDH intercalated for neutralizing the charge of the double hydroxide. Thus, hybrid nanoarchitectures were prepared profiting from the anion exchange properties of a MgAl-LDH/sepiolite (Figure 1D) and also by co-precipitation of the MgAl-LDH in the presence of an aqueous dispersion of

sepiolite in which MCPA was also present (Figure 1E). Differences in composition, structure and release behavior in the developed hybrid nanoarchitectures prepared by the two methods were examined and analyzed. In view to apply these materials in agriculture, the efficiency of formulations based on the hybrid nanoarchitectures was explored in *in vitro* tests of MCPA release, confirming the improvement of retention properties and so their potential interest in applications related to controlled herbicide delivery. For a better control in the MCPA release, the hybrid nanoarchitectures were also associated with mixtures of alginate-zein biopolymers to produce bionaocmposite beads that may improve retention properties and so, procure sustainable release for longer periods of time.

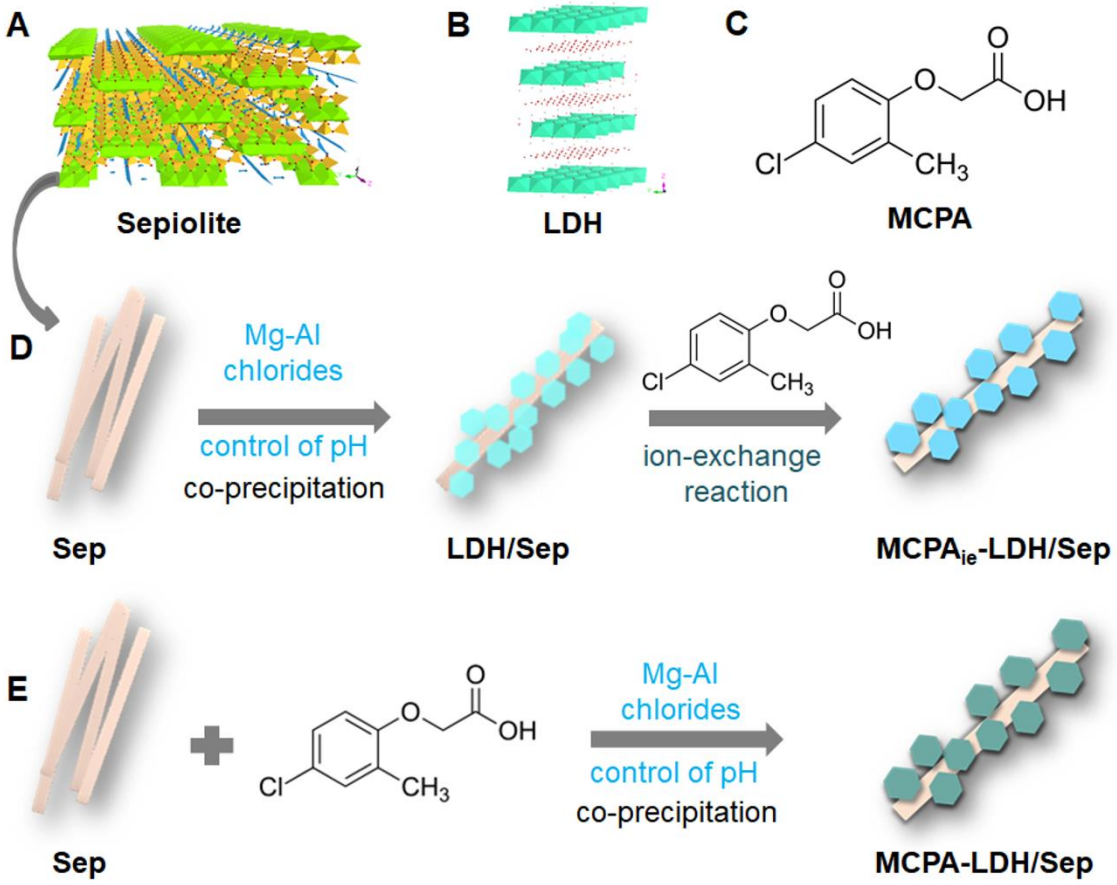

Figure 5. 1. Schematic representations of sepiolite (A) and layered double hydroxide (B) structures, molecular formula of the 2-methyl-4-chlorophenoxyacetic acid (MCPA) herbicide (C). Schemes of the synthesis process follow for the preparation of hybrid MCPA-LDH/sepiolite nanoarchitectures by ion-exchange (D) and by one-step co-precipitation (E) methods.

5. 2 LAYERED DOUBLE HYDROXIDE-MCPA HYBRIDS

5.2.1 MCPA-LDH hybrid prepared by the ion-exchange and co-precipitation methods

The LDH of the general formula $[Mg_2Al_3(OH)_6]Cl.xH_2O]$ was synthesized by co-precipitation method as described in detailed in Chapter 2 #section 2.2.3. The XRD pattern (Figure 5. 2) of this LDH shows the characteristic reflections of the inorganic solid structure with the most intense diffraction peak at approximately

11.35º in 2 theta angle that corresponds to the d_{003} (003) reflection. Additionally, (006), (012), (015), (018), (110) and (113) reflections of the LDH structure can be also observed in the diffractogram (Miyata, 1977; Bish, 1980; Meyn et al., 1990; Rives, 2001). Considering the (00l) reflection peaks it can be deduced a basal spacing of 0.77 nm, and as the thickness of the brucite layer is approximately 0.48 nm then a basal space increase of 0.29 nm confirms the presence of Cl^- anion in the interlayer region (Constantino and Pinnavaia, 1995). The intercalation of MCPA in hybrids prepared by ion-exchange and co-precipitation methods is evidenced by the displacement of the (00l) reflections towards lower 2 theta angle, giving rise to basal spacing of 2.15 and 2.32 nm for the $MCPA_{ie}$-LDH and MCPA-LDH hybrid materials, respectively. Values that give rise to a basal spacing increase of around 1.67 and 1.84 nm, suggesting that the MCPA is intercalated forming a bilayer between the LDH sheets, similarly to that observed in other studies (Lakraimi et al., 2000; Inacio et al., 2001; Cardoso and Valim, 2006). Considering the short time required for the preparation of the hybrids by the co-precipitation method, 24 h instead of 72 h, that one seems advantageous over ion-exchange protocols to produce the MCPA-based hybrids. In addition, from the CHN elemental chemical analysis it was deduce a content of 278 mEq and 303 mEq of MCPA per 100 g LDH for the $MCPA_{ie}$-LDH and MCPA-LDH hybrids, respectively. Actually, the amount of MCPA per 100 g LDH incorporated by the co-precipitation method almost fulfills the ion-exchange capacity of this 2:1 MgAl-LDH, which ranges from approx. 330 mEq per 100 g of LDH (Badreddine et al., 1998; Inacio et al., 2001; Pavlovic et al., 2005; Cardoso et al., 2006; Bruna et al., 2009; Alromeed et al., 2015b).

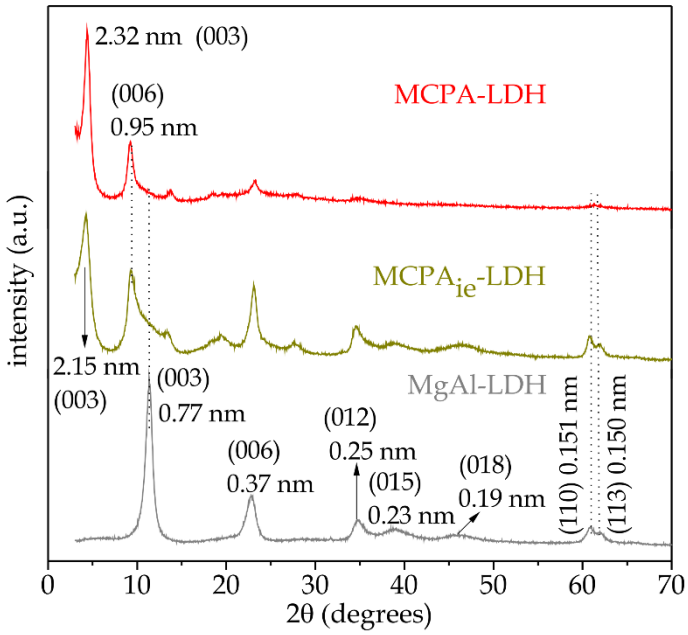

Figure 5. 2. XRD patterns of MgAl-LDH and the $MCPA_{ie}$-LDH and MCPA-LDH hybrids prepared by ion-exchange and co-precipitation, respectively.

The interactions between the LDH and the MCPA herbicide in the hybrids were studied by infrared spectroscopy (Figure 5. 3). The intense bands at 3460 cm^{-1} and 1630 cm^{-1} that appears in the spectra of the neat LDH and also the hybrids correspond to the valence vibrations of hydroxyl groups and the bending vibration of water δ(H_2O), respectively (Badreddine et al., 1998; Lakraimi et al., 2000). The bands observed in the LDH in the low frequency region of the spectrum correspond to the reticular vibration modes and can be attributed to the M-O (758 and 665 cm^{-1}) and O-M-O (435 cm^{-1}) vibrations where "M" refers to Mg or Al (Miyata, 1977; Cavani et al., 1991; Badreddine et al., 1998; Houri et al., 1999; Lakraimi et al., 2000; Pavlovic et al., 2005). Despite the precautions taken during the synthesis of the materials, a small contamination by CO_3^{-2} can be considered in the solid due to the apparition of the characteristic vibration band at 1360 cm^{-1} (Miyata, 1975).

The FTIR spectrum of the MCPA shows bands at 1495 and 1430 cm^{-1} corresponding to the vibrations of the aromatic ring C=C, bands at 1300 and 1080 cm^{-1} assigned to the asymmetric and symmetric stretching vibration of C-O-C,

respectively, and bands at 1740 cm^{-1} corresponding to the $\nu_{C=O}$ of carboxyl group (Pavlovic et al., 2005; Cardoso et al., 2006).

In the $MCPA_{ie}$-LDH and MCPA-LDH hybrids the intercalation is confirmed due to the disappearance of the $\nu_{C=O}$ band 1740 cm^{-1} and the presence of a broad band at 1610 cm^{-1} that can be assigned to the asymmetric stretching vibration of the ionized COO^- groups. Next to it, a weaker band about 1490 cm^{-1} corresponding to the $\nu_{C=O}$ of the COO^- group corroborates that MCPA is incorporated between the LDH layers in its anionic form. In addition, other bands appearing at 2925 cm^{-1}, which can be attributed to the aliphatic C-H stretching vibrations of the herbicide, and at around 1245 and 1080 cm^{-1}, which can be assigned to the phenyl-alkyl ether groups present in MCPA, are also observed in the spectrum of the hybrid materials (Figure 5. 3) (Lakraimi et al., 2000; Inacio et al., 2001; Pavlovic et al., 2005; Cardoso et al., 2006; Bruna et al., 2009). In addition, bands at around 1360 and 1365 cm^{-1} in the starting LDH and in the $MCPA_{ie}$-LDH, point out to a possible a little contamination by carbonate ions during the preparation of the materials (Miyata, 1975).

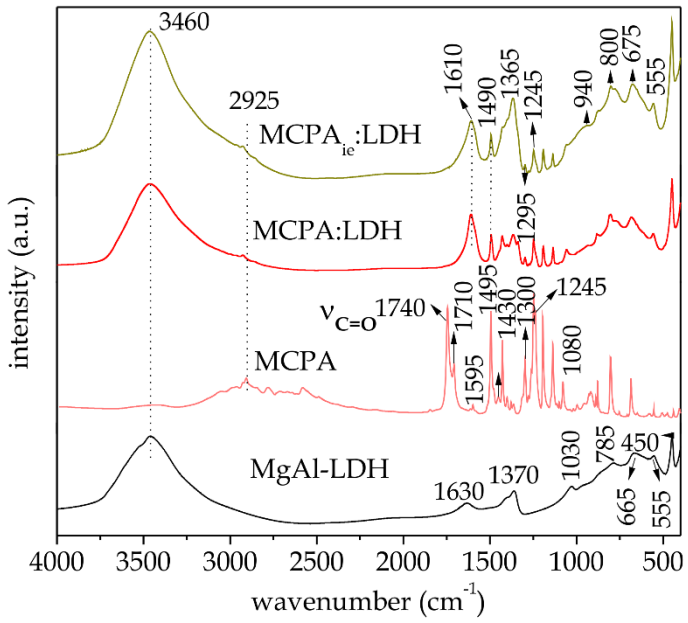

Figure 5. 3. FTIR spectra of MgAl-LDH, MCPA, and the MCPA-LDH and $MCPA_{ie}$-LDH hybrids.

The morphology of the neat LDH and that of the MCPA-LDH and $MCPA_{ie}$-LDH hybrid materials was analyzed by field emission scanning eletron microscopy (FESEM) and electron transmission microscopy (TEM) (Figure 5. 4). Figure 5. 4A shows that LDH flat nanoparticles an agglomerated as a *sandrose* structure (Leroux et al., 2004), with a particle size of around 100 nm. According to Figure 5. 4B & E, the incorporation of MCPA into MgAl-LDH, by ion-exchange and co-precipitation, gives rise to a more spongy morphology, where the nanopaticles seem to be less aglomerated, with a particle size around 100 nm. The TEM images (Figure 5. 4B, D & F) show that of the morphology of all the LDH materials are firmed by flat round disc particles some of them almost of hexagonal form typical of hydrotalcite materials (Costantino et al., 1998; Okamoto et al., 2007). Particle size is in all the samples in the nanometric scale with diameter typically around 100 nm.

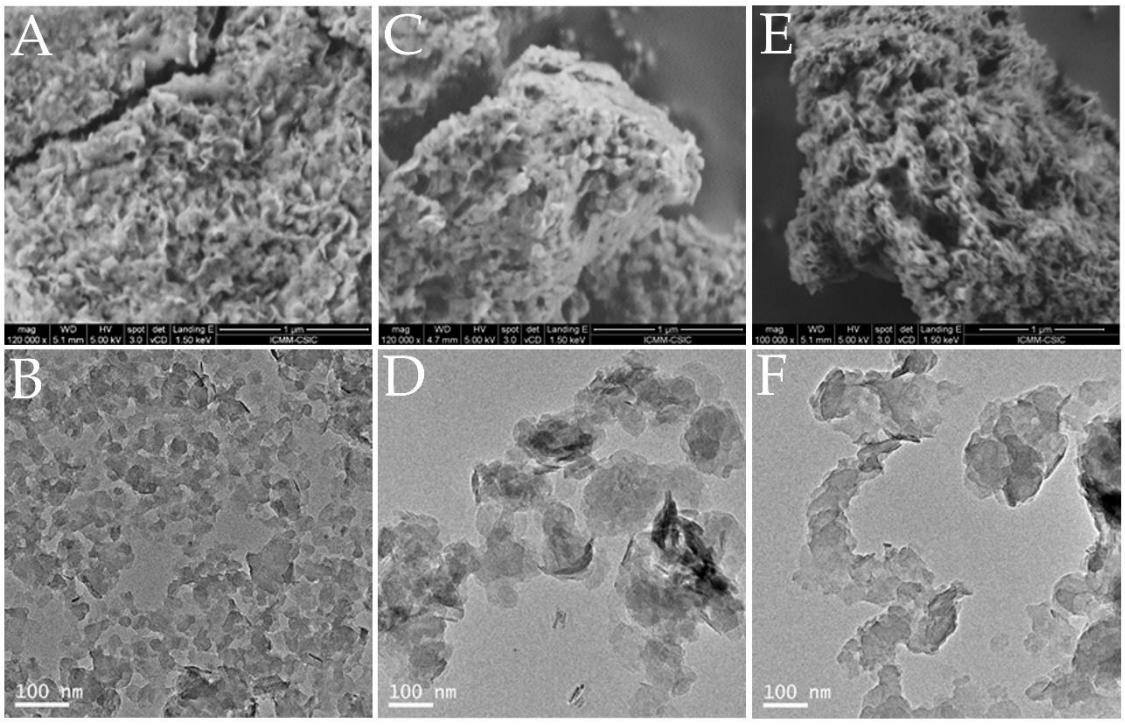

Figure 5. 4. FESEM (upper row) and TEM (bottom row) images of the MgAl-LDH(A, B), $MCPA_{ie}$-LDH (C, D) and MCPA-LDH (E, F) (co-precipitation) hybrids.

5.3 MCPA:LDH/SEPIOLITE HYBRID NANOARCHITECTURES

5.3.1. LDH/sepiolite nanoarchitectures prepared by the co-precipitation method

The preparation of HDL/sepiolite (LDH/Sep) nanoarchitectures is based on a method developed and patented by Ruiz Hitzky et al. (2008) where the LDH is prepared by co-precipitation of the LDH in the presence of sepiolite, with some adaptations according to the needs of the current study. Thus, LDH with formula $[Mg_3Al_2(OH)_6]Cl \cdot xH_2O$ was prepared in the presence of a dispersion of sepiolite at pH ≈ 9, as described in Chapter 2 #section 2.2.3. In order to study the materials systematically, nanoarchitectures with different LDH/sepiolite ratios were prepared. Thus, the amount of reagents used for the formation of LDH was varied and sepiolite was fixed in order to ready the formation of LDH/sepiolite nanoarchitecture with 2:1, 1:1, 0.5:1 and 0.3:1 LDH:sepiolite proportions. Once formed, the nanoarchitectures were recovered by centrifugation and submitted to a thermal treatment at 60 or 150ºC to produce their consolidation (Chapter 2 #section 2.2.3). Table 5. 1 shows the yield of LDH formed with respect to the one expected in the formation of the various nanoarchitectures, which in all the cases is around 90%.

Table 5. 1. Yield of MgAl-LDH and nanoarchitectures prepared based on LDH:sepiolite.

Sample	**Yield (%)**
MgAl-LDH	93.38
LDH/Sep2:1	91.01
LDH/Sep1:1	90.00
LDH/Sep0.5:1	91.45
LDH/Sep0.3:1	93.13

The resulting LDH/sepiolite nanoarchitectures, were initially characterized by X-ray diffraction (Figure 5. 5) to confirm the presence of the LDH. In the nanoarchitectures, at least the (003) reflection peak of the LDH is observed, being determined from them a basal spacing d_{003} = 0.77 nm in all the cases. Additionally, the peaks ascribed to (110) and (113) characteristic reflections of the LDH are also observed at 0.152 and 0.150 nm, respectively together with other reflection peaks assigned to sepiolite, being clearly visible the one at d_{110} = 1.21 nm corresponding to the characteristic (110) reflection(Gómez-Avilés et al., 2016). By comparing the patterns of different nanoarchitectures, it is also observed that the peak ascribed to the (003) reflection of the LDH increases in intensity with respect to the (110) peak of sepiolite as the amount of LDH in the nanoarchitecture increases, similarly to that found by Gómez-Avilés et al., (2016) and Tian et al., (2016) in the formation of other nanoarchitectures based on LDH supported on sepiolite.

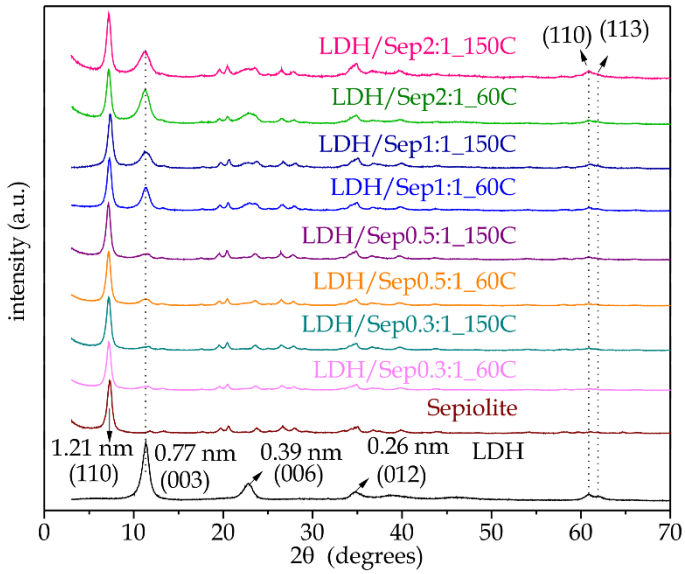

Figure 5. 5. XRD patterns of LDH, sepiolite and LDH/Sep nanoarchitectures prepared to contain different LDH:clay ratio.

The FESEM images (Figure 5. 6) of the different of LDH/Sep nanoarchitectures show the growth of LDH on the surface of the sepiolite fibers. As the LDH present in the nanoarchitectures increases and the fibers became further covered by nanoparticles of the hydroxide more compacted materials are produced.

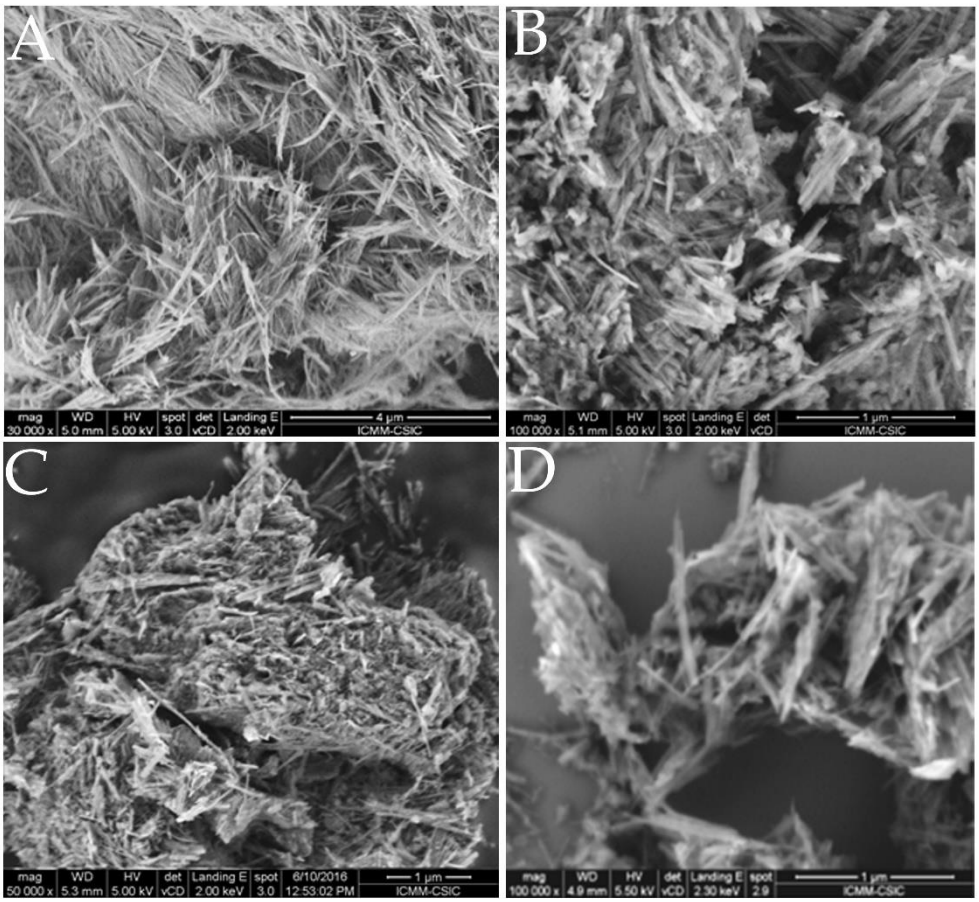

Figure 5. 6. FESEM images of sepiolite (A), and the LDH/Sep 2:1 (B), LDH/Sep 1:1 (C) and LDH/Sep 0.5:1 (D) nanoarchitectures.

The chemical interactions between the nanoparticles assembled in the nanoarchitectures can be corroborated by infrared spectroscopy analyzing the spectral zone where appears the characteristic stretching OH vibration of the Si-OH and Mg-OH groups of sepiolite structure at approximately 3720 and 3680 cm^{-1}, respectively, in pure sepiolite (Figure 5. 7A) (Ahlrichs, 1975). Thus, these two bands are observed in all the prepared systems (Figure 5. 7A), but with significant difference that account of the interactions. The $\nu_{Si\text{-}OH}$ band at 3720 cm^{-1}, appears with much lower intensity in the LDH/Sep nanoarchitectures thermally treated

at 60 or 150 °C, which confirms the existence of chemical interactions between the Si-OH on the surface of the sepiolite and the LDH particles. A similar behavior was observed in other materials adsorbed on sepiolite, as for instance thioflavine-T (Casal et al., 2001), sacran biopolymer (Alcântara et al., 2014) and ZnO nanoparticles (Akkari et al., 2016) perturbing the band till practically no being observable in certain cases. In the LDH/Sep nanoarchitectures the existence of hydrogen interactions between the silanol groups of the silicate and the LDH particles, also provoked the shift of this band to lower frequencies and then it becomes practically imperceptible overlapped by other bands appearing in that region.

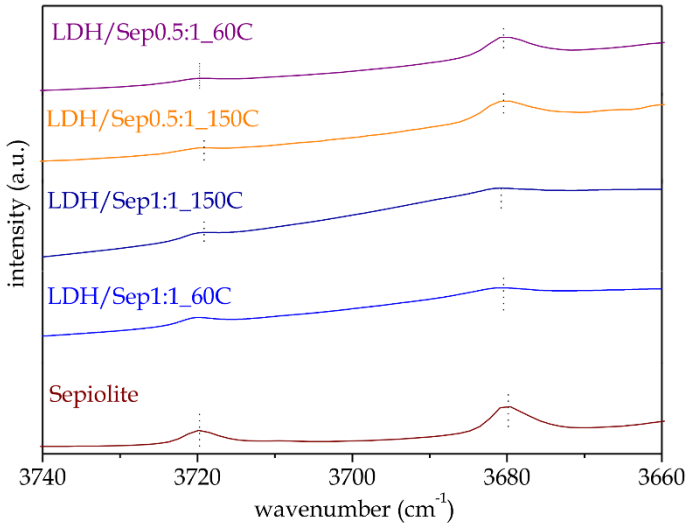

Figure 5. 7. FTIR of the spectra 3740 to 3660 cm^{-1} region of pure sepiolite and LDH/Sep nanoarchitectures prepared in proportions of 1:1 and 0.5:1 consolidated at 60 and 150 °C.

The chemical interactions between the LDH and sepiolite in the nanoarchitectures prepared by the co-precipitation method was also corroborated by ^{29}Si MAS NMR spectroscopy. The ^{29}Si NMR spectrum of sepiolite in Figure 5. 8 shows the presence of three Q^3 signals corresponding to Si atoms located within the structure and a Q^2 signal associated with Si atoms of the silanol groups at the external surface of sepiolite fibers (de la Caillerie and Fripiat, 1992). As previously reported by Gómez-Avilés et al. (2016), those three

characteristic Q^3 signals are observed in the spectra of the LDH/sepiolite nanoarchitectures at around -92.5, -95 and -98.4 ppm, together with a new Q^3 signal that appears at -96.6 ppm. The Q^2 signal (Figure 5. 8) associated with the silanol groups decrease in intensity till become practically undetectable as the LDH content increase and the fibers become more and more covered by LDH nanoparticles. Thus, the new Q^3 signal can be univocally associated with a new type of Si environment coming from the condensation of the OH of silanol groups on the surface of the sepiolite fibers with hydroxyl groups of the co-precipitated LDH particles. This result was also observed in the formation of other nanoarchitectures based on sepiolite (Belver et al., 2013; Gómez-Avilés et al., 2013, 2016), confirming that so that in the materials here developed the LDH are chemically bounded though the silanol groups that cover the silicate fibers. Moreover, from the results of the current work it seems that the temperature of consolidation step is not as critical in the formation of the nanoarchitectures as there are not significant differences in the spectra of the nanoarchitectures consolidated at 60 and 150ºC.

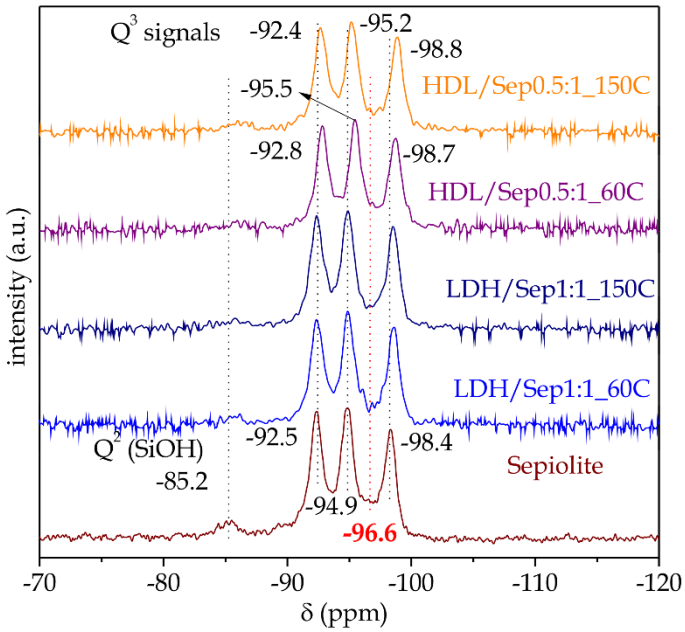

Figure 5.8. ^{29}Si MAS NMR spectra of sepiolite (a) and the LDH/Sep0.5:1_60C (b), LDH/Sep0.5:1_150C (c), LDH/Sep1:1_60C (d) and LDH/Sep1:1_150C (e) nanoarchitectures.

5.3.2 MCPA$_{ie}$-LDH /sepiolite hybrid nanoarchitectures prepared by the ion-exchange method

The preparation of hybrid nanoarchitectures LDH/Sep based on the association of the 2-methyl-4-chlorophenoxylacetic acid herbicide was first achieved by ionic exchange of MCPA anions with the chloride ions present in previously prepared LDH/Sep nanoarchitectures with different LDH:sepolite ratio (Figure 1D). The XRD patterns (Figure 5. 9) of the nanoarchitectures before and after the ion-exchange reaction, showed the presence of the most intense characteristics peaks of pure sand LDH structures. Moreover, differences in the position of the (003) reflection peak of the LDH in the pristine nanoarchitectures and most of the hybrid nanoarchitectures confirm the intercalation of MCPA in the LDH. Therefore, the reflection (003) of the starting LDH with a basal spacing of 0.77 nm shifts to lower 2θ angles, resulting in a basal spacing of 2.15 nm in the hybrid nanoarchitectures, coincident with that observed in the MCPA$_{ie}$:LDH hybrid (#section 5.2).

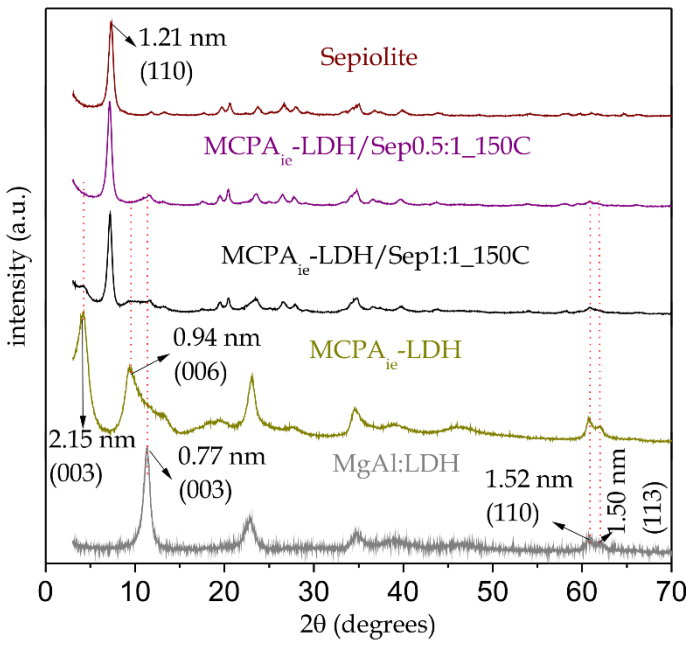

Figure 5. 9. XRD patterns of individual components (sepiolite, LDH, and MCPA), MCPA$_{ie}$-LDH intercalation compound and the neat LDH/Sep and MCPA$_{ie}$-LDH/Sep hybrid nanoarchitectures.

FTIR spectra of the hybrid nanoarchitecturas (Figure 5. 10) confirm the presence of bands attributed to the organic component in all of them, although, as in the intercalation compound $MCPA_{ie}$-LDH, the existence of interactions with the inorganic substrate modified the position of the bands. This especially affects the very intense bands at 1748 and 1707 cm^{-1} assigned to the $\nu_{C=O}$ vibration modes of the carboxylic group of the MCPA molecule, which was not observed in the spectra of $MCPA_{ie}$-LDH neither in those of the MCPAie-LDH/Sep1:1_150C hybrids (Figure 5. 10). They should move towards a lower wavelength being so expected at around 1610 cm^{-1} the symmetric and asymmetric stretching vibration of ionized COO^- groups since the carboxylic group must be present as a carboxylate (Alromeed et al., 2015b). In fact, the spectra of the hybrid nanoarchitectures show a large band in the region of 1630-1600 cm^{-1} region due to the overlapping of such bands with the one ascribed to δ_{HOH} vibration modes of water molecules adsorbed on inorganic solids, LDH and sepiolite, that appear around 1630 cm^{-1}.

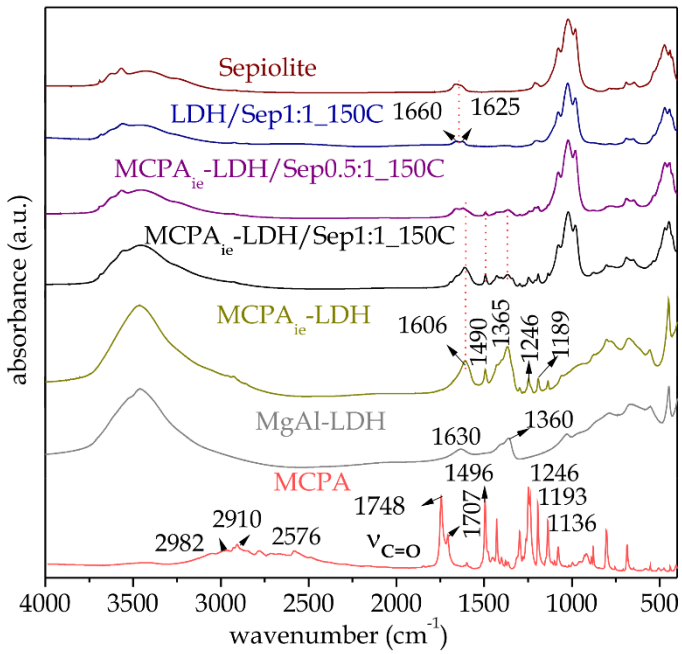

Figure 5.10. FTIR spectra of individual components (sepiolite, LDH, and MCPA), $MCPA_{ie}$-LDH intercalation compound and the neat LDH/Sep and $MCPA_{ie}$-LDH/Sep hybrid nanoarchitectures.

The presence of MCPA in the nanoarchitectures was confirmed by CHN elemental chemical analysis, values show in Table 5. 2 where MCPA content is expressed in relation to the amount of LDH present in the nanoarchitectures. The expected anion exchange capacity (AEC) of the LDH is around 330 mEq/100 g LDH and taking into account the content in MCPA in the $MCPA_{ie}$-LDH intercalation compound the calculated amount of MCPA in the hybrid nanoarchitectures suggests the ion-exchange process varies depending of the sample. The content of MCPA in the $MCPA_{ie}$-LDH/Sep1:1_150C hybrid nanoarchitecture is similar to that of the $MCPA_{ie}$-LDH hybrid, however the expected content for a complete ion-exchange is only reacheed in nanoarchitectures with lower LDH:ratio as it is the case of the $MCPA_{ie}$-LDH/Sep0.5:1_150C sample. This effect could be ascribed to a lower degree of agglomeration of the LDH particles grown on the sepiolite fibers in the nanoarchitecture with lower content in LDH, which may favor a faster ion-exchange reaction, being possible to complete the process in the adopted experimental conditions. In fact, when the sepiolite fibers are less covered by LDH nanoparticles, as in $MCPA_{ie}$-LDH/Sep0.3:1_150C, the amount of MCPA overpassed the ion-exchange capacity of the LDH. This can be explained by the fact that sepiolite fiber are not completely cover by LDH nanoparticles and so MCPA anions may be adsorbed on the surface of sepiolite, the hydrogen atoms of the silanol groups acting as new points for MCPA anions adsorption.

Table 5. 2. Amount of MCPA adsorbed in the hybrid nanoarchitectures by the ion-exchange method.

Sample	**LDH/Sep real ratio**	**MCPA-LDH/Sep real ratio**	**mEq of MCPA/100 g of LDH**
$MCPA_{ie}$-LDH	--	--	278
$MCPA_{ie}$-LDH/Sep1:1_150C	0.94:1	0.90:1	269
$MCPA_{ie}$-LDH/Sep0.5:1_150C	0.47:1	0.45:1	325
$MCPA_{ie}$-LDH/Sep0.3:1_150C	0.28:1	0.27:1	452

Figure 5.11 shows images obtained by FESEM and TEM of various $MCPA_{ie}$:LDH/Sep hybrid nanoarchitectures. From the FESEM images, it is clearly observed how sepiolite fibers appear covered and compacted after the co-precipitation process to produce the corresponding nanoarchitecture. The aspect of the as prepared material and the one recovered after the intercalation of MCPA in the LDH component does not vary significantly. This fact is confirmed by TEM (Figure 5. 11C & D), where it is possible to distinguish the presence of small flat particles attached to the fibers in both nanoarchitectures. These images also confirm that the ion-exchange treatment is in fact a topotactic intercalation process that does not affect the nature of the LDH/sepiolite nanoarchitecture, confirming also the stability of this type of materials. In fact, the content of LDH in the nanoarchitecture practically is the same often the ion-exchange reaction (Table 5. 2).

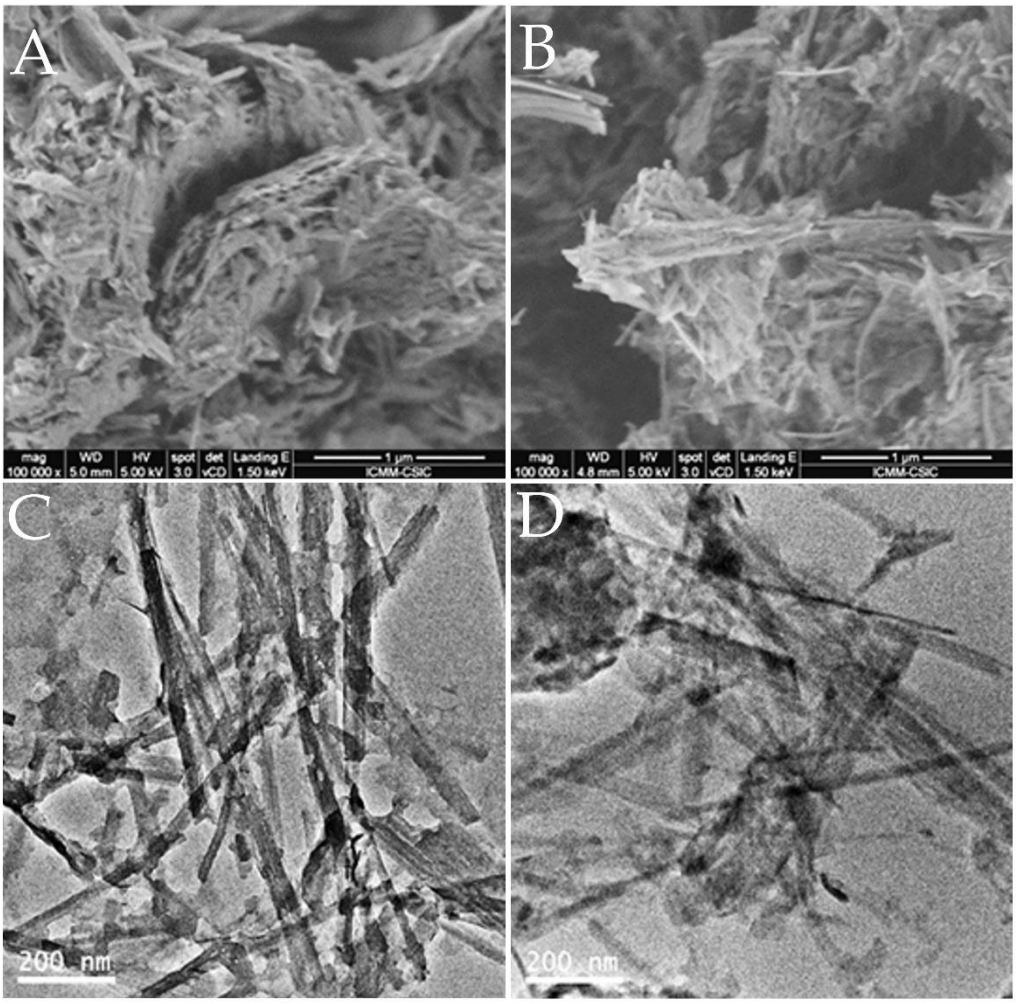

Figure 5.11. FESEM images of LDH/Sep1:1_150C (A), and $MCPA_{ie}$-LDH/Sep1:1_150C (B) nanoarchitectures; and TEM images of the LDH/Sep1:1_150C nanoarchitecture before (C) and after (D) the ion-exchange treatment with MCPA.

5.3.3. MCPA-LDH /sepiolite hybrid nanoarchitectures prepared by the co-precipitation method

In a second study, it was sought to prepare hybrid nanoarchitectures in a single step through the co-precipitation method, which involves the preparation of the LDH in the presence of sepiolite and the herbicide MCPA in an aqueous dispersion (Chapter 2 #section 2.2.3). XRD patterns of the resulting hybrid nanoarchitectures (Figure 5.12) confirmed that in all cases the MCPA is intercalated in the interlayer space of the co-precipitated LDH, as indicated by the presence of the (003) reflection peak characteristic of the LDH structure at 2θ

angle around 4.5 degrees. From that reflection, basal spacing values of 2.32 nm in the LDH present in the hybrid nanoarchitectures are deduced, which is similar to the value determined in MCPA-LDH intercalation compounds prepared by the co-precipitation method. The structure of sepiolite is maintained in all samples, independent of the proportion of LDH, while the most intense peak of the LDH decreased in intensity at the same time that the proportion of LDH/sepiolite is lowered. In addition, the (110) and (113) peaks characteristic of LDH solids are observed in all the nanoarchitectures formed, confirming the formation of the LDH structure for all the studied LDH:sepiolite ratios.

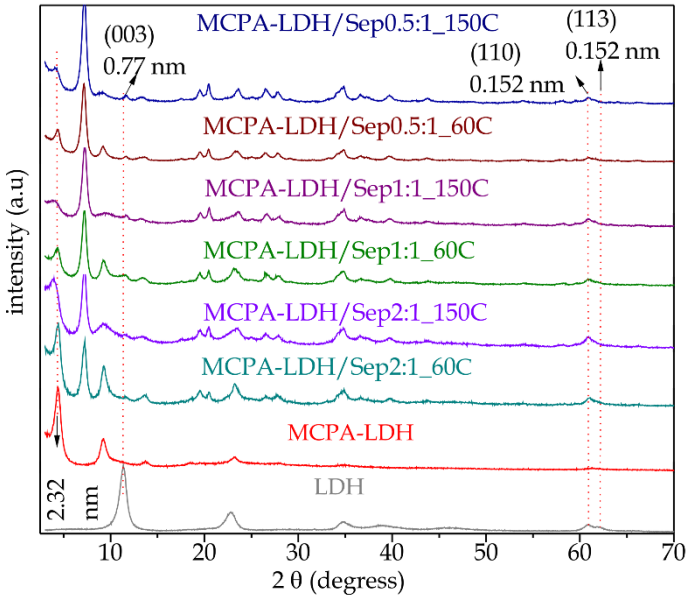

Figure 5.12. XRD patterns of MgAl-LDH, MCPA-LDH and the hybrid nanoarchitectures prepare by co-precipitation of the LDH in the presence of sepiolite and MCPA at a different LDH:sepiolite theoretical ratio (X:1).

The amount of adsorbed MCPA varies with the LDH:sepiolite ratio in the hybrid nanoarchitectures, unexpectedly with large amounts of MCPA retained as the amount of LDH is reduced (Table 5. 3). Moreover, it seems that the presence of large amounts of MCPA is reflected in lower yield in the production of assembled LDH particles in the nanoarchitecture, which can be reduced to a half for nanoarchitectures with a 0.5:1 LDH:sepiolite theoretical composition. In most of

the prepared hybrid nanoarchitectures, the amount of MCPA exceeds the anionic exchange capacity of the LDH (≈ 330 mEq/100 g), which suggests that a part of the MCPA is adsorbed by other mechanism, perhaps on the external surface of the sepiolite clay or in interaction with the clay and the LDH particles. In previous studies it has been reported that sepiolite does not absorb large amounts of this herbicide (Atçay and Yurdakoç, 2000). Figure 5. 13 displays the adsorption isotherm of MCPA on sepiolite, showing that the maximum adsorbed amount of MCPA varies and does not reach a clear plateau but it is possible to adsorb upto 100 mg of MCPA per g of sepiolite. However, we have observed that larger adsorption of MCPA on sepiolite could take place in the presence of Mg^{2+} and Al^{3+} ions at pH values below those required for the precipitation of the LDH (Table 5. 3). Table 5. 3 summarizes the mixtures of sepiolite, MCPA and the Mg and Al salts, in the same proportions than the hybrid nanoarchitectures, which were prepared to determine the uptake of MCPA on sepiolite under these conditions. The materials were kept under stirring for approximately 18 hours. The solid was recovered by centrifugation, washed 3 times with water and dried in an oven at 60 °C. The amount of adsorbed MCPA was determined by CHN and expressed as amount of MCPA per 100 grams of total material (not referred to the amount of sepiolite or salts added). In this case, the amount of MCPA incorporated by the effect of co-adsorption of MCPA with the Mg and Al salts is about 5 times higher than that obtained by the direct adsorption from MCPA solution and it does not seem to be dependent on the MCPA:salts ratio present in the solution. This co-adsorption of MCPA not intercalated in the LDH could be the reason of the higher content on MCPAin some of the prepared hybrid nanoarchitectures.

The hybrid nanoarchitectures were consolidated at 150 ^{o}C as in the protocol reported by Gómez-Avilés et al. (Gómez-Avilés et al., 2016), and at a lower temperature as well, 60 ^{o}C in this case, to assure no degradation of the organic species present in them. Both thermal treatments resulted in similar materials, showing that lower temperatures could be used if the method was applied to prepare hybrid nanoarchitectures involving less stable organic species.

Table 5. 3. LDH yield, experimental LDH/Sep ratio and amount of MCPA incorporated in the MCPA:LDH/sepiolite hybrid nanoarchitectures prepared by the co-precipitation method.

Sample	**LDH yield (%)**	**LDH/Sep real ratio**	**mEq MCPA per 100 g LDH**
MCPA-LDH	89.7	--	303
MCPA-LDH/Sep2:1_60C	84.0	1.68:1	336
MCPA-LDH/Sep2:1_150C	82.0	1.64:1	356
MCPA-LDH/Sep1:1_60C	81.0	0.81:1	385
MCPA-LDH/Sep1:1_150C	78.0	0.78:1	421
MCPA-LDH/Sep0.5:1_60C	78.0	0.39:1	433
MCPA-LDH/Sep0.5:1_150C	77.0	0.38:1	445
MCPA-LDH/Sep0.3:1_60C	54.4	0.19:1	1266
MCPA-LDH/Sep0.3:1_150C	41.4	0.18:1	1180

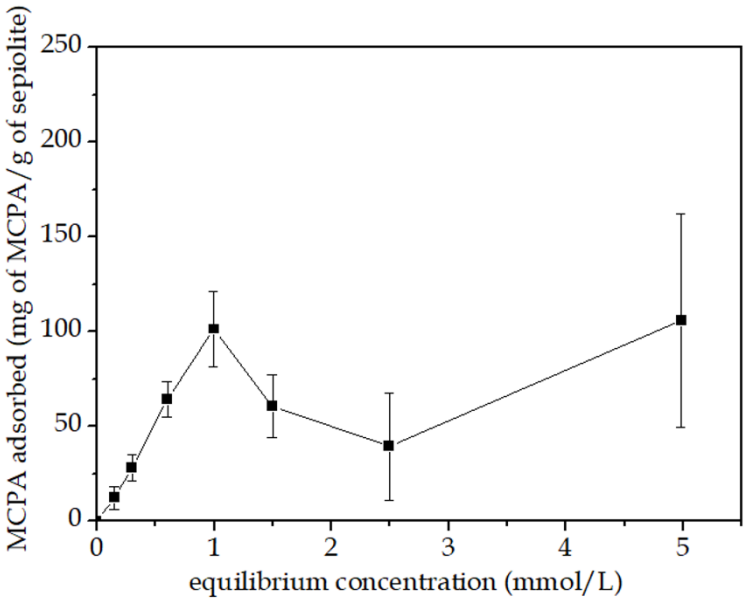

Figure 5. 13. Adsorption isotherm 23 °C of MCPA from water solutions in sepiolite.

Table 5. 4. Amount of MCPA adsorbed on sepiolite in the presence of Mg^{2+} and Al^{3+} ions (metal chlorides).

Samples	g MCPA per 100g of material	mEq MCPA per 100g of material
Sep/MgAl-MCPA1:1	59.3	295.3
Sep/MgAl-MCPA0.5:1	54.7	272.5
Sep/MgAl-MCPA0.3:1	44.8	222.9

The interactions of the MCPA herbicide with the LDH inorganic host in both the MCPA-LDH hybrid and in the MCPA-LDH/Sep hybrid nanoarchitectures prepared by the co-precipitation method were studied by infrared spectroscopy (Figure 5. 14). The spectra obtained in KBr diluted samples (Figure 5. 14A) show the presence of the main characteristic bands of MCPA, confirming the presence of the herbicide in all the prepared materials. The absence of the characteristic C=O stretching vibration mode of protonated carboxylic groups in MCPA molecule that appears as a double band at 1745 and 1710 cm^{-1} in the pure MCPA suggest the presence of the herbicide as anionic species in the MCPA-LDH hybrid and in the hybrid nanoarchitectures as well. This is confirmed by the presence of a strong absorption band at approximately 1610 cm^{-1} that can be assigned to the asymmetric stretching vibration of the ionized COO^- groups, which may be overlapping with the 1630 cm^{-1} band of $\delta_{H\text{-}O\text{-}H}$ vibration modes of water molecules present in the inorganic solids (Casal et al., 2001; Pavlovic et al., 2005; Cardoso et al., 2006; Bruna et al., 2009; Alromeed et al., 2015b). The bands that appear in the low frequency region of the spectrum of hybrid nanoarchitectures are related to vibration modes of the two inorganic solids present in them.

The FTIR spectra (Figure 5. 14B) of sepiolite and the hybrid nanoarchitecture obtained in pure sample was used to confirm the existence of chemical interaction between sepiolite and the formed LDH. Thus, it was analyzed the 3800 to 3600 cm^{-1} region where bands ascribed to Si-OH and Mg-OH vibration modes of sepiolite appear (Ahlrichs, 1975). The band attributed to the OH vibration of the Mg-OH groups is observed in the hybrid nanoarchitectures with apparently the same intensity. In contrast, the intensity of the band at 3720 cm^{-1}

related to the ν_{O-H} vibration modes of silanol groups is attenuated in the hybrid nanoarchitectures, indicating that part of them are in close interaction with other species (Casal et al., 2001; Alcântara et al., 2014; Akkari et al., 2016; Marwa Akkari et al., 2016). In the hybrid nanoarchitectures this perturbation can be again ascribed to hydrogen interactions between the silanol groups of the external surface of the sepiolite fibers and the grown LDH particles, inducing a shift of that IR band towards lower frequencies. This interaction is supported by the fact that the band practically becomes imperceptible in the MCPA-LDH/Sep hybrid nanoarchitectures when increase the temperature using for the consolidation of the nanoarchitecture (Figure 5. 14B) and also when the LDH content with respect to sepiolite increases and so LDH particles may be completely covering the sepiolite fibers. In addition, when comparing the FTIR of LDH/Sep of nanoarchitectures (Figure 5.6) with those of MCPA-LDH/Sep hybrid nanoarchitectures of the same LDH:sepiolite ratio (Figure 5. 14B), it is observed a greater decrease in the intensity of the 3720 cm^{-1} band for the later probably due to the presence of MCPA species also in interaction with Si-OH groups of sepiolite that were not banded to LDH nanoparticle. This interpretation is in agreement with the fact that a larger amount of MCPA, overpassing the AEC of the LDH, is present in the hybrid nanoarchitecture prepared with the lowest LDH:sepiolite ratio.

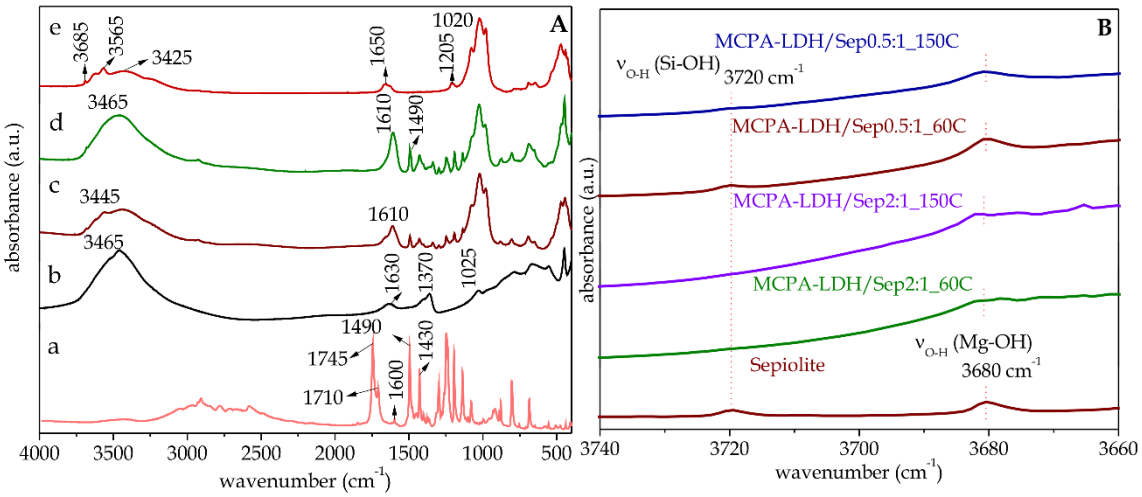

Figure 5. 14. FTIR spectra (4000 to 400 cm^{-1} region) of (a) MCPA, (b) LDH, (c) MCPA-LDH/Sep0.5:1_60 and (d) MCPA-LDH/Sep2:1_60 hybrid nanoarchitectures and (e) pristine sepiolite obtained in sample diluted in KBr (A) and FTIR spectra (3740 to 3660 cm^{-1} region) of various MCPA-LDH/Sepiolite hybrid nanoarchitectures prepared by co-precipitation obtained in pure sample (B).

The FESEM images of the MCPA-LDH/Sep hybrid nanoarchitectures (Figure 5. 15) confirm that sepiolite fibers are covered by LDH nanoparticles, being more agglomerated in the hybrid nanoarchitecture containing the higher amount of LDH. In those materials with lower content in LDH, the layered solid grows as particles of smaller size and TEM images clearly confirm that they remain attached to the silicate fibers (figure 5. 15).

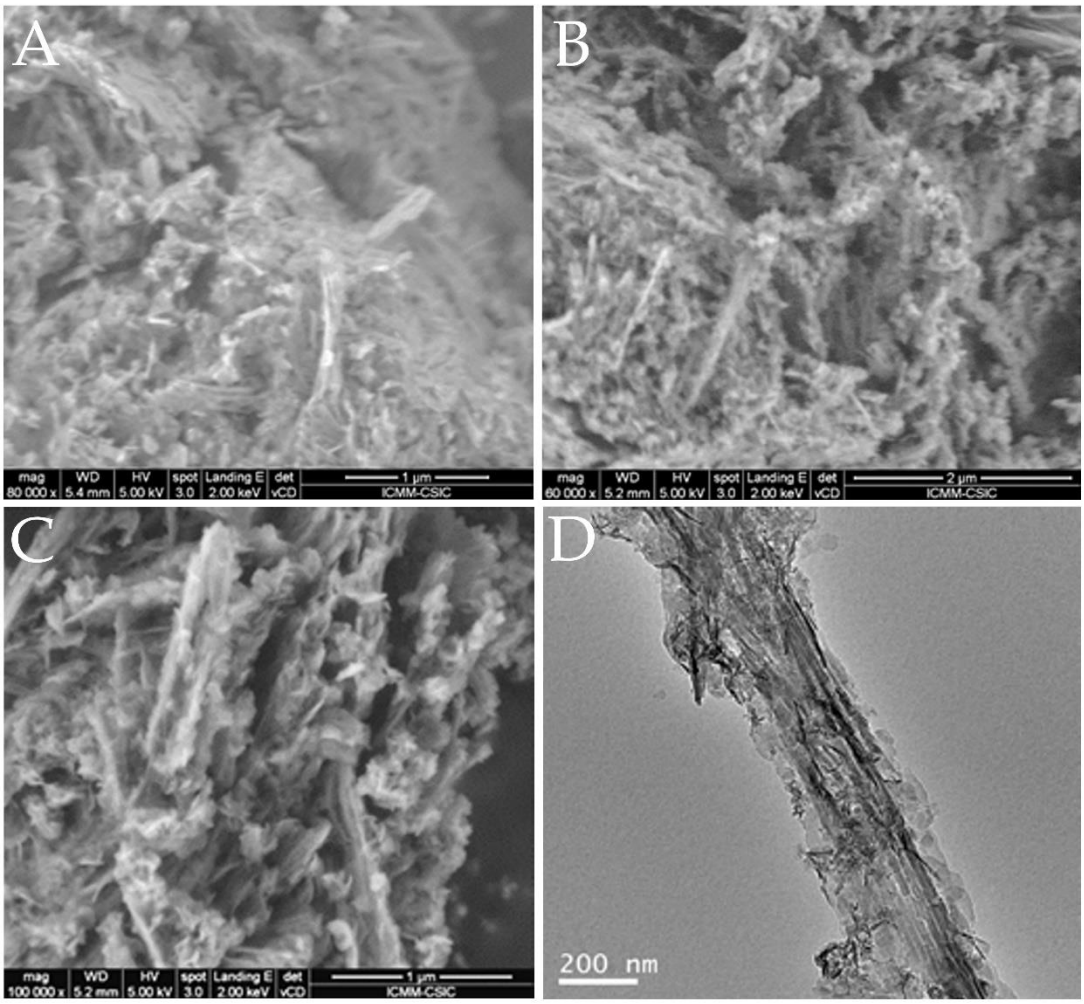

Figure 5. 15. FESEM images of MCPA-LDH/Sep2:1_150C (A), MCPA-LDH/Sep0.5:1_60C (B), MCPA-LDH/Sep0.5:1_150C (C) hybrid nanoarchitectures and TEM image of the (D) MCPA-LDH/Sep0.5:1_60C hybrid nanoarchitecture.

5.4 BIONANOCOMPOSITE SYSTEMS

The MCPA:LDH/sepiolite hybrid nanoarchitectures prepared for application in herbicide release systems were dispersed in an alginate/zein matrix resulting in the formation of bionanocomposite systems that were processed as beads by dripping in a 5% $CaCl_2$ solution. Based on a previous work with these biopolymers blends (Alcântara et al., 2010b; Aranda et al., 2012), the bionanocomposites produced in this study contain 17% zein with respect to total biopolymers. The MCPA-LDH/Sep 0.5:1_60C nanoarchitecture was chosen as reservoir of the MCPA it is the one with the larger amount of herbicide

intercalated into the LDH component and so ALG-Z@MCPA:LDH/Sep0.5:1_60C beads were prepared for the release experiments. The bionanocomposite material was evaluated for its encapsulation efficiency, which resulted in 51.2%, an expected result based on previous studies for bionanocomposite beads based on this combination of biopolymers (Alcântara et al., 2010b). This encapsulation corresponds to 0.17 mg per gram of biopolymers.

Figure 5. 16A show an image of one alginate-zein@MCPA-LDH/Sep bead obtained with an optical microscope where the actual size of the microsphere, approximately 2000 um, can be determined. Figure 5. 16B shows the surface of the bead observed by FESEM, while the cross-section of the bead is shown in figure 5. 16C. Both FESEM images reveal a rough morphology, but the material is homogeneous and without agglomerates, which indicates good interaction between both biopolymers, in addition to a good dispersion of the nanoarchitecture particles within the biopolymeric formed by the alginate and zein blend.

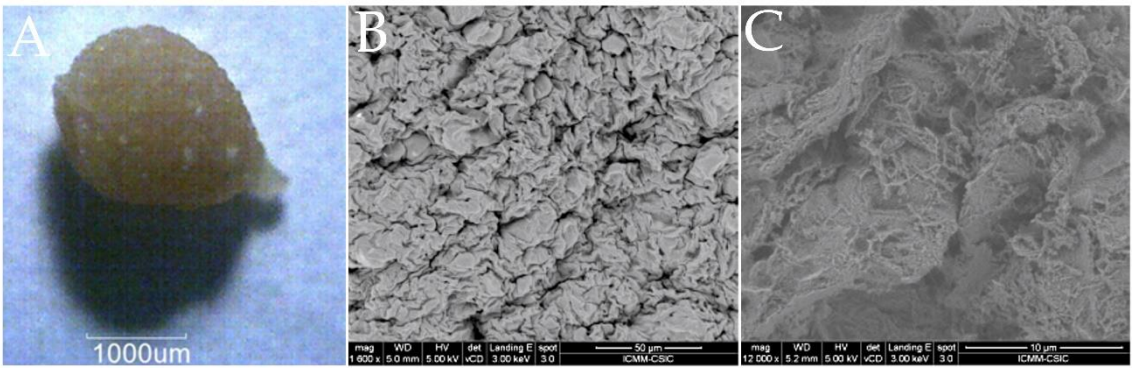

Figure 5. 16. Optical microscopy image of the alginate-zein@MCPA-LDH/Sep (A) bionanocomposite bead and FESEM images of the surface (B) and a cross section (C) of the bionanocomposite bead.

The interaction between alginate and zein were studied using FTIR spectroscopy, which confirms the existence of molecular interactions between biopolymers. The spectrum of the pristine alginate shows bands at 3435, 1615, 1415 and 1035 cm^{-1} that can be attributed to the ν_{OH} (H_2O y OH), ν_{asCO} ($-COO^-$), ν_{sCO} ($-COO^-$) y

ν_{asCO} (C-O-C) vibrations, respectively (Figure 5. 17) (Pongjanyakul and Puttipipatkhachorn, 2007; Ivancic et al., 2016). The FTIR spectrum of zein is characterized by the presence of a band at 3350 cm^{-1} which is assigned to the ν_{NH} vibration mode of the amide A groups of the protein (Figure 5. 17). The bands at 1660 and 1530 cm^{-1} are attributed to the ν_{CO} vibrations of C=O of amide I and ν_{CN} of the C-N-H bond of amide II of peptide groups, respectively. The amide band I is essentially associated with the stretching vibration mode of the carbonyl group (C=O), although it also receives a contribution from the C-N stretching vibration and the C-C-N deformation vibrations. However, the amide II band is mainly due to the N-H bending vibration mode, with contribution of the N-H plane, the C-N and C-C stretching vibrations (Miyazawa et al., 1956; Ozcalik and Tihminlioglu, 2013; Alcântara et al., 2016). In the FTIR spectrum of the ALG-Z@MCPA:LDH/Sep0.5:1_60C bionanocomposite, the band at 1660 cm^{-1}, characteristic of the ν_{CO} (amide I) vibrations of zein appears to be overlapped by the band at 1615 cm^{-1} characteristic of alginate, being them observed as a single a relatively large band centered at 1635 cm^{-1} (Figure 5. 17). In fact, this band is asymmetric, suggesting that, it includes a band at low frequency, related to the amide component I, and a high frequency associated with the amide component II, which is an indication that an aggregate bound through hydrogen interaction is formed. Similar results of interactions between the alginate carboxylate groups associated with protonated amino groups of the protein were found in a previous study in which both biopolymers were blended for incorporating ibuprofen (Alcântara et al., 2010) Furthermore, it is not possible to identify bands referring to the nanoarchitectures which is due to its low content compared to the total of the biopolymers mass in the bionanocomposite.

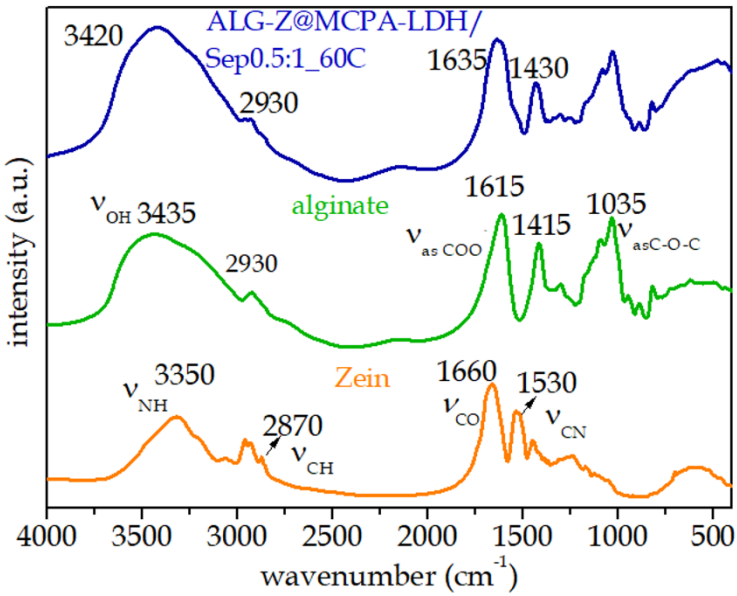

Figure 5. 17. FTIR spectra of zein, alginate and ALG-Z@MCPA-LDH/Sep0.5:1_60C bionanocomposite.

5.4.1. In vitro release of MCPA in water

The release of MCPA from various hybrid nanoarchitectures was evaluated in *in vitro* tests in deionized water (approx. pH 5.5), simulating conditions of the rainwater. The kinetics of the release depends on the nanoarchitecture composition (Figure 5. 18A & B). The MCPA-LDH hybrid showed the slowest release of MCPA, with around 35% lixiviated from the inorganic host after 8 h, similar values than those found when released from the $MCPA_{ie}$-LDH hybrid (Alcântara et al., 2013). In contrast the $MCPA_{ie}$-LDH/Sep1:1_150C hybrid nanoarchitecture, where the MCPA was incorporated by ion-exchange, showed a very rapid release, with practically 75% of the MCPA leached in the first 8 hours. This result clearly confirms that the presence of the LDH as small nanoparticles attached to the fibrous clay may favor a rapid release of the intercalated species. In the hybrid nanoarchitectures with analogous LDH:sepiolite ratio but prepared by the co-precipitation method the release is slower, showing the slowest kinetics the nanoarchitecture consolidated at 60 ºC. A similar trend was observed when comparing the release from co-precipitated hybrid nanoarchitectures of other compositions consolidated at 60 and 150 ºC

(Figure 5. 18A & B). There is not yet a clear explanation of this behavior that perhaps could be ascribed to the different degree of hydration or to the presence of OH^- species in the systems consolidated at lower temperature, which determines a different mechanism of attack of H^+ to produce the degradation of the LDH, and so the release of entrapped MCPA. As the LDH proportion in the hybrid nanoarchitecture varies, a fastest kinetics is observed with the lowest content in LDH (Figure 18A & Figure 18B). This behavior is probably related to the fact that size and aggregation state of the LDH nanoparticles increase with the LDH content in the nanoarchitecture, lowering the kinetics of the process. The release reached after 8 h of contact with water varies with values of around 50% in nanoarchitectures consolidated at 60 ºC (e.g., 43 and 51% for the 1:1 and 0.5:1 LDH/Sep nanoarchitectures, respectively) to around 70% in the ones consolidated at 150 ºC (e.g, 73% MCPA-LDH/Sep1.1_150C) (Figure 18A & 18B). After 8 hours the release evolves differently towards a steady state and after 48 h only the MCPA-LDH/Sep0.5:1_60C system provided a complete release of MCPA. These results confirm that the release of the herbicide from the hybrid nanoarchitectures may be tuned by selecting the specific composition and characteristics of the system, which makes them of interest for agricultural purposes.

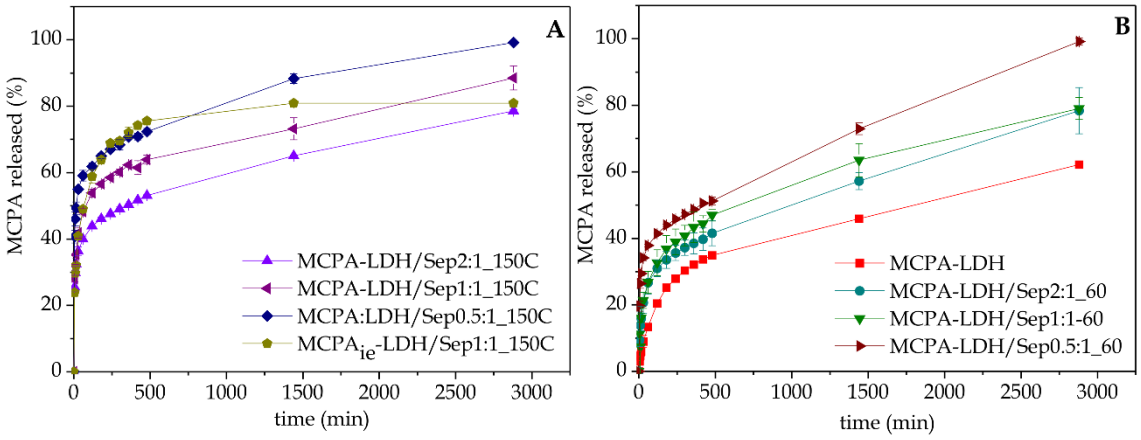

Figure 5. 18. *In vitro* release of MCPA from the hybrid formulations in bidistilled water (pH around 5.5)

Given that the amount of initial release of MCPA in all the formulations is quite high, the encapsulation of the hybrid nanoarchitectures in a protective biopolymer matrix was proposed to afford a better control in the release of the herbicide. In a previous study (Alcântara et al., 2013) it was reported that a mixture of alginate and zein biopolymers incorporating the $MCPA_{ie}$-LDH hybrid was able to reduce the initial release of MCPA by approximately 10 to 15% in the first 8 hours. In the present study, the MCPA-LDH/Sep0.5:1_60C nanoarchitecture was selected to prepare the bionanocomposite system, as it releases 100% of the herbicide at the end of 48 hours. In the ALG-Z@MCPA-LDH/Sep0.5:1_60C bionanocomposite beads, the hydrophilicity of alginate is reduced by the presence of zein, contributing to increase the control in the herbicide release. Figure 5.19 shows that the release of MCPA from the ALG-Z@MCPA-LDH/Sep system gives rise to a slower release in the first 8 hours than the non-encapsulated systems, reaching approx. 40% in 48 hours. After 8 days the ALG-Z@MCPA-LDH/Sep0.5:1_60C formulation reaches a release of MCPA close to the 70% due to the presence of the biopolymer matrix. This result suggests that the bionanocomposite may reach 100% of MCPA release in about two weeks.

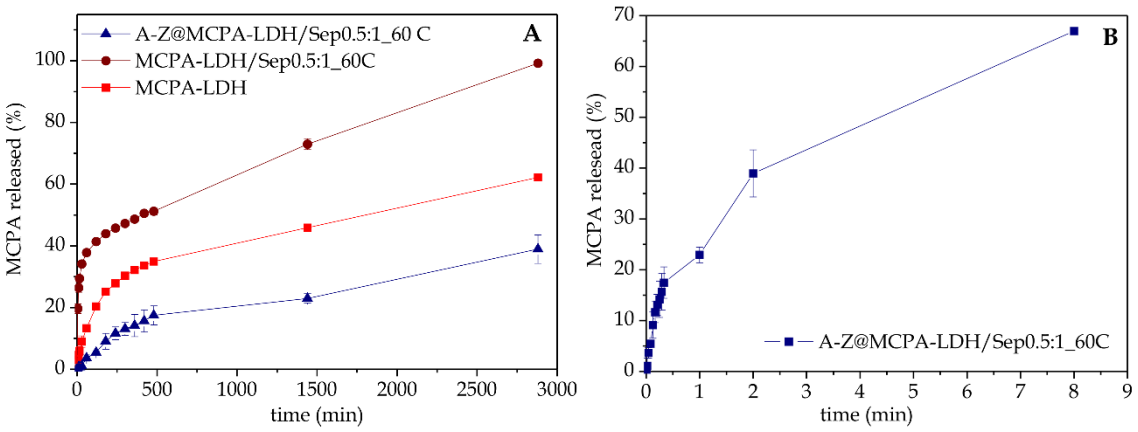

Figure 5. 19. *In vitro* release in water of MCPA from in different formulations (A) and release of the bionanocomposite systems in 8 days (B).

5.4.2. Soil column experiments

The objective of the soil column experiments was to track the behavior of the pesticide alone and its formulations within a soil column profile under conditions similar to those found in Mediterranean regions. Pure MCPA and the MCPA incorporated in the different formulations were selected to compare the effectiveness of these materials in a controlled release (pure MCPA, MCPA-LDH, MCPA-LDH/Sep0.5:1_60C and ALG-Z@MCPA-LDH/Sep0.5:1_60C). In the course of these experiments, the volume of water added was approximately equivalent to the pore volume of the columns. After 24 hours of contact with the soil column, the supernatant was collected and analyzed in order to determine the amount of herbicide that passed through the entire depth of the soil column (Figure 5. 20). Practically 80% of the MCPA in the formulation of the pure MCPA was recovered after passing through the 16 cm of the soil column, while the formulations where the MCPA is incorporated in a MgAl-LDH matrix or in the MgAl-LDH/Sep nanoarchitecture is recovered at the end 5 to 12% of the pesticide. The formulation involving the alginate and zein matrix practically did not present leaching of the herbicide, being identified traces of less than 1% of the pesticide at the end of the 24 hours. This means that a large part of the herbicide incorporated in the LDH and hybrid nanoarchitectures, but mainly in the bionanocomposite system, is still in the carrier, in the upper part of the soil and that is available to act for a longer time against the weeds.

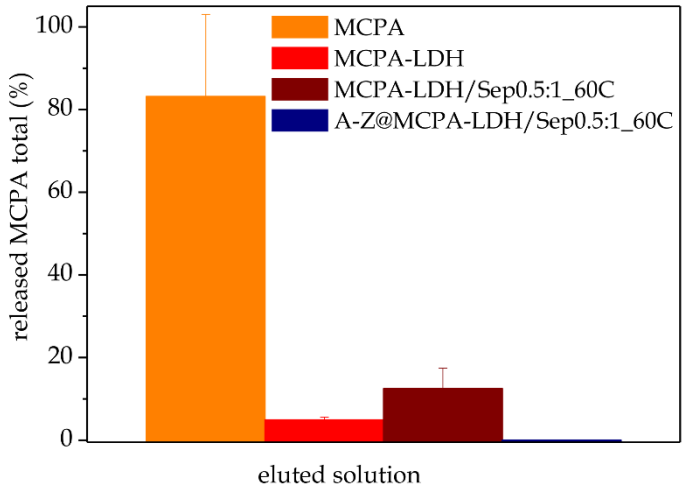

Figure 5. 20. Percentage of MCPA collected after passing through the segments of the soil column. Vertical bars indicate standard errors.

5.6 CONCLUDING REMARKS

This work reports two procedures that allow the preparation of hybrid LDH/sepiolite nanoarchitectured materials by association of the herbicide MCPA, profiting from the intercalation properties of the inorganic layered component. The stability of the prepared LDH/sepiolite nanoarchitecures allows the ion-exchange reaction of interlayer anions by the anionic MCPA species. Moreover, it has been proven that is possible to produce hybrid MCPA-LDH/sepiolite nanoarchitectures in a single step by co-precipitation of the LDH in presence of the clay and organic compound. This last approach allows the incorporation of higher amounts of MCPA than the ion-exchange reaction, with the additional advantage of being less time consuming. FTIR and ^{29}Si NMR spectroscopic analysis corroborated that the LDH particles in the co-precipitated hybrid nanoarchitecture are chemically linked to the silanol groups that cover the silicate fibers, producing stable systems even using consolidation temperatures as low as 60 ^{o}C. In order to prove a potential application of the developed hybrid nanoarchitectures, they have been *in vitro* tested as systems for controlled release of the incorporated organic species, in this case the herbicide MCPA. *In vitro* tests carried out in bidistilled water showed that the herbicide

release kinetics depended on the nanoarchitecture composition and the method of preparation, showing slower release rates those materials with higher content in LDH. The herbicide could be completely released from the hybrid nanoarchitectures, confirming their suitability for the controlled release of pesticides in the agricultural area. In order to have better control in the release process the hybrid nanoarchitectures can be encapsulated in a protective biopolymer matrix, like alginate-zein, which delays the complete release up to several weeks. In the release tests in soil columns it has been possible to observe the same release behavior as in the water tests. With these results it has been seen that a high percentage of the herbicide is in the carrier, available in the upper part of the soil, being able to act even for several days in the weeds and at the same time avoiding contamination at more depths of the soil. Moreover, the presence of sepiolite in the hybrid nanoarchitectures could be profited to associate other active species to the formulation, profiting from the high capacity of this clay to adsorb numerous types of molecules. Finally, it is worthy to mention that the reported MCPA-LDH/sepiolite hybrid nanoarchitectures prepared by co-precipitation is a first example of LDH/sepiolite hybrid nanoarchitectures, and so, the obtained results open the way to a new methodology for the production of other hybrid systems incorporating diverse organic and polymeric anionic species associated with nanometric LDH particles and sepiolite for controlled drug delivery uses and other applications.

CHAPTER 6

CONCLUSIONS

This Thesis demonstrated the successful preparation of controlled delivery systems based on the incorporation of bioactive species in inorganic layered solids and further encapsulation in biopolymer matrices, which allow control in the liberation and facilitate specific conformation of the resulting bionanocomposites, such as in the form of beads or films, to procure an easy use for specific release of pharmaceuticals and pesticides in biomedical and agricultural applications, respectively.

- Metformin, the most common oral drug for treatment of type II diabetes, has been successfully intercalated in layered silicates of the smectite clay minerals group. Cationic metformin, dissociated from the commercial metformin hydrochloride product in aqueous solution, spontaneously intercalates into smectites by an ion-exchange mechanism, replacing the interlayer cations and, depending on the characteristics of the clay, being possible to have it also retained by just adsorption of metformin hydrochloride on the external surface of the clay. The Wyoming montmorillonite evaluated in this study allows the incorporation of metformin up to 3 times its exchange capacity, though the species adsorbed at the external surface can be easily removed by just washing with water, remaining only the intercalated metformin stabilized by electrostatic interaction as interlayer ions that compensate the CEC of the clay. The extension of the preparation method to synthetic hectorite of small particle size, such as Laponite® XLG commonly used in cosmetics and pharmaceutics, shows that in spite of using aqueous solutions that contain metformin three times fold the CEC of the

clay, only an amount equivalent to the CEC can be retained, being intercalated as compensating interlayer cations, confirming also the possibility to produce clay-metformin hybrids for production in large scale as that required in real applications. Computational studies confirm the experimental results, indicating an energetically favorable cation exchange reaction with MF forming a monolayer in the interlayer space of both clays, and more favorable adsorption energy values for the process taking place in hectorite rather than in montmorillonite, which points out that structural and compositional dissimilarities of the involved clay will affect the final characteristic of the hybrid. *In vitro* test of metformin release from the clay-metformin hybrids shows a quite rapid liberation at low pH as that in the stomach, overruling the use of the developed hybrids as controlled drug delivery systems for metformin. The incorporation of the hybrid in a biopolymer matrix of chitosan or pectin allows the conformation of beads that can be further coated to produce pectin@chitosan/clay-metformin and pectin@chitosan@pectin/clay-metformin core-shell beads that allow a better controlled release kinetics, being more effective systems for a sustainable release of metformin compared to those based on clay-metformin hybrids or in the incorporation of metformin hydrochloride directly in a biopolymer matrix (e.g., chitosan, pectin, pectin@chitosan core-shell beads…). *In vitro* release test simulating the sequence of pH changes and residence time of the drug passing through the gastrointestinal tract show that the pectin@chitosan@pectin/clay-metformin core-shell beads shows a more controlled release than the pectin@chitosan/clay-metformin core-shell beads, with the additional advantage that the former have an encapsulation efficiency of almost 90% versus a maximum of 60% in the latter. The designed bionanocomposite core-shell systems take advantage of the functionalities of all their components as the external pectin coating procures stability and low release at the pH conditions of the stomach, the chitosan affords mucoadhesive properties to improve absorption at the intestine, and the clay acts as a protective substrate that creates a reservoir of metformin, and possibly could also act as an antidiarrheal agent for reducing other side effects of metformin accumulation in

the intestinal tract, all of them together increasing the residence time of metformin in the body and preventing practically 50 to 60% from being eliminated in the first hours. The proposed bionanocomposite core-shell beads system has shown very promising results for the controlled release of metformin, but it could be further explored using other oral drug treatments for other diseases where the properties of the bionanocomposite system could be used to afford both a controlled and located release.

- Various materials based on the association of allantoin, a molecule of great versatility for uses in cosmetics and pharmaceutics but difficult to become stabilized with other components, with layered hydroxides were explored with the aim to produce controlled release systems for potential topical application in skin disease treatments. Incorporation of allantoin in a 2:1 MgAl layered double hydroxides (LDH) was intended by ion-exchange reaction in the presence of an aqueous solution of allantoin, and by precipitation of the LDH in the presence of the molecule, observing that though the final hybrids contain allantoin, it is in a quite small amount in the solid resulting from the ion-exchange reaction, with practically the same amount of Cl^- ions that the parent LDH. In contrast, larger amounts of allantoin are found in the co-precipitated solid , with less content in Cl^- ions, but the XRD patterns do not shown the presence of an intercalated phase, confirming the formed hybrid is not an intercalation compound though it allows the stabilization of allantoin. The co-precipitation of a 2:1 ZnAl LDH in the presence of allantoin results in a hybrid that contains larger amount of allantoin, which coincides practically with the ion-exchange capacity of the inorganic solid. This material shows the presence of XRD peaks that can be associated with a new intercalated phase, but where the content in Al is very low to confirm the formed phase is the intended 2:1 ZnAl LDH. The co-precipitation in presence of just Zn^{2+} leads to the formation of a Zn layered simple hydroxide (LSH) where allantoin species remain intercalated and coordinated to some of the Zn atoms in the solid, probably stabilized as in certain Zn-allantoin coordination compounds reported in various patented works, constituting the first report of a intercalated

compound of allantoin. Comparison of allantoin release from the prepared co-precipitated ZnAl-LDH hybrid, the Zn-LSH hybrid and the Zn-allantoin complex in conditions simulating the pH of the skin (buffer solution of pH ≈ 5.5) shows that the intercalation compound is the most efficient system. The incorporation of these three Zn-allantoin systems in biopolymers (e.g., agar, HPMC, nanocellulose,…) allows the formation of bionanocomposite films that could be used for the sustained release of allantoin, and may show also bactericide properties (e.g., against Gram-negative bacteria such as *Staphylococcus aureus*), though optimization of the resulting bionanocomposites is still required in order to procure films of good stability, convenient mechanical properties and appropriate doses of the allantoin-hybrid in order to reach a suitable allantoin release system for topical uses in skin disease treatments and other applications.

- Nanoarchitectured materials where 2:1 Mg-Al LDH nanoparticles remain assembled to sepiolite nanofibers were used as inorganic hosts of anionic species of the herbicide know as 2-methyl-4-chlorophenoxyacetic acid (MCPA), which were associated by ion-exchange reaction with interlayer anions of the LDH already assembled to sepiolite or by co-precipitation of the LDH in the presence of sepiolite and the herbicide to produce directly in one step the hybrid nanoarchitecture. The use of a single-step co-precipitation method to produce hybrid LDH/sepiolite nanoarchitectures was applied for the first time in this study, and it shows the possibility to incorporate larger amounts of the organic species than with the use of ion-exchange reactions in already formed LDH/sepiolite material, being possible to prepare also nanoarchitectures with variable LDH:sepiolite ratio. The *in vitro* release tests of MCPA from these materials in deionized water (approx. pH 5.5), simulating conditions of the rainwater, shows that the release kinetics depend on the proportion of components in the hybrid nanoarchitecture, which could be of interest in view of tuning a slower or faster release system for a given application. The hybrid nanoarchitecures could be used as reservoir of MCPA as well and included in a biopolymer matrix to produce the controlled delivery system. In this way, bionanocomposite beads prepared with a mixture of alginate and zein allow a

controlled release for up to days. Tests performed on soil columns show that the alginate-zein bionanocomposite system prevents the leaching of the herbicide deeper into the soil and thus contamination of the soil at greater depths, which could be relevant in view to use this type of bionacomposite systems for application in agriculture. A further advantage of the LDH/sepiolite nanoarchitectures not explored in this Thesis addresses the use of the sepiolite fibers to associate other active species in the formulation, taking advantage of the high capacity of this clay to adsorb numerous types of molecules.

CAPÍTULO 6

CONCLUSIONES

Esta Tesis demostró la preparación exitosa de sistemas de entrega controlados basados en la incorporación de especies bioactivas en sólidos inorgánicos lamelares y una mayor encapsulación en matrices de biopolímeros, que permiten el control en la liberación y facilitan la conformación específica de los compuestos *bionanocomposites* resultantes, como en forma de *beads* o películas, para obtener un uso fácil para la liberación específica de productos farmacéuticos y pesticidas en aplicaciones biomédicas y agrícolas, respectivamente.

- La metformina, es el fármaco oral más común para el tratamiento de la diabetes tipo II, que se ha intercalado con éxito en silicatos lamelares del grupo de minerales de arcilla de las esmectitas. La metformina catiónica, disociada del producto comercial de hidrocloruro de metformina en solución acuosa, se intercala espontáneamente en esmectitas mediante un mecanismo de intercambio iónico, reemplazando los cationes de la capa intermedia y, dependiendo de las características de la arcilla, es posible que también se retenga mediante la simple adsorción de clorhidrato de metformina en la superficie externa de la arcilla. La montmorillonita de Wyoming evaluada en este estudio permite la incorporación de metformina hasta 3 veces su capacidad de intercambio, aunque las especies adsorbidas en la superficie externa pueden eliminarse fácilmente con solo lavarlas con agua, quedando solo la metformina intercalada estabilizada por interacción electrostática como iones entre capas que compensan el CEC de la arcilla. La extensión del método de preparación a hectorita sintética de pequeño tamaño de partícula, como Laponite® XLG comúnmente utilizada en cosmética y farmacia, muestra que a pesar de usar soluciones acuosas que contienen metformina tres veces el CEC de la arcilla, solo

una cantidad equivalente se puede retener el CEC, intercalando como cationes compensadores en la capa interlaminar, confirmando también la posibilidad de producir híbridos de arcilla-metformina para la producción a gran escala como se requiere en aplicaciones reales. Los estudios computacionales confirman los resultados experimentales, indicando una reacción de intercambio catiónico energéticamente favorable con metformina formando una monocapa en el espacio interlaminar de ambas arcillas, y valores de energía de adsorción más favorables para el proceso que tiene lugar en hectorita en lugar de en montmorillonita, lo que indica que la estructura y las diferencias de composición de la arcilla involucrada afectarán la característica final del híbrido. La prueba *in vitro* de la liberación de metformina de los híbridos arcilla-metformina muestra una liberación bastante rápida a pH bajo como en el estómago, anulando el uso de los híbridos desarrollados como sistemas controlados de administración de fármacos para metformina. La incorporación del híbrido en una matriz de biopolímero de quitosano o pectina permite la conformación de perlas que pueden recubrirse para producir pectina@quitosano/arcilla-metformina y pectina@quitosano@pectina/arcilla-metformina *beads* que permiten una mejor cinética de liberación controlada, siendo sistemas más efectivos para una liberación sostenible de metformina en comparación con aquellos basados en híbridos de arcilla-metformina o en la incorporación de clorhidrato de metformina directamente en una matriz de biopolímero (p. ej., quitosano, pectina, pectina@quitosano *beads*...). Las pruebas de liberación in vitro que simulan la secuencia de cambios de pH y el tiempo de residencia del fármaco que pasa a través del tracto gastrointestinal muestran que los *beads* de pectina@quitosana@pectina/arcilla-metformina muestran una liberación más controlada que los *beads* de pectina@quitosano/arcilla-metformina, con la ventaja adicional de que las primeras tienen una eficiencia de encapsulación de casi 90% frente a un máximo de 60% en las últimas. Los sistemas *bionanocomposites* diseñados aprovechan las funcionalidades de todos sus componentes, ya que el revestimiento externo de pectina proporciona estabilidad y baja liberación a las condiciones de pH del estómago, el quitosano ofrece

propiedades mucoadhesivas para mejorar la absorción en el intestino y la arcilla actúa como un sustrato protector que crea un reservorio de metformina, y posiblemente también podría actuar como un agente antidiarreico para reducir otros efectos secundarios de la acumulación de metformina en el tracto intestinal. Todos juntos aumentan el tiempo de residencia de metformina en el cuerpo y evitan que se elimine prácticamente del 50 al 60% en las primeras horas. El sistema propuesto de *bionanocomposites* ha mostrado resultados muy prometedores para la liberación controlada de metformina, pero podría explorarse más a fondo utilizando otros tratamientos con medicamentos orales para otras enfermedades.

- Se exploraron diversos materiales basados en la asociación de alantoína, una molécula de gran versatilidad para usos en cosmética y farmacia, pero difícil de estabilizar con otros componentes, con hidróxidos lamelares, con el objetivo de producir sistemas de liberación controlada para una posible aplicación tópica en enfermedades de la piel. La incorporación de alantoína en un hidróxido doble laminar de MgAl 2:1 (LDH) se pretendía por reacción de intercambio iónico en presencia de una solución acuosa de alantoína, y por co-precipitación del LDH en presencia de la molécula, aunque que los híbridos finales contienen alantoína, está en una cantidad bastante pequeña en el sólido resultante de la reacción de intercambio iónico, con prácticamente la misma cantidad de iones cloruros que el LDH original. En contraste, se encuentran grandes cantidades de alantoína en hibrido del método de co-precipitación, con menos contenido en iones cloruros, pero los patrones de DRX no muestran la presencia de una fase intercalada, lo que confirma que el híbrido formado no es un compuesto de intercalación, aunque permite la estabilización de la alantoína. La coprecipitación de una LDH ZnAl 2: 1 en presencia de alantoína da como resultado un híbrido que contiene una mayor cantidad de alantoína, que coincide prácticamente con la capacidad de intercambio iónico del sólido inorgánico. Este material muestra la presencia de picos de XRD que pueden asociarse con una nueva fase intercalada, pero donde el contenido en Al es muy bajo para confirmar la fase formada de LDH

ZnAl 2: 1 prevista. La coprecipitación en presencia de solo Zn^{2+} conduce a la formación de un hidróxido simple laminar de Zn (LSH) donde las especies de alantoína permanecen intercaladas y coordinadas con algunos de los átomos de Zn en el sólido, probablemente estabilizados como en ciertos compuestos de coordinación de Zn-alantoína reportados en varios trabajos patentados, que constituyen el primer informe de un compuesto intercalado de alantoína. La comparación de la liberación de alantoína del híbrido ZnAl-LDH co-precipitado preparado, el híbrido Zn-LSH y el complejo Zn-alantoína en condiciones que simulan el pH de la piel (solución tampón de pH ≈ 5.5) muestra que el compuesto de intercalación es el sistema más eficiente. La incorporación de estos tres sistemas de Zn-alantoína en biopolímeros (p. Ej., Agar, HPMC, nanocelulosa, ...) permite la formación de películas de *bionanocompsosites* que podrían usarse para la liberación sostenida de alantoína, y pueden mostrar también propiedades bactericidas (p. Ej., contra Gram -bacterias negativas como *Staphylococcus aureus*), aunque todavía se requiere la optimización de los compuestos *bionanocomposites* resultantes para obtener películas de buena estabilidad, propiedades mecánicas convenientes y dosis apropiadas del híbrido de alantoína para alcanzar un sistema de liberación de alantoína adecuado para usos tópicos en tratamientos para enfermedades de la piel y otras aplicaciones.

- Los materiales nanoarquitecturados donde las nanopartículas 2:1 de Mg-Al LDH permanecen ensambladas en nanofibras de sepiolita se usaron como huéspedes inorgánicos de especies aniónicas del herbicida conocido como ácido 2-metil-4-clorofenoxiacético (MCPA), que se asociaron por reacción de intercambio iónico con aniones entre las láminas del LDH ya ensamblados en sepiolita o por co-precipitación de LDH en presencia de sepiolita y herbicida, produciendo directamente en un solo paso la nanoarquitectura híbrida. El uso de un método de co-precipitación de un solo paso para producir nanoarquitecturas híbridas de LDH/sepiolita se aplicó por primera vez en este estudio, y muestra la posibilidad de incorporar mayores cantidades de especies orgánicas que con el uso de reacciones de intercambio iónico en material LDH/sepiolita ya

formado, siendo posible preparar también nanoarquitecturas con una relación LDH:sepiolita variable. Las pruebas de liberación in vitro de MCPA de estos materiales en agua desionizada (aprox. PH 5.5), que simulan las condiciones del agua de lluvia, muestran que la cinética de liberación depende de la proporción de componentes en la nanoarquitectura híbrida, lo que podría ser de interés en vista de ajustar un sistema de liberación más lento o más rápido para una aplicación determinada. Las nanoarquitecturas híbridas también podrían usarse como reservorio de MCPA e incluirse en una matriz de biopolímeros para producir el sistema de suministro controlado. De esta manera, los *beads* de *bionanocomposites* preparadas con una mezcla de alginato y zeína permiten una liberación controlada durante hasta días. Las pruebas realizadas en columnas de suelo muestran que los sistemas de *bionanocomposites* de alginato-zeína evitan la lixiviación del herbicida más profundamente en el suelo y, por lo tanto, la contaminación del suelo a mayores profundidades, lo que podría ser relevante para utilizar este tipo de sistemas *bionanocomposites* para su aplicación en la agricultura. Una ventaja adicional de las nanoarquitecturas LDH/sepiolita, no exploradas en esta Tesis, aborda el uso de las fibras de sepiolita para asociar otras especies activas en la formulación, aprovechando la alta capacidad de esta arcilla para adsorber numerosos tipos de moléculas.

BIBLIOGRAPHY

Abdul Latip, A.F., Hussein, M.Z., Stanslas, J., Wong, C.C., Adnan, R., 2013. Release behavior and toxicity profiles towards A549 cell lines of ciprofloxacin from its layered zinc hydroxide intercalation compound. Chemistry Central Journal 7, 119. https://doi.org/10.1186/1752-153X-7-119

Aguzzi, C., Cerezo, P., Viseras, C., Caramella, C., 2007. Use of clays as drug delivery systems: Possibilities and limitations. Applied Clay Science 36, 22–36. https://doi.org/10.1016/j.clay.2006.06.015

Ahlrichs, J.L., 1975. Structural Hydroxyls in Sepiolites. Clays and Clay Minerals 23, 119–124. https://doi.org/10.1346/CCMN.1975.0230207

Akena Fine Chemicals S.r.l., 2012. Alantoína CTFA.

Akkari, M., Aranda, P., Ben Haj Amara, A., Ruiz-Hitzky, E., 2016. Organoclay hybrid materials as precursors of porous ZnO/silica-clay heterostructures for photocatalytic applications. Beilstein Journal of Nanotechnology 7, 1971–1982. https://doi.org/10.3762/bjnano.7.188

Akkari, M., Aranda, P., Ben Rhaiem, H., Ben Haj Amara, A., Ruiz-Hitzky, E., 2016. ZnO/clay nanoarchitectures: Synthesis, characterization and evaluation as photocatalysts. Applied Clay Science 131, 131–139. https://doi.org/10.1016/j.clay.2015.12.013

Akkari, M., Aranda, P., Ben Rhaiem, H., Ben Haj Amara, A., Ruiz-Hitzky, E., 2016. ZnO/clay nanoarchitectures: Synthesis, characterization and evaluation as photocatalysts. Applied Clay Science 131, 131–139. https://doi.org/10.1016/j.clay.2015.12.013

Alam, M.J., Ahmad, S., 2015. FTIR, FT-Raman, UV–Visible spectra and quantum chemical calculations of allantoin molecule and its hydrogen bonded dimers. Spectrochimica Acta Part A: Molecular and Biomolecular Spectroscopy 136, 961–978. https://doi.org/10.1016/j.saa.2014.09.119

Alcântara, A.C.S., Aranda, P., Darder, M., Ruiz-Hitzky, E., 2010. Bionanocomposites based on alginate–zein/layered double hydroxide materials as drug delivery systems. Journal of Materials Chemistry 20, 9495. https://doi.org/10.1039/c0jm01211d

Alcântara, A.C.S., S. López-Capdevila, M. Darder, P. Aranda, E.R.-H., 2013. Bionanocomposites como sistemas de liberación controlda de pesticidas, in: C. Belver, J. Cuevas, J. Luque, eds. (Ed.), Jornada Científica de La Sociedad Española de Arcillas. Madrid 2013, p. 3563.

Alcântara, A.C.S., Darder, M., 2018. Building Up Functional Bionanocomposites from the Assembly of Clays and Biopolymers. The Chemical Record 18, 696–712. https://doi.org/10.1002/tcr.201700076

Alcântara, A.C.S., Darder, M., Aranda, P., Ruiz-Hitzky, E., 2016. Effective intercalation of zein into Na-montmorillonite: role of the protein components and use of the developed biointerfaces. Beilstein Journal of Nanotechnology 7, 1772–1782. https://doi.org/10.3762/bjnano.7.170

Alcântara, A.C.S., Darder, M., Aranda, P., Tateyama, S., Okajima, M.K., Kaneko, T., Ogawa, M., Ruiz-Hitzky, E., 2014. Clay-bionanocomposites with sacran megamolecules for the selective uptake of neodymium. J. Mater. Chem. A 2, 1391–1399. https://doi.org/10.1039/C3TA14145D

Aldea, M., Craciun, L., Tomuleasa, C., Berindan-Neagoe, I., Kacso, G., Florian, I.S., Crivii, C., 2014. Repositioning metformin in cancer: genetics, drug targets, and new ways of delivery. Tumor Biology 35, 5101–5110. https://doi.org/10.1007/s13277-014-1676-8

Allègre, J. (2012). Les silicates d'alumine (argiles) en therapeutique. Une pratique coutumière ancienne relayée dans la médecine mo- derne. PhD Thesis,

Université Paris XIII, Paris.

Alromeed, A.A., Scrano, L., A. Bufo, S., Undabeytia, T., 2015a. Slow-release formulations of the herbicide MCPA by using clay-protein composites. Pest Management Science 71, 1303–1310. https://doi.org/10.1002/ps.3929

Alromeed, A.A., Scrano, L., A. Bufo, S., Undabeytia, T., 2015b. Slow-release formulations of the herbicide MCPA by using clay-protein composites. Pest Management Science 71, 1303–1310. https://doi.org/10.1002/ps.3929

Altuntasoglu, O., Matsuda, Y., Ida, S., Matsumoto, Y., 2010. Syntheses of Zinc Oxide and Zinc Hydroxide Single Nanosheets. Chemistry of Materials 22, 3158–3164. https://doi.org/10.1021/cm100152q

Ambrogi, V., Perioli, L., Ricci, M., Pulcini, L., Nocchetti, M., Giovagnoli, S., Rossi, C., 2008. Eudragit® and hydrotalcite-like anionic clay composite system for diclofenac colonic delivery. Microporous and Mesoporous Materials 115, 405–415. https://doi.org/10.1016/j.micromeso.2008.02.014

Aono, M., Bando, Y., Ariga, K., 2012. Nanoarchitectonics: Pioneering a New Paradigm for Nanotechnology in Materials Development. Advanced Materials 24, 150–151. https://doi.org/10.1002/adma.201104614

Aranda P., Belver C., and R.-H.E., 2015. Hybrid nanoarchitectures by sol-gel from silica and silicate building blocks, in: Zayat, D.L.& M. (Ed.), The Sol-Gel Handbook: Synthesis, Characterization and Aplllications. Wiley-VCH, pp. 443–470.

Aranda, P., Alcântara, A.C.S., Ribeiro, L.N.M., Darder, M., Ruiz-Hitzky, E., 2012. Bionanocomposites based on layered double hydroxides as drug delivery systems, in: Choi, S.H., Choy, J.-H., Lee, U., Varadan, V.K. (Eds.), Progress in Biomedical Optics and Imaging - Proceedings of SPIE. p. 85486D. https://doi.org/10.1117/12.2008317

Aranda, P., Ruiz-Hitzky, E., 2018. Immobilization of Nanoparticles on Fibrous Clay Surfaces: Towards Promising Nanoplatforms for Advanced Functional Applications. The Chemical Record 18, 1125–1137.

https://doi.org/10.1002/tcr.201700113

Araújo, L.U., Grabe-Guimarães, A., Mosqueira, V.C.F., Carneiro, C.M., Silva-Barcellos, N.M., 2010. Profile of wound healing process induced by allantoin. Acta Cirurgica Brasileira 25, 460–461. https://doi.org/10.1590/S0102-86502010000500014

Ariga, K., Jia, X., Shrestha, L.K., 2019. Soft material nanoarchitectonics at interfaces: molecular assembly, nanomaterial synthesis, and life control. Molecular Systems Design & Engineering 4, 49–64. https://doi.org/10.1039/C8ME00094H

Armisén, R., 1991. Agar and agarose biotechnological applications. Hydrobiologia 221, 157–166. https://doi.org/10.1007/BF00028372

Atçay, G., Yurdakoç, K., 2000. Removal of Various Phenoxyalkanoic Acid Herbicides from Water by Organo-clays. Acta hydrochimica et hydrobiologica 28, 300–304. https://doi.org/10.1002/1521-401X(200012)28:6<300::AID-AHEH300>3.0.CO;2-L

Babu, R. V., Rao, K.S. V., Sairam, M., Naidu, B.V.K., Hosamani, K.M., Aminabhavi, T.M., 2006. pH sensitive interpenetrating network microgels of sodium alginate-acrylic acid for the controlled release of ibuprofen. Journal of Applied Polymer Science 99, 2671–2678. https://doi.org/10.1002/app.22760

Bacakova, L., Pajorova, J., Bacakova, M., Skogberg, A., Kallio, P., Kolarova, K., Svorcik, V., 2019. Versatile Application of Nanocellulose: From Industry to Skin Tissue Engineering and Wound Healing. Nanomaterials 9, 164. https://doi.org/10.3390/nano9020164

Badreddine, M., Khaldi, M., Legrouri, A., Barroug, A., Chaouch, M., De Roy, A., Besse, J.P., 1998. Chloride-hydrogenophosphate ion exchange into the zinc–aluminium–chloride layered double hydroxide. Materials Chemistry and Physics 52, 235–239. https://doi.org/10.1016/S0254-0584(97)02050-6

Becker, L.C., Bergfeld, W.F., Belsito, D. V, Klaassen, C.D., Marks, J.G., Shank,

R.C., Slaga, T.J., Snyder, P.W., Andersen, F.A., 2010. Final Report of the Safety Assessment of Allantoin and Its Related Complexes. International Journal of Toxicology 29, 84S–97S. https://doi.org/10.1177/1091581810362805

Belver, C., Aranda, P., Ruiz-Hitzky, E., 2013. Silica–alumina/sepiolite nanoarchitectures. Journal of Materials Chemistry A 1, 7477. https://doi.org/10.1039/c3ta01686b

Bergaya, F. and Lagaly, G. (Eds. ., 2013. Handbook of Clay Science, 2nd edition. Elsevier, Oxford, UK.

Bergaya, F., Lagaly, G., 2006. Chapter 1 General Introduction: Clays, Clay Minerals, and Clay Science, in: Developments in Clay Science. pp. 1–18. https://doi.org/10.1016/S1572-4352(05)01001-9

Bergaya, F., Lagaly, G., Vayer, M., 2013. Chapter 2.11 - Cation and Anion Exchange, in: Science, F.B. and G.L.B.T.-D. in C. (Ed.), Handbook of Clay Science. Elsevier, pp. 333–359. https://doi.org/https://doi.org/10.1016/B978-0-08-098259-5.00013-5

Bini, M., Monteforte, F., 2018. Layered Double Hydroxides (LDHs): Versatile and Powerful Hosts for Different Applications. Journal of Analytical & Pharmaceutical Research 7, 1–4. https://doi.org/10.15406/japlr.2018.07.00206

Biovia, 2018. Materials Studio.

Bish, D.L., 1980. Anion-exchange in takovite: applications to other hydroxide minerals. Bulletin de Mineralogie 103, 170–175.

Bonnet, S., Forano, C., de Roy, A., Besse, J.P., Maillard, P., Momenteau, M., 1996. Synthesis of Hybrid Organo−Mineral Materials: Anionic Tetraphenylporphyrins in Layered Double Hydroxides. Chemistry of Materials 8, 1962–1968. https://doi.org/10.1021/cm960020t

Borrego-Sánchez, A., Gómez-Pantoja, E., Morillo, E., Undabeytia, T., Sainz-Díaz, C.I., 2018. Adsorption of the tallow amine ethoxylate surfactant Ethomeen

T/15 on montmorillonite. Applied Clay Science 161, 533–543. https://doi.org/10.1016/j.clay.2018.03.026

Borrego-Sánchez, A., Viseras, C., Aguzzi, C., Sainz-Díaz, C.I., 2016. Molecular and crystal structure of praziquantel. Spectroscopic properties and crystal polymorphism. European Journal of Pharmaceutical Sciences 92, 266–275. https://doi.org/10.1016/j.ejps.2016.04.023

Brauner, K., Preisinger, A., 1956. Struktur und Entstehung des Sepioliths. Tschermaks Mineralogische und Petrographische Mitteilungen 6, 120–140. https://doi.org/10.1007/BF01128033

Brigatti, M.F., Galan, E., Theng, B.K.G., 2006. Chapter 2 Structures and Mineralogy of Clay Minerals, in: Developments in Clay Science. pp. 19–86. https://doi.org/10.1016/S1572-4352(05)01002-0

Brigatti, M.F., Galán, E., Theng, B.K.G., 2013. Chapter 2 - Structure and Mineralogy of Clay Minerals, in: Science, F.B. and G.L.B.T.-D. in C. (Ed.), Handbook of Clay Science. Elsevier, pp. 21–81. https://doi.org/https://doi.org/10.1016/B978-0-08-098258-8.00002-X

Brindley, G.W., Sempels, R.E., 1977. Preparation and properties of some hydroxy-aluminium beidellites. Clay Minerals 12, 229–237. https://doi.org/10.1180/claymin.1977.012.3.05

Bristol-Myers Squibb. U.S. FDA., 2009. (metformin hydrochloride) Tablets Mechanism of Action 1–35.

Bruna, F., Celis, R., Pavlovic, I., Barriga, C., Cornejo, J., Ulibarri, M.A., 2009. Layered double hydroxides as adsorbents and carriers of the herbicide (4-chloro-2-methylphenoxy)acetic acid (MCPA): Systems Mg–Al, Mg–Fe and Mg–Al–Fe. Journal of Hazardous Materials 168, 1476–1481. https://doi.org/10.1016/j.jhazmat.2009.03.038

BYK Additives & Instruments, 2014. Laponite : performance additives. Technical Information B-RI 21 22.

Caflisch, K.M., Schmidt-Malan, S.M., Mandrekar, J.N., Karau, M.J., Nicklas, J.P.,

Williams, L.B., Patel, R., 2018. Antibacterial activity of reduced iron clay against pathogenic bacteria associated with wound infections. International Journal of Antimicrobial Agents 52, 692–696. https://doi.org/10.1016/j.ijantimicag.2018.07.018

Campos, E.V.R., de Oliveira, J.L., Fraceto, L.F., 2014. Applications of Controlled Release Systems for Fungicides, Herbicides, Acaricides, Nutrients, and Plant Growth Hormones: A Review. Advanced Science, Engineering and Medicine 6, 373–387. https://doi.org/10.1166/asem.2014.1538

Cardoso, L.P., Celis, R., Cornejo, J., Valim, J.B., 2006. Layered Double Hydroxides as Supports for the Slow Release of Acid Herbicides. Journal of Agricultural and Food Chemistry 54, 5968–5975. https://doi.org/10.1021/jf061026y

Cardoso, L.P., Valim, J.B., 2006. Study of acids herbicides removal by calcined Mg—Al—CO3—LDH. Journal of Physics and Chemistry of Solids 67, 987–993. https://doi.org/10.1016/j.jpcs.2006.01.015

Carretero, M.I., 2002. Clay minerals and their beneficial effects upon human health. A review. Applied Clay Science 21, 155–163. https://doi.org/10.1016/S0169-1317(01)00085-0

Carretero, M.I., Gomes, C.S.F., Tateo, F., 2013. Clays, Drugs, and Human Health, in: Developments in Clay Science. Elsevier Ltd., pp. 711–764. https://doi.org/10.1016/B978-0-08-098259-5.00025-1

Carretero, M. I., Lagaly, G., 2007. Clays and health: An introduction. Applied Clay Science 36, 1–3. https://doi.org/10.1016/j.clay.2006.09.001

Carretero, M.I., Pozo, M., 2010. Clay and non-clay minerals in the pharmaceutical and cosmetic industries Part II. Active ingredients. Applied Clay Science 47, 171–181. https://doi.org/10.1016/j.clay.2009.10.016

Carretero, M. I. and Pozo, M., 2009. Clay and non-clay minerals in the pharmaceutical industry. Applied Clay Science 46, 73–80. https://doi.org/10.1016/j.clay.2009.07.017

Casal, B., Merino, J., Serratosa, J.-M., Ruiz-Hitzky, E., 2001. Sepiolite-based

materials for the photo- and thermal-stabilization of pesticides. Applied Clay Science 18, 245–254. https://doi.org/10.1016/S0169-1317(01)00030-8

Castro-Smirnov, F.A., Ayache, J., Bertrand, J.-R., Dardillac, E., Le Cam, E., Piétrement, O., Aranda, P., Ruiz-Hitzky, E., Lopez, B.S., 2017. Cellular uptake pathways of sepiolite nanofibers and DNA transfection improvement. Scientific Reports 7, 5586. https://doi.org/10.1038/s41598-017-05839-3

Castro-Smirnov, F.A., Piétrement, O., Aranda, P., Bertrand, J.-R., Ayache, J., Le Cam, E., Ruiz-Hitzky, E., Lopez, B.S., 2016. Physical interactions between DNA and sepiolite nanofibers, and potential application for DNA transfer into mammalian cells. Scientific Reports 6, 36341. https://doi.org/10.1038/srep36341

Cavani, F., Trifirò, F., Vaccari, A., 1991. Hydrotalcite-type anionic clays: Preparation, properties and applications. Catalysis Today 11, 173–301. https://doi.org/10.1016/0920-5861(91)80068-K

Celis, R., Adelino, M.A., Hermosín, M.C., Cornejo, J., 2012. Montmorillonite–chitosan bionanocomposites as adsorbents of the herbicide clopyralid in aqueous solution and soil/water suspensions. Journal of Hazardous Materials 209–210, 67–76. https://doi.org/10.1016/j.jhazmat.2011.12.074

Celis, R., Hermosín, M.C., Carrizosa, M.J., Cornejo, J., 2002. Inorganic and Organic Clays as Carriers for Controlled Release of the Herbicide Hexazinone. Journal of Agricultural and Food Chemistry 50, 2324–2330. https://doi.org/10.1021/jf011360o

Charles J. MacAlister and Arthur Walsh Titherley, 1936. Narrative of an investigation concerning an ancient medicinal remedy and its modern utilities. The symphytum officinale and its contained allantoin: By Charles J Macalister, M.D., F.R.C.P., Hon. Consulting Physician to the Liverpool Royal Southern Hospita, John Bale. ed, The Journal of Laboratory and Clinical Medicine. Elsevier, London. https://doi.org/10.5555/uri:pii:S002221433890527X

Chatterjee, S., Khunti, K., Davies, M.J., 2017. Type 2 diabetes. The Lancet 389, 2239–2251. https://doi.org/10.1016/S0140-6736(17)30058-2

Chauhan, N., Dilbaghi, N., Gopal, M., Kumar, R., Kim, K.-H., Kumar, S., 2017. Development of chitosan nanocapsules for the controlled release of hexaconazole. International Journal of Biological Macromolecules 97, 616–624. https://doi.org/10.1016/j.ijbiomac.2016.12.059

Cheung, R., Ng, T., Wong, J., Chan, W., 2015. Chitosan: An Update on Potential Biomedical and Pharmaceutical Applications. Marine Drugs 13, 5156–5186. https://doi.org/10.3390/md13085156

Childs, S.L., Chyall, L.J., Dunlap, J.T., Coates, D.A., Stahly, B.C., Stahly, G.P., 2004. A Metastable Polymorph of Metformin Hydrochloride: Isolation and Characterization Using Capillary Crystallization and Thermal Microscopy Techniques. Crystal Growth & Design 4, 441–449. https://doi.org/10.1021/cg034243p

Chinnaiyan, S.K., Deivasigamani, K., Gadela, V.R., 2019. Combined synergetic potential of metformin loaded pectin-chitosan biohybrids nanoparticle for NIDDM. International Journal of Biological Macromolecules 125, 278–289. https://doi.org/10.1016/j.ijbiomac.2018.12.009

Choi, G., Eom, S., Vinu, A., Choy, J.-H., 2018. 2D Nanostructured Metal Hydroxides with Gene Delivery and Theranostic Functions; A Comprehensive Review. The Chemical Record 18, 1033–1053. https://doi.org/10.1002/tcr.201700091

Chourasia, M.K., Jain, S.K., 2003. Pharmaceutical approaches to colon targeted drug delivery systems. Journal of pharmacy & pharmaceutical sciences : a publication of the Canadian Society for Pharmaceutical Sciences, Societe canadienne des sciences pharmaceutiques 6, 33–66.

Choy, J.-H., Kwak, S.-Y., Jeong, Y.-J., Park, J.-S., 2000. Inorganic Layered Double Hydroxides as Nonviral Vectors. Angewandte Chemie 39, 4041–4045. https://doi.org/10.1002/1521-3773(20001117)39:22<4041::AID-

ANIE4041>3.0.CO;2-C

Choy, J., Choi, S., Oh, J., Park, T., 2007. Clay minerals and layered double hydroxides for novel biological applications. Applied Clay Science 36, 122–132. https://doi.org/10.1016/j.clay.2006.07.007

Christidis, G., Aldana, C., Chryssikos, G., Gionis, V., Kalo, H., Stöter, M., Breu, J., Robert, J.-L., 2018. The Nature of Laponite: Pure Hectorite or a Mixture of Different Trioctahedral Phases? Minerals 8, 314. https://doi.org/10.3390/min8080314

Clark, S.J., Segall, M.D., Pickard, C.J., Hasnip, P.J., Probert, M.I.J., Refson, K., Payne, M.C., 2005. First principles methods using CASTEP. Zeitschrift für Kristallographie - Crystalline Materials 220, 567–570. https://doi.org/10.1524/zkri.220.5.567.65075

Colilla, M., Darder, M., Aranda, P., Ruiz-Hitzky, E., 2005. Amperometric sensors based on mercaptopyridine - Montmorillonite intercalation compounds. Chemistry of Materials 17, 708–715.

Constantino, V.R.L., Pinnavaia, T.J., 1995. Basic Properties of Mg2+1-xAl3+x Layered Double Hydroxides Intercalated by Carbonate, Hydroxide, Chloride, and Sulfate Anions. Inorganic Chemistry 34, 883–892. https://doi.org/10.1021/ic00108a020

Costantino, U., Ambrogi, V., Nocchetti, M., Perioli, L., 2008. Hydrotalcite-like compounds: Versatile layered hosts of molecular anions with biological activity. Microporous and Mesoporous Materials 107, 149–160. https://doi.org/10.1016/j.micromeso.2007.02.005

Costantino, U., Marmottini, F., Nocchetti, M., Vivani, R., 1998. New Synthetic Routes to Hydrotalcite-Like Compounds 2 Characterisation and Properties of the Obtained Materials. Eur. J. Inorg. Chem 143921446.

Cox, S.R., Williams, D.E., 1981. Representation of the molecular electrostatic potential by a net atomic charge model. Journal of Computational Chemistry 2, 304–323. https://doi.org/10.1002/jcc.540020312

Cunha, V.R.R., Lima, F.C.D.A., Sakai, V.Y., Véras, L.M.C., Leite, J.R.S.A., Petrilli, H.M., Constantino, V.R.L., 2017. LAPONITE®-pilocarpine hybrid material: experimental and theoretical evaluation of pilocarpine conformation. RSC Advances 7, 27290–27298. https://doi.org/10.1039/C7RA02017A

Dalcanale, E., Pinalli, R., Chimica, D., 2015. Encyclopedia of Polymeric Nanomaterials, Encyclopedia of Polymeric Nanomaterials. Springer Berlin Heidelberg, Berlin, Heidelberg. https://doi.org/10.1007/978-3-642-29648-2

Darder, M., Aranda, P., Ruiz-Hitzky, E., 2007. Bionanocomposites: A New Concept of Ecological, Bioinspired, and Functional Hybrid Materials. Advanced Materials 19, 1309–1319. https://doi.org/10.1002/adma.200602328

de la Caillerie, J.-B. d'Espinos., Fripiat, J.J., 1992. AL modified sepiolite as catalyst or catalyst support. Catalysis Today 14, 125–140. https://doi.org/10.1016/0920-5861(92)80017-H

Del Hoyo, C., 2007. Layered double hydroxides and human health: An overview. Applied Clay Science 36, 103–121. https://doi.org/10.1016/j.clay.2006.06.010

Ding, L., Hu, Y., Luo, Y., Zhu, J., Wu, Y., Yu, Z., Cao, X., Peng, C., Shi, X., Guo, R., 2016. LAPONITE®-stabilized iron oxide nanoparticles for in vivo MR imaging of tumors. Biomaterials Science 4, 474–482. https://doi.org/10.1039/C5BM00508F

Domszy, J.G., Roberts, G.A.F., 1985. Evaluation of infrared spectroscopic techniques for analysing chitosan. Die Makromolekulare Chemie 186, 1671–1677. https://doi.org/10.1002/macp.1985.021860815

Donnelly, R., Shaikh, R., Raj Singh, T., Garland, M., Woolfson, Ad., 2011. Mucoadhesive drug delivery systems. Journal of Pharmacy and Bioallied Sciences 3, 89. https://doi.org/10.4103/0975-7406.76478

Du, H., Liu, W., Zhang, M., Si, C., Zhang, X., Li, B., 2019. Cellulose nanocrystals and cellulose nano fi brils based hydrogels for biomedical applications.

Carbohydrate Polymers 209, 130–144. https://doi.org/10.1016/j.carbpol.2019.01.020

Duan, X., Lu, J., Evans, D.G., Wei, X., Chen, J.S., 2017. Functional Host–Guest Materials, in: Modern Inorganic Synthetic Chemistry. Elsevier, pp. 493–543. https://doi.org/10.1016/B978-0-444-63591-4.00018-5

Dupin, J.-C., Martinez, H., Guimon, C., Dumitriu, E., Fechete, I., 2004. Intercalation compounds of Mg–Al layered double hydroxides with dichlophenac: different methods of preparation and physico-chemical characterization. Applied Clay Science 27, 95–106. https://doi.org/10.1016/j.clay.2004.03.001

El-Nahhal, Y., Undabeytia, T., Polubesova, T., Mishael, Y.G., Nir, S., Rubin, B., 2001. Organo-clay formulations of pesticides: reduced leaching and photodegradation. Applied Clay Science 18, 309–326. https://doi.org/10.1016/S0169-1317(01)00028-X

Emami Riedmaier, A., Fisel, P., Nies, A.T., Schaeffeler, E., Schwab, M., 2013. Metformin and cancer: from the old medicine cabinet to pharmacological pitfalls and prospects. Trends in Pharmacological Sciences 34, 126–135. https://doi.org/10.1016/j.tips.2012.11.005

F. Kooli, C. Depège, A. Ennaqadi, A. de R.& J.P.B., 1997. Rehydratation of ZnAl-Layered Double Hydroxides. Clays and Clay Minerals 45, 92–98. https://doi.org/10.1346/CCMN.1997.0450111

Fadel, G., Luiz, C., Rita, M., Aurélio, M., Novak, C., Fernandes, C., Souza, D., Amado, A., Alves, R., Freitas, D., 2017. International Journal of Biological Macromolecules Bacterial cellulose in biomedical applications : A review. International Journal of Biological Macromolecules 104, 97–106. https://doi.org/10.1016/j.ijbiomac.2017.05.171

Fekete, E., Bella, É., Csiszár, E., Móczó, J., 2019. Improving physical properties and retrogradation of thermoplastic starch by incorporating agar.

International Journal of Biological Macromolecules 136, 1026–1033. https://doi.org/10.1016/j.ijbiomac.2019.06.109

Fernandes, F.M., Vázquez, L., Ruiz-Hitzky, E., Carnicero, A., Castro, M., 2014. Elastic properties of natural single nanofibres. RSC Advances 4, 11225. https://doi.org/10.1039/c3ra47452f

Fernández-Pérez, M., Villafranca-Sánchez, M., González-Pradas, E., Flores-Céspedes, F., 1999. Controlled Release of Diuron from an Alginate−Bentonite Formulation: Water Release Kinetics and Soil Mobility Study. Journal of Agricultural and Food Chemistry 47, 791–798. https://doi.org/10.1021/jf980878y

Forano, C., Costantino, U., Prévot, V., Gueho, C.T., 2013. Layered Double Hydroxides (LDH), in: Developments in Clay Science. pp. 745–782. https://doi.org/10.1016/B978-0-08-098258-8.00025-0

Forano, C., Hibino, T., Leroux, F., Taviot-Guého, C., 2006. Chapter 13.1 Layered Double Hydroxides, in: Developments in Clay Science. pp. 1021–1095. https://doi.org/10.1016/S1572-4352(05)01039-1

Ford, J.L., 2014. Design and Evaluation of Hydroxypropyl Methylcellulose Matrix Tablets for Oral Controlled Release: A Historical Perspective, in: Timmins, P., Pygall, S.R., Melia, C.D. (Eds.), AAPS Advances in the Pharmaceutical Sciences Series. Springer New York, New York, NY, pp. 17–51. https://doi.org/10.1007/978-1-4939-1519-4_2

Foretz, M., Guigas, B., Bertrand, L., Pollak, M., Viollet, B., 2014. Metformin: From Mechanisms of Action to Therapies. Cell Metabolism 20, 953–966. https://doi.org/10.1016/j.cmet.2014.09.018

Francisco-Márquez, M., Soriano-Correa, C., Sainz-Díaz, C.I., 2017. Adsorption of Sulfonamides on Phyllosilicate Surfaces by Molecular Modeling Calculations. The Journal of Physical Chemistry C 121, 2905–2914. https://doi.org/10.1021/acs.jpcc.6b12467

Fu, L., Zhang, J., Yang, G., 2013. Present status and applications of bacterial

cellulose-based materials for skin tissue repair. Carbohydrate Polymers 92, 1432–1442. https://doi.org/10.1016/j.carbpol.2012.10.071

Fu, Y.-C., Ferng, L.-H.A., Huang, P.-Y., 2006. Quantitative analysis of allantoin and allantoic acid in yam tuber, mucilage, skin and bulbil of the Dioscorea species. Food Chemistry 94, 541–549. https://doi.org/10.1016/j.foodchem.2004.12.006

Gadape, H., Parikh, K., 2011. Quantitative determination and validation of Carvedilol in pharmaceuticals using quantitative nuclear magnetic resonance spectroscopy. Analytical Methods 3, 2341. https://doi.org/10.1039/c1ay05247k

Galarneau, A., Barodawalla, A., Pinnavaia, T.J., 1997. Porous clay heterostructures (PCH) as acid catalysts. Chemical Communications 1661–1662. https://doi.org/10.1039/a703101g

Galarneau, A., Barodawalla, A., Pinnavaia, T.J., 1995. Porous clay heterostructures formed by gallery-templated synthesis. Nature 374, 529–531. https://doi.org/10.1038/374529a0

Galed, G., Miralles, B., Panos, I., Santiago, A., Heras, A., 2005. -Deacetylation and depolymerization reactions of chitin/chitosan: Influence of the source of chitin. Carbohydrate Polymers 62, 316–320. https://doi.org/10.1016/j.carbpol.2005.03.019

García-Briones, G.S., Ocampo-Pérez, R., Gómez-Durán, C.F.A., Neri-Gómez, T., Palestino, G., 2019. Porous silicon microcarriers for extended release of metformin: Design, biological evaluation and 3D kinetics modeling. Chemical Engineering Journal 365, 415–428. https://doi.org/10.1016/j.cej.2019.02.022

George, A., Shah, P.A., Shrivastav, P.S., 2019. Natural biodegradable polymers based nano-formulations for drug delivery: A review. International Journal of Pharmaceutics 561, 244–264.

https://doi.org/10.1016/j.ijpharm.2019.03.011

Gerstl, Z., Nasser, A., Mingelgrin, U., 1998. Controlled Release of Pesticides into Water from Clay−Polymer Formulations. Journal of Agricultural and Food Chemistry 46, 3803–3809. https://doi.org/10.1021/jf980184p

Ghazaie, M., Ghiaci, P., Ghiaci, M., 2017. Study on release of naproxen and metformin encapsulated in biopolymer-inorganic mesoporous matrices as controlled drug-delivery systems. Microporous and Mesoporous Materials 244, 291–300. https://doi.org/10.1016/j.micromeso.2016.11.004

Ghosal, K., Chakrabarty, S., Nanda, A., 2011. Hydroxypropyl methylcellulose in drug delivery. Pelagia research Library 2, 152–168.

Gil, A.; Korili, S. A.; Trujillano, R.; Vicente, M.A. V. (Ed.), 2010. Pillared Clays and Related Catalysts, Springer. ed. New York.

Gil, A., Korili, S.A., Vicente, M.A., 2008. Recent Advances in the Control and Characterization of the Porous Structure of Pillared Clay Catalysts. Catalysis Reviews 50, 153–221. https://doi.org/10.1080/01614940802019383

Giles, C.H., MacEwan, T.H., Nakhwa, S.N., Smith, D., 1960. Studies in adsorption. Part XI. A system of classification of solution adsorption isotherms, and its use in diagnosis of adsorption mechanisms and in measurement of specific surface areas of solids. Journal of the Chemical Society (Resumed) 846, 3973. https://doi.org/10.1039/jr9600003973

Gnanasambandam, R., 2000. Determination of pectin degree of esterification by diffuse reflectance Fourier transform infrared spectroscopy. Food Chemistry 68, 327–332. https://doi.org/10.1016/S0308-8146(99)00191-0

Gombotz, W., 1998. Protein release from alginate matrices. Advanced Drug Delivery Reviews 31, 267–285. https://doi.org/10.1016/S0169-409X(97)00124-5

Gómez-Avilés, A., Aranda, P., Fernandes, F.M., Belver, C., Ruiz-Hitzky, E., 2013. Silica-Sepiolite Nanoarchitectures. Journal of Nanoscience and Nanotechnology 13, 2897–2907. https://doi.org/10.1166/jnn.2013.7429

Gómez-Avilés, A., Aranda, P., Ruiz-Hitzky, E., 2016. Layered double hydroxide/sepiolite heterostructured materials. Applied Clay Science 130, 83–92. https://doi.org/10.1016/j.clay.2015.12.011

González-Pradas, E., Fernández-Pérez, M., Villafranca-Sánchez, M., Martínez-López, F., Flores-Céspedes, F., 1999. Use of bentonite and humic acid as modifying agents in alginate-based controlled-release formulations of imidacloprid. Pesticide Science 55, 546–552. https://doi.org/10.1002/(SICI)1096-9063(199905)55:5<546::AID-PS938>3.0.CO;2-P

Gordijo, C.R., Barbosa, C.A.S., Da Costa Ferreira, A.M., Constantino, V.R.L., Oliveira Silva, D. de, 2005. Immobilization of Ibuprofen and Copper-Ibuprofen Drugs on Layered Double Hydroxides. Journal of Pharmaceutical Sciences 94, 1135–1148. https://doi.org/10.1002/jps.20336

Goyal, M.R., 2017. Engineering Practices for Agricultural Production and Water Conservation, Engineering Practices for Agricultural Production and Water Conservation: An Interdisciplinary Approach. Apple Academic Press, Waretown, NJ : Apple Academic Press, 2017. https://doi.org/10.1201/9781315365954

Graham, G.G., Punt, J., Arora, M., Day, R.O., Doogue, M.P., Duong, J.K., Furlong, T.J., Greenfield, J.R., Greenup, L.C., Kirkpatrick, C.M., Ray, J.E., Timmins, P., Williams, K.M., 2011. Clinical Pharmacokinetics of Metformin. Clinical Pharmacokinetics 50, 81–98. https://doi.org/10.2165/11534750-000000000-00000

Gunasekaran, S., Natarajan, R.K., Renganayaki, V., Natarajan, S., 2006. Vibrational spectra and thermodynamic analysis of metformin. Indian Journal of Pure and Applied Physics 44, 495–500.

Gupta, G., de Jesus Andreoli Pinto, T., Chellappan, D.K., Mishra, A., Malipeddi, H., Dua, K., 2018. A clinical update on metformin and lung cancer in diabetic patients. Panminerva Medica 70–75. https://doi.org/10.23736/S0031-0808.18.03394-3

Gupta, S., Agarwal, D.D., Banerjee, S., 2009. Synergistic combination of metal stearates and β-diketones with hydrotalcites in poly(vinyl chloride) stabilization. Journal of Applied Polymer Science 112, 1056–1062. https://doi.org/10.1002/app.29484

Gupta, S.C., Sung, B., Prasad, S., Webb, L.J., Aggarwal, B.B., 2013. Cancer drug discovery by repurposing : teaching new tricks to old dogs. Trends in Pharmacological Sciences 1–10. https://doi.org/10.1016/j.tips.2013.06.005

Harris, L., Foster, S., Richards, R., 2002. An introduction to staphylococcus aureus, and techniques for identifying and quantifying s. aureus adhesins in relation to adhesion to biomaterials: review. European Cells and Materials 4, 39–60. https://doi.org/10.22203/eCM.v004a04

Heinz, H., Koerner, H., Anderson, K.L., Vaia, R.A., Farmer, B.L., 2005. Force Field for Mica-Type Silicates and Dynamics of Octadecylammonium Chains Grafted to Montmorillonite. Chemistry of Materials 17, 5658–5669. https://doi.org/10.1021/cm0509328

Heller-Kallai, L., 2013. Thermally Modified Clay Minerals, in: Developments in Clay Science. Elsevier Ltd., pp. 411–433. https://doi.org/10.1016/B978-0-08-098258-8.00014-6

Herrera, N.N., Letoffe, J.-M., Reymond, J.-P., Bourgeat-Lami, E., 2005. Silylation of laponite clay particles with monofunctional and trifunctional vinyl alkoxysilanes. Journal of Materials Chemistry 15, 863. https://doi.org/10.1039/b415618h

Hoffman, A.S., 2008. The origins and evolution of "controlled" drug delivery systems. Journal of Controlled Release 132, 153–163. https://doi.org/10.1016/j.jconrel.2008.08.012

Houri, B., Legrouri, A., Barroug, A., Forano, C., Besse, J.-P., 1999. Removal of Chromate Ions from Water by Anionicc CLAYS. J. Chim. Phys. 96, 455–463.

Hudzicki, J., 2012. Kirby-Bauer Disk Diffusion Susceptibility Test Protocol Author Information. American Society For Microbiology 1–13.

Hun Kim, M., Choi, G., Elzatahry, A., Vinu, A., Bin Choy, Y., Choy, J.-H., 2016. Review of Clay-drug Hybrid Materials for Biomedical Applications: Administration Routes. Clays and Clay Minerals 64, 115–130. https://doi.org/10.1346/CCMN.2016.0640204

Hussein, M.Z., Abdul Rahman, N.S.S., Sarijo, S.H., Zainal, Z., 2012. Herbicide-Intercalated Zinc Layered Hydroxide Nanohybrid for a Dual-Guest Controlled Release Formulation. International Journal of Molecular Sciences 13, 7328–7342. https://doi.org/10.3390/ijms13067328

Inacio, J., Taviot-Guého, C., Forano, C., Besse, J.., 2001. Adsorption of MCPA pesticide by MgAl-layered double hydroxides. Applied Clay Science 18, 255–264. https://doi.org/10.1016/S0169-1317(01)00029-1

Ivancic, A., Macaev, F., Aksakal, F., Boldescu, V., Pogrebnoi, S., Duca, G., 2016. Preparation of alginate–chitosan–cyclodextrin micro- and nanoparticles loaded with anti-tuberculosis compounds. Beilstein Journal of Nanotechnology 7, 1208–1218. https://doi.org/10.3762/bjnano.7.112

Jafarbeglou, M., Abdouss, M., Shoushtari, A.M., Jafarbeglou, M., 2016. Clay nanocomposites as engineered drug delivery systems. RSC Adv. 6, 50002–50016. https://doi.org/10.1039/C6RA03942A

John P. Perdew, Kieron Burke, and M.E., 1997. Generalized Gradient Approximation Made Simple. Physical review letters 77, 3865–3868. https://doi.org/10.1103/PhysRevLett.77.3865

Jorfi, M., Foster, E.J., 2015. Recent advances in nanocellulose for biomedical applications. Journal of Applied Polymer Science 132, n/a-n/a. https://doi.org/10.1002/app.41719

Kaur, G., Grewal, J., Jyoti, K., Jain, U.K., Chandra, R., Madan, J., 2018. Oral controlled and sustained drug delivery systems, in: Drug Targeting and Stimuli Sensitive Drug Delivery Systems. Elsevier, pp. 567–626. https://doi.org/10.1016/B978-0-12-813689-8.00015-X

Ke, M., Wahab, J.A., Hyunsik, B., Song, K.-H., Lee, J.S., Gopiraman, M., Kim, I.S.,

2016. Allantoin-loaded porous silica nanoparticles/polycaprolactone nanofiber composites: fabrication, characterization, and drug release properties. RSC Advances 6, 4593–4600. https://doi.org/10.1039/C5RA22199D

Khan, A.H., Ghosh, S., Pradhan, B., Dalui, A., Shrestha, L.K., Acharya, S., Ariga, K., 2017. Two-Dimensional (2D) Nanomaterials towards Electrochemical Nanoarchitectonics in Energy-Related Applications. Bulletin of the Chemical Society of Japan 90, 627–648. https://doi.org/10.1246/bcsj.20170043

Kim, M.H., Park, D.H., Yang, J.H., Choy, Y. Bin, Choy, J.H., 2013. Drug-inorganic-polymer nanohybrid for transdermal delivery. International Journal of Pharmaceutics 444, 120–127. https://doi.org/10.1016/j.ijpharm.2012.12.043

Kinaan, M., Ding, H., Triggle, C.R., 2015. Metformin: An Old Drug for the Treatment of Diabetes but a New Drug for the Protection of the Endothelium. Medical Principles and Practice 24, 401–415. https://doi.org/10.1159/000381643

King, P., Peacock, I., Donnelly, R., 2001. The UK Prospective Diabetes Study (UKPDS): clinical and therapeutic implications for type 2 diabetes. British Journal of Clinical Pharmacology 48, 643–648. https://doi.org/10.1046/j.1365-2125.1999.00092.x

Klemm, D., Schumann, D., Kramer, F., Heßler, N., Hornung, M., Schmauder, H.-P., Marsch, S., 2006. Nanocelluloses as Innovative Polymers in Research and Application, in: Advances in Polymer Science. pp. 49–96. https://doi.org/10.1007/12_097

Klippel, A.P., Margraf, H.W., Covey, T.H., 1977. The use of silver-zinc-allantoin powder for the prehospital treatment of burns. Journal of the American College of Emergency Physicians 6, 184–186. https://doi.org/10.1016/S0361-1124(77)80492-9

Komiyama, M., Yoshimoto, K., Sisido, M., Ariga, K., 2017. Chemistry Can Make Strict and Fuzzy Controls for Bio-Systems: DNA Nanoarchitectonics and

Cell-Macromolecular Nanoarchitectonics. Bulletin of the Chemical Society of Japan 90, 967–1004. https://doi.org/10.1246/bcsj.20170156

Krentz, A.J., Bailey, C.J., 2005. Oral Antidiabetic Agents. Drugs 65, 385–411. https://doi.org/10.2165/00003495-200565030-00005

Kuş, N., Bayarı, S.H., Fausto, R., 2009. Thermal decomposition of allantoin as probed by matrix isolation FTIR spectroscopy. Tetrahedron 65, 9719–9727. https://doi.org/10.1016/j.tet.2009.09.088

Labropoulos, K.C., Niesz, D.E., Danforth, S.C., Kevrekidis, P.G., 2002. Dynamic rheology of agar gels: theory and experiments. Part II: gelation behavior of agar sols and fitting of a theoretical rheological model. Carbohydrate Polymers 50, 407–415. https://doi.org/10.1016/S0144-8617(02)00085-1

Lai, M.-F., Lii, C., 1997. Rheological and thermal characteristics of gel structures from various agar fractions. International Journal of Biological Macromolecules 21, 123–130. https://doi.org/10.1016/S0141-8130(97)00051-2

Lakraimi, M., Legrouri, A., Barroug, A., De Roy, A., Pierre Besse, J., 2000. Preparation of a new stable hybrid material by chloride–2,4-dichlorophenoxyacetate ion exchange into the zinc–aluminium–chloride layered double hydroxide. Journal of Materials Chemistry 10, 1007–1011. https://doi.org/10.1039/a909047i

Laliberte, B.K., Neumiller, J.J., 2010. Review of Medications Used in the Treatment of Diabetes Mellitus. Journal of Pharmacy Technology 26, 136–146. https://doi.org/10.1177/875512251002600307

Langry, A., Cellier, J., Hintze-Bruening, H., Leroux, F., 2018. In situ generation of layered single- or double-hydroxide inorganic platelets (LSH and LDH) assisted by bola amphiphiles. Dalton Transactions 47, 3005–3013. https://doi.org/10.1039/C7DT03191B

Lawton, J.W., 2002. Zein: A History of Processing and Use. Cereal Chemistry Journal 79, 1–18. https://doi.org/10.1094/CCHEM.2002.79.1.1

Lee, K.Y., Mooney, D.J., 2012. Alginate: Properties and biomedical applications. Progress in Polymer Science 37, 106–126. https://doi.org/10.1016/j.progpolymsci.2011.06.003

Lenhard, J.M., Gottschalk, W.K., 2002. Preclinical developments in type 2 diabetes. Advanced Drug Delivery Reviews 54, 1199–1212. https://doi.org/10.1016/S0169-409X(02)00092-3

Leroux, F., Adachi-Pagano, M., Intissar, M., Chauvière, S., Forano, C., Besse, J.-P., 2001. Delamination and restacking of layered double hydroxides. Journal of Materials Chemistry 11, 105–112. https://doi.org/10.1039/b002955f

Leroux, F., Besse, J.-P., 2001. Polymer Interleaved Layered Double Hydroxide: A New Emerging Class of Nanocomposites. Chemistry of Materials 13, 3507–3515. https://doi.org/10.1021/cm0110268

Leroux, F., Gachon, J., Besse, J.-P., 2004. Biopolymer immobilization during the crystalline growth of layered double hydroxide. Journal of Solid State Chemistry 177, 245–250. https://doi.org/10.1016/j.jssc.2003.08.013

Levetan, C., 2007. Oral antidiabetic agents in type 2 diabetes. Current Medical Research and Opinion 23, 945–952. https://doi.org/10.1185/030079907X178766

Li, T., Miras, H., Song, Y.-F., 2017. Polyoxometalate (POM)-Layered Double Hydroxides (LDH) Composite Materials: Design and Catalytic Applications. Catalysts 7, 260. https://doi.org/10.3390/catal7090260

Li, X., Nie, X., Qu, F., 2017. Development of small intestine-specific delivery system for metformin hydrochloride delivery. Journal of Sol-Gel Science and Technology 81, 762–768. https://doi.org/10.1007/s10971-016-4247-1

Lin, N., Dufresne, A., 2014. Nanocellulose in Biomedicine : Current Status and Future Prospect. European Polymer Journal 59, 302–325. https://doi.org/10.1016/j.eurpolymj.2014.07.025

Lisuzzo, L., Cavallaro, G., Milioto, S., Lazzara, G., 2019. Layered composite based on halloysite and natural polymers: a carrier for the pH controlled release of

drugs. New Journal of Chemistry 43, 10887–10893. https://doi.org/10.1039/C9NJ02565K

Lisuzzo, L., Wicklein, B., Lo Dico, G., Lazzara, G., del Real, G., Aranda, P., Ruiz-Hitzky, E., 2020. Functional biohybrid materials based on halloysite, sepiolite and cellulose nanofibers for health applications. Dalton Transactions. https://doi.org/10.1039/C9DT03804C

Liu, J., Zhang, L., Jia, Y., Hu, W., Zhang, J., Jiang, H., 2012. Preparation and evaluation of pectin-based colon-specific pulsatile capsule in vitro and in vivo. Archives of Pharmacal Research 35, 1927–1934. https://doi.org/10.1007/s12272-012-1109-4

López-Galindo, A., Viseras, C., Aguzzi, C., Cerezo, P., 2011. Pharmaceutical and Cosmetic Uses of Fibrous Clays, in: Developments in Clay Science. pp. 299–324. https://doi.org/10.1016/B978-0-444-53607-5.00013-X

Lord, J.M., 2003. Metformin in polycystic ovary syndrome: systematic review and meta-analysis. BMJ 327, 951–0. https://doi.org/10.1136/bmj.327.7421.951

Loren, R.P., 1995. Allantoin-metal complexes for skin and hair. US19940218392.

Madejová, J., Arvaiova, B., Komadel, P., 1999. FTIR spectroscopic characterization of thermally treated Cu 2 + , Cd 2 + , and Li + montmorillonites. Spectrochimica acta. Part A, Molecular and biomolecular spectroscopy 55, 2467–2476. https://doi.org/10.1016/j.clay.2006.11.002

Madejová, K.P. and J., 2001. Baseline studies of the clay minerals society source clays: infrared methods. Clays and Clay Minerals 49, 410–432. https://doi.org/10.1346/CCMN.2001.0490502

Maes, A., Stul, M.S., Cremers, A., 1979. Layer charge - cation-exchange capacity relationships in montmorillonite. Clays and Clay Minerals 27, 387–392. https://doi.org/10.1346/CCMN.1979.0270510

Margraf, H., 1974. Anti-microbial compositions utilizing allantoin compounds and complexes. 165.753.

Margulies, L., Rozen, H., Cohen, E., 1985. Energy transfer at the surface of clays and protection of pesticides from photodegradation. Nature 315, 658–659. https://doi.org/10.1038/315658a0

Markowicz-Piasecka, M., Sikora, J., Szydłowska, A., Skupień, A., Mikiciuk-Olasik, E., Huttunen, K.M., 2017. Metformin – a Future Therapy for Neurodegenerative Diseases. Pharmaceutical Research 34, 2614–2627. https://doi.org/10.1007/s11095-017-2199-y

Martínez-Gómez, F., Guerrero, J., Matsuhiro, B., Pavez, J., 2017. In vitro release of metformin hydrochloride from sodium alginate/polyvinyl alcohol hydrogels. Carbohydrate Polymers 155, 182–191. https://doi.org/10.1016/j.carbpol.2016.08.079

Massaro, M., Colletti, C., Lazzara, G., Riela, S., 2018. The Use of Some Clay Minerals as Natural Resources for Drug Carrier Applications. Journal of Functional Biomaterials 9, 58. https://doi.org/10.3390/jfb9040058

Mehtani, D., Seth, A., Sharma, P., Maheshwari, N., Kapoor, D., Shrivastava, S.K., Tekade, R.K., 2019. Biomaterials for Sustained and Controlled Delivery of Small Drug Molecules, in: Biomaterials and Bionanotechnology. Elsevier, pp. 89–152. https://doi.org/10.1016/B978-0-12-814427-5.00004-4

Meirelles, L., Carazo, E., Borrego-Sánchez, A., Barbosa, R., Moura, T., Aguzzi, C., Sainz-Diaz, C.I., Viseras, C., Raffin, F., 2019. Design and characterization of a tuberculostatic hybrid based on interaction of ethambutol with a raw palygorskite. Applied Clay Science 181, 105213. https://doi.org/10.1016/j.clay.2019.105213

Meyn, M., Beneke, K., Lagaly, G., 1990. Anion-exchange reactions of layered double hydroxides. Inorganic Chemistry 29, 5201–5207. https://doi.org/10.1021/ic00351a013

Miller, P. and Westra, P., 2004. Herbicide Behavior in Soils. Colorado State University cooperative extension, Boulder.

Miller, R., Fainerman, V.B., Möhwald, H., 2002. Adsorption Behavior of

Oxyethylated Surfactants at the Air/Water Interface. Journal of Colloid and Interface Science 247, 193–199. https://doi.org/10.1006/jcis.2001.8120

Mishael, Y.G., Undabeytia, T., Rabinovitz, O., Rubin, B., Nir, S., 2003. Sulfosulfuron Incorporated in Micelles Adsorbed on Montmorillonite for Slow Release Formulations. Journal of Agricultural and Food Chemistry 51, 2253–2259. https://doi.org/10.1021/jf0261497

Mishra, G., Dash, B., Pandey, S., 2018. Layered double hydroxides: A brief review from fundamentals to application as evolving biomaterials. Applied Clay Science 153, 172–186. https://doi.org/10.1016/j.clay.2017.12.021

Miyata, S., 1977. Synthesis of Hydrotalcite-Like Compounds and their Physico-Chemical Properties—The Systems Mg2+-Al3+-SO42− and Mg2+-Al3+-CrO42−. Clays and Clay Minerals 25, 14–18. https://doi.org/10.1346/CCMN.1977.0250103

Miyata, S., 1975. The Syntheses of Hydrotalcite-Like Compounds and Their Structures and Physico-Chemical Properties I: The Systems Mg2+-Al3+-NO3−, Mg2+-Al3+-Cl−, Mg2+-Al3+-ClO4−, Ni2+-Al3+-Cl− and Zn2+-Al3+-Cl−. Clays and Clay Minerals 23, 369–375. https://doi.org/10.1346/CCMN.1975.0230508

Miyazawa, T., Shimanouchi, T., Mizushima, S., 1956. Characteristic Infrared Bands of Monosubstituted Amides. The Journal of Chemical Physics 24, 408–418. https://doi.org/10.1063/1.1742489

Mohite, B. V., Patil, S. V., 2014. A novel biomaterial: bacterial cellulose and its new era applications. Biotechnology and Applied Biochemistry 61, 101–110. https://doi.org/10.1002/bab.1148

Moraes, J.D.D., Bertolino, S.R.A., Cuffini, S.L., Ducart, D.F., Bretzke, P.E., Leonardi, G.R., 2017. Clay minerals: Properties and applications to dermocosmetic products and perspectives of natural raw materials for therapeutic purposes—A review. International Journal of Pharmaceutics 534, 213–219. https://doi.org/10.1016/j.ijpharm.2017.10.031

Munarin, F., Tanzi, M.C., Petrini, P., 2012. Advances in biomedical applications of pectin gels. International Journal of Biological Macromolecules 51, 681–689. https://doi.org/10.1016/j.ijbiomac.2012.07.002

Negrea, P., Caunii, A., Sarac, I., Butnariu, M., 2015. The study of infrared spectrum of chitin and chitosan extract as potential sources of biomass. Digest Journal of Nanomaterials and Biostructures 10, 1129–1138.

Nennemann, A., Mishael, Y., Nir, S., Rubin, B., Polubesova, T., Bergaya, F., van Damme, H., Lagaly, G., 2001. Clay-based formulations of metolachlor with reduced leaching. Applied Clay Science 18, 265–275. https://doi.org/10.1016/S0169-1317(01)00032-1

Nir, S., El-Nahhal, Y., Undabeytia, T., Rytwo, G., Polubesova, T., Mishael, Y., Rabinovitz, O., Rubin, B., 2013. Clays, Clay Minerals, and Pesticides, in: Developments in Clay Science. Copyright © 2013, 2006 Elsevier Ltd. All rights reserved., pp. 645–662. https://doi.org/10.1016/B978-0-08-098259-5.00022-6

Nir, S., El Nahhal, Y., Undabeytia, T., Rytwo, G., Polubesova, T., Mishael, Y., Rabinovitz, U., Rubin, B., 2006. Chapter 11.2 Clays and Pesticides, in: Developments in Clay Science. pp. 677–691. https://doi.org/10.1016/S1572-4352(05)01021-4

Oh, J.-M., Park, D.-H., Choi, S.-J., Choy, J.-H., 2012. LDH Nanocontainers as Bio-Reservoirs and Drug Delivery Carriers. Recent Patents on Nanotechnology 6, 200–217. https://doi.org/10.2174/187221012803531538

Oh, J.-M., Park, M., Kim, S.-T., Jung, J.-Y., Kang, Y.-G., Choy, J.-H., 2006. Efficient delivery of anticancer drug MTX through MTX-LDH nanohybrid system. Journal of Physics and Chemistry of Solids 67, 1024–1027. https://doi.org/10.1016/j.jpcs.2006.01.033

Oh, Y.-J., Choi, G., Choy, Y. Bin, Park, J.W., Park, J.H., Lee, H.J., Yoon, Y.J., Chang, H.C., Choy, J.-H., 2013. Aripiprazole-Montmorillonite: A New Organic-Inorganic Nanohybrid Material for Biomedical Applications. Chemistry - A

European Journal 19, 4869–4875. https://doi.org/10.1002/chem.201203384

Okamoto, K., Iyi, N., Sasaki, T., 2007. Factors affecting the crystal size of the MgAl-LDH (layered double hydroxide) prepared by using ammonia-releasing reagents. Applied Clay Science 37, 23–31. https://doi.org/10.1016/j.clay.2006.10.008

Oliveira, A.S., Alcântara, A.C.S., Pergher, S.B.C., 2017. Bionanocomposite systems based on montmorillonite and biopolymers for the controlled release of olanzapine. Materials Science and Engineering: C 75, 1250–1258. https://doi.org/10.1016/j.msec.2017.03.044

Oliveira, S.M. de, Silva, J.B.P. da, Hernandes, M.Z., Lima, M. do C.A. de, Galdino, S.L., Pitta, I.D.R., 2008. Estrutura, reatividade e propriedades biológicas de hidantoínas. Química Nova 31, 614–622. https://doi.org/10.1590/S0100-40422008000300029

Olphen, H. V., 1977. An Introduction to Clay Colloid Chemistry, Berichte der Bunsengesellschaft für physikalische Chemie. Wiley-VCH Verlag GmbH & Co. KGaA, New York, London, Sydney, Toronto. https://doi.org/10.1002/bbpc.197800022

Ortega-Castro, J., Hernandez-Haro, N., Dove, M.T., Hernandez-Laguna, A., Sainz-Diaz, C.I., 2010. Density functional theory and Monte Carlo study of octahedral cation ordering of Al/Fe/Mg cations in dioctahedral 2:1 phyllosilicates. American Mineralogist 95, 209–220. https://doi.org/10.2138/am.2010.3273

Ozcalik, O., Tihminlioglu, F., 2013. Barrier properties of corn zein nanocomposite coated polypropylene films for food packaging applications. Journal of Food Engineering 114, 505–513. https://doi.org/10.1016/j.jfoodeng.2012.09.005

Pala, L., Rotella, C.M., 2014. The "slower" the better. Journal of Endocrinological Investigation 37, 497–498. https://doi.org/10.1007/s40618-014-0065-x

Paliwal, R., Palakurthi, S., 2014. Zein in controlled drug delivery and tissue engineering. Journal of Controlled Release 189, 108–122.

https://doi.org/10.1016/j.jconrel.2014.06.036

Pálková, H., Madejová, J., Zimowska, M., Serwicka, E.M., 2010. Laponite-derived porous clay heterostructures: II. FTIR study of the structure evolution. Microporous and Mesoporous Materials 127, 237–244. https://doi.org/10.1016/j.micromeso.2009.07.012

Park, D.-H., Hwang, S.-J., Oh, J.-M., Yang, J.-H., Choy, J.-H., 2013. Polymer–inorganic supramolecular nanohybrids for red, white, green, and blue applications. Progress in Polymer Science 38, 1442–1486. https://doi.org/10.1016/j.progpolymsci.2013.05.007

Park, J.K., Choy, Y. Bin, Oh, J.-M., Kim, J.Y., Hwang, S.-J., Choy, J.-H., 2008. Controlled release of donepezil intercalated in smectite clays. International Journal of Pharmaceutics 359, 198–204. https://doi.org/10.1016/j.ijpharm.2008.04.012

Park, K., 2014. Controlled drug delivery systems: Past forward and future back. Journal of Controlled Release 190, 3–8. https://doi.org/10.1016/j.jconrel.2014.03.054

Pavlovic, I., Barriga, C., Hermosín, M.C., Cornejo, J., Ulibarri, M.A., 2005. Adsorption of acidic pesticides 2,4-D, Clopyralid and Picloram on calcined hydrotalcite. Applied Clay Science 30, 125–133. https://doi.org/10.1016/j.clay.2005.04.004

Pepperman, A.B., Jui-Chang W. Kuan, McCombs, C., 1991. Alginate controlled release formulations of metribuzin. Journal of Controlled Release 17, 105–111. https://doi.org/10.1016/0168-3659(91)90136-2

Perioli, L., Nocchetti, M., Ambrogi, V., Latterini, L., Rossi, C., Costantino, U., 2008. Sunscreen immobilization on ZnAl-hydrotalcite for new cosmetic formulations. Microporous and Mesoporous Materials 107, 180–189. https://doi.org/10.1016/j.micromeso.2007.02.021

Petersen, N., Gatenholm, P., 2011. Bacterial cellulose-based materials and medical devices: current state and perspectives. Applied Microbiology and

Biotechnology 91, 1277–1286. https://doi.org/10.1007/s00253-011-3432-y

Piétrement, O., Castro-Smirnov, F.A., Le Cam, E., Aranda, P., Ruiz-Hitzky, E., Lopez, B.S., 2018. Sepiolite as a New Nanocarrier for DNA Transfer into Mammalian Cells: Proof of Concept, Issues and Perspectives. The Chemical Record 18, 849–857. https://doi.org/10.1002/tcr.201700078

Pongjanyakul, T., Puttipipatkhachorn, S., 2007. Xanthan–alginate composite gel beads: Molecular interaction and in vitro characterization. International Journal of Pharmaceutics 331, 61–71. https://doi.org/10.1016/j.ijpharm.2006.09.011

Porubcan, L.S., Serna, C.J., White, J.L., Hem, S.L., 1978. Mechanism of adsorption of clindamycin and tetracycline by montmorillonite. Journal of Pharmaceutical Sciences 67, 1081–1087. https://doi.org/10.1002/jps.2600670815

Prete, M.C., de Oliveira, F.M., Tarley, C.R.T., 2017. Assessment on the performance of nano-carbon black as an alternative material for extraction of carbendazim, tebuthiuron, hexazinone, diuron and ametryn. Journal of Environmental Chemical Engineering 5, 93–102. https://doi.org/10.1016/j.jece.2016.11.022

Rajpurohit, H., Sharma, S., Sharma, P., Bhandari, A., 2010. Polymers for colon targeted drug delivery. Indian Journal of Pharmaceutical Sciences 72, 689. https://doi.org/10.4103/0250-474X.84576

Rappe, A.K., Goddard, W.A., 1991. Charge equilibration for molecular dynamics simulations. The Journal of Physical Chemistry 95, 3358–3363. https://doi.org/10.1021/j100161a070

Rebitski, E.P., Alcântara, A.C.S., Darder, M., Cansian, R.L., Gómez-Hortigüela, L., Pergher, S.B.C., 2018. Functional Carboxymethylcellulose/Zein Bionanocomposite Films Based on Neomycin Supported on Sepiolite or Montmorillonite Clays. ACS Omega 3, 13538–13550. https://doi.org/10.1021/acsomega.8b01026

Rebitski, E.P., Souza, G.P., Santana, S.A.A., Pergher, S.B.C., Alcântara, A.C.S., 2019. Bionanocomposites based on cationic and anionic layered clays as controlled release devices of amoxicillin. Applied Clay Science 173, 35–45. https://doi.org/10.1016/j.clay.2019.02.024

Rees, D.A., 1981. Polysaccharide shapes and their interactions - some recent advances. Pure and Applied Chemistry 53, 1–14. https://doi.org/10.1351/pac198153010001

Ribeiro, L.N.M., Alcântara, A.C.S., Darder, M., Aranda, P., Araújo-Moreira, F.M., Ruiz-Hitzky, E., 2014. Pectin-coated chitosan–LDH bionanocomposite beads as potential systems for colon-targeted drug delivery. International Journal of Pharmaceutics 463, 1–9. https://doi.org/10.1016/j.ijpharm.2013.12.035

Ribeiro, L.N.M., Alcântara, A.C.S., Darder, M., Aranda, P., Herrmann, P.S.P., Araújo-Moreira, F.M., García-Hernández, M., Ruiz-Hitzky, E., 2014c. Bionanocomposites containing magnetic graphite as potential systems for drug delivery. International Journal of Pharmaceutics 477, 553–563. https://doi.org/10.1016/j.ijpharm.2014.10.033

Rick, S.W., Stuart, S.J., Bader, J.S., Berne, B.J., 1995. Fluctuating charge force fields for aqueous solutions, in: Studies in Physical and Theoretical Chemistry. pp. 31–40. https://doi.org/10.1016/S0167-6881(06)80758-5

Rives, V., 2001. Layered double hydroxides: present and future, Nova Publishers. Nova Publishers, New York.

Robert, C., Wilson, C.S., Venuta, A., Ferrari, M., Arreto, C.-D., 2017. Evolution of the scientific literature on drug delivery: A 1974–2015 bibliometric study. Journal of Controlled Release 260, 226–233. https://doi.org/10.1016/j.jconrel.2017.06.012

Rogez, G., Massobrio, C., Rabu, P., Drillon, M., 2011. Layered hydroxide hybrid nanostructures: a route to multifunctionality. Chemical Society Reviews 40, 1031. https://doi.org/10.1039/c0cs00159g

Rojas, L.B.A., Gomes, M.B., 2013. Metformin: an old but still the best treatment

for type 2 diabetes. Diabetology & Metabolic Syndrome 5, 6. https://doi.org/10.1186/1758-5996-5-6

Roy, A., Singh, S.K., Bajpai, J., Bajpai, A.K., 2014. Controlled pesticide release from biodegradable polymers. Central European Journal of Chemistry 12, 453–469. https://doi.org/10.2478/s11532-013-0405-2

Ruiz-Hitzky, E., 2001. Molecular access to intracrystalline tunnels of sepiolite. Journal of Materials Chemistry 11, 86–91. https://doi.org/10.1039/b003197f

Ruiz-Hitzky, E., Aranda, P., Serratosa, M. "Organic/Polymeric Interactions with Clays". Chapter 3 Handbook of Layered Materials, pág. 91–154, S.M. Auerbach, K.A. Carrado & P.K. Dutta, Eds., Marcel Dekker, New York, 2004

Ruiz-Hitzky, E., Aranda, P., 2014. Novel architectures in porous materials based on clays. Journal of Sol-Gel Science and Technology 70, 307–316. https://doi.org/10.1007/s10971-013-3237-9

Ruiz-Hitzky, E., Aranda, P., Belver, C., 2012. Nanoarchitectures based on clay materials. RSC Nanoscience and Nanotechnology.

Ruiz-Hitzky, E., Darder, M., Aranda, P., del Burgo, M.Á.M., del Real, G., 2009. Bionanocomposites as New Carriers for Influenza Vaccines. Advanced Materials 21, 4167–4171. https://doi.org/10.1002/adma.200900181

Ruiz-Hitzky, E., Aranda, P., Gómez-Avilés, A., 2008. Micro- and nano-structured composite materials based on laminar double hydroxides ofhydrotalcite type and silicates of the clay family. Patent N. WO2010072870.

Ruiz-Hitzky, E., Darder, M., Wicklein, B., Castro-Smirnov, F.A., Aranda, P., 2019. Clay-based biohybrid materials for biomedical and pharmaceutical applications. Clays and Clay Minerals 67, 44–58. https://doi.org/10.1007/s42860-019-0005-0

Rytwo, G., Tropp, D., Serban, C., 2002. Adsorption of diquat, paraquat and methyl green on sepiolite: experimental results and model calculations. Applied Clay Science 20, 273–282. https://doi.org/10.1016/S0169-1317(01)00068-0

Sánchez-Espejo, R., Aguzzi, C., Salcedo, I., Cerezo, P., Viseras, C., 2014. Clays in complementary and alternative medicine. Materials Technology 29, B78–B81. https://doi.org/10.1179/1753555714Y.0000000173

Sande, S.A., 2005. Pectin-based oral drug delivery to the colon. Expert Opinion on Drug Delivery 2, 441–450. https://doi.org/10.1517/17425247.2.3.441

Sangeetha, K., Vinodhini, P.A., Sudha, P.N., 2019. Clay based biopolymer nanocomposites and their applications in environmental and biomedical fields. Sustainable Polymer Composites and Nanocomposites 1159–1183. https://doi.org/10.1007/978-3-030-05399-4_40

Santaren, J., Sanz, J., Ruiz-hitzky, E., 1990. Structural fluorine in sepiolite. Clays and Clay Minerals 38, 63–68.

Santos, A.F.O., Jr, I.D.B., Souza, F.S. de, Medeiros, A.F.D., Pinto, M.F., Santana, D.P. de, Macêdo, R.O., 2008. Application of thermal analysis of binary mixtures with metformin. Journal of Thermal Analysis and Calorimetry 93, 361–364. https://doi.org/10.1007/s10973-007-7876-3

Settanni, L., Corsetti, A., 2008. Application of bacteriocins in vegetable food biopreservation. International Journal of Food Microbiology 121, 123–138. https://doi.org/10.1016/j.ijfoodmicro.2007.09.001

Shariatinia, Z., Zahraee, Z., 2017. Controlled release of metformin from chitosan–based nanocomposite films containing mesoporous MCM-41 nanoparticles as novel drug delivery systems. Journal of Colloid and Interface Science 501, 60–76. https://doi.org/10.1016/j.jcis.2017.04.036

Shimoda, J., Onishi, H., Machida, Y., 2001. Bioadhesive Characteristics of Chitosan Microspheres to the Mucosa of Rat Small Intestine. Drug Development and Industrial Pharmacy 27, 567–576. https://doi.org/10.1081/DDC-100105182

Shingade, G.M., 2012. Review on: recent trend on transdermal drug delivery system. Journal of Drug Delivery and Therapeutics 2. https://doi.org/10.22270/jddt.v2i1.74

Shukla, M.K., Singh, R.P., Reddy, C.R.K., Jha, B., 2012. Synthesis and characterization of agar-based silver nanoparticles and nanocomposite film with antibacterial applications. Bioresource Technology 107, 295–300. https://doi.org/10.1016/j.biortech.2011.11.092

Shukla, R., Cheryan, M., 2001. Zein: the industrial protein from corn. Industrial Crops and Products 13, 171–192. https://doi.org/10.1016/S0926-6690(00)00064-9

Si, S., Taubert, A., Mantion, A., Rogez, G., Rabu, P., 2012. Peptide-intercalated layered metal hydroxides: effect of peptide chain length and side chain functionality on structural, optical and magnetic properties. Chemical Science 3, 1945. https://doi.org/10.1039/c2sc01087a

Siepmann, J., Peppas, N.A., 2001. Modeling of drug release from delivery systems based on hydroxypropyl methylcellulose (HPMC). Advanced Drug Delivery Reviews 48, 139–157. https://doi.org/10.1016/S0169-409X(01)00112-0

Siepmann, J., Siegel, R.A., Rathbone, M.J., 2012. Fundamentals and Applications of Controlled Release Drug Delivery, Fundamentals and Applications of Controlled Release Drug Delivery. Springer US, Boston, MA. https://doi.org/10.1007/978-1-4614-0881-9

Šimkovic, I., 2013. Unexplored possibilities of all-polysaccharide composites. Carbohydrate Polymers 95, 697–715. https://doi.org/10.1016/j.carbpol.2013.03.040

Singh, A., Dhiman, N., Kar, A.K., Singh, D., Purohit, M.P., Ghosh, D., Patnaik, S., 2020. Advances in controlled release pesticide formulations: Prospects to safer integrated pest management and sustainable agriculture. Journal of Hazardous Materials 385, 121525. https://doi.org/10.1016/j.jhazmat.2019.121525

Singh DK, R.A., 2000. Biomedical Applications of Chitin, Chitosan, and Their Derivatives. Journal of Macromolecular Science, Part C: Polymer Reviews

40, 69–83. https://doi.org/10.1081/MC-100100579

Sirtori, C., 1994. Re-evaluation of a biguanide, metformin: mechanism of action and tolerability. Pharmacological Research 30, 187–228. https://doi.org/10.1016/1043-6618(94)80104-5

Sriamornsak, P., 2011. Application of pectin in oral drug delivery. Expert Opinion on Drug Delivery 8, 1009–1023. https://doi.org/10.1517/17425247.2011.584867

Starukh, G., Rozovik, O., Oranska, O., 2016. Organo/Zn-Al LDH Nanocomposites for Cationic Dye Removal from Aqueous Media. Nanoscale Research Letters 11, 228. https://doi.org/10.1186/s11671-016-1402-0

Sterrett, J.J., Bragg, S., Weart, C.W., 2016. Type 2 Diabetes Medication Review. The American Journal of the Medical Sciences 351, 342–355. https://doi.org/10.1016/j.amjms.2016.01.019

Stimpfling, T., Langry, A., Hintze-bruening, H., Leroux, F., 2016. In situ platelets formation into aqueous polymer colloids: The topochemical transformation from single to double layered hydroxide (LSH–LDH) uncovered. Journal of Colloid and Interface Science 462, 260–271. https://doi.org/10.1016/j.jcis.2015.10.010

Synytsya, A., 2003. Fourier transform Raman and infrared spectroscopy of pectins. Carbohydrate Polymers 54, 97–106. https://doi.org/10.1016/S0144-8617(03)00158-9

Taki, S., Badens, E., Charbit, G., 2001. Controlled release system formed by supercritical anti-solvent coprecipitation of a herbicide and a biodegradable polymer. The Journal of Supercritical Fluids 21, 61–70. https://doi.org/10.1016/S0896-8446(01)00076-6

Thakur, B.R., Singh, R.K., Handa, A.K., Rao, M.A., 1997. Chemistry and uses of pectin — A review. Critical Reviews in Food Science and Nutrition 37, 47–73. https://doi.org/10.1080/10408399709527767

Thirawong, N., Nunthanid, J., Puttipipatkhachorn, S., Sriamornsak, P., 2007. Mucoadhesive properties of various pectins on gastrointestinal mucosa: An in vitro evaluation using texture analyzer. European Journal of Pharmaceutics and Biopharmaceutics 67, 132–140. https://doi.org/10.1016/j.ejpb.2007.01.010

Tian, N., Tian, X., Liu, X., Zhou, Z., Yang, C., Ma, L., Tian, C., Li, Y., Wang, Y., 2016. Facile synthesis of hierarchical dendrite-like structure iron layered double hydroxide nanohybrids for effective arsenic removal. Chemical Communications 52, 11955–11958. https://doi.org/10.1039/C6CC05659H

Tian, S., Li, J., Tao, Q., Zhao, Y., Lv, Z., Yang, F., Duan, H., Chen, Y., Zhou, Q., Hou, D., 2018. Controlled drug delivery for glaucoma therapy using montmorillonite/Eudragit microspheres as an ion-exchange carrier. International Journal of Nanomedicine Volume 13, 415–428. https://doi.org/10.2147/IJN.S146346

Tiwari, G., Tiwari, R., Bannerjee, S., Bhati, L., Pandey, S., Pandey, P., Sriwastawa, B., 2012. Drug delivery systems: An updated review. International Journal of Pharmaceutical Investigation 2, 2. https://doi.org/10.4103/2230-973X.96920

Tkatchenko, A., Scheffler, M., 2009. Accurate Molecular Van Der Waals Interactions from Ground-State Electron Density and Free-Atom Reference Data. Physical Review Letters 102, 073005. https://doi.org/10.1103/PhysRevLett.102.073005

Tomás, H., Alves, C.S., Rodrigues, J., 2018. Laponite®: A key nanoplatform for biomedical applications? Nanomedicine: Nanotechnology, Biology and Medicine 14, 2407–2420. https://doi.org/10.1016/j.nano.2017.04.016

Turner, R., 1998. Effect of intensive blood-glucose control with metformin on complications in overweight patients with type 2 diabetes (UKPDS 34). The Lancet 352, 854–865. https://doi.org/10.1016/S0140-6736(98)07037-8

UK Prospective Diabetes Study Group, 1998. Tight blood pressure control and

risk of macrovascular and microvascular complications in type 2 diabetes: UKPDS 38. UK Prospective Diabetes Study Group. BMJ (Clinical research ed.) 317, 703–13.

Undabeytia, T., Mishael, Y.G., Nir, S., Papahadjopoulos-Sternberg, B., Rubin, B., Morillo, E., Maqueda, C., 2003. A Novel System for Reducing Leaching from Formulations of Anionic Herbicides: Clay-Liposomes. Environmental Science & Technology 37, 4475–4480. https://doi.org/10.1021/es0343508

Undabeytia, T., Nir, S., Rubin, B., 2000. Organo-Clay Formulations of the Hydrophobic Herbicide Norflurazon Yield Reduced Leaching. Journal of Agricultural and Food Chemistry 48, 4767–4773. https://doi.org/10.1021/jf9907945

Undabeytia, T., Recio, E., Maqueda, C., Sánchez-Verdejo, T., Balek, V., 2012. Slow diuron release formulations based on clay–phosphatidylcholine complexes. Applied Clay Science 55, 53–61. https://doi.org/10.1016/j.clay.2011.10.005

Vanderbilt, D., 1990. Soft self-consistent pseudopotentials in a generalized eigenvalue formalism. Physical Review B 41, 7892. https://doi.org/10.1080/15376520590890677

Verma, S., Ahuja, M., 2017. Carboxymethyl sesbania gum: Synthesis, characterization and evaluation for drug delivery. International Journal of Biological Macromolecules 98, 75–83. https://doi.org/10.1016/j.ijbiomac.2017.01.070

Viseras, C., Aguzzi, C., Cerezo, P., Lopezgalindo, A., 2007. Uses of clay minerals in semisolid health care and therapeutic products. Applied Clay Science 36, 37–50. https://doi.org/10.1016/j.clay.2006.07.006

Viseras, C., Carazo, E., Borrego-Sánchez, A., García-Villén, F., Sánchez-Espejo, R., Cerezo, P., Aguzzi, C., 2019. Clay Minerals in Skin Drug Delivery. Clays and Clay Minerals 67, 59–71. https://doi.org/10.1007/s42860-018-0003-7

Viseras, C., Cerezo, P., Sanchez, R., Salcedo, I., Aguzzi, C., 2010. Current challenges in clay minerals for drug delivery. Applied Clay Science 48, 291–

295. https://doi.org/10.1016/j.clay.2010.01.007

Wang, L.F., Rhim, J.W., 2015. Preparation and application of agar/alginate/collagen ternary blend functional food packaging films. International Journal of Biological Macromolecules 80, 460–468. https://doi.org/10.1016/j.ijbiomac.2015.07.007

Ways, T. M., Lau, M. W., Khutoryanskiy, V. V, 2018. Chitosan and Its Derivatives for Application in Mucoadhesive Drug Delivery Systems. Polymers 10, 267. https://doi.org/10.3390/polym10030267

Wei, X., Fan, Y., Bi, C., Yan, X., Zhang, X., Li, X., 2014. Crystal Structure and Tautomerism Study of the Mono-protonated Metformin Salt. Bulletin of the Korean Chemical Society 35, 3495–3501. https://doi.org/10.5012/bkcs.2014.35.12.3495

Wenyang Xu, Xiaoju Wang, Niklas Sandler, Stefan Willfor, and C.X., 2018. Three-dimensional printing of wood-derived biopolymers : A review focused on biomedical applications. ACS Sustainable Chem. Eng 6, 5663–5680. https://doi.org/10.1021/acssuschemeng.7b03924

Wicklein, B., Darder, M., Aranda, P., Del Burgo, M.A.M., Del Real, G., Esteban, M., Ruiz-Hitzky, E., 2016. Clay-lipid nanohybrids: towards influenza vaccines and beyond. Clay Minerals 51, 529–538. https://doi.org/10.1180/claymin.2016.051.4.01

Wicklein, B., Darder, M., Aranda, P., Ruiz-Hitzky, E., 2010. Bio-organoclays Based on Phospholipids as Immobilization Hosts for Biological Species. Langmuir 26, 5217–5225. https://doi.org/10.1021/la9036925

Wicklein, B., Martín del Burgo, M.Á., Yuste, M., Darder, M., Llavata, C.E., Aranda, P., Ortin, J., del Real, G., Ruiz-Hitzky, E., 2012. Lipid-Based Bio-Nanohybrids for Functional Stabilisation of Influenza Vaccines. European Journal of Inorganic Chemistry 2012, 5186–5191. https://doi.org/10.1002/ejic.201200579

Williams, L.B., 2017. Geomimicry: harnessing the antibacterial action of clays.

Clay Minerals 52, 1–24. https://doi.org/10.1180/claymin.2017.052.1.01

Williams, L.B., Haydel, S.E., 2010. Evaluation of the medicinal use of clay minerals as antibacterial agents. International Geology Review 52, 745–770. https://doi.org/10.1080/00206811003679737

Xu, B., Sung, C., Han, B., 2011. Crystal Structure Characterization of Natural Allantoin from Edible Lichen Umbilicaria esculenta. Crystals 1, 128–135. https://doi.org/10.3390/cryst1030128

Xu, X., Chen, S., Wu, B., Ma, M., Shi, Y., Wang, X., 2015. Effect of allantoin on the stabilization efficiency of Ca–Zn thermal stabilizers for poly(vinyl chloride). Journal of Thermal Analysis and Calorimetry 119, 597–603. https://doi.org/10.1007/s10973-014-4168-6

Y. Xue, Z. Mou, H.X., 2017. Nanocellulose as Sustainable Biomass Material: Structure, Properties, Present Status and Future Prospects in Biomedical Applications. Nanoescale 9, 14758–14781. https://doi.org/10.1039/C7NR04994C

Yadu N. V.K., Raghvendra K. M., Aswathy V., Parvathy P., Sunija S., Neelakandan M. S., Nitheesha S., Vishnu K.A., 2017. Chitosan as Promising Materials for Biomedical Application: Review. Research & Development in Material Science 2, 170–185.https://doi.org/10.31031/RDMS.2017.02.000543

Yang, J.-H., Lee, J.-H., Ryu, H.-J., Elzatahry, A.A., Alothman, Z.A., Choy, J.-H., 2016. Drug–clay nanohybrids as sustained delivery systems. Applied Clay Science 130, 20–32. https://doi.org/10.1016/j.clay.2016.01.021

Yun, Y.H., Lee, B.K., Park, K., 2015. Controlled Drug Delivery: Historical perspective for the next generation. Journal of Controlled Release 219, 2–7. https://doi.org/10.1016/j.jconrel.2015.10.005

Zhang, H., Zhang, F., Yuan, R., 2020. Applications of natural polymer-based hydrogels in the food industry, in: Hydrogels Based on Natural Polymers. Elsevier, pp. 357–410. https://doi.org/10.1016/B978-0-12-816421-1.00015-X

Zhang, K., Xu, Z., Lu, J., Tang, Z., Zhao, H., Good, D., Wei, M., 2014. Potential for Layered Double Hydroxides-Based, Innovative Drug Delivery Systems. International Journal of Molecular Sciences 15, 7409–7428. https://doi.org/10.3390/ijms15057409

Zhang, X., Cresswell, M., 2016. Materials for Inorganic Controlled Release Technology, in: Inorganic Controlled Release Technology. Elsevier, pp. 1–16. https://doi.org/10.1016/B978-0-08-099991-3.00001-6

Zhao, D., Yu, S., Sun, B., Gao, S., Guo, S., Zhao, K., 2018. Biomedical Applications of Chitosan and Its Derivative Nanoparticles. Polymers 10, 462. https://doi.org/10.3390/polym10040462